DRVNA INDUSTRIJA

SCIENTIFIC JOURNAL
OF WOOD TECHNOLOGY

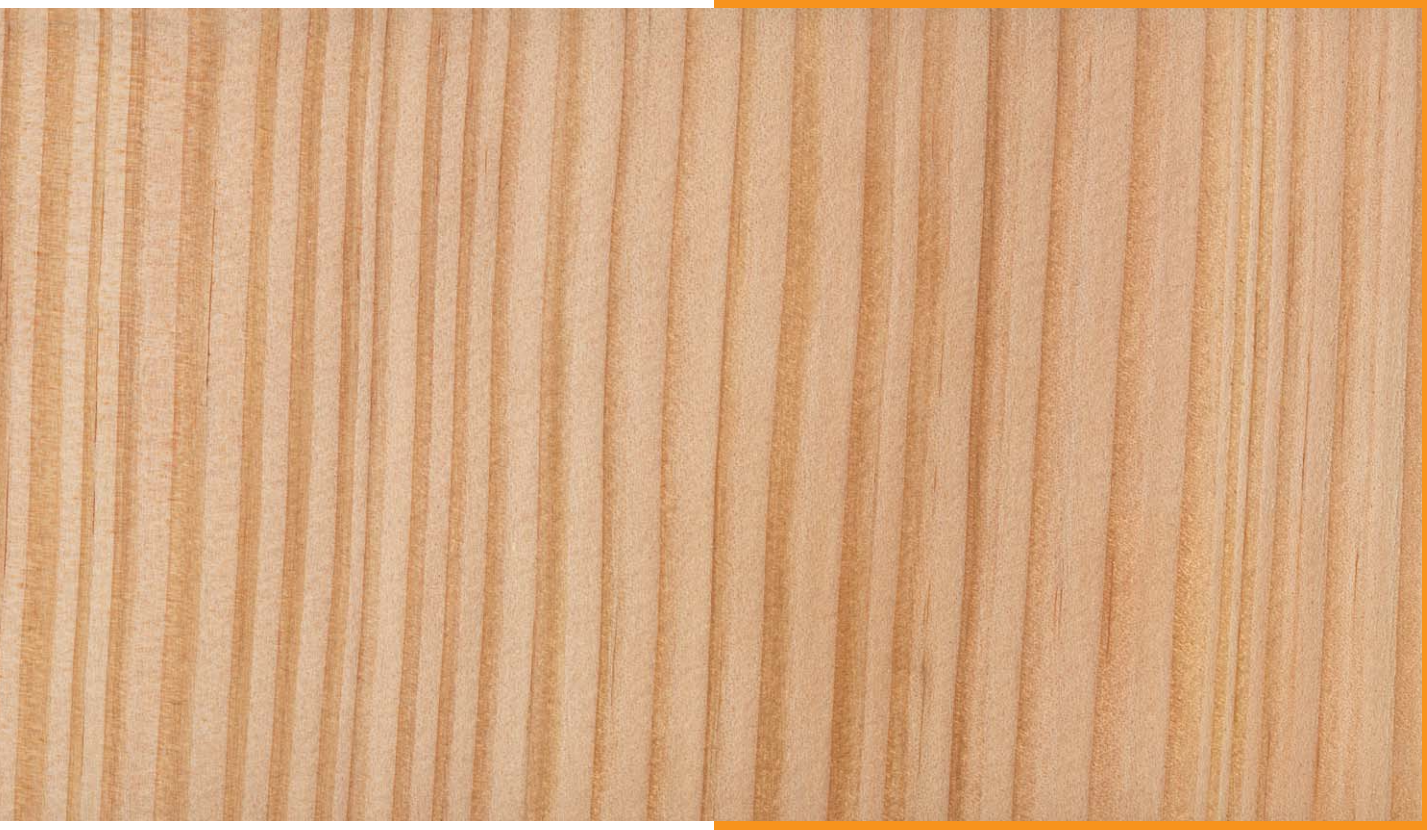

ZNANSTVENI ČASOPIS
ZA PITANJA DRVNE TEHNOLOGIJE

Pseudotsuga menziesii (Mirb.) Franco

UDK 674.031.677.7
ISO: Drv. Ind.
CODEN: DRINAT
JCR: DRVNA IND
ISSN 0012-6772

2/22
VOLUME 73

UDK 630*8+674 Coden: Drinat ISSN 0012-6772

DRVNA INDUSTRIJA

SCIENTIFIC JOURNAL OF WOOD TECHNOLOGY

Znanstveni časopis za pitanja drvne tehnologije

PUBLISHER AND EDITORIAL OFFICE
Izdavač i uredništvo
Faculty of Forestry and Wood Technology
University of Zagreb, Croatia
Fakultet šumarstva i drvne tehnologije
Sveučilišta u Zagrebu
www.sumfak.unizg.hr

CO-PUBLISHER / Suizdavač
Hrvatska komora inženjera šumarstva i drvne tehnologije

FOUNDER / Osnivač
Institut za drvnoindustrijska istraživanja, Zagreb

The journal Drvna industrija is a public scientific journal for publishing research results on structure, properties and protection of wood and wood materials, application of wood and wood materials, mechanical woodworking, hydrothermal treatment and chemical processing of wood, all aspects of wood materials and wood products production and trade in wood and wood products.
The journal is published quarterly and financially supported by the Ministry of Science and Education of the Republic of Croatia

Časopis Drvna industrija javno je znanstveno glasilo za objavu rezultata istraživanja građe, svojstava i zaštite drva i drvnih materijala, primjene drva i drvnih materijala, mehaničke i hidrotermičke obrade te kemijske prerade drva, svih aspekata proizvodnje drvnih materijala i proizvoda te trgovine drvom i drvnim proizvodima.
Časopis izlazi četiri puta u godini uz financijsku potporu Ministarstva znanosti i obrazovanja Republike Hrvatske.

Contents
Sadržaj

CIRCULATION: *400 pieces*

INDEXED IN: *Science Citation Index Expanded, Scopus, CAB Abstracts, Compendex, Environment Index, Veterinary Science Database, Geobase, DOAJ*

MANUSCRIPTS ARE TO BE SUBMITTED *by the link http://journal.sdewes.org/drvind*

CONTACT WITH THE EDITORIAL *e-mail: editordi@sumfak.hr*

SUBSCRIPTION: *Annual subscription for foreign subscribers is 55 EUR. Subscription in Croatia is 300 kn. For pupils, students and retired persons the subscription is 100 kn. Subscription shall be paid to the IBAN HR0923600001101340148 with the indication "Drvna industrija"*

PRINTED BY: *DENONA d.o.o., Getaldićeva 1, Zagreb, www.denona.hr*

DESIGN: *Bernardić Studio*

THE JOURNAL IS AVAILABLE ONLINE: *https://drvnaindustrija.com*

COVER: *Radial section of Pseudotsuga menziesii (Mirb.) Franco, xylotheca of Institute for Wood Science, Faculty of Forestry and Wood Technology University of Zagreb*

DRVNA INDUSTRIJA · VOL. 73, 2 · P. 113-256· SUMMER 2022. · ZAGREB EDITORIAL COMPLETED 2. 5. 2022.

NAKLADA: *400 komada*

ČASOPIS JE REFERIRAN U: *Science Citation Index Expanded, Scopus, CAB Abstracts, Compendex, Environment Index, Veterinary Science Database, Geobase, DOAJ*

ČLANKE TREBA SLATI *putem poveznice http://journal.sdewes.org/drvind*

KONTAKT S UREDNIŠTVOM: *e-mail: editordi@sumfak.hr*

PRETPLATA: *Godišnja pretplata za pretplatnike iz inozemstva iznosi 55 EUR. Pretplata u Hrvatskoj iznosi 300 kn, a za đake, studente i umirovljenike 100 kn. Pretplata se plaća na IBAN HR0923600001101340148 s naznakom "Drvna industrija".*

TISAK: *DENONA d.o.o., Getaldićeva 1, Zagreb, www.denona.hr*

DESIGN: *Bernardić Studio*

ČASOPIS JE DOSTUPAN NA INTERNETU: *https://drvnaindustrija.com*

NASLOVNICA: *Radijalni presjek drva Pseudotsuga menziesii (Mirb.) Franco, ksiloteka Zavoda za znanost o drvu, Fakultet šumarstva i drvne tehnologije Sveučilišta u Zagrebu*

DRVNA INDUSTRIJA · VOL. 73, 2 · STR. 113-256 · LJETO 2022. · ZAGREB REDAKCIJA DOVRŠENA 2. 5. 2022.

ORIGINAL SCIENTIFIC PAPERS
Izvorni znanstveni radovi 115

REVIEW PAPERS
Pregledni radovi 227

Darius Albrektas[1], Agnė Styraitė[2]

Modelling and Investigating Real-World Drying Defects in Wood

Modeliranje i istraživanje stvarnih grešaka sušenja drva

ORIGINAL SCIENTIFIC PAPER
Izvorni znanstveni rad
Received – prispjelo: 20. 10. 2020.
Accepted – prihvaćeno: 23. 3. 2022.
UDK: 630*81; 674.047.3
https://doi.org/10.5552/drvind.2022.2040

ABSTRACT • *Depending upon the conditions in which they are used, wood products are required to have been produced with the necessary moisture levels for the intended job. In many cases, this means that drying is required in order to achieve these moisture levels. Wood is also often thermally modified. During the required processing, stresses often occur in wood assortments. If such stresses exceed the limits of durability in the wood, cracks will appear. Similar cracks in wood can occur prior to the drying and/or heat treatment stage. These defects are usually internal and invisible, but they can significantly alter the mechanical properties of the product. This study has shown that wood defects can often be detected using the original method, which involved transverse resonant vibrations, invisible drying, and others. It has been found that a defect of at least 12.5 % of the specimen's overall length will change the mechanical properties of that specimen. When the defect length makes 25 % of the specimen's overall length, or even more, the assortment sometimes behaves as a system of several bodies. In addition, when the defect reaches half the total length of the specimen, the modulus of elasticity may decrease to 20 %, and the coefficient of damping may increase to 80 %.*

KEYWORDS: *wood moisture content; drying defects; resonant frequency; amplitude characteristics; transverse vibrations; modulus of elasticity; coefficient of damping*

SAŽETAK • *Proizvodi od drva u konačnici moraju imati određen sadržaj vode, ovisno o mjestu njihove uporabe. To najčešće znači da je drvo potrebno osušiti kako bi se postigao željeni sadržaj vode u njemu. Drvo je često i toplinski modificirano. Tijekom sušenja u drvnim se sortimentima često pojavljuju naprezanja. Ako ona prelaze razinu graničnih naprezanja drva, nastat će pukotine. Slične pukotine u drvu mogu se pojaviti prije faze sušenja i/ili toplinske obrade. Te se greške obično nalaze unutar drvnog elementa i nevidljive su, ali znatno utječu na mehanička svojstva proizvoda. Ovo je istraživanje pokazalo da se greške drva često mogu otkriti originalnom metodom koja podrazumijeva poprečne rezonantne vibracije, nevidljivo sušenje i druge postupke. Utvrđeno je da će greška drva duga najmanje 12,5 % ukupne duljine uzorka promijeniti mehanička svojstva tog uzorka. Kada duljina greške iznosi 25 % ili više ukupne duljine uzorka, drvni se element u nekim primjerima ponaša kao sustav nekoliko tijela. Osim toga, ako greška drva dosegne polovicu ukupne duljine uzorka, modul elastičnosti može se smanjiti do 20 %, a koeficijent prigušenja porasti do 80 %.*

KLJUČNE RIJEČI: *sadržaj vode u drvu; greške sušenja; rezonantna frekvencija; amplitudna obilježja; poprečne vibracije; modul elastičnosti; koeficijent prigušenja*

[1] Author is associate professor at Kaunas University of Applied Sciences, Faculty of Technology, Kaunas, Lithuania.
[2] Author is student at Kaunas University of Technology, Faculty of Mechanical Engineering and Design, Kaunas, Lithuania.

1 INTRODUCTION
1. UVOD

Depending upon the intended conditions of use of wood products, such products will need to contain a moisture content of between 6-20 %. The moisture content in uncut, living wood, which is part of a growing tree, tends to vary from about 40 % to 90 % or more, depending upon the tree species, the season of the year, and various other factors ('Wood handbook', 2010; Perré *et al.,* 2004). If wood is selected with the wrong moisture content for the job at hand, then later, during its use, the moisture levels will reach a value that corresponds to the environmental conditions. However, during the drying or wetting process, products or parts of those products may change dimensions and shape, possibly losing their aesthetic appearance and functionality, while visible or even invisible cracks or other defects may show up (Dietsch, 2017). In order to be able to avoid such problems, wood, in most cases, must be dried.

In order to reduce drying times and achieve higher economic benefits, wood is subject to a harsher drying regime. It is processed at higher temperatures and in drier air. However, as a result of such a drying process, in most cases a cross-section of dried wood assortments will show considerable levels of humidity difference, which can lead to stress formation (Perré *et al.,* 2004; Karabagli *et al*., 1997). Exceeding the strength limit of wood causes the appearance of cracks and other defects. These defects are often internal and invisible and, therefore, they can often only be noticed following mechanical treatment. Furthermore, they significantly impair the mechanical properties of wood (Oltean *et al.,* 2007).

Thermal modification of wood changes some of its properties (being heated at an even higher temperature, between 160-260 °C), making it resistant to environmental influences (Oltean *et al.,* 2007; Poncsak *et al.,* 2006). Heat treatment results in changes in the chemical composition of wood, as well as in the removal of extractives, etc. Furthermore, in many cases the wood also dries out, creating stresses due to the varying shrinkages of separate zones and temperature differences. Again, exceeding the strength limit of wood causes the appearance of cracks and other defects, often not visible to the naked eye. Therefore, the wood must be treated to an optimised regime during both the drying and thermal modification stages. Furthermore, internal, invisible defects may occur prior to the drying or heat treatment phases.

The process of assessing mechanical properties, along with defect-finding and modelling, uses various acoustic and other non-destructive methods (Poncsak *et al*., 2020; Kamal *et al*., 2017; Perlsaksson, 2018; Hamdi *et al*., 2016). The values in the mechanical properties of wood, as determined by using dynamic methods, tend to correlate well with values obtained by using static methods (Wang *et al.,* 2000; Vobolis *et al.,* 2013; Hossein *et al.,* 2011). The relationship between the dynamic and static modulus of elasticity was found to be about 0.91. However, when a defect occurs, this relationship decreases to 0.51 (Hossein *et al.,* 2011).

The aim of this study was to evaluate the possibility of being able to detect wood defects by applying a transverse resonant vibration method so that it becomes possible to determine the influence of such defects on the mechanical properties of the product.

2 MATERIALS AND METHODS
2. MATERIJALI I METODE

The study involved timber specimens of the birch family (*betula pendula*), with varying dimensions as follows: 400 mm × 50 mm × 20 mm (involving twenty items, and categorised as Group 1); 400 mm × 50 mm × 30 mm (twenty items, Group 2); and 400 mm × 50 mm × 40 mm (twenty items, Group 3). The moisture content in the wood following conditioning varied from 10.7 % to 11.5 %, with density levels of between 590-650 kg/m^3 (moisture content and density values were determined according to the standards LST EN 13183-2:2003 and LST EN 323:1999).

The specimens were weighed on an electronic scale with an accuracy level of 0.01 g, and were measured using callipers (the length with an accuracy of 0.05 mm, and thickness and width with an accuracy of 0.02 mm). Amplitude frequency characteristics fell within the 20-2000 Hz frequency range, being determined using the original methodology and equipment (Albrektas *et al.,* 2003).

A test stand (Figure 1) was used to determine the modulus of elasticity (*MOE*) and the coefficient of damping based on non-destructive testing (employing

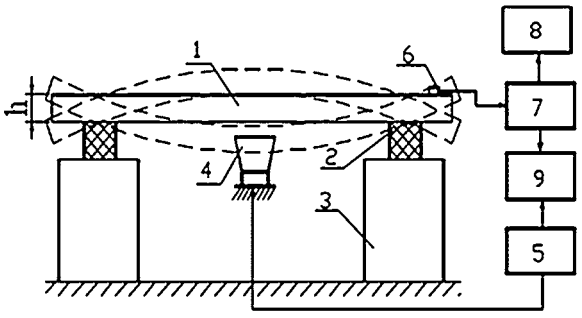

Figure 1 Schematic for test stand: 1 – specimen; 2 – vibration damping material (foam rubber); 3 – solid supports; 4 – loudspeaker; 5 – vibration generator; 6 – sensor; 7 – measuring instrument; 8 – oscilloscope; 9 – phase meter; *h* – thickness of specimen

Slika 1. Shema ispitnog postolja: 1 – uzorak; 2 – materijal za prigušivanje vibracija (pjenasta guma); 3 – čvrsti nosači; 4 – zvučnik; 5 – generator vibracija; 6 – senzor; 7 – mjerni instrument; 8 – osciloskop; 9 – mjerač faza; *h* – debljina uzorka

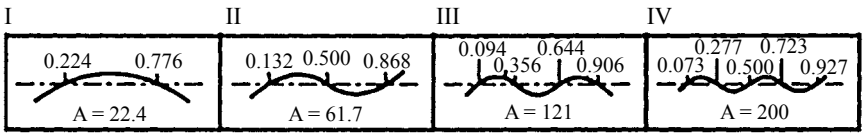

Figure 2 The first four modes of theoretical isotropic beam, when both ends are fixed 'freely.' The curve shows the vibration mode of theoretical isotropic beam (I, II, III, IV, respectively), numerical values show relative distances from the end of theoretical isotropic beam to the point where the vibration amplitude is 0 and 'A' is a coefficient, depending on fastening method of specimen and on vibration mode.

Slika 2. Prva četiri načina vibracije teorijske izotropne grede kada su oba njezina kraja „slobodno" učvršćena. Krivulja predočuje način vibracije teorijske izotropne grede (I, II, III, IV), brojčane vrijednosti pokazuju relativne udaljenosti od kraja teorijske izotropne grede do točke gdje je amplituda vibracije 0, a A označava koeficijent, ovisno o načinu pričvršćenja uzorka i načinu vibracije.

transverse resonant vibrations), which also made it possible to assess the mechanical properties of the specimens (Albrektas *et al.,* 2003; Vobolis *et al*., 2013; Timoshenko *et al*., 1985). The studies were carried out at a frequency of 20-2000 Hz.

A beam-shaped body, which vibrates at a resonance (natural) frequency, depending on its anchorage, curves to a corresponding shape (mode), which, in many cases, is close to the mode of a theoretical isotropic beam. The first four modes of the theoretical isotropic beam - with the beam fixed 'freely' at both ends (as on the stand for the tested specimens) - are presented in Figure 2 (Broch, 1984).

The *MOE* was calculated based on the following Eq. 1 (Timoshenko *et al.,* 1985):

$$E = \frac{f_{rez}^2 \cdot 4 \cdot \pi^2 \cdot \rho \cdot s \cdot l^4}{I \cdot A^2} \quad (1)$$

Where: E is modulus of elasticity; f_{rez} is frequency of transverse vibrations; ρ is density of wood; s is cross-sectional area; l is beam length; I is cross-sectional moment of inertia; and A is e fastening method being used, as represented by a coefficient (Figure 2).

The viscous properties (coefficient of damping) of the specimens being studied were evaluated based on the following Eq. 2:

$$tg\delta \approx \frac{\Delta f}{f_{rez}} \quad (2)$$

Where: f_{rez} is frequency of transverse vibrations; Δf is frequency bandwidth when vibration amplitude decreases by 0.7 times.

After determining the characteristic (first) mode of vibration specimens, the *MOE* and coefficient of damping of wood were both calculated (Timoshenko *et al*., 1985).

Subsequently, the specimens from all three groups were divided into subgroups: Group 1 into Subgroups 1.1 and 1.2; Group 2 into Subgroups 2.1 and 2.2; and Group 3 into 3.1 and 3.2. There were ten samples in each subgroup.

Drying defects were simulated for specimens in subgroups 1.1, 2.1, and 3.1. An incision was made along the specimen (between every 50 mm to 200 mm, over the entire thickness of that specimen (Figure 3).

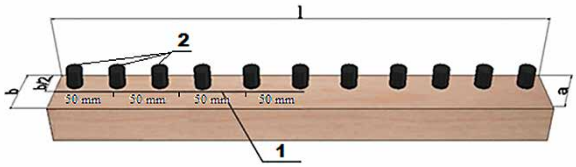

Figure 3 The principle used for forming incisions in the specimen: 1 – incision, gradually increasing every 50 mm to 200 mm; 2 – locations of sensor mounting points, with *a* being the sample thickness, *b* the sample width, and *l* the sample length

Slika 3. Načelo koje se primjenjuje za oblikovanje rezova na uzorku: 1 – rez koji se postupno povećava svakih 50 do 200 mm; 2 – položaj točaka ugradnje senzora, pri čemu je *a* debljina uzorka, *b* širina uzorka, a *l* duljina uzorka

After each incision increase, the amplitude-frequency characteristics of the specimens - the characteristic vibration modes - were determined in the 20-2000 Hz frequency range. In addition, the *MOE* and coefficient of damping were also calculated.

Specimens from subgroups 1.2, 2.2, and 3.2 were soaked in distilled water for about 170 hours and then dried at a temperature of 140 °C for twenty-four hours in order to force the formation of cracks (otherwise known as drying defects) due to excessive drying speed and the resultant stresses. After drying took place, the amplitude-frequency characteristics, characteristic vibration modes, *MOE*, and coefficient of damping of these specimens were also determined (Timoshenko *et al.,* 1985).

3 RESULTS AND DISCUSSION
3. REZULTATI I RASPRAVA

It was found that Group 1 specimens tend to vibrate at two resonant frequencies in the 20-2000 Hz frequency range. Vibrating at each of the frequencies, the specimens deflected in modes that were similar to the first and second modes for the theoretical isotropic beam (Timoshenko *et al.,* 1985). The amplitude-frequency characteristics and vibration modes of one of the specimens are presented in Figure 4.

For other Group 1 specimens, the analogous amplitude-frequency characteristics and similar vibration modes were both obtained.

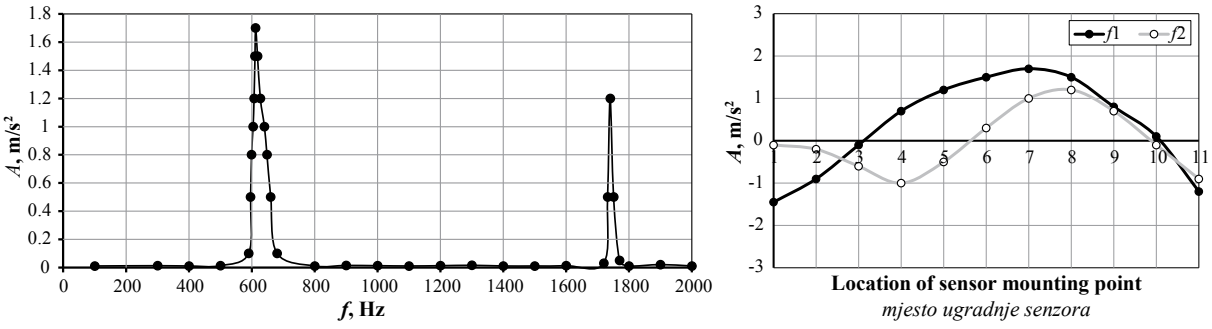

a) b)

Figure 4 a) Amplitude-frequency characteristics, b) vibration modes for one of Group 1 samples close to the first and second modes of theoretical isotropic rod
Slika 4. a) Obilježja amplitude i frekvencije, b) načini vibracija za jedan od uzoraka grupe 1. koji su slični prvome i drugome modu teorijske izotropne šipke

In the case of groups 2 and 3, only one clear resonant frequency was recorded in the aforementioned frequency range. This can be explained by the fact that these specimens were thicker, and that their resonant frequency in the second mode was higher than 2000 Hz. Vibrating at these frequencies, the specimens deflected in modes that were similar to the first mode for the theoretical isotropic beam. The amplitude-frequency characteristics in the 20-2000 Hz frequency range and the vibration modes for one of the specimens in groups 2 and 3 are presented in Figure 5.

Other specimens in the above groups and 20-2000 Hz frequency range 'behaved' analogously. Later, using the theory for the theoretical isotropic beam, the MOE and coefficient of damping were calculated analogously according to the determined resonant frequencies and other parameters for the specimens. The values are presented in Table 1.

Defects were then simulated in specimens from subgroups 1.1, 2.1, and 3.1. The parameters for the specimens - their resonant frequencies and their rating in the 20-2000 Hz frequency range, along with MOE and coefficient of damping - have changed after the incision has been made and increased. The characteristic change in the parameters for one of the samples in Subgroup 1.1 after making and increasing the incision is given in Table 2.

The amplitude-frequency characteristics for the above specimen in the absence of a defect, and when the length of any defect was 200 mm and the length of

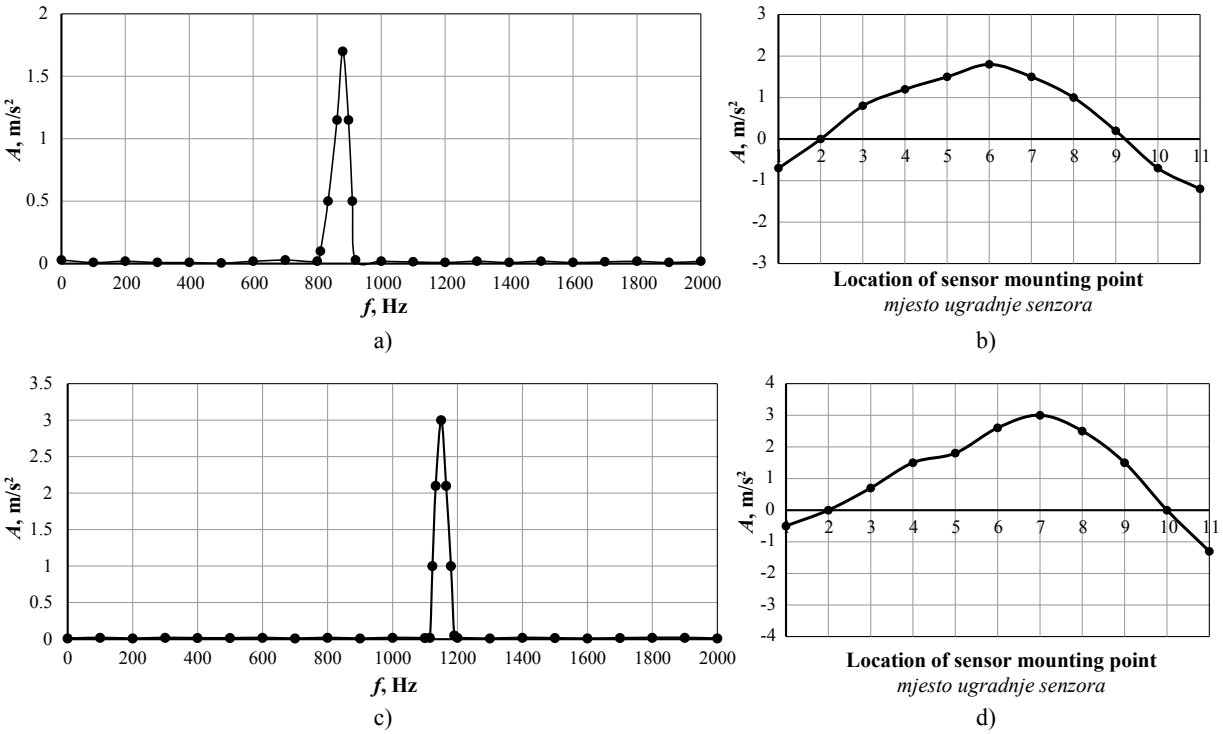

a) b)

c) d)

Figure 5 a) Amplitude-frequency characteristics and b) vibration mode of one of Group 2 samples, c) amplitude-frequency characteristics and d) vibration mode of one of Group 3 samples
Slika 5. a) Obilježja amplitude i frekvencije te b) način vibracije jednoga od uzoraka grupe 2.; c) obilježja amplitude i frekvencije te d) način vibracije jednoga od uzoraka grupe 3.

Table 1 Values for resonant frequencies, *MOE*, and coefficient of damping for each sample
Tablica 1. Vrijednosti rezonantne frekvencije, *MOE* i koeficijenta prigušenja za svaki uzorak

Sample group *Grupa uzoraka*	**Resonant frequency, Hz** *Rezonantna frekvencija,* Hz	**Modulus of elasticity, MPa** *Modul elastičnosti,* MPa	**Coefficient of damping, r.u.** *Koeficijent prigušenja,* r.u.
1	600-670, *1660-1745*	14330-16525	0.017-0.020
2	840-915	11995-15845	0.018-0.021
3	1085-1205	10600 -14475	0.020-0.032

Note: Frequencies at which specimens deflected in a mode close to the second theoretical mode for isotropic beam are given in italics.
Napomena: frekvencije napisane kurzivom jesu frekvencije pri kojima su uzorci skretali u mod sličan drugome teorijskom modu za izotropnu gredu.

Table 2 Variation in resonant frequencies, *MOE*, and coefficient of damping for one of the samples of Subgroup 1.1 with increasing incision length
Tablica 2. Varijacije rezonantnih frekvencija, modula elastičnosti i koeficijenta prigušenja za jedan od uzoraka podskupine 1.1. s povećanjem duljine reza

Length of incision, mm *Duljina reza,* mm	**Resonant frequencies, Hz** *Rezonantna frekvencija,* Hz	**Modulus of elasticity, MPa** *Modul elastičnosti,* MPa	**Coefficient of damping, r.u.** *Koeficijent prigušenja,* r.u.
0	615, 1670	14270	0.020
50	612, 1650	14130	0.021
100	600, 1620	13580	0.024
150	580,1380,1580	12690	0.025
200	571,1290,1566	12300	0.027

any defect in the form of vibration modes was 200 mm, are shown in Figure 6.

As is obvious, in the absence of a defect, the specimen vibrated at two resonant frequencies in the 20-2000 Hz frequency range. When the defect size reached 150 mm, a third resonant frequency appeared. Furthermore, the frequency in the 'first mode' significantly decreased when the incision length reached 150 mm in length. The shape of both the first and second modes became more complex and less similar to the theoretical mode for the isotropic beam as the defect developed (Figure 6, b).

Other specimens 'behaved' analogously during the defect simulation. It has been found that, after making and increasing the incision in the 20-2000 Hz frequency in all the specimens in Subgroup 1.1, the resonance frequency reading increased from two to between three and four, and from one to between two and three for subgroups 2.1 and 3.1. Furthermore, vibration-related modes became more complicated. This can be explained by the fact that the incision destroyed the solid body. The specimen became a more complex system consisting of several bodies when the incision reached a certain size. In most cases, more significant changes in mode were found when the incision length reached 150mm, equal to approximately a third of the entire specimen length. A solid beam-shaped body no longer existed, which means that it did not vibrate in a mode that could be analogous to the isotropic beam (Timoshenko *et al.,* 1985; Albrektas *et al.,* 2003).

According to the theory of vibration in isotropic beams (Timoshenko *et al.,* 1985), when a beam-shaped body vibrates, the amplitude of the vibrations is distributed according to specific patterns (for example, when the body vibrates in the 'first mode', the maximum amplitude is in the middle). This was observed until the incision length reached between 100-150mm. Then it became clear that, in some specimens, the reso-

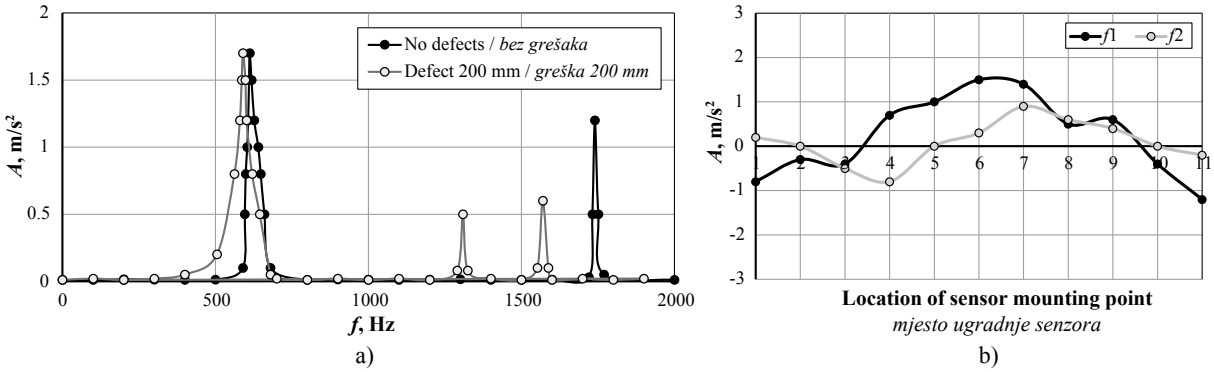

a) b)

Figure 6 (a) Amplitude-frequency characteristics for one of the samples of Subgroup 1.1 with no defect and when the defect length is 200 mm, and (b) in the first and second mode of vibration when the defect length is 200 mm
Slika 6. (a) Obilježja amplitude i frekvencije za jedan od uzoraka podskupine 1.1. bez greške i uz duljinu greške 200 mm te (b) u prvome i drugom načinu vibracija pri duljini greške 200 mm

Table 3 Change of resonant frequencies, *MOE*, and coefficient of damping of specimens after forming a 200 mm incision
Tablica 3. Promjena rezonantnih frekvencija, modula elastičnosti i koeficijenta prigušenja uzoraka nakon formiranja reza od 200 mm

Specimen subgroup *Podskupina uzorka*	**Resonant frequency, Hz** *Rezonantna frekvencija,* Hz		**Modulus of elasticity, MPa** *Modul elastičnosti,* MPa		**Coefficient of damping, r.u.** *Koeficijent prigušenja,* r.u.	
	Without defect *Bez greške*	With defect *S greškom*	Without defect *Bez greške*	With defect *S greškom*	Without defect *Bez greške*	With defect *S greškom*
1.1	600-625 *1660-1745*	560-590 *1535-1570*	14330-16325	12330-14520	0.018-0.020	0.027-0.032
2.1	860-920	790-850	13515-15840	11260-13390	0.019-0.021	0.030-0.037
3.1	1125-1205	1035-1105	12525-14470	12125-10495	0.020-0.024	0.032-0.039

Note: The second (second mode) resonant frequency for samples in Subgroup 1.1 is given in italics.
Napomena: kurzivom je napisana druga rezonantna frekvencija (drugi način vibracija) za uzorke u podskupini 1.1.

nant frequencies of a body vibrating in the same mode and amplitudes differed significantly (by up to 4 %) at different sensor mounting locations (Figure 3) (in the absence of an incision, no such difference was observed). This can be explained by the fact that the specimen has already vibrated, not as a solid body but as a system of several bodies.

Changes in the parameters for the specimens after forming a 200 mm incision are given in Table 3.

The existing incision served to deteriorate the specimen mechanical properties (Oltean *et al.,* 2007; Albrektas *et al.,* 2003). It became apparent that, by making incisions which extended along half of the entire length of the samples, the resonant frequencies for the first

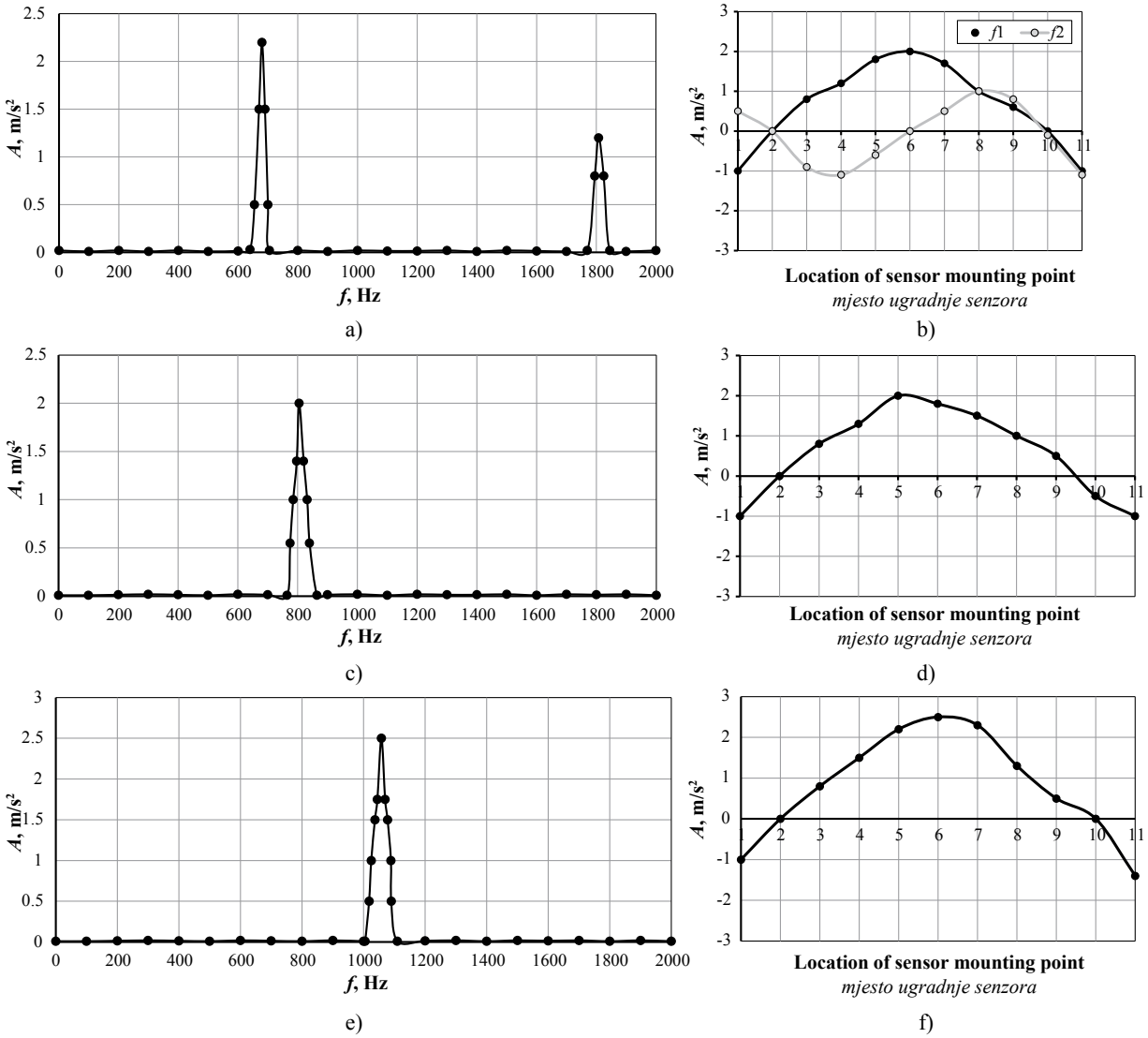

Figure 7 Amplitude-frequency characteristics (a, c, and e, respectively), and vibration modes (b, d, and f, respectively) for representative samples in subgroups 1.2, 2.2, and 3.2
Slika 7. Obilježja amplitude i frekvencije (a, c, e) te načini vibracija (b, d, f) za reprezentativne uzorke u podskupinama 1.2., 2.2. i 3.2.

mode in the thinnest specimens tended to decrease by 6 % on average, and in the medium thickness and the thickest specimens this figure increased to about 8 %. The average *MOE* decreased by 12.5 %, 16.0 %, and 16.2 %, respectively, while the average damping ratio increased by 60 %, 70 %, and 64 %, respectively.

Similarly, specimens in subgroups 1.2, 2.2, and 3.2 were tested in the 20-2000 Hz frequency range. The amplitude-frequency characteristics and vibration modes of a representative specimen of each subgroup are shown in Figure 7.

In the above frequency range, analogous to the specimens in subgroups 1.1, 2.1, and 3.1, two resonant frequencies were observed for the thinnest specimens (these specimens tended to vibrate in the first and second mode in a way similar to that of the theoretical isotropic rod vibration modes). For thicker specimens, one resonant frequency was observed for each specimen, vibrating at a rate at which they deflected in modes that were similar to the first mode for the theoretical isotropic beam. The specimens were then soaked and dried to force high stresses and form significant drying defects (internal cracks). The amplitude-frequency characteristics and vibration modes for the specimens, which were determined following the drying process, are presented in Figure 8.

Specimens from Subgroup 1.2 vibrated at two resonant frequencies in the 20-2000 Hz frequency range prior to forming any drying defects. Following the formation of such defects, the resonant frequencies increased to between three and four. In all specimens from subgroups 2.2 and 3.2, one resonant frequency was observed in each of them prior to the appearance of any defect formation, and in two to three frequencies

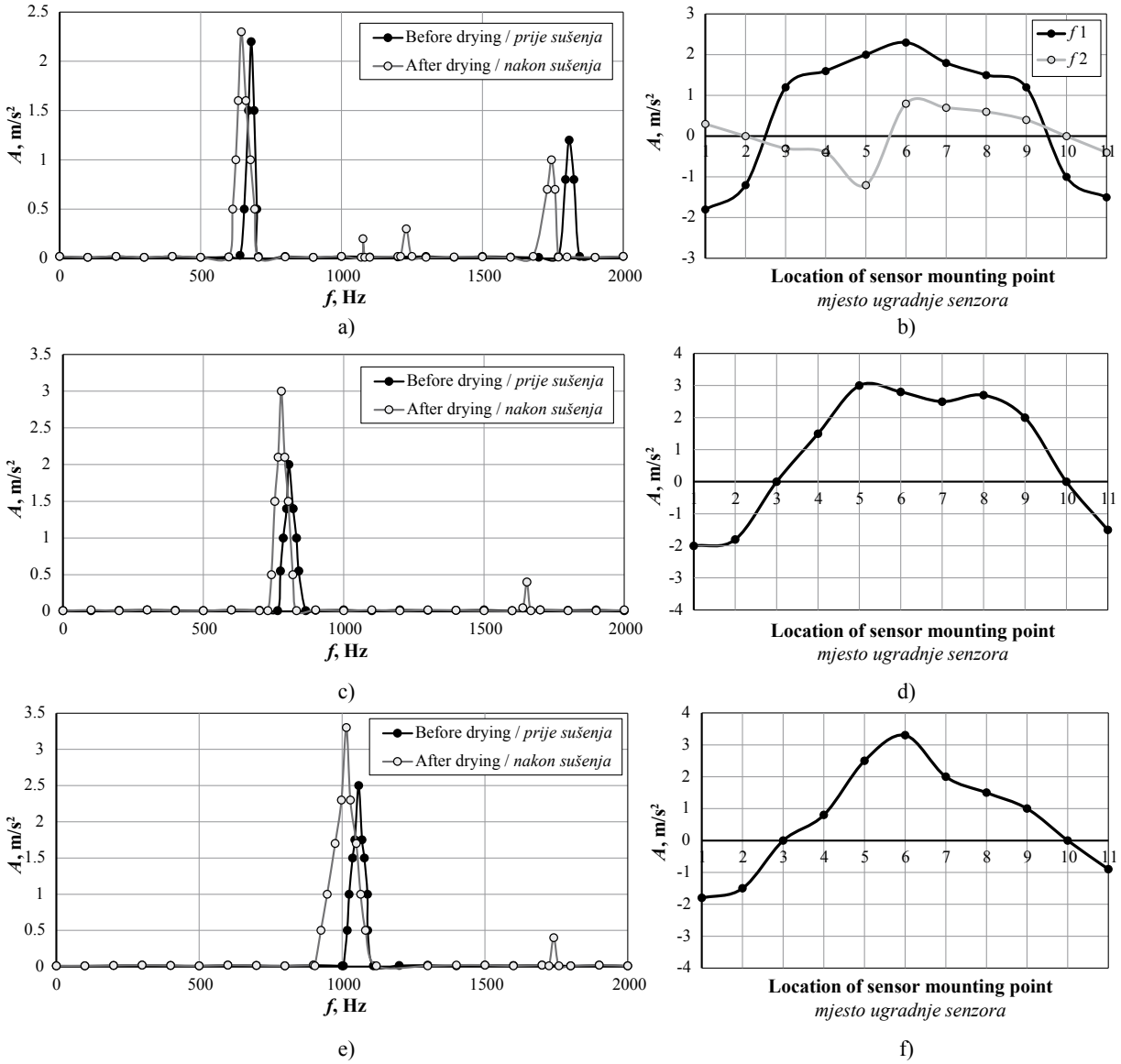

Figure 8 Amplitude-frequency characteristics for representative samples in subgroups 1.2, 2.2, and 3.2 before and after drying (a, c, and e, respectively), and vibration modes after drying (b, d, and f, respectively)
Slika 8. Obilježja amplitude i frekvencije za reprezentativne uzorke u podskupinama 1.2., 2.2. i 3.2. prije i nakon sušenja (a, c, e), te načini vibracija nakon sušenja uzoraka (b, d, f)

Table 4 Change in resonant frequencies, *MOE*, and coefficient of damping of samples following the formation of drying defects
Tablica 4. Promjena rezonantnih frekvencija, modula elastičnosti i koeficijenta prigušenja uzoraka nakon nastanka grešaka sušenja

Specimen subgroup *Podgrupa uzorka*	**Resonant frequency, Hz** *Rezonantna frekvencija,* Hz		**Modulus of elasticity, MPa** *Modul elastičnosti,* MPa		**Coefficient of damping, r.u.** *Koeficijent prigušenja,* r.u.	
	Without defect *Bez greške*	With defect *S greškom*	Without defect *Bez greške*	With defect *S greškom*	Without defect *Bez greške*	With defect *S greškom*
1.2	635-665	605-635	14480-16520	11500-13800	0.017-0.020	0.021-0.025
2.2	840-905	815-900	11990-15440	11075-14530	0.018-0.020	0.023-0.031
3.2	1085-1145	1005-1130	10600-12385	9100-11780	0.021-0.032	0.026-0.036

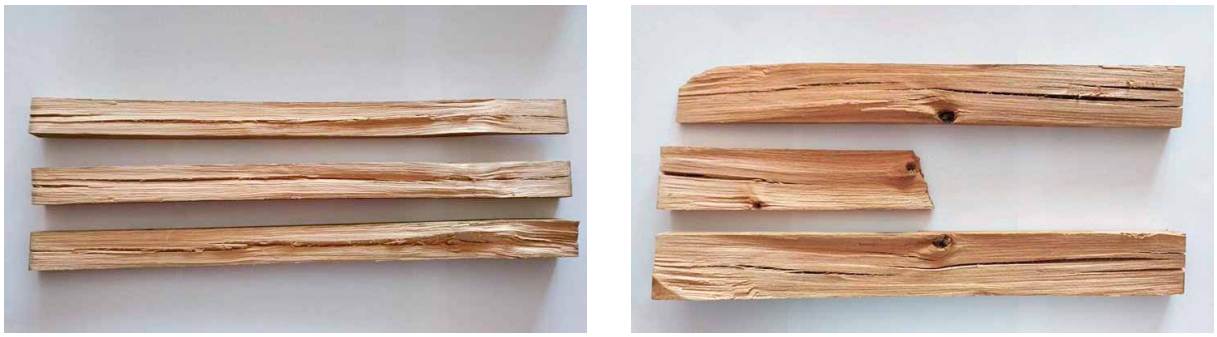

Figure 9 Characteristic defects after extreme drying and/or thermal modification
Slika 9. Karakteristične greške nakon intenzivnog sušenja i/ili toplinske modifikacije

following the appearance of defects. This can be explained by the fact that the specimen became a system of individual bodies, as in the case of an incision.

Changes in the mechanical properties of specimens from the above subgroups due to drying defects are presented in Table 4.

Photographs revealing the characteristic defects formed during the phase of extreme drying are shown in Figure 9.

It was found that there were significant changes in the mechanical properties of the samples with the formation of drying defects, as was also true in the case of making the initial incision. The resonant frequency of the thinnest specimens, when they deflect in a mode similar to that of the first mode for the isotropic beam, tended to decrease by an average of about 4.6 %, with their *MOE* decreasing by an average of 18.4 %, and the coefficient of damping increasing by about 21 %. Accordingly, the average resonant frequency for medium-thickness specimens tended to decrease by about 1.7 %, the *MOE* decreased by an average of 6.7 %, and the coefficient of damping increased by 42 %. The frequency of the thickest specimens decreased by an average of 4.2 %, while the MOE decreased by an average of 9.2 %, and the coefficient of damping increased by 13 %.

All of the data obtained from the tests had to be statistically processed. It was found that the coefficient of variation for the *MOE* values for those specimens in the subgroups that had no defects changed from a reading of 3.87 % to one of 5.30 %, while the coefficient of damping changed from 4.71 % to 6.19 %. After forming a single defect (making an incision) with a length of 200 mm, these values fell within the limits of 4.81-6.00 % and 5.15-6.57 %, respectively. The most significant scatter of values for the mechanical properties could be observed in the sample subgroups where drying defects were observed. The variation coefficient for values in terms of the *MOE* changed within limits that fell between 6.38-9.72 %, while the coefficient of damping changed within the range of 7.99-9.37 %.

The analysis of results obtained shows that the above drying defects had a similar effect on the mechanical properties of the specimens, as did the 200 mm incision. This can be explained by the fact that the defects (cracks) were formed along with the wood fibre and were sufficiently significant. On the other hand, the incision had a more uniform effect on the mechanical properties of all specimens, regardless of their dimensions, fibre arrangement, etc. Drying defects were formed in various ways, with their eventual size and location differing from one other. The higher scattering of mechanical properties obtained following the completion of the drying process is also shown in the statistics. In addition, the smallest scatter of values could be found in subgroups that included the thinnest assortments. This is most likely due to the fact that, as the volume of the specimen decreases, the specimens become less ‘anisotropic’.

4 CONCLUSIONS
4. ZAKLJUČAK

It was found that a defect that amounts to a quarter or more of the entire length of a specimen can significantly change its amplitude-frequency characteristics.

The number of resonant frequencies increases within the same frequency range, while the characteristic (resonant) vibrations decrease. The emerging 'new' frequencies do not correspond to the first, second, or later specimen mode frequencies. The detection of such frequencies is the simplest way to detect a defect in a specimen.

It was found that a defect that amounts to a quarter or more of the entire length of a specimen clearly replaces the first and second modes for the beam-shaped specimen, which, in the absence of any defect, corresponds to the vibration modes for the theoretical isotropic beam. The defect destroys the beam-shaped specimen, as a solid body, breaking it into a multi-mass system. As a result, the vibration modes for such a specimen are no longer similar to the vibration modes for the theoretical isotropic beam, and the resonant frequency may differ more significantly (by up to 4 %) in different specimen areas.

It was also found that a defect that amounts to at least 12.5 % of the entire length of a specimen can reduce the *MOE,* while increasing the coefficient of damping. As the defect increases, the *MOE* decreases even more, while the coefficient of damping increases (when the defect reaches half the entire length of the specimen, the *MOE* may decrease to 20 % of the total, while the coefficient of damping may increase to 80 %).

It was found that, due to wood anisotropy, any drying defects are formed differently in that wood, exhibiting a different effect on the *MOE* and coefficient of damping for the wood. This is indicated by the increased scatter of the values for these parameters in the presence of such defects.

It has been shown that the method used based on transverse resonant vibrations can detect and evaluate invisible drying and other wood defects.

5 REFERENCES
5. LITERATURA

1. Albrektas, D.; Vobolis, J., 2003: Investigation of mechanical parameters and defects of solid wood glued panels. Materials Science, 9 (4): 368-373.
2. Broch, J. T., 1984: Mechanical Vibrations and Shock Measurements. Grostrum. K. Larsen and Son, pp. 370.
3. Dietsch, P., 2017: Effect of reinforcement on shrinkage stresses in timber members. Construction and Building Materials, 150: 903-915. https://doi.org/10.1016/j.conbuildmat.2017.06.033
4. Hamdi, S. E.; Pitt, R. M.; Dubois, F., 2016: Temperature variation effect on crack growth in orthotropic medium: Finite element formulation for the viscoelastic behavior in thermal cracked wood-based materials. International Journal of Solids and Structures, 115-116: 1-13. https://doi.org/10.1016/j.ijsolstr.2016.09.019
5. Hossein, M. A.; Shahverdi, M.; Roogna, M., 2011: The effect of wood knot as a defect on modulus of elasticity (MOE) and damping correlation. Notulae Scientia Biologicae, 3 (3): 145-149. https://doi.org/10.15835/nsb336119
6. Kamal, K.; Qayyum, R.; Mathavan, S.; Zafar, T., 2017: Wood defects classification using laws texture energy measures and supervised learning approach. Advanced Engineering Informatics, 34: 125-135. https://doi.org/10.1016/j.aei.2017.09.007
7. Karabagli, A.; Mougel, E.; Chrusciel, L.; Zoulalian, A., 1997: Study on a low temperature convective wood drier of some operating parameters on drier modelling and on the quality of dried wood. Holz als Roh- und Werkstoff, 55: 221-226.
8. Oltean, L.; Teischinger, A.; Hasmann, Ch., 2007: Influence of temperature on cracking and mechanical properties of wood during wood drying – a review. BioResources, 2 (4): 789-811.
9. Perlsaksson, J. C., 2018: Dynamic crack propagation in wood fibre composites analysed by high speed photography and a dynamic phase field model. International Journal of Solids and Structures, 144-145: 78-85. https://doi.org/10.1016/j.ijsolstr.2018.04.015
10. Perré, P.; Passard, J., 2004: A physical and mechanical model able to predict the stress field in wood over a wide range of drying conditions. Drying Technology, 22 (1-2): 27-44. https://doi.org/10.1081/DRT-120028202
11. Poncsak, S.; Kocaefe, D.; Bouazara, M.; Pichette, A., 2006: Effect of high temperature treatment on the mechanical properties of birch (*Betula papyrifera*). Wood Science and Technology, 40: 647-663. https://doi.org/10.1007/s00226-006-0082-9
12. Timoshenko, S.; Young, D. H.; Weaver, W. jr., 1985: Vibration problems in engineering. Moscow. Mashinostroenie, pp. 472.
13. Vobolis, J.; Albrektas, D., 2013: Resonant vibration-based evaluation of wood drying defects. Journal of Measurements in Engineering, 1 (2): 113-120.
14. Wang, X.; Ross, R. J.; McClellan, M.; Barbour, R. J.; Erickson, J. R.; Forsman, J. W., 2000: Strength and stiffness assessment of standing trees using a non destructive stress wave technique. Madison: U.S. Department of Agriculture.
15. ***Forest Products Laboratory, 2010: Wood handbook – Wood as an engineering material. General Technical Report FPL-GTR-190. Madison, WI: U.S. Department of Agriculture, Forest Service, Forest Products Laboratory, pp. 508.
16. ***Standard LST EN 13183-2:2003 Moisture content of a piece of sawn timber. Part 2: Estimatios by electrical resistance method.
17. ***Standard LST EN 323:1999. Wood-based panels – Determination of density.

Corresponding address:

Assoc. Prof. DARIUS ALBREKTAS, PhD
Kaunas University of Applied Sciences, Faculty of Technology, Pramonės pr. 20, LT – 50468 Kaunas, LITHUANIA, e-mail: Darius.Albrektas@ktu.lt

VLin

Testing laboratory for furniture and playground equipment

accredited testing laboratory for furniture and playground equipment according to HRN EN ISO/IEC 17025

more than 40 methods in the scope of the testing of furniture, coatings and parts for furniture, children's playgrounds and playground equipment

outside the scope of accreditation:

research of constructions and ergonomics of furniture

testing of finishing materials and proceses

testing of flammability and ecology of upholstered furniture

furniture expertise

Laboratory **is a member of the Laboratoria Croatica CROLAB – an association whose goal is the development of Croatian laboratories as an infrastructure for the development of production and the economy within a demanding open market, using common potentials and synergy effects of the association, while the**

Faculty of Forestry and Wood technology **is a full member of the INNOVAWOOD – association whose aim it to contribute to business successes in forestry, wood industry and furniture industry, stressing the increase of competitiveness of the European industry.**

Research of beds and sleeping, research of children's beds, optimal design of tables, chairs and corpus furniture, healthy and comfort sitting at school, office and in home are some of numerous researches performed by the *Institute for furniture and wood in construction*, which enriched the treasury of knowledge on furniture quality.

17025-HAA 1338 TEST

Good cooperation with furniture manufacturers, importers and distributors makes us recognizable

Knowledge is our capital

CROLAB

INNOVAWOOD

University of Zagreb • Faculty of forestry and wood technology
Testing laboratory for furniture and playground equipment
Institute for furniture and wood in construction
Svetošimunska cesta 23
HR-10000 Zagreb, Croatia

Mustafa Burak Arslan[1], Selçuk Küçükaydın[2], Meltem Taş-Küçükaydın[3], Mehmet Emin Duru[3], Halil Turgut Şahin[4]

Composition of Essential Oils in Needles and Barks of Turkish Red Pine (*Pinus brutia* Ten.) Infested by *Marchalina hellenica* Genn.

Sastav eteričnih ulja u iglicama i kori turskoga crvenog bora (*Pinus brutia* Ten.) zaraženoga insektom *Marchalina hellenica* Genn.

ORIGINAL SCIENTIFIC PAPER
Izvorni znanstveni rad
Received – prispjelo: 20. 11. 2020.
Accepted – prihvaćeno: 13. 12. 2021.
UDK: 630*81; 674.032.475.4
https://doi.org/10.5552/drvind.2022.2045

ABSTRACT • *The scale insect Marchalina hellenica Genn. plays a key role in pine honey production and is hosted mainly by Turkish red pine (Pinus brutia Ten.). The needles of Turkish red pine are rich in essential oils. Moreover, essential oils can affect the host selection of insects. The essential oils in the needles and barks of Marchalina hellenica-infested and non-infested Turkish red pine were obtained via water distillation and their composition was determined by GC-MS analyses. The composition of the essential oils was found to differ in the needles of non-infested Turkish red pine and in those of pine infested by Marchalina hellenica. The Mann-Whitney U test results showed that the β-caryophyllene level was higher in the needles of Turkish red pine infested by Marchalina hellenica, whereas the junipen level was higher in the essential oil of non-infested Turkish red pine bark. Pimaral and α-guaiene were detected only in the needles of infested trees, but were absent in the needles of non-infested trees. These components may be markers that can act on their own or as part of the whole in the host tree selection of Marchalina hellenica. In addition, the cis-verbenone component found in Turkish red pine bark might play a role in attracting Marchalina hellenica. This phenomenon should be further investigated through additional studies.*

KEYWORDS: *Marchalina hellenica; Pinus brutia; essential oils; GC-MS; needles; bark*

SAŽETAK • *Ljuskavica Marchalina hellenica Genn. ima ključnu ulogu u proizvodnji meda od borovine, a uglavnom živi na turskome crvenom boru (Pinus brutia Ten.). Iglice tog bora bogate su eteričnim uljima. Štoviše, eterična ulja za insekte mogu biti presudna pri odabiru domaćina na kojemu će se nastaniti. Eterična ulja iz iglica turskoga crvenog bora zaraženoga i nezaraženoga ljuskavicom Marchalina hellenica dobivena su vodenom destilacijom, a njihov je sastav određen GC-MS analizama. Utvrđeno je da je sastav eteričnih ulja u iglicama ne-*

[1] Author is researcher at General Directorate of Forestry, Ege Forestry Research Institute, İzmir, Turkey.
[2] Author is researcher at Department of Medical Services and Techniques, Köyceğiz Vocational School of Health Services, Muğla Sıtkı Koçman University, Muğla, Turkey.
[3] Author is researcher at Department of Chemistry, Faculty of Sciences, Muğla Sıtkı Koçman University, Muğla, Turkey.
[4] Author is researcher at Department of Forest Products Engineering, Faculty of Forestry, Isparta University of Applied Sciences, Isparta, Turkey.

zaraženoga turskoga crvenog bora i u iglicama bora zaraženoga s Marchalina hellenica različit. Rezultati Mann-Whitneyjeva U-testa pokazali su da je razina β-kariofilena veća u iglicama crvenoga turskog bora zaraženoga s Marchalina hellenica, dok je razina kleke viša u eteričnom ulju nezaražene kore turskoga crvenog bora. Pimaral i α-guaiene otkriveni su samo u zaraženim iglicama stabala, ali ih nije bilo u iglicama nezaraženih borova. Te komponente mogu biti markeri koji pri selekciji stabla domaćina Marchaline hellenice mogu djelovati sami ili kao dio cjeline. Osim toga, komponenta cis-verbenon, pronađena u kori turskoga crvenog bora, mogla bi imati važnu ulogu u privlačenju Marchaline hellenice. Tu je pojavu potrebno detaljnije istražiti u dodatnim studijama.

KLJUČNE RIJEČI: *Marchalina hellenica; Pinus brutia; eterična ulja; GC-MS; iglice; kora*

1 INTRODUCTION
1. UVOD

The majority of the world's pine honey production takes place in Turkey. However, the essence of pine honey is created by *Marchalina hellenica* Genn (*M. hellenica*), which is mainly hosted by Turkish red pine (*Pinus brutia* Ten.). The scale insect *M. hellenica* lives in the cracks under the scales of bark. After sucking the sap of the host tree and receiving the nutrients it requires, the insect secretes the remainder rectally. This secretion, called *honeydew*, is then collected by bees and converted into pine honey, the worldwide production of which is only carried out in Turkey and Greece (Besçeli and Ekici, 1968; Santas, 1983; Gürkan and Boşgelmez, 1989; Thrasyvoulou and Manikis, 1996; Gösterit and Gürel, 2011).

M. hellenica is distributed on the mainland and throughout some islands of Turkey and Greece as well as on the Italian island of Ischia. Although the widest distribution area of *M. hellenica* in Turkey is found in the Muğla region, it is also spread along the Aegean coast. *M. hellenica* selects *Pinus brutia* in particular in Turkey, and both *Pinus halapensis* and *Pinus brutia* in Greece. However, it has previously been reported that it can infest *Pinus pinea, Pinus nigra, Pinus sylvestris,* and *Pinus pinaster*. Moreover, suggestions that *M. hellenica* is also hosted by *Cedrus libani* in Turkey and by *Abies cephalonica* in Greece have been proposed (Besçeli and Ekici, 1968; Selmi, 1983; Margaritopoulos *et al.,* 2003; Bacandritsos, 2004; Gounari, 2006; Ülgentürk *et al.,* 2012). According to the Food and Agriculture Organization (FAO) report AUS-69/1 dated 13.07.2015, *M. hellenica* has begun to appear in *Pinus radiata* and *Pinus halapensis* in Australia as well (Anonymous, 2017).

Furthermore, there is disagreement over the instar periods of *M. hellenica* in Greece. Although Erlinghagen (2001) and Bacandritsos *et al.* (2004) reported two instar periods, Gounari (2006; 2008) suggested three instar periods. Nevertheless, it is generally agreed that *M. hellenica* exhibits three instar periods in Turkey (Gürkan and Boşgelmez, 1989; Ülgentürk *et al.* 2012).

Coniferous trees and their parts contain rich extractives. Sahin and Yalcin (2017) determined the most common essential oil components in coniferous tree needles and a wide range of studies have been carried out on the determination of essential oil components in various parts of *Pinus brutia,* including the needles (Roussis *et al.,* 1995; Sezik *et al.,* 2008; Mateus, 2008; Koutsaviti *et al.,* 2014; Yener *et al.,* 2014), bark (Salman, 2009; Bagci *et al.,* 2011), cones (Loizzo *et al.,* 2008; Tumen *et al.,* 2010), and twigs (Ghosn *et al.,* 2006; Ustun *et al.,* 2012).

In coniferous trees, essential oils and some other extractives may be effective in the selection of host trees by insects. It was reported that some of the extractive components in coniferous trees might have attractive or deterrent effects on insects (Metcalf and Kogan, 1987; Jactel *et al.,* 1996; Franceschi *et al.,* 2005; Erbilgin *et al.,* 2006; Keeling and Bohlmann, 2006).

However, very limited research has been conducted on the interaction of *M. hellenica* with the extractive content of host trees. The terpene composition of the oleoresin (Mita *et al.,* 2002) and needles (Gallis *et al.,* 2011) of Aleppo pine infested by *M. hellenica* and the needles (Topcan, 2017) of Turkish red pine hosting *M. hellenica* have been investigated.

Although a few studies have been conducted to determine the interaction of *M. hellenica* with some tree species, a better understanding of specific tree chemical properties under controlled conditions was clearly needed. Consequently, the essential oil composition of Turkish red pine needles and bark from selected regions was evaluated against *M. hellenica* infections. After collecting samples, the level of essential oil compounds was determined based on the degree of changes. By performing the sample collection process in different areas and seasons and using the bark as a material as well as the needle, this study provides an additional new dimension compared to previous studies. The essential oil compounds of the needles and bark of *M. hellenica*-infested and uninfested Turkish red pine were examined. The results found in this study were evaluated in terms of the use of these components as a mark of host tree selection for *M. hellenica*.

2 MATERIALS AND METHODS
2. MATERIJALI I METODE

The Turkish red pine needle and bark samples from trees infested by *M. hellenica* and from non-infested trees were collected in three different seasons from

Table 1 Needle sample collection areas and periods
Tablica 1. Područja i razdoblja prikupljanja uzoraka iglica

Area/Season *Područje/Sezona*	**First (Season 1)** *1. sezona*	**Second (Season 2)** *2. sezona*	**Third (Season 3)** *3. sezona*
Area 1 (A1): Ula – Muğla	July 2016	October 2016	February 2017
Area 2 (A2): Yerkesik – Muğla	July 2016	October 2016	February 2017
Area 3 (A3): Gökova – Muğla	July 2016	November 2016	January 2017

three different trial areas consisting of natural stands in Muğla Province. Table 1 presents the collection areas and seasons. The coexistence of Turkish red pine trees hosting and not hosting *M. hellenica* was considered as the criterion in the selection of the study area. In total, twenty trees were selected in each trial area, ten of which were infested with *M. hellenica* and ten were not infested. Needle and bark samples were taken from the same trees in all three seasons. Samples from *M. hellenica*-infested trees were mixed together homogeneously. The same procedure was applied to samples from non-infested trees.

To obtain the essential oils of the needles and barks, 350 g samples were subjected to hydro distillation for 3 h using a Clevenger-type apparatus. The essential oils were kept in the refrigerator at -18 °C until gas chromatography-mass spectrometry (GC-MS) analysis. The Varian 2100 GC-MS system was used to characterize the essential oil components of the samples. The NIST 2008 library data and the "Eight Peak Index of Mass Spectra", "Monoterpenes", and "Identification of Essential Oils by Ion Trap Mass Spectroscopy" spectrophotometer atlases were used to identify the components. In addition, characterization was supported by taking into account the retention times of the components and calculating the Kovats index values. Standard substances were also characterized in the column under the same conditions and their retention times and essential oil components were compared. The GC-MS analysis conditions for the experimental procedure were as follows:

- Carrier gas: Helium
- Injection temperature: 250 °C
- Column temperature: The oven temperature was held at 60 °C for 5 min, and then increased up to 280 °C in increments of 4 °C/min and held at this temperature for 15 min.
- Split ratio: 1:50
- Ion source temperature: 150 °C
- Ionization energy: 70 eV
- Mass range: 28 - 650 m/z
- Injection volume: 0.2 µL
- Column properties: DB-1 nonpolar capillary column (Agilent), length: 30 m, inner diameter: 0.25 mm, film thickness: 0.25 µm

The evaluation of the normal distribution status of the dataset was performed using the Shapiro-Wilk test. The non-parametric Mann-Whitney U test was used to determine whether the two groups (infested by *M. hellenica* and non-infested) differed from each other.

3 RESULTS AND DISCUSSION
3. REZULTATI I RASPRAVA

3.1 Chemical composition of essential oils in pine needles
3.1. Kemijski sastav eteričnih ulja u borovim iglicama

As shown in Table 4 (Supplement), the presence of 51 and 63 components, respectively, were revealed in the needles of *M. hellenica*-infested and non-infested Turkish red pine in Area 1. The main components of the essential oils of infested and non-infested tree needles were detected as α-pinen, β-pinen, β-caryophyllene, germacrene D, cembrene, and thunbergol. In all three seasons, the β-caryophyllene ratio of the infested tree needles (12.84, 13.15, and 15.55 %) was higher than in the non-infested tree needles (11.29, 8.24, and 12.89 %); however, the α-pinen and β-pinen ratios differed. Pimaral and α-guaiene were identified only in the infested tree needles and these were in low amounts. The existence of 34 and 37 components, respectively, appeared in the infested and non-infested Turkish red pine needles in Area 2 (Table 5, Supplement). The main components of the essential oil composition of the infested and non-infested tree needles in A2 were similar to those in A1. Cembrene and thunbergol were not determined as major components in A2. A contrasting situation was seen in the ratios of α-pinen and β-pinen. Pimaral and α-guaiene were found only in the needles of infested trees, as was the case in A1.

The 32 and 30 components, respectively, identified in infested and non-infested Turkish red pine needles in Area 3, are shown in Table 6 (Supplement). The major components of the essential oils of infested and non-infested tree needles were detected as α-pinene, β-pinene, β-caryophyllene, and germacrene D, as was the case in A2. A comparison of the infested and non-infested tree needles revealed that the rate of β-caryophyllene was higher in the infested tree needles, whereas the ratios of α-pinene and β-pinene were higher in the non-infested tree needles. The seasonal β-caryophyllene ratios were determined to be 16.22, 20.61, and 14.54 % in the infested tree needles and 7.68, 9.98, and 11.05 % in the non-infested tree needles, respectively. Pimaral appeared only in the needles of infested trees, as observed in A1 and A2.

The rate of β-caryophyllene was higher in infested tree needles in all three seasons and all three trial

areas, except for the second season of A2 (Figure 1). However, no such relation was observed between the *α*-pinene and *β*-pinene ratios or the infested and non-infested tree needles. Therefore, according to the results of the Mann-Whitney U test (Table 2), only the *β*-caryophyllene ratio was found higher in infested trees at $\alpha = 0.05$ ($p = 0.038$). Although the germacrene D ratio showed a tendency similar to that of *β*-caryophyllene, there was statistically no correlation between it and the infested tree needles. Moreover, no significant difference was found among the other components. In all trial areas, pimaral was identified only in the needles of infested trees (Figure 2), whereas *α*-guaiene was detected in the needles of infested trees only in A1 and A2 , but was not found in either infested or non-infested tree needles in the A3 trial region (Figure 3). The findings of the pimaral and α-guaiene were seen as remarkable.

Gallis *et al.* (2011) reported that, when *β*-caryophyllene, *α*-humulene, and neoabietol ratios were higher in the needles of Aleppo pine infested with *M. hellenica*, the ratio of the cembrene was higher in non-infested trees. Kleinhentz *et al.* (1999) indicated that the *β*-caryophyllene ratio was higher in the needles of maritime pine infested by *Dioryctria sylvestrella* Ratz.

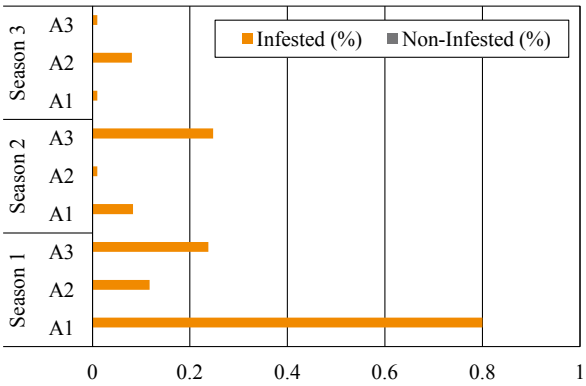

Figure 2 Pimaral levels in needles of *M. hellenica*-infested and non-infested Turkish red pine
Slika 2. Razine pimarala u iglicama turskoga crvenog bora zaraženoga s *M. hellenica* i u iglicama nezaraženoga turskog crvenog bora

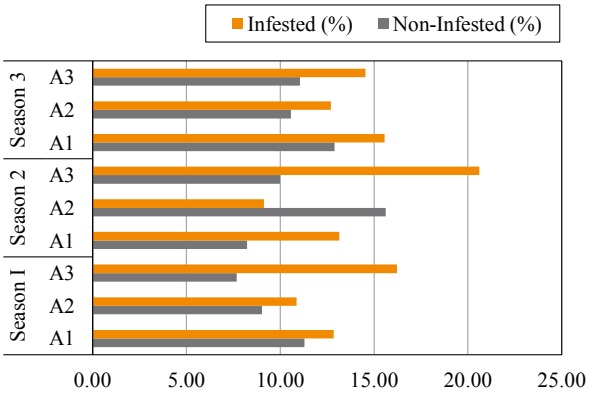

Figure 1 β-caryophyllene levels in needles of *M. hellenica*-infested and non-infested Turkish red pine
Slika 1. Razine β-kariofilena u iglicama turskoga crvenog bora zaraženoga insektom *M. hellenica* i u iglicama nezaraženoga turskog crvenog bora

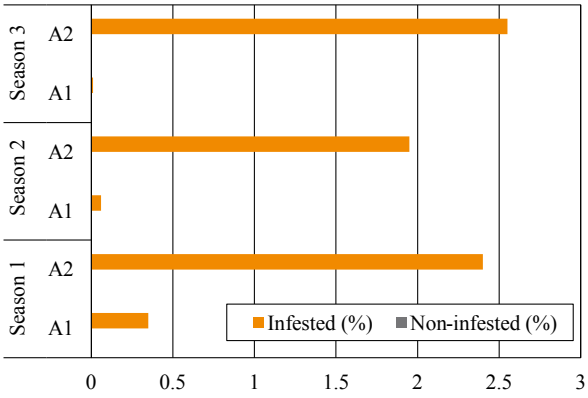

Figure 3 α-guaiene levels in needles of *M. hellenica*-infested and non-infested Turkish red pine
Slika 3. Razine α-guaiene u iglicama turskoga crvenog bora zaraženoga s *M. hellenica* i u iglicama nezaraženoga turskog crvenog bora

Table 2 Results of Mann-Whitney U test of essential oil components of needles from *M. hellenica*-infested and non-infested trees
Tablica 2. Rezultati Mann-Whitneyjeva U-testa komponenata eteričnog ulja iglica s borova zaraženih i nezaraženih insektom *M. hellenica*

Component *Komponenta*	**Mann-Whitney U**	**Z**	**Asymp. Sig. (2-tailed)**	**Mean ranks** *Prosječni rankovi*		**Sample number** *Broj uzorka*	
				Non-Infested *Nezaražen*	**Infested** *Zaražen*	**Non-Infested** *Nezaražen*	**Infested** *Zaražen*
α-Pinene	26.000	-1.281	.200	11.11	7.89	9	9
β-Pinene	29.000	-1.015	.310	10.78	8.22	9	9
α-Terpineol	23.000	-1.545	.122	11.44	7.56	9	9
***β*-Caryophyllene**	**17.000**	**-2.075**	**.038***	**6.89**	**12.11**	**9**	**9**
Germacrane D	22.000	-1.634	.102	7.44	11.56	9	9
δ-Cadinene	40.000	-.044	.965	9.44	9.56	9	9
Cembrene	36.500	-.353	.724	9.06	9.94	9	9
Thunbergol	36.000	-.397	.691	9.00	10.00	9	9

*significant for $\alpha = 0.05$ / *značajno za* $\alpha = 0{,}05$

In our study, the *β*-caryophyllene level was found to be statistically higher in the needles of Turkish red pine infested by *M. hellenica*. However, no correlation was found between *M. hellenica* and cembren.

Mita *et al.* (2002) reported that the sensitivity of Aleppo pine to attack by *M. hellenica* was significantly correlated with a high ratio of *α*-pinene and low ratios of limonene and *α*- terpinyl acetate. Topcan (2017) demonstrated that the amount of *α*-pinene decreased in the needles of Turkish red pine infested by *M. hellenica* during times of their intense feeding. In our research, although **α**-pinene was a major component in the needles of infested and non-infested trees, statistically, no correlation was found between the *α*-pinene level in the needles of Turkish red pine and *M. hellenica.*

Sakai and Yamasaki (1990) demonstrated that the pimaral isolated from *Pinus densiflora* and *Pinus tunbergii* exhibited an attractive effect for *Monochamus alternatus* females. In our work, pimaral was detected only in the needles of Turkish red pine infested by *M. hellenica,* despite being quantitatively low. Likewise, **α**-guaiene was determined only in the needles of Turkish red pine infested by *M. hellenica*. No previous studies were found correlating *α*-guaiene with *M. hellenica* or other insects. Therefore, this finding is of great importance as it is being presented to the literature for the first time. The similarities and differences appeared when our results on the needles were compared to the literature findings.

3.2 Chemical composition of essential oils in pine bark
3.2. Kemijski sastav eteričnih ulja u borovoj kori

The presence of 40 and 44 components, respectively, were determined in the bark of infested and non-infested Turkish red pine trees in the Area 1 trial region (Table 7, Supplement). The major components of the infested and non-infested tree bark were *α*-terpineol, *β*-caryophyllene, borneol, myrtenol, junipen, *cis*-myrtanol, and caryophyllene oxide. The junipen and caryophyllene oxide ratios in the bark of infested trees were revealed as 9.85, 15.11, 16.22, 4.01, 4.64, and 8.17 %, respectively, whereas the ratio of these components in the bark of non-infested trees were found as 6.44, 7.42, 7.13, 1.92, 2.66, and 2.22 %, respectively. For all three seasons, *cis*-verbenone was detected only in the bark of infested trees (25.65, 4.65, and 3.79 %), but was absent in the bark of non-infested trees.

A total of 39 components appeared in both infested and non-infested Turkish red pine bark in the Area 2 trial region. These components are shown in Table 8 (Supplement). As with the A1 trial region, for all three seasons, although *cis*-verbenone was only seen in the bark of infested trees (2.75, 3.13, and 1.24 %), it was not found in the bark of non-infested trees. Like in the A1 trial region, in the A2 trial region, the main components of infested and non-infested tree bark were *α*-terpineol, junipen, *β*-caryophyllene, myrtenol, caryophyllene oxide, borneol, and *cis*-myrtanol.

The existence of 34 and 37 components, as listed in Table 9 (Supplement), were revealed in the bark of infested and non-infested Turkish red pine in the A3 trial region. The main components in the essential oils of the infested and non-infested tree bark were identified as α-terpineol, junipen, *β*-caryophyllene, caryophyllene oxide, and borneol, as in the A1 and A2 trial regions. Unlike the other two trial areas, although *cis*-verbenone was determined in the bark of both infested and non-infested trees, it was found to be higher in the bark of infested trees for all three seasons. According to the seasons, *cis*-verbenone ratios were determined as 1.51, 3.44, and 2.64 % in the bark of infested trees and

Table 3 Results of Mann-Whitney U test of essential oil components of *M. hellenica*-infested and non-infested barks
Tablica 3. Rezultati Mann-Whitneyjeva U-testa komponenata eteričnog ulja kore zaražene s *M. hellenica* i nezaražene borove kore

Component *Komponenta*	**Mann-Whitney U**	**Z**	**Asymp. Sig. (2-tailed)**	**Mean ranks** *Prosječni rankovi*		**Sample number** *Broj uzorka*	
				Non-Infested *Nezaražen*	**Infested** *Zaražen*	**Non-Infested** *Nezaražen*	**Infested** *Zaražen*
Fenchol	26.000	-1.280	.200	11.11	7.89	9	9
trans-pinocarveol	34.000	-.574	.566	8.78	10.22	9	9
Borneol	32.000	-.751	.200	10.44	8.56	9	9
Myrtenol	26.000	-1.280	.200	7.89	11.11	9	9
cis-myrtanol	34.000	-.574	.566	10.22	8.78	9	9
Junipen	**20.000**	**-1.810**	**.070***	**11.78**	**7.22**	**9**	**9**
β-Caryophyllene	28.000	-1.104	.270	10.89	8.11	9	9
α-Caryophyllene	36.000	-.397	.691	10.00	9.00	9	9
Caryophyllene oxide	39.000	-.132	.895	9.67	9.33	9	9
Isoaromadendrene oxide	36.000	-.397	.691	9.00	10.00	9	9
Aaromadendrene oxide	27.000	-1.192	.233	8.00	11.00	9	9

*significant for α = 0.05 / *značajno za α* = 0,05

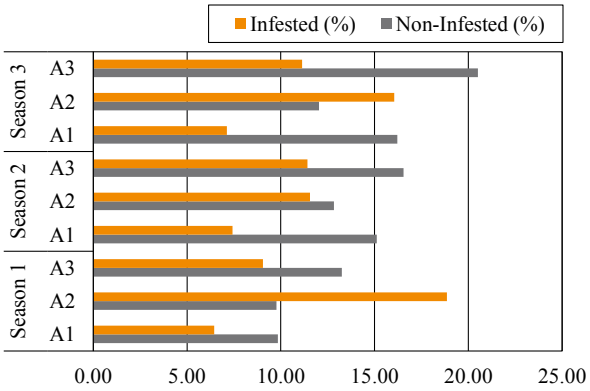

Figure 4 Junipen levels in barks of *M. hellenica*-infested and non-infested Turkish red pine
Slika 4. Razine kleke u iglicama turskoga crvenog bora zaraženoga s *M. hellenica* i u iglicama nezaraženoga turskog crvenog bora

1.04, 1.75, and 1.05 % in the bark of non-infested trees, respectively.

According to the results of the Mann-Whitney U test (Table 3), the junipen ratio was higher in the bark of non-infested trees at $\alpha = 0.10$ ($p = 0.07$). No significant difference was observed in the other components. Figure 4 presents the junipen levels of the infested and non-infested tree bark. Although the *cis*-verbenone was identified only in the bark of infested trees in the A1 and A2 trial regions, it was detected in the bark of both infested and non-infested trees in the A3 trial region, but was quantitatively higher in the bark of infested trees. The *cis*-verbenone ratios of the infested and non-infested tree bark are presented in Figure 5.

Verbenon is one of the components used in creating pheromone traps (Rudinsky, 1973; Bedard *et al.*, 1980). In our study, although *cis*-verbenone was determined only in the bark of Turkish red pine infested by *M. hellenica* in the A1 and A2 trial regions, it was found in the bark of both infested and non-infested trees in the A3 trial region, but at a higher level in the infested bark. When the data obtained from our research and the findings in the related literature were evaluated together, it was concluded that the *cis*-verbenone component in Turkish red pine bark might have an effect that attracts *M. hellenica*.

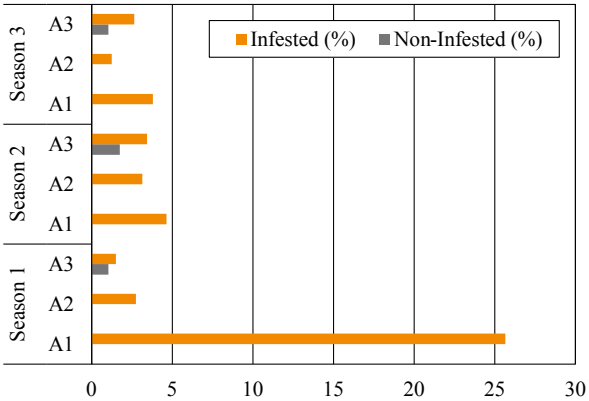

Figure 5 *Cis*-verbenon levels in barks of *M. hellenica*-infested and non-infested Turkish red pine
Slika 5. Razine *Cis*-verbenona u iglicama turskoga crvenog bora zaraženoga s *M. hellenica* i u iglicama nezaraženoga turskog crvenog bora

Kleinhentz *et al.* (1999) reported that the junipen ratio was higher in the liber and resin of maritime pine not infested by *Dioryctria sylvestrella* Ratz. In addition, Kovalcuk *et al.* (2015) stated that the junipen rate was higher in the bark of Scots pine not infested by *Hylobius abietis* L. In our study, the junipen level was determined to be statistically higher in the bark of Turkish red pine not infested by *M. hellenica*. The results for junipen obtained in our study were compatible with the literature findings.

4 CONCLUSIONS
4. ZAKLJUČAK

Essential oils can play a key role in the selection of host trees by insects. Therefore, the GC-MS analyses of the essential oils are of great importance. The GC-MS results of this study indicated that the essential oil composition of non-infested Turkish red pine trees and of those infested by *M. hellenica* were different. This could suggest that the *cis*-verbenone in Turkish red pine bark might exhibit an attractive effect for *M. hellenica*. The *β*-caryophyllene, junipen, *cis*-verbenone, pimaral, and *α*-guaiene determined via GC-MS analyses may be markers that can act on their own or as a part of the whole in the host tree selection of *M. hellenica*. However, in order to verify our claim, additional studies are needed, both in *M. hellenica*-infested forests and under laboratory conditions. Our findings have created an important basis for future studies focusing on the selection of host trees of *M. hellenica* and including olfactometer and orientation tests.

Acknowledgements – Zahvala

This study was supported by the Republic of Turkey General Directorate of Forestry (Project Number 15.7801). The authors would like to thank Forest Subdistrict Directors Mr. Mehmet Akbıyıkoğlu and Mr. Saner Demirtaş for their contribution in determining trial areas and collecting samples.

5 REFERENCES
5. LITERATURA

1. Bacandritsos, N., 2004: Establishment and honeydew honey production of *Marchalina hellenica* (Coccoidea Margarodidae) on fir tree (*Abies cephalonica*). Bulletin of Insectology, 57 (2): 127-130.
2. Bacandritsos, N.; Saitanis, C.; Papanastasiou, I., 2004: Morphology and life cycle of *Marchalina hellenica* (Gennadius) (Hemiptera: Margarodidae) on pine (Parnis Mt.) and fir (Helmos Mt.) forests of Greece. Annals Soci-

ete Entomologique France, 40: 169-176. https://doi.org/10.1080/00379271.2004.10697413
3. Bagci, E.; Hayta, S.; Dogan, G., 2011: Chemical composition of essential oils from bark and leaves of *Pinus brutia* Ten. from Turkey. Asian Journal of Chemistry, 23 (6): 2782-2784.
4. Bedard, W. D.; Tilden, P. E.; Lindahl, K. Q. Jr.; Wood, D. L.; Rauch, P. A., 1980: Effects of verbenone and *trans*-verbenol on the response of *Dendroctonus brevicomis* to natural and synthetic attractant in the field. Journal of Chemical Ecology, 6: 997-1013. https://doi.org/10.1007/BF00994657
5. Beşçeli, Ö.; Ekici, M., 1968: Çam pamuklu biti (*Monophlebus hellenicus* Genn) ve arıcılık. Journal of the Turkish Forest Research Institute, 14 (1): 73-78.
6. Erbilgin N.; Christiansen, E.; Krokene, P.; Zeneli, G.; Gershenzon, J., 2006: Exogenous application of methyl jasmonate elicits defenses in Norway spruce (*Picea abies*) and reduces host colonization by the bark beetle Ips typographus. Oecologia, 148: 426-436. https://doi.org/10.1007/s00442-006-0394-3
7. Erlinghagen, F., 2001: Portrait of an insect: *Marchalina hellenica* Genn. (Sternorrhyncha: Coccina: Margarodidae), important producer of honeydew in Greece. Apiacta, 36 (3): 131-137.
8. Franceschi, V. R.; Krokene, P.; Christiansen, E.; Krekling, T., 2005: Anatomical and chemical defenses of conifer bark against bark beetles and other pests. New Phytologist, 167: 353-376. https://doi.org/10.1111/j.1469-8137.2005.01436.x
9. Gallis, A.; Carlos, A.; Papageorgiou, A. C.; Garcia Vallejo, M. C., 2011: Needle terpenoid composition of *Pinus halepensis* (Mill.) trees infested by the scale insect *Marchalina hellenica* (Genn.) in Greece. In: Proceedings of the Fourth İnternational Workshop on the Genetics of Host-Parasite Interactions in Forestry: Disease and Insect Resistance in Forest Trees, Oregon, pp. 304-308.
10. Ghosn, M. W.; Saliba, N. A.; Talhouk, S. Y., 2006: Chemical composition of the needle-twig oils of *Pinus brutia* Ten. Journal of Essential Oil Research, 18: 445-447. https://doi.org/10.1080/10412905.2006.9699137
11. Gounari, S., 2006: Studies on the phenology of *Marchalina hellenica* (Gen.) (Hemiptera: Coccoidea, Margarodidae) in relation to honeydew flow. Journal of Apicultural Research, 45 (1): 8-12. https://doi.org/10.1080/00218839.2006.11101305
12. Gounari, S., 2008: Aspects on biology of *Marchalina hellenica* (Coccoidea, Marchalinidae). In: Proceedings of First International Mugla Beekeeping Pine Honey Congress, Muğla, Turkey, pp. 133-140.
13. Gösterit, A.; Gürel, F., 2011: Orman-arıcılık ilişkisi ve arıcılığın orman köylüleri ve kırsal kesimin kalkınmasındaki önemi. Orman ve Av Dergisi, 2: 26-29.
14. Gürkan, B.; Boşgelmez, A., 1989: Çam pamuklu koşnili *Marchalina hellenica* (Gennadius)'ın biyo-ekolojisi ve populasyon dinamiği. PhD Thesis, Hacettepe University, Ankara, Turkey.
15. Jactel, H.; Kleinhentz, M.; Marpeau-Bezard, A.; Marion-Poll, F.; Menassieu, P.; Burban, C., 1996: Terpene variations in maritime pine constitutive oleoresin related to host tree selection by *Dioryctria sylvestrella* Ratz. (Lepidoptera: Pyralidae). Journal of Chemical Ecology, 22 (5): 1037-1050. https://doi.org/10.1007/BF02029953
16. Keeling, C. I.; Bohlmann, J., 2006: Genes, enzymes and chemicals of terpenoid diversity in the constitutive and induced defence of conifers against insects and pathogens. New Phytologist, 170: 657-675. https://doi.org/10.1111/j.1469-8137.2006.01716.x
17. Kleinhentz, M.; Jactel, H.; Menassieu, P., 1999: Terpene attractant candidates of *Dioryctria sylvestrella* in maritime pine (*Pinus pinaster*) oleoresin, needles, liber and headspace samples. Journal of Chemical Ecology, 25 (12): 2741-2756. https://doi.org/10.1023/A:1020803608406
18. Koutsaviti, K.; Giatropoulos, A.; Pitarokili, D.; Papachristos, D.; Michaelakis, A.; Tzakou, O., 2014: Greek *Pinus* essential oils: larvicidal activity and repellency against *Aedes albopictus* (Diptera: Culicidae). Parasitology Research, 114 (2): 583-592. https://doi.org/10.1007/s00436-014-4220-2
19. Kovalchuk, A.; Raffaello, T.; Jaber, E.; Keriö, S.; Ghimire, R.; Lorenz, W. W.; Dean, J. F. D.; Holopainen, J. K.; Asiegbu, F. O., 2015: Activation of defence pathways in Scots pine bark after feeding by pine weevil (*Hylobius abietis*). BMC Genomics, 16: 1-15. https://doi.org/10.1186/s12864-015-1546-9
20. Loizzo, M. R.; Saab, A. M.; Tundis, R.; Menichini, F.; Bonesi, M.; Statti, G. A.; Menichini F., 2008: Chemical composition and antimicrobial activity of essential oils from *Pinus brutia* (Calabrian pine) growing in Lebanon. Chemistry of Natural Compounds, 44: 784-786. https://doi.org/10.1007/s10600-009-9167-7
21. Margaritopoulos, J. T.; Bacandritsos, N.; Pekas, A. N.; Stamatis, C.; Mamuris, Z.; Tsitsipis, J. A., 2003: Genetic variation of *Marchalina hellenica* (Hemiptera: Margarodidae) sampled from different hosts and localities in Greece. Bulletin of Entomological Research, 93: 447-453. https://doi.org/10.1079/BER2003260
22. Mateus, E. M. H. P., 2008: Characterization of pinus spp. needles by gas chromatography and mass spectrometry: Application to plant-ınsect ınteractions. PhD Thesis, Nova de Lisboa University, Lisbon, Portugal.
23. Metcalf, R. L.; Kogan, M., 1987: Plant volatiles as insect attractants. Critical Reviews in Plant Sciences, 5 (3): 251-301. https://doi.org/10.1080/07352688709382242
24. Mita, E.; Tsitsimpikou, C.; Tsiveleka, L.; Petrakis, P. V.; Ortiz, A.; Vagias, C.; Roussis, V., 2002: Seasonal variation of oleoresin terpenoids from *Pinus halepensis* and *Pinus pinea* and host selection of the scale insect *Marchalina hellenica* (Homoptera, Coccoidea, Margarodidae, Coelostonidiinae). Holzforschung, 56: 572-578. https://doi.org/10.1515/HF.2002.087
25. Roussis, V.; Petrakis, P. V.; Ortiz, A.; Basllis, E.; Mazomenos, B. E., 1995: Volatile constituents of needles of five *Pinus* species grown in Greece. Phytochemistry, 39 (2): 357-361. https://doi.org/10.1016/0031-9422(94)00885-W
26. Rudinsky, J. A., 1973: Multiple functions of the southern pine beetle pheromone verbenone. Environmental Entomology, 2 (4): 511-514. https://doi.org/10.1093/ee/2.4.511
27. Sahin, H. T.; Yalcin, O. U., 2017: Chemical composition and utilization of conifer needles-a review. Journal of Applied Life Sciences International, 14 (3): 1-11. https://doi.org/10.9734/JALSI/2017/37076
28. Sakai, M.; Yamasaki, T., 1990: (+)-juniperol and (+)-pimaral: attractants for the cerambycid beetle, *Monochamus alternatus* Hope. Journal of Chemical Ecology, 16 (12): 3383-3392. https://doi.org/10.1007/BF00982105
29. Salman, M. T., 2009: Chromatographic identification of some volatile oils from the of *Pinus brutia* Ten. growing in Iraq. Foundation of Technical Education, 22: 1-7.
30. Santas, L. A., 1983: Insects producing honeydew exploited by bees in Greece. Apidologie, 14 (2): 93-103. https://doi.org/10.1051/apido:19830204

31. Selmi, E., 1983: *Marchalina hellenica* (Gennadius) (Homoptera, Margarodidae)'nın Marmara Bölgesindeki biyolojisi. Journal of the Faculty of Forestry Istanbul University, 33: 93-103.
32. Sezik, E.; Üstün, O.; Kürkçüoğlu, M.; Başer, K. H. C., 2008: Chemical compositions of the needle essential oils obtained from *Pinus brutia* Ten. growing in Turkey. Acta Pharmaceutica Sciencia, 50: 85-96.
33. Thrasyvoulou, A.; Manikis, J., 1996: Some physicochemica and microscopic characteristics of Greek unifloral honeys. Apidologie, 26: 441-452. https://doi.org/10.1051/apido:19950601
34. Topcan, Z. P., 2017: An investigation of the effect on needle terpene profile of Pinus brutia Ten. infested by *Marchalina hellenica Genn.* MSc Thesis, Pamukkale University, Denizli, Turkey.
35. Tumen, I.; Hafizoglu, H.; Kilic, A.; Dönmez, I. E.; Sivrikaya, H.; Reunanen, M., 2010: Yields and constituents of essential oil from cones of *Pinaceae* spp. natively grown in Turkey. Molecules, 15 (8): 5797-5806. https://doi.org/10.3390/molecules15085797
36. Ustun, O.; Senol, F. S.; Kurkcuoglu, M.; Orhan, I. E.; Murat Kartal, M.; Baser, K. H. C., 2012: Investigation on chemical composition, anticholinesterase and antioxidant activities of extracts and essential oils of Turkish *Pinus* species and pycnogenol. Industrial Crops and Products, 38: 115-123. https://doi.org/10.1016/j.indcrop.2012.01.016
37. Ülgentürk, S.; Civelek, H. S.; Şahin, Ö.; Evren, H.; Sarıbaşak, H., 2012: Çam pamuklu koşnili biti *Marchalina hellenica* Genn. (Hemiptera: Margarodidae)'nın biyoekolojisi, Ege ve Akdeniz Bölgesindeki yayılış alanları. Turkish Scientific and Technical Research Council Project Final Report, 108-359. Ankara, Turkey.
38. Yener, H. O.; Saygıdeğer, S. D.; Sarikurkcu, C.; Yumrutas, O., 2014: Evaluation of antioxidant activities of essential oils and methanol extracts of *Pinus* species. Journal of Essential Oil Bearing Plants, 17 (2): 295-302. https://doi.org/10.1080/0972060X.2014.895164
39. ***Anonymous, 2017: Detection of *Marchalina hellenica* in Victoria and South Australia. Report Number: AUS-69/1. https://www.ippc.int/en/countries/australia/pestreports/2015/07/detection-of-marchalina-hellenica-in-victoria-and-south-australia-1/

SUPPLEMENT – DODATAK

Table 4 A1 trial region: Essential oil composition in needles of *M. hellenica*-infested and non-infested Turkish red pine
Tablica 4. Probno područje A1: sastav eteričnog ulja u iglicama turskoga crvenog bora nezaraženoga i zaraženoga s *M. hellenica*

		SEASON 1 (Area, %) *1. sezona (površina, %)*		SEASON 2 (Area, %) *2. sezona (površina, %)*		SEASON 3 (Area, %) *3. sezona (površina, %)*	
Component / *Komponenta*	**RI**	**NI**	**I**	**NI**	**I**	**NI**	**I**
***α*-pinen**	940	0.07	tr	11.77	8.55	13.79	21.51
Camphene	948	tr	tr	0.30	0.26	0.27	0.41
α-fenchene	955	tr	-	tr	-	35.10	-
***β*-pinen**	961	0.32	0.09	31.40	29.99	1.92	3.98
3-caren	1004	0.09	tr	0.91	0.66	1.01	0.72
Pseudolimonen	1012	0.04	tr	1.98	2.38	tr	42.68
α-Phellandrene	1015	-	tr	-	0.06	-	tr
D-limonen	1026	0.12	tr	2.04	0.27	0.45	tr
Terpineolen	1080	0.19	tr	0.53	0.76	0.34	0.33
Linalol	1106	0.28	tr	0.21	0.14	0.32	tr
Fenchol	1108	0.22	tr	tr	0.11	tr	tr
trans-Pinocarveol	1121	0.02	-	tr	-	tr	-
cis-β-Terpineol	1131	0.10	tr	tr	0.05	tr	tr
Isoborneol	1138	0.26	tr	0.11	0.11	0.08	tr
Myrtenol	1154	0.04	-	tr	-	tr	-
Terpinen-4-ol	1159	0.26	tr	0.11	0.16	0.08	tr
α-Terpineol	1175	7.04	0.53	1.98	2.79	1.30	0.59
Estragole	1221	0.03	tr	tr	0.04	tr	tr
cis-Geraniol	1225	0.03	-	tr	-	tr	-
Thymol Methyl ether	1228	0.03	tr	tr	0.02	tr	tr
Linalyl acetate (Bergamiol)	1239	0.72	tr	0.50	0.09	1.51	0.17
α-Terpineol acetate (Terpinyl acetate)	1357	1.98	0.18	1.37	0.75	2.56	0.93
Aromadendrene	1363	0.04	tr	tr	0.29	tr	tr
Isobornyl acetate	1268	0.44	tr	0.28	0.50	0.29	0.35
T-Gurjunene	1374	0.04	-	tr	-	tr	-
β-Elemen	1382	0.96	0.11	0.49	0.65	0.66	0.13

Table 4 continuation / **Tablica 4.** nastavak

		SEASON 1 (Area, %) *1. sezona (površina, %)*		**SEASON 2 (Area, %)** *2. sezona (površina, %)*		**SEASON 3 (Area, %)** *3. sezona (površina, %)*	
Component / *Komponenta*	**RI**	**NI**	**I**	**NI**	**I**	**NI**	**I**
Eugenol methyl ether	1387	0.79	0.05	0.25	0.41	tr	0.26
β-Cubebene	1412	0.52	tr	0.24	0.24	0.27	0.18
***β*-Caryophyllene**	1415	11.29	12.84	8.24	13.15	12.89	15.55
α-Caryophyllene	1443	31.49	-	18.15	-	2.63	-
α-Amorphene	1452	0.16	-	0.08	-	tr	-
α-Selinene	1465	2.63	-	1.79	-	tr	-
α-Guaiene	1470	-	0.35	-	0.06	-	tr
Germacrene D	1472	1.26	3.13	0.67	19.72	tr	3.11
Phenethyl pivalate	1477	-	0.20	-	0.72	-	0.56
α-Muurolene	1487	0.58	-	0.28	-	0.59	-
Isoeugenol methyl ether	1491	0.75	-	0.10	-	0.59	-
T-Muurolene	1493	1.06	0.16	0.39	0.41	tr	0.43
α-Himachalene	1495	1.21	-	0.79	-	1.65	-
cis-*α*-Bisabolene	1499	-	0.25	-	1.22	-	1.51
Nerolidol	1512	-	0.10	-	0.09	-	tr
δ-Cadinene	1513	2.97	0.44	1.26	1.25	1.63	1.20
Caryophyllene oxide	1561	0.41	0.23	0.08	0.22	0.16	0.17
Aromadendrene oxide	1576	0.25	0.19	0.05	0.06	tr	tr
Germacrene-D-4-ol	1578	tr	0.07	tr	0.16	0.16	0.15
Lauric acid ethyl ester (Dodecanoic acid ethyl ester)	1582	-	tr	-	tr	-	0.11
trans-*α*-longipinocarveol	1596	0.09	-	tr	-	tr	-
α-Cubenol	1601	0.64	-	0.18	-	tr	-
tau-Cadinol	1616	1.27	0.85	0.34	0.37	0.35	0.16
α-Cadinol	1622	2.13	1.60	0.56	0.57	0.54	tr
δ-Cadinol	1631	0.39	0.29	0.10	0.12	tr	tr
tau-Muurolol	1639	0.12	-	tr	-	tr	-
trans-farnesol	1677	-	tr	-	tr	-	0.23
Benzylbenzoate	1719	0.21	0.10	0.04	0.07	tr	tr
Sclaren	1801	0.08	-	tr	-	0.12	-
trans farnesyl acetate	1814	0.31	0.84	0.17	0.31	0.12	0.12
Benzoic acid phenethyl ester	1830	0.07	-	tr	-	tr	-
Cis-3-Hexenyl cinnamate	1846	0.04	0.15	tr	0.02	tr	tr
Kaur-16-ene	1908	0.38	-	0.22	-	tr	-
Undefinitied	-	-	1.76	-	0.45	-	tr
Verticillol	2226	3.09	5.84	1.08	1.40	1.41	0.27
Thunbergol	2235	14.14	46.40	3.97	5.31	9.71	3.14
Pimaral	2241	-	0.80	-	0.08	-	tr
Cembrene	2253	6.69	15.28	3.10	3.97	3.93	0.74
Undefinitied	-	-	2.21	-	0.66	-	0.31
Scloreol	2174	-	3.05	-	0.14	-	tr
Ethyl Linoleate	2191	0.22	-	3.54	-	tr	-
Pimara-7.15-dien-3-one	2257	0.63	-	0.11	-	0.14	-
Methyl abiatate	2342	0.24	-	0.16	-	tr	-
Androst-4-ene-3,17 dione	2392	-	1.09	-	0.12	-	tr
Methyl neoabietate	2411	0.39	0.82	0.09	0.08	tr	tr
Methyl 7,13,15-abietatrienoate	2421	0.15	-	tr	-	tr	-
Undefinitied	-	tr	-	tr	-	0.25	

RI – Retention Index, I – Infested, NI – Non-Infested, I. Season – July 2016, II. Season – October 2016, III. Season – February 2017, tr – traces, tr <0.01

RI – indeks retencije, I – zaražen bor, NI – nezaražen bor, 1. sezona – srpanj 2016., 2. sezona – listopad 2016., 3. sezona – veljača 2017., tr – u tragovima, tr <0,01

Table 5 A2 trial – region: Essential oil composition in needles of *M. hellenica*-infested and non-infested Turkish red pine
Tablica 5. Probno područje A2: sastav eteričnog ulja u iglicama turskoga crvenog bora nezaraženoga i zaraženoga s *M. hellenica*

		SEASON 1 (Area, %) *1. sezona (površina, %)*		**SEASON 2 (Area, %)** *2. sezona (površina, %)*		**SEASON 3 (Area, %)** *3. sezona (površina, %)*	
Component / *Komponenta*	**RI**	**NI**	**I**	**NI**	**I**	**NI**	**I**
***α*-pinen**	940	12.09	9.92	1.92	14.10	14.35	13.31
Camphene	948	0.41	0.31	0.06	0.35	0.30	0.27
***β*-pinen**	961	32.07	28.89	7.56	36.94	30.51	27.33
3-Caren	1004	1.01	0.69	0.55	0.71	0.87	0.46
Pseudolimonen	1012	2.43	1.81	0.79	2.03	2.66	2.08
D-limonen	1026	2.71	2.32	1.25	2.28	2.37	2.04
Terpineolen	1080	1.52	0.89	0.51	0.51	0.39	0.32
Linalol	1106	0.24	0.20	0.23	0.11	0.22	0.14
Fenchol	1108	0.27	0.16	0.09	tr	tr	tr
cis-*β*-Terpineol	1131	0.09	0.07	0.05	tr	tr	tr
Isoborneol	1138	0.22	0.15	0.13	tr	tr	tr
Terpinen-4-ol	1159	0.24	0.17	0.18	0.12	0.09	0.08
α-Terpineol	1175	5.14	3.18	2.68	1.90	1.16	0.92
Linalyl acetate (Bergamiol)	1239	0.21	0.25	1.04	0.43	1.00	0.76
Isobornyl acetate	1268	0.35	0.59	0.74	0.64	0.46	0.65
α-Terpineol acetate (Terpinyl acetate)	1357	0.81	1.53	1.61	1.64	1.28	3.18
β-Bourbonene	1379	0.13	0.13	0.16	0.10	0.15	Tr
β-Elemen	1382	0.56	0.75	1.22	0.69	0.44	0.36
Eugenol methyl ether	1387	0.47	0.04	0.84	0.40	0.46	0.42
β-Cubebene	1412	0.27	0.33	0.39	0.23	0.18	0.20
***β*-Caryophyllene**	1415	9.03	10.86	15.61	9.14	10.56	12.70
α-Caryophyllene	1443	2.02	-	3.40	-	2.17	-
α-Guaiene	1470	-	2.40	-	1.95	-	2.55
Germacrene D	1472	16.45	23.89	34.50	20.04	22.43	25.69
T-Muurolene	1493	0.40	0.58	0.65	0.41	0.36	0.51
α-Himachalene	1495	0.91	-	1.97	-	0.96	-
δ-Cadinene	1513	1.30	1.60	2.05	1.24	0.98	1.34
Caryophyllene oxide	1561	0.19	0.32	0.36	0.17	0.12	tr
α-Cubenol	1601	0.40	-	0.26	-	0.12	-
tau-Cadinol	1616	0.63	0.67	0.83	0.30	0.24	0.29
δ-Cadinol	1631	1.10	1.16	1.49	0.49	0.40	0.42
Benzylbenzoate	1719	0.07	-	0.08	-	tr	-
trans farnesyl acetate	1814	0.14	0.18	0.28	0.18	0.11	0.06
Verticillol	2226	0.68	0.74	2.01	0.33	0.37	0.33
Thunbergol	2235	2.81	2.45	7.93	1.42	2.93	2.30
Pimaral	2241	-	0.12	-	tr	-	0.08
Cembrene	2253	2.56	2.57	6.45	1.15	1.35	1.11
Methyl neoabietate	2411	0.11	0.09	0.14	tr	tr	0.11

RI – Retention Index, I – Infested, NI – Non-Infested, I. Season – July 2016, II. Season – October 2016, III. Season – February 2017, tr – traces, tr <0.01
RI – indeks retencije, I – zaražen bor, NI – nezaražen bor, 1. sezona – srpanj 2016., 2. sezona – listopad 2016., 3. sezona – veljača 2017., tr – u tragovima, tr <0,01

Table 6 A3 trial region: Essential oil composition in needles of *M. hellenica*-infested and non-infested Turkish red pine
Tablica 6. Probno područje A3: sastav eteričnog ulja u iglicama turskoga crvenog bora nezaraženoga i zaraženoga s *M. hellenica*

		SEASON 1 (Area, %) *1. sezona (površina, %)*		**SEASON 2 (Area, %)** *2. sezona (površina, %)*		**SEASON 3 (Area, %)** *3. sezona (površina, %)*	
Component / *Komponenta*	**RI**	**NI**	**I**	**NI**	**I**	**NI**	**I**
***α*-pinene**	940	19.74	2.29	17.07	tr	17.59	11.54
Camphene	948	0.52	0.08	0.39	tr	0.43	0.22
***β*-pinene**	961	34.39	6.04	35.97	0.41	26.25	20.98
3-Caren	1004	0.94	0.56	1.73	0.43	1.33	1.27
Pseudolimonen	1012	2.11	0.69	2.05	0.17	2.32	2.16

Table 6 continuation / **Tablica 6.** nastavak

		SEASON 1 (Area, %) *1. sezona (površina, %)*		**SEASON 2 (Area, %)** *2. sezona (površina, %)*		**SEASON 3 (Area, %)** *3. sezona (površina, %)*	
Component / *Komponenta*	**RI**	**NI**	**I**	**NI**	**I**	**NI**	**I**
D-limonen	1026	2.34	0.94	3.43	0.27	2.12	1.59
Terpineolen	1080	0.86	0.44	0.60	0.18	0.39	0.22
Linalol	1106	0.26	0.08	0.30	0.21	0.11	tr
Isoborneol	1138	0.16	0.10	tr	0.08	0.04	tr
Terpinen-4-ol	1159	0.16	0.10	0.13	0.10	0.07	tr
α-Terpineol	1175	3.49	2.36	2.67	2.47	1.07	0.71
Linalyl acetate (Bergamiol)	1239	0.45	-	0.51	-	0.41	-
Isobornyl acetate	1268	0.45	0.43	0.41	0.53	0.43	0.33
α-Terpineol acetate (Terpinyl acetate)	1357	-	1.37	-	2.71	-	1.77
β-Bourbonene	1379	0.10	0.30	0.15	0.29	0.23	0.28
β-Elemen	1382	0.42	0.89	0.37	0.89	0.35	0.39
Eugenol methyl ether	1387	0.36	0.44	0.21	0.26	0.31	0.15
β-Cubebene	1412	0.21	0.52	0.13	0.51	0.23	0.29
***β*-Caryophyllene**	1415	7.68	16.22	9.98	20.61	11.05	14.54
α-Caryophyllene	1443	1.67	3.55	1.98	4.46	2.34	3.05
Germacrene D	1472	16.22	41.85	15.49	39.29	25.56	29.10
T-Muurolene	1493	0.52	1.13	0.34	1.09	0.37	0.72
α-Himachalene	1495	0.90	1.79	1.20	2.34	1.65	1.52
δ-Cadinene	1513	1.55	3.28	1.17	3.20	1.91	2.10
α-Cubenol	1601	0.22	0.23	tr	0.16	tr	0.19
tau-Cadinol	1616	0.39	0.94	0.17	0.74	0.44	0.28
δ-Cadinol	1631	0.57	1.47	0.32	0.91	0.86	0.40
Benzylbenzoate	1719	0.06	0.12	tr	tr	0.01	tr
trans farnesyl acetate	1814	-	0.59	-	0.56	-	0.20
Verticillol	2226	0.38	-	0.32	-	1.59	-
Thunbergol	2235	1.63	5.48	1.75	8.27	0.49	3.87
Pimaral	2241	-	0.24	-	0.25	-	tr
Cembrene	2253	1.25	5.35	1.15	8.48	0.07	2.03
Methyl neoabietate	2411	-	0.14	-	0.14	-	0.06

RI – Retention Index, I – Infested, NI – Non-Infested, I. Season – July 2016, II. Season – October 2016, III. Season – February 2017, tr – traces, tr <0.01
RI – indeks retencije, I – zaražen bor, NI – nezaražen bor, 1. sezona – srpanj 2016., 2. sezona – listopad 2016., 3. sezona – veljača 2017., tr – u tragovima, tr <0,01

Table 7 A1 trial region: Essential oil composition in bark of *M. hellenica*-infested and non-infested Turkish red pine
Tablica 7. Probno područje A1: sastav eteričnog ulja u kori turskoga crvenog bora nezaraženoga i zaraženoga s *M. hellenica*

		SEASON 1 (Area, %) *1. sezona (površina, %)*		**SEASON 2 (Area, %)** *2. sezona (površina, %)*		**SEASON 3 (Area, %)** *3. sezona (površina, %)*	
Component / *Komponenta*	**RI**	**NI**	**I**	**NI**	**I**	**NI**	**I**
α-pinen	940	0.09	1.97	0.34	tr	0.70	2.51
Camphane	948	-	0.20	-	tr	-	0.24
***β*-pinen**	961	0.26	0.54	0.16	tr	0.46	0.78
3-Caren	1004	0.25	1.38	0.60	tr	1.83	1.82
p-Simen	1013	tr	0.41	0.18	tr	0.24	0.60
D-Limonen	1026	0.11	0.86	0.39	tr	0.57	1.03
Dehidro p-simen	1058	tr	0.19	0.19	0.04	0.21	0.29
Fenchone	1075	-	0.26	-	0.09	-	0.64
Terpineolen	1080	0.51	1.01	1.02	0.15	1.42	1.49
Fenchol	1108	1.80	2.45	2.91	1.44	1.18	2.83
α-Campholenal	1116	0.42	0.19	0.84	0.09	0.41	0.27
Trans-Pinocarveol	1121	2.03	1.15	4.23	0.17	1.43	2.40
Camphor	1128	0.99	1.03	2.50	1.02	0.93	2.59
Cis-β-Terpineol	1131	0.79	0.86	1.27	0.90	0.62	1.42
Isoborneol	1138	1.07	1.38	1.66	1.16	0.71	2.03
Borneol	1147	5.20	5.04	7.99	6.44	2.88	7.43
Myrtenol	1154	5.37	2.74	7.31	4.14	3.50	5.53

Table 7 continuation / **Tablica 7.** nastavak

		SEASON 1 (Area, %) *1. sezona (površina, %)*		**SEASON 2 (Area, %)** *2. sezona (površina, %)*		**SEASON 3 (Area, %)** *3. sezona (površina, %)*	
Component / *Komponenta*	**RI**	**NI**	**I**	**NI**	**I**	**NI**	**I**
Terpinen-4-ol	1159	3.03	1.60	3.35	2.12	1.66	2.41
Para-Simen-8-ol	1168	1.18	-	1.68	-	0.53	-
***α*-Terpineol**	1175	34.69	27.42	3.91	40.21	19.66	33.04
Berbenone	1191	1.50	-	3.62	-	1.09	-
***Cis*-Verbenon**	1196	-	25.65	-	4.65	-	3.79
Cis-Carveol	1200	0.73	0.43	0.87	1.01	0.49	1.12
***Cis*-Myrtanol**	1208	3.80	2.21	5.23	5.36	1.55	3.39
Perilla aldehyde (Perillal)	1217	0.47	-	0.38	-	0.21	-
Estragole	1221	0.68	0.62	0.79	0.51	0.41	0.38
Perilla alchol (Perillol)	1290	0.41	0.38	0.24	0.18	tr	
Carvacrol	1295	0.17	0.12	0.22	0.39	0.15	0.29
α-Longipinen	1338	0.74	0.42	1.19	0.34	1.09	0.38
α-Gurjunene	1387	0.53	0.76	0.90	0.78	0.84	0.49
Junipen	1401	9.85	6.44	15.11	7.42	16.22	7.13
***β*-Caryophyllene**	1415	9.69	3.79	12.87	4.48	11.26	4.90
α-Caryophyllene	1443	2.16	0.89	2.88	1.11	2.77	1.07
β-Farnesene	1450	0.20	-	0.23	-	0.20	-
Methyl eugenol	1456	0.23	0.19	0.27	0.34	0.60	0.23
Germacrene-D	1472	-	0.38	-	0.53	-	Tr
Caryophyllene oxide	1561	4.01	1.92	4.64	2.66	8.17	2.22
Isoaromadendrene oxide	1572	1.33	0.76	2.12	2.30	2.77	0.74
Aromadendrene oxide	1576	1.49	1.00	2.58	3.97	4.65	1.34
Benzylbenzoate	1719	0.12	0.11	0.21	0.24	0.06	Tr
Isopimaric acid methyl ester	2217	0.13	-	0.24	-	1.06	-
Verticillol	2226	0.99	0.62	1.35	1.43	2.57	1.48
Pimaral	2241	0.58	0.83	0.91	2.50	2.93	0.75
Cembrene	2253	0.35	-	0.43	-	0.69	-
Dehydroabietic aldehyde	2263	0.60	-	0.66	-	0.56	-
Undefinitied	-	0.44	-	0.36	-	0.32	-
Methyl dehydroabiatate	2301	0.81	1.20	0.94	1.34	0.33	0.41
Methyl abiatate	2342	0.20	0.58	0.20	0.49	0.07	0.08

RI – Retention Index, I – Infested, NI – Non-Infested, I. Season – July 2016, II. Season – October 2016, III. Season – February 2017, tr – traces, tr <0.01
RI – indeks retencije, I – zaražen bor, NI – nezaražen bor, 1. sezona – srpanj 2016., 2. sezona – listopad 2016., 3. sezona – veljača 2017., tr – u tragovima, tr <0,01

Table 8 A2 trial region: Essential oil composition in bark of *M. hellenica*-infested and non-infested Turkish red pine
Tablica 8. Probno područje A2: sastav eteričnog ulja u kori turskoga crvenog bora nezaraženoga i zaraženoga s *M. hellenica*

		SEASON 1 (Area, %) *1. sezona (površina, %)*		**SEASON 2 (Area, %)** *2. sezona (površina, %)*		**SEASON 3 (Area, %)** *3. sezona (površina, %)*	
Component / *Komponenta*	**RI**	**NI**	**I**	**NI**	**I**	**NI**	**I**
α-pinen	940	3.40	0.20	0.03	tr	2.77	4.05
Camphene	948	0.36	-	tr	-	0.18	-
β-pinen	961	1.16	0.16	0.02	tr	1.33	0.08
3-Caren	1004	2.44	0.69	0.10	0.05	3.25	1.70
p-Simen	1013	0.47	0.15	0.02	tr	0.35	0.05
D-limonen	1026	0.85	0.38	0.04	0.03	1.06	3.72
γ-Terpinen	1048	0.17	-	0.02	-	0.20	-
Dehidro para-simen	1058	0.24	-	0.05	-	0.18	-
Terpineolen	1080	1.77	1.07	0.28	0.28	1.71	1.82
Fenchol	1108	1.62	1.43	1.24	0.72	1.41	1.62
α-Campholenal	1116	0.71	0.61	0.35	0.12	0.51	0.85
trans-Pinocarveol	1121	2.53	1.23	1.60	0.67	2.08	2.48
Camphor	1128	1.51	0.78	0.91	0.42	1.39	1.13
cis-β-Terpineol	1131	0.64	0.65	0.77	0.44	0.87	0.70
Isoborneol	1138	0.67	0.58	0.76	0.37	3.37	3.44

Table 8 continuation / **Tablica 8.** nastavak

		SEASON 1 (Area, %) *1. sezona (površina, %)*		**SEASON 2 (Area, %)** *2. sezona (površina, %)*		**SEASON 3 (Area, %)** *3. sezona (površina, %)*	
Component / *Komponenta*	**RI**	**NI**	**I**	**NI**	**I**	**NI**	**I**
Borneol	1147	4.01	2.91	3.90	2.24	2.68	2.41
Myrtenol	1154	20.32	3.11	4.11	2.80	6.24	5.31
Terpinen-4-ol	1159	2.31	1.73	1.89	1.08	2.06	2.04
***α*-Terpineol**	1175	21.86	23.66	33.76	22.72	24.30	20.74
***Cis*-Verbenon**	1191	-	2.75	-	3.15	-	1.24
Cis-Carveol	1200	0.88	0.59	0.96	0.69	0.79	0.47
***Cis*-Myrtanol**	1208	4.86	1.95	3.91	2.97	3.77	1.81
Perilla aldehyde (Perillal)	1217	0.66	-	0.56	-	0.32	-
Estragole	1221	1.07	1.16	0.77	0.56	0.46	0.83
Perilla alchol (Perillol)	1290	0.30	0.44	0.48	0.51	Tr	tr
Carvacrol	1295	0.27	0.25	0.42	0.35	0.26	0.12
α-Longipinen	1338	0.87	1.96	1.09	1.04	1.05	1.57
α-Gurjunene	1387	0.70	1.57	0.90	0.84	0.64	0.91
Junipen	1401	9.77	18.86	12.83	11.55	12.04	16.05
***β*-Caryophyllene**	1415	6.11	9.12	9.25	8.05	8.96	11.16
***α*-Caryophyllene**	1443	1.23	2.18	2.38	2.36	1.97	2.42
Methyl eugenol	1456	0.50	0.89	0.41	1.19	0.53	0.71
Caryophyllene oxide	1561	1.64	5.96	5.26	4.61	5.45	4.87
Isoaromadendrene oxide	1572	1.29	2.67	1.92	4.78	2.79	1.24
Aromadendrene oxide	1576	1.39	3.36	1.92	6.30	2.79	1.75
Benzylbenzoate	1719	0.14	0.30	0.24	0.59	0.09	0.08
Verticillol	2226	-	1.83	-	4.19	-	0.78
Pimaral	2241	0.64	1.35	2.21	3.84	1.44	0.64
Cembrene	2253	-	0.53	-	0.97	-	0.30
Pimara-7.15-dien-3-one	2257	-	1.18	-	2.01	-	0.26
Dehydroabietic aldehyde	2263	0.32	0.94	1.90	2.89	0.34	0.40
Methyl dehydroabiatate	2301	0.31	0.64	1.77	3.23	0.24	0.21
Methyl abiatate	2342	tr	0.16	0.98	1.36	0.10	0.06

RI – Retention Index, I – Infested, NI – Non-Infested, I. Season – July 2016, II. Season – October 2016, III. Season – February 2017, tr – traces, tr <0.01
RI – indeks retencije, I – zaražen bor, NI – nezaražen bor, 1. sezona – srpanj 2016., 2. sezona – listopad 2016., 3. sezona – veljača 2017., tr – u tragovima, tr <0,01

Table 9 A3 trial region: Essential oil composition in bark of *M. hellenica*-infested and non-infested Turkish red pine
Tablica 9. Probno područje A3: sastav eteričnog ulja u kori turskoga crvenog bora nezaraženoga i zaraženoga s *M. hellenica*

		SEASON 1 (Area, %) *1. sezona (površina, %)*		**SEASON 2 (Area, %)** *2. sezona (površina, %)*		**SEASON 3 (Area, %)** *3. sezona (površina, %)*	
Component / *Komponenta*	**RI**	**NI**	**I**	**NI**	**I**	**NI**	**I**
α-pinen	940	tr	tr	10.93	1.26	3.79	0.28
Camphene	948	tr	-	0.82	-	0.16	-
β-pinen	961	tr	tr	3.72	0.46	2.26	0.24
3-Caren	1004	tr	tr	6.11	0.70	1.80	0.44
D-limonen	1026	tr	tr	2.00	0.94	0.64	0.39
γ-Terpinen	1048	tr	-	0.26	-	0.10	-
Dehidro para-simen	1058	tr	tr	0.38	1.57	0.11	1.49
Terpineolen	1080	tr	-	2.69	-	1.04	-
Fenchol	1108	1.37	0.43	1.71	1.75	0.90	1.89
α-Campholenal	1116	0.13	tr	0.78	0.59	0.72	0.73
trans-Pinocarveol	1121	0.89	0.32	2.00	1.66	1.90	-
Camphor	1128	0.41	0.05	1.59	2.09	0.60	1.44
cis-*β*-Terpineol	1131	0.76	0.60	0.39	1.36	0.63	1.43
Isoborneol	1138	1.36	0.85	1.09	1.40	2.32	1.43
Borneol	1147	6.03	5.06	4.36	5.88	1.77	5.27
Myrtenol	1154	2.59	3.54	1.98	1.92	2.79	3.55
Terpinen-4-ol	1159	1.49	0.71	1.59	1.87	1.06	1.60

Table 9 continuation / **Tablica 9.** nastavak

		SEASON 1 (Area, %) *1. sezona (površina, %)*		**SEASON 2 (Area, %)** *2. sezona (površina, %)*		**SEASON 3 (Area, %)** *3. sezona (površina, %)*	
Component / *Komponenta*	**RI**	**NI**	**I**	**NI**	**I**	**NI**	**I**
***α*-Terpineol**	1175	30.68	30.17	18.90	31.73	8.28	26.22
***Cis*-Verbenon**	1191	1.04	1.51	1.75	3.44	1.05	2.64
Cis-Carveol	1200	0.62	0.66	0.42	0.52	0.53	0.97
Cis-Myrtanol	1208	2.95	3.83	1.33	1.04	0.61	1.24
Estragole	1221	0.85	0.50	0.78	0.64	0.28	0.21
Carvacrol	1295	0.21	0.65	tr	0.30	0.07	0.13
α-Longipinen	1338	0.73	0.28	1.64	0.79	1.99	0.88
α-Gurjunene	1387	1.11	0.71	1.16	0.68	1.20	1.06
Junipen	1401	13.26	9.05	16.55	11.42	20.51	11.14
***β*-Caryophyllene**	1415	6.41	7.03	9.76	11.32	21.49	14.91
α-Caryophyllene	1443	1.60	2.20	2.00	2.78	5.04	3.47
Methyl eugenol	1456	0.34	0.57	0.43	1.74	Tr	0.42
Caryophyllene oxide	1561	2.68	6.55	1.41	2.87	9.15	5.88
Isoaromadendrene oxide	1572	1.84	4.86	0.52	2.10	1.64	1.66
Aromadendrene oxide	1576	2.32	6.02	0.68	2.80	2.33	2.78
Benzylbenzoate	1719	0.17	2.00	tr	tr	0.02	0.03
Pimaral	2241	0.89	3.15	0.31	1.80	1.48	2.35
Cembrene	2253	-	3.66	-	tr	-	0.68
Dehydroabietic aldehyde	2263	14.67	-	tr	-	0.74	-
Methyl dehydroabiatate	2301	1.60	3.63	tr	0.61	0.85	0.47
Methyl abiatate	2342	1.02	1.42	tr	tr	0.17	0.39

RI – Retention Index, I – Infested, NI – Non-Infested, I. Season – July 2016, II. Season – October 2016, III. Season – February 2017, tr – traces, tr <0.01
RI – indeks retencije, I – zaražen bor, NI – nezaražen bor, 1. sezona – srpanj 2016., 2. sezona – listopad 2016., 3. sezona – veljača 2017., tr – u tragovima, tr <0,01

Corresponding address:

MUSTAFA BURAK ARSLAN
General Directorate of Forestry, Ege Forestry Research Institute, İzmir, TURKEY,
e-mail: mustafaburakarslan@ogm.gov.tr

Ersin Ercan[1], Musa Atar[2], Mustafa Kucuktuvek[3], Hakan Keskin[2]

Characterization of Formaldehyde Emission and Combustion Properties of Peanut (*Arachis Hypogaea*) Husk-Based Green Composite Panels for Building Applications

Karakterizacija emisije formaldehida i svojstava gorenja ekoloških kompozitnih ploča za graditeljstvo proizvedenih na bazi ljusaka kikirikija (*Arachis hypogaea*)

ORIGINAL SCIENTIFIC PAPER
Izvorni znanstveni rad
Received – prispjelo: 2. 2. 2021.
Accepted – prihvaćeno: 13. 12. 2021.
UDK: 547.281.1; 674.049.3; 674.81
https://doi.org/10.5552/drvind.2022.2105

ABSTRACT • *The building sectors are increasingly in need of more wood-based panels. Forests and environments are being destroyed to produce these wood-based panels. The aim of this study is to protect forest assets by recycling peanut (Arachis hypogaea) husk and manufacturing particleboard for green building design. The manufactured composite panels were subjected to combustion and formaldehyde tests. According to the test results, peanut husk reduced the combustion time and increased the combustion temperature. Phenol-formaldehyde adhesive decreased illuminance values and the peanut husk ratio increased the illuminance values. It was understood that, when the peanut husk additive ratio increased, combustion times decreased. Slow-combustion of green building composite panels delays the danger of collapse in case of a fire in a building. The combustion performance of the composite panels can be improved by adding non-combustible materials that do not affect the adhesion performance of the composite panels. When the adhesive type is taken into consideration, it is seen that the FF additive ratio reduces the combustion time. According to the formaldehyde emission test results, 24 hours after the manufacturing process all composite panels met the requirements of the board formaldehyde class E1. These composite panels can be used in green buildings as a sustainable building material. The furniture industry can also use these agro-fiber composite panels as green materials.*

KEYWORDS: *particleboard; peanut husk; combustion properties; formaldehyde emission; green building materials*

[1] Author is researcher at Turkish Standards Institute, Inspection and Surveillance System Directorate, Ankara, Turkey.
[2] Authors are researchers at Gazi University, Faculty of Technology, Department of Wood Products Industrial Engineering, Teknikokullar, Ankara, Turkey.
[3] Author is researcher at Iskenderun Technical University, Faculty of Architecture, Department of Interior Architecture, Iskenderun, Hatay, Turkey.

SAŽETAK • *Građevni sektor ima sve veću potrebu za pločama na bazi drva za čiju se proizvodnju uništavaju šume i okoliš. Cilj ovog istraživanja bio je zaštititi šumska dobra recikliranjem ljusaka kikirikija (Arachis hypogaea) i proizvodnjom iverica namijenjenih zelenoj gradnji. Na tako proizvedenim kompozitnim pločama provedena su ispitivanja gorenja i emisije formaldehida. Rezultati su pokazali da se dodavanjem ljusaka kikirikija smanjuje vrijeme gorenja i povećava temperatura izgaranja ploča. Fenol-formaldehidno ljepilo pridonosi smanjenju vrijednosti osvjetljenja, a uz veći udio dodanih ljusaka kikirikija povećava se razina osvjetljenja pri gorenju. Pretpostavljeno je da će se s povećanjem udjela ljusaka kikirikija smanjiti vrijeme gorenja. Sporo gorenje kompozitnih ploča namijenjenih zelenoj gradnji odgađa opasnost od urušavanja u slučaju požara u zgradi. Svojstva gorenja kompozitnih ploča mogu se poboljšati dodavanjem nezapaljivih materijala koji ne utječu na adheziju kompozitnih ploča. S obzirom na vrstu ljepila, ustanovljeno je da se s povećanjem udjela FF ljepila skraćuje vrijeme gorenja. Prema rezultatima ispitivanja emisije formaldehida 24 sata nakon procesa proizvodnje, sve su kompozitne ploče zadovoljile klasu emisije formaldehida E1. Zaključeno je da se ispitivane kompozitne ploče u zelenoj gradnji mogu upotrebljavati kao održivi građevni materijal. Kao ekološki prihvatljive, te se kompozitne ploče na bazi agrovlakana mogu primjenjivati i u industriji namještaja.*

KLJUČNE RIJEČI: *iverica; ljuska kikirikija; svojstva izgaranja; emisija formaldehida; zeleni građevni materijali*

1 INTRODUCTION
1. UVOD

There are important initiatives around the world to find sustainable, affordable building materials and technologies that meet the required comfort and safety standards. Along with the manufacturing of green building materials, improving the technological properties of recycled composite material based on agricultural residues is also an important approach to achieve this goal.

The use of building materials with minimum environmental impact contributes to the sustainable development of countries. Considering the environmental impact of selected materials in buildings can be an important method to improve the environmental performance of buildings. Today, there are many technologies to reduce environmental impacts, but these technologies need to be developed (Seyfang, 2010; Fernandez, 2006). Since 40 % of natural resources are used in the construction sector, buildings have a significant environmental impact. Besides, buildings are the cause of 30 % greenhouse gas emissions and an additional 18 % emission in the transport and use of building materials (Yudelson, 2008; Venkatarama *et al.,* 2003).

In recent years, sustainable design in the construction sector has been an important factor in preventing environmental problems. Architectural decisions such as orientation and mass and facade design have a significant impact on the strength and health of the building.

The physical, mechanical, and chemical properties of the chosen materials that are the basic components of a building are vital for a sustainable design. As a green design strategy, choosing eco-friendly sustainable building materials can be the fastest way to integrate into a sustainable design concept (Umar *et al.,* 2012). Therefore, the effective use of local and recycled building materials in the design can be a good strategy (Hulme and Radford, 2010; Fernandez, 2006). Peanut, which is one of the most produced agricultural residues in southern Turkey, is a local raw material that can be used for this purpose.

Non-wood lignocellulosic raw materials, as more sustainable materials, are in great demand due to the shortage of wood (Ulker and Burdurlu, 2016). The composite panel is produced by bonding wood fibers under heat and pressure with an adhesive. The building and furniture industries are in search of sustainable raw materials that can be used in composite panel production as an alternative to forest products. Recycling of lignocellulose agricultural wastes is a good alternative to composite panel production (Nemli and Aydin, 2007). In this way, forests can be protected and sustainable building and furniture material can be produced. Some agricultural wastes used in composite panel production are poppy husk (Keskin *et al.,* 2015), kiwi pruning wastes (Nemli *et al.,* 2007), pine cone (Buyuksari *et al.,* 2010), coffee husk and hulls (Bekalo and Reinhardt, 2010), vine pruning (Ntalos and Grigoriou, 2012), coconut fiber and castor oil (Fiorelli *et al.,* 2012) and cottonseed hulls (Gurjar, 1993). Composite panels to be used in the construction industry must meet some strength, combustion and surface quality standards. In general, it is tried to benefit from the wastes of annual plants in the production of composite panels. The Limit Oxygen Index (LOI) of the panels produced from poppy husk was determined as 48 % (Keskin *et al.,* 2015). It is seen that most agricultural wastes affect the strength values negatively.

Formaldehyde-based binders are commonly used to produce composite products found in furniture, cabinets, worktops, shelves and stair systems, floor coverings, and many other interior building materials. Formaldehyde (HCHO) adhesive is a poisonous material for the body especially for the nose and throat, but the eyes are the most sensitive to formaldehyde exposure. Moreover, it also causes more serious health problems such as asthma and cancer (Kim *et al.,* 2006). Poor in-

door air quality affects human beings and causes health problems. Also, indoor air quality is one of the important factors that decrease the performance of the user (Reis *et al.,* 2006). Efforts are underway for interiors to reduce formaldehyde emissions by changing the chemical formulas of adhesives. Therefore, many wood manufacturers and researchers focus primarily on reducing or controlling the emission of formaldehyde from urea-formaldehyde adhesive-bonded composites. One of the reasons for formaldehyde emission is the presence of free formaldehyde in UF resins (Kim and Kim, 2005).

Wood has some advantages in case of fire. The most important advantage is the slow-burning of wood, which delays the danger of collapse, thus minimizing the loss of life. Improving the combustion properties of wood material and wood-based composites can further reduce the loss of life and property during fires (Terzi, 2008).

This study aims to produce a green building material that can reduce the effects of environmental problems and can be used for healthy building and furniture production. For this purpose, peanut husks were recycled under laboratory conditions to produce a sustainable, low formaldehyde emission and fire-retardant building material.

2 MATERIALS AND METHODS
2. MATERIJALI I METODE

2.1 Peanut (*Arachis hypogaea*) husk
2.1. Ljuske kikirikija (*Arachis hypogaea*)

When the chemical structure of peanut husk was examined, it was found to be suitable for composite panel production, because it contains a high amount of cellulose and lignin. Peanut husk is reported to consist of 35-45 % cellulose, 27-33 % lignin, 60-67 % fiber, 6-7 % protein, 2-4 % ash, and 1-2 % fat (Kadiroglu, 2018). Peanut husks (*Arachis hypogaea*) used in the production of composite panels were obtained from Adana and Osmaniye provinces. Thinner peanut husk used in the outer layers were obtained by using a grinder. Coarse peanut husk used in the core layer were produced by using a 5 mm × 5 mm sieve. The thickness of the peanut husk is 0.1-0.5 mm, width is 2.1-7.8 mm and length is 1.1-7.9 mm. Peanut husks used in the core and outer layers are shown in Figure 1a and b.

a) b)

Figure 1 Peanut fibers: a) core layer fibers, b) outer layer fibers
Slika 1. Vlakna kikirikija: a) vlakna središnjeg sloja, b) vlakna vanjskog sloja

2.2 Wood particles
2.2. Drvne čestice

The fibers used in the production of composite panels were dried in an industrial dryer up to 1.4-3 % moisture and obtained from Yıldız Entegre, joint-stock company's composite panel factory in Bolu, Turkey. Wood fibers consist of 35 % Eastern Black Sea oak (*Quercus Pontica*), 45 % Black Pine (*Pinus nigra*), 10 % Aspen (*Populus tremula*), and 10 % workshop shav-

a) b)

Figure 2 Wood fibers: a) core layer fibers, b) outer layer fibers
Slika 2. Drvna vlakna: a) vlakna središnjeg sloja, b) vlakna vanjskog sloja

Table 1 Technical properties of adhesives
Tablica 1. Tehnička svojstva ljepila

Properties / *Svojstvo*	**UF**	**MF**	**FF**
Appearance / *Izgled*	White / *bijelo*	Transparent / *prozirno*	Red-brown / *crvenosmeđe*
Density (ρ) / *Gustoća (ρ)*	1.235-1.240 g/cm^3	1.225-1240 g/cm^3	1.200-1.210 g/cm^3
pH	7.5-8.7	8.5-9.5	10.5-13
Viscosity / *Viskoznost*	140-200 cP	100-200 cP	250-500 cP
Gelling time / *Vrijeme želiranja*	15 – 25 s.	70-110 s.	10-20 s.
Free formaldehyde / *Slobodni formaldehid*	Max.- 0.8 %	Max.- 0.8 %	Max.- 1 %
Mole ratio / *Molarni omjer*	1.45-1.55	1.80-1.85	1.50-1.55
Solid matter / *Suha tvar*	(55 ±1) %	(54 ±1) %	(55 ±1) %
Storage period / *Vrijeme skladištenja*	30 days/*dana*	20 days/*dana*	45 days/*dana*

Table 2 Experimental design
Tablica 2. Plan istraživanja

Panel type *Vrsta ploče*	**Peanut husk fiber, %** *Vlakna ljuske kikirikija, %*	**Wood fibers, %** *Drvna vlakna, %*	**Adhesive ratio, %** *Udio ljepila, %*	**Average density, g/cm³** *Srednja gustoća,* g/cm³
P1	100	0	100 UF	0.65
P2	100	0	95 UF + 5 MF	0.65
P3	100	0	95 UF + 5 FF	0.65
P4	75	25	100 UF	0.65
P5	75	25	95 UF + 5 MF	0.65
P6	75	25	95 UF + 5 FF	0.65
P7	50	50	100 UF	0.65
P8	50	50	95 UF + 5 MF	0.65
P9	50	50	95 UF + 5 FF	0.65
P10	25	75	100 UF	0.65
P11	25	75	95 UF + 5 MF	0.65
P12	25	75	95 UF + 5 FF	0.65

ings. There are no barks in the mixture formed. The thickness of the fibers varies between 0.2-0.6 mm, width 2.0-3.84 mm, and length 2.09-10.44 mm. The wood fibers used in the core and outer layers are shown in Figure 2a and b.

2.3 Adhesives
2.3. Ljepila

Urea-formaldehyde (UF), melamine-formaldehyde (MF) and phenol-formaldehyde adhesives are used in this study. Since these adhesives are widely used in the composite panel production industry, they were preferred for use in this research.

2.4 Methodology
2.4. Metodologija

Sustainable buildings and eco-design principles require low formaldehyde emissions and high fire resistance building materials. Composite panels used in the building and furniture sector should be produced in accordance with EN 312 (2010) product standard. The composite panels produced in this study were subjected to a combustion test according to ASTM E 160-50 (1975) standard and formaldehyde emission test according to EN 717-1 (2004) standard.

2.5 Preparation of testing samples
2.5. Priprema ispitnih uzoraka

The average density of manufactured composite panels was 0.65 g/cm³. The size of the composite panels was 18 mm × 500 mm × 500 mm. Since there are many studies on this subject, for the integrity of the results, we searched those studies and compared them. The experimental design of test samples can be seen in Table 2.

In order to determine a suitable adhesive rate, our previous studies and literature knowledge were taken into consideration. For this purpose, the ratio of the amount of adhesive used in the outer layers and the core layer to the total dry fiber mass was determined as 10 %. Press area was 50 cm ×50 cm and draft board panel thickness was assumed to be 18 mm with a total volume value of 4500 cm³.

The hardener was used in the prepared adhesive solution of 1 % ammonium sulfate $(NH_4)_2SO_4$. The production parameters of composite panels are displayed in Table 3.

Gluing was carried out using an adhesive gun in a circular moving mixer. A 60 cm × 60 cm guide forming frame was used in the preparation of the composite panel outline. The laying process was carried out in the forming frame, and three layers were produced by laying the surface, middle and other surface layers, respectively. 65 % of the thickness of the slab was formed by the core layer and 35 % by outer layers. The laying process was carried out homogeneously without disturbing the composite panel layers. The spreading process is shown in Figure 3a, b, and c.

Table 3 Production parameters of composite panels
Tablica 3. Proizvodni parametri kompozitnih ploča

Parameter / *Parametar*	**Value** / *Vrijednost*
Press temperature, °C *temperatura prešanja,* °C	165
Pressing time, min *vrijeme prešanja,* mm	7
Peak pressure, N/mm² *najveći tlak,* N/mm²	0.25
Thickness, mm *debljina,* mm	18
Dimensions, mm *dimenzije*, mm	500 × 500
$(NH_4)_2SO_4$, %	1
Outer layer, % *vanjski sloj,* %	35
Core layer, % *središnji sloj*, %	65
Number of panels for each type *broj ploča iste vrste*	5

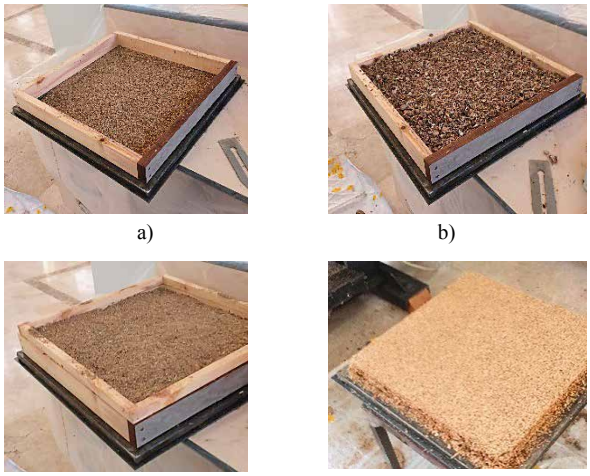

a) b) c) d)

Figure 3 Spreading process: a) outer layer, b) core layer, c) outer layer, d) after cold press
Slika 3. Postupak natresanja: a) vanjskog sloja, b) središnjeg sloja, c) vanjskog sloja, d) nakon hladnog prešanja

After completing the laying, the guide frame was removed and a cold-press was applied to the composite panel outline. After the cold-press, the composite panel draft was put into a hot press process. The composite panel outline after the cold-press is shown in Figure 3d.

In the hot pressing process, an electrically heated press, having an area of 60 cm × 60 cm, was used. After the hot press process, the composite panels were kept in the air conditioning cabinet for 24 hours.

2.6 Combustion test
2.6. Ispitivanje gorenja

The composite panels were manufactured in accordance with ASTM E 160-50 standard for the determination of the combustion properties. Before the combustion test, 72 test samples were prepared for each board type with the dimensions of 76 mm × 76 mm × 13 mm. Each sample group was weighed and stacked on the stand according to the test standard. The flame height was kept constant at (25±1.3) cm when the maker was empty and the gas pressure at the manometer was 0.5 kg/cm². In the funnel part, where the thermocouple is mounted, combustion was carried out at a temperature of (215±8) °C. The flame source was centered under the stack and flame-induced combustion (CWF) was continued for 3 minutes. Following the extinction of the flame source, the self-combustion (CWOF) and the core combustion (ECP) stages were performed. Measurements in the combustion stages were made at 15 s. 30 s. and 30 s. respectively, and temperature changes were read from the thermometer.

2.7 Formaldehyde emission test
2.7. Ispitivanje emisije formaldehida

The formaldehyde (HCHO) emission (FE) of the manufactured composite panels was determined in accordance with the European Norm EN 717-1. Formaldehyde emission levels of the manufactured composite panels were determined at Gazi University, Faculty of Technology Woodworking Industrial Engineering Department Wood Laboratory. Tests were carried out with a Multi-RAE lite PGM 6208 formaldehyde detector that works with photoionization technology. The test samples were placed in the test chamber, which allowed the test samples to remain under constant temperature and humidity, and formaldehyde emission (FE) values were measured.

FE was evaluated in accordance with EN 717-1. According to this method, test samples were placed in a constant humidity chamber with controlled temperature,

Table 4 Formaldehyde emission standards for composite panels in Europe and the USA (Groah *et al*., 1991)
Tablica 4. Norme za emisiju formaldehida kompozitnih ploča u Europi i SAD-u (Groah *et al*., 1991.)

Country *Država*	**Standard** *Norma*	**Test method** *Ispitna metoda*	**Board class** *Klasa ploče*	**Limit value** *Granična vrijednost*
Europe	EN 13986, 2004	EN 717-1	E1	≤ 0.1ppm (≤ 0.124 mg/m³)
		EN 120		≤ 8 mg/100
		EN 717-2		≤ 3.5 mg/m² h
		EN 717-1	E2	> 0.1 ppm (> 0.124 mg/m³)
		EN 120		> 8 ≤ 30 mg/100
		EN 717-2		> 3.5 ≤ 8.0 mg/m³ h
Australia & New Zealand	AS/NZS 1859-1, 2004	AS/NZS	E0	≤ 0.5 mg/L
		4266.16, 2004	E1	≤ 1.5 mg/L
		(Desiccator)	E2	≤ 4.5 mg/L
USA	ANSI A 208.1, 2009	ASTM E 1333	PB	≤ 0.18 ppm Phase 1 (2009)
		(large chamber)		≤ 0.09 ppm Phase 2 (2011)
Japan	JIS A 5908, 2003	JIS A 1460		≤ 1.5 mg/L
		(Desiccator)		≤ 0.5 mg/L
				≤ 0.3 mg/L

[a] At 23 °C and 1013 hPa, the following relationship exists for formaldehyde measured by EN 717-1: 1 ppm = 1.24 mg/m³ or 1 mg/m³ = 0.81 ppm
[a] *Pri 23 °C i 1013 hPa za formaldehid izmjeren prema EN 717-1 odnos je ovakav: 1 ppm = 1,24 mg/m³ ili 1 mg/m³ = 0,81 ppm.*

the air was continuously replaced and the test was completed when the emission reached a stable value. The international limiting values for the formaldehyde parameters of composite panels are presented in Table 4.

2.8 Data analyses
2.8. Analiza podataka

The aim of this study was to determine the effect of the peanut husk ratio, adhesive type, and its contents on the formaldehyde emission and combustion properties of the composite panel. One-way analysis of variance (ANOVA) was used to check the significant difference between factors and levels. When the ANOVA showed a prominent difference among factors and levels, a comparison of the means was defined by the Duncan test to see whether the differences between the groups were consequential or not.

3 RESULTS AND DISCUSSION
3. REZULTATI I RASPRAVA

3.1 Combustion temperatures
3.1. Temperature gorenja

In this study, combustion temperatures were measured in three steps. These steps can be expressed as combustion with flame (CWF), combustion without flame source (CWOF), and ember combustion phase (ECP). The highest temperatures of 187.00 °C, 406.67 °C and 145.00 °C during CWF, CWOF, and ECP, respectively, were observed in P1 type composite panels. The lowest temperatures of 313.67 °C, 147.67 °C and 99.67 °C during CWOF, CWF and ECP, respectively, were observed in P12 type composite panels. Combustion temperatures according to composite panel types are shown in Table 5.

According to the combustion steps, the highest temperature was measured during the CWOF process. In the combustion phase, the lowest temperature was achieved in the ECP. The highest combustion temperature was determined as 406.67 °C in the composite panels produced solely from peanut husk. The combustion temperatures of the composite panels produced with 100 % peanut husk additive (P1) were found highest. According to this; combustion temperatures (°C) were found as 187.00 °C in CWF stage, 406.67 °C in CWOF stage and 145 °C in ECP stage. It was observed that, when the peanut husk ratio decreased, the combustion temperatures also decreased. We have not found a relationship between adhesives and combustion temperatures. Considering the Duncan test results, in combustion stages, peanut husk ratio increases CWF, CWOF and ECP.

Peanut husk contains cellulose, lignin, and fat (Kadiroglu, 2018). The fat contained in peanut husk may have increased the combustion temperature.

By increasing the ratio of phenol-formaldehyde adhesive and adding boron minerals, the combustion properties of the composite panels produced with peanut husk can be improved. During CWF, CWOF, and ECP stages, combustion temperatures were 480 °C, 603 °C and 333 °C, respectively, in the combustion test of the Caucasian spruce (*Picea orientalis* L.) wood (Groah *et al.,* 1991).

As a result of research on the effect of glass wool and Rock wool on the combustion properties of particleboards, adhesive type did not affect ignition time and

Table 5 Combustion temperatures during combustion stages
Tablica 5. Temperature gorenja tijekom faza gorenja

Panel type *Vrsta ploče*	**Combustion with flame (CWF), °C** *Gorenje s plamenom (CWF)* °C	**HG[a]**	**Std$_{cwf}$**	**Combustion without flame source (CWOF), °C** *Izgaranje bez izvora plamena (CWOF),* °C	**HG[a]**	**Std$_{cwfo}$**	**Ember combustion (ECP), °C** *Sagorijevanje žara (ECP),* °C	**HG[a]**	**Std$_{ecp}$**
P1	187.00	a	12.74	406.67	a	29.93	145.00	a	13.28
P2	167.00	de	10.86	372.00	cd	26.91	120.00	f	11.79
P3	152.00	ij	11.51	343.67	h	27.31	108.33	jk	12.67
P4	154.33	hi	11.29	321.67	i	29.39	116.67	fg	11.94
P5	171.67	bc	11.04	391.00	ab	28.13	136.33	bc	12.27
P6	160.33	g	10.92	350.33	fg	26.98	114.00	hi	12.12
P7	164.67	ef	10.84	362.00	de	26.74	125.67	de	11.73
P8	149.33	jk	11.80	321.00	ij	29.47	112.00	ij	12.29
P9	167.33	d	10.87	372.00	cd	26.91	126.00	cd	11.73
P10	174.33	b	11.21	380.33	bc	27.30	138.67	ab	12.50
P11	156.33	h	11.14	355.00	ef	26.83	114.33	gh	12.10
P12	147.67	lm	12.01	313.67	jk	30.47	99.67	l	13.87
LSD = ± 6.74 °C				LSD = ± 24.32 °C			LSD = ± 8.51 °C		

[a] Homogeneous group ($p<0.05$) / *homogene skupine ($p<0,05$)*

mass loss. While flaming combustion temperature of PB with UF was 19 % higher, flaming combustion duration and smoldering combustion duration was 32 % and 29 % lower than that of PB with MF, respectively.

3.2 Illuminance values
3.2. Vrijednosti osvjetljenja

During the first combustion stage, combustion with flame (CWF), the highest illuminance values were observed in composite panels P8 produced using 50 % peanut husk fibers and 50 % wood fibers and 95 % UF and 5 % MF. During CWF, the lowest illuminance values were observed in composite panels P8 produced using 50 % peanut husk fibers and 50 % wood fibers, and 95 % UF and 5 % FF. According to these results, FF adhesive decreased illuminance values.

During the second combustion stage (CWOF), the highest illuminance value was measured in composite panels P3 produced with 100 % peanut husk and 95 % UF, 5 % FF. The lowest illuminance values were observed in composite panels P10 produced using 25 % peanut husk and 100 % urea-formaldehyde adhesive.

During the third combustion stage, the ember combustion phase (ECP), the highest illuminance values were observed in composite panels P8 produced using 50 % peanut husk fibers and 50 % wood fibers, and 95 % UF and 5 % MF. During ECP, the lowest illuminance values were found in composite panels P5 produced using 75 % peanut husk fibers and 25 % wood fibers, and 95 % UF and 5 % MF. According to these results, FF adhesive decreased illuminance values. Table 6 shows the illuminance values according to composite panel types.

According to combustion type, the highest illuminance values of 976.07 lux were observed in the ECP and the lowest of 952.55 lux in the CWF stage. According to the peanut additive ratio, the highest illuminance values of 968.92 lux were observed in 50 % peanut added composite panels. The lowest illuminance values of 952.21 lux were observed in composite panels with 75 % peanut husk additive. When the adhesive type is considered, the illuminance values of 5 % FF + 95 % UF glued composite panels are measured as 974.03 lux. The illuminance value of the composite panels produced with 100 % UF adhesive was 954.03 lux.

Considering the data obtained from the experiments and Duncan test results, it was observed that there were statistical differences between the produced panels. However, there was no correlation between the peanut husk ratio and adhesive type with illuminance values during combustion stages. The results of production on an industrial scale may produce more pronounced results than the panels produced in the laboratory.

A high illuminance value means less smoke. Less smoke reduces the risk of smoke poisoning. It is seen that there is no significant difference between the test samples in terms of smoke density. Therefore, it can be said that composite panels produced with wood fibers and composite panels produced with peanut husk have similar properties.

3.3 Combustion times and mass loss
3.3. Vrijeme gorenja i gubitak mase

During combustion stages, the shortest combustion time was observed in P3 type composite panels as 1440.00 sec. The longest combustion time was ob-

Table 6 Illuminance values during combustion stages
Tablica 6. Vrijednosti osvjetljenja tijekom faza gorenja

Panel type *Vrsta ploče*	**Combustion with flame (CWF), lux** *Gorenje s plamenom (CWF),* lux	**HG[a]**	**Std$_{cwf}$**	**Combustion without flame source (CWOF), lux** *Izgaranje bez izvora plamena (CWOF),* lux	**HG[a]**	**Std$_{cwfo}$**	**Ember combustion (ECP), lux** *Sagorijevanje žara (ECP),* lux	**HG[a]**	**Std$_{ecp}$**
P1	987.67	bc	35.07	944.00	gh	27.64	973.00	gh	32.82
P2	952.06	i	34.37	938.77	hi	27.80	908.07	mn	37.84
P3	983.94	cd	34.87	995.78	a	30.04	984.42	f	32.89
P4	960.59	gh	34.28	983.78	ab	28.87	1006.71	bc	33.89
P5	915.69	l	36.51	934.89	ij	27.97	931.39	lm	35.07
P6	909.24	lm	37.17	946.28	fg	27.59	981.30	fg	32.84
P7	996.91	ab	35.70	979.48	bc	28.53	1004.51	cd	33.74
P8	1005.24	a	36.41	975.76	cd	28.28	1012.14	a	34.30
P9	896.97	mn	38.61	910.97	k	29.86	938.28	l	34.44
P10	983.07	de	34.82	903.54	kl	30.71	965.07	hi	32.95
P11	965.58	fg	34.31	949.41	f	27.55	999.98	de	33.47
P12	975.11	ef	34.50	967.98	de	27.87	1008.00	ab	33.98
LSD = ± 19.46 lux				LSD = ±17.64 lux			LSD = ±12.49 lux		

[a]Homogeneous group (p<0.05) / *homogene skupine (p<0,05)*

Table 7 Combustion times and mass loss during combustion stages
Tablica 7. Vrijeme gorenja i gubitak mase tijekom faza gorenja

Panel type *Vrsta ploče*	**Combustion, sec** *Gorenje,* s	**HG** [a]	**Std$_c$**	**Mass loss, %** *Gubitak mase, %*	**HG**[a]	**Std$_{wl}$**
P1	1547.78	h	244.99	46.50	a	7.33
P2	1506.67	hg	248.89	34.87	ea	6.50
P3	1440.00	i	256.16	30.82	g	6.57
P4	1715.56	fg	234.23	29.42	gb	6.64
P5	1783.33	e	232.39	42.23	b	6.86
P6	1733.33	f	233.60	30.20	ga	6.60
P7	2021.11	c	237.90	35.02	e	6.51
P8	1973.33	cd	235.32	25.70	h	6.93
P9	1984.44	cd	235.86	40.51	c	6.73
P10	2080.00	ab	242.03	39.02	d	6.63
P11	2093.33	A	243.11	33.55	f	6.51
P12	2098.89	A	243.58	23.97	i	7.11
LSD = ± 828.17 sec			LSD = ± 1.28 %			

[a] Homogeneous group ($p<0.05$) / *homogene skupine ($p<0,05$)*

served in P12 type composite panels as 2098.89. The highest mass loss (46.50 %) was observed in P1 type composite panels. The lowest mass loss (23.97 %) was observed in P12 type composite panels. Combustion times and mass loss are shown in Table 7.

Combustion times, according to the peanut additive ratio and adhesive type, were detected longest in P12 as 2098.89 seconds, while the shortest time decreased by 31.33 %, seen in P3 boards as 1440.00 seconds. It has been determined that the boards with more peanut husk additives burned faster and that their burning time was shorter than that of the boards with less additives. This could be explained by the fact that the peanut husk burned faster than wood fibers and the charring time was longer in wood fibers. As a result of the experiments, it was understood that when the peanut husk additive ratio increased, combustion time was reduced.

The total mass loss was measured as 46.50 % in P1 boards. As the peanut husk additive ratio decreased, total mass loss also decreased and it was 23.97 % in P12 boards. Regarding the total mass losses, it has been determined that the peanut husk showed incineration faster at lower temperatures than wood fibers. As a result, it was determined that the total mass loss at the end of the combustion process increased as the peanut husk additive ratio increased. When the adhesive type is taken into consideration, it is seen that the FF additive ratio reduced the combustion time because of the characteristics of the adhesive.

According to the result of research on the effect of glass wool and rock wool on the combustion properties of particleboards, adhesive type did not affect ignition time and mass loss. While flaming combustion temperature of PB with UF was 19 % higher, flaming combustion duration and smoldering combustion duration was 32 % and 29 % lower than that of PB with MF, respectively (Ulker and Burdurlu, 2015).

3.4 Formaldehyde emissions
3.4. Emisija formaldehida

Engineered wood composites, including plywood, particleboard, and fiberboard, used as furniture components, mostly contain formaldehyde resins as adhesive. Adhesives, flame-retardant chemicals, and paints are used in engineered wood products (EWPs) to increase some of the properties of wood. (Ulker and Ulker, 2019). Some issues should be considered when using recycled wood wastes for further reutilization, such as the release of formaldehyde from particleboard used as an interior building product due to incompletely reacted urea-formaldehyde (UF), melamine-formaldehyde (MF), and phenol-formaldehyde (PF) resins in particleboard. As a result, indoor air quality can worsen, posing a major health concern, particularly in modern homes and workplaces, which are often more airtight than older buildings.

Formaldehyde emissions were measured twice for each board - one hour and 24 hours after production. Formaldehyde emission test results after composite panel production are shown in Table 8.

The results of formaldehyde emission one hour after manufacturing were approximately 70 % higher than the results after 24 hours. The emission values returned to an acceptable level after 24 hours. The result is displayed in Figure 4.

We found a negative relationship between wood fiber additive ratios and formaldehyde emissions. This can be explained by the lower bonding performance among the peanut husks. When the peanut husk additive ratio increased, formaldehyde emission values also increased.

The lowest formaldehyde emission values were observed in the mixture of 95 % UF + 5 % MF adhesives in P11 type composite panel, and the highest formaldehyde emission values were obtained in compos-

Table 8 Formaldehyde emissions
Tablica 8. Emisije formaldehida

Panel type *Vrsta ploče*	**One hour after composite panel manufacturing, ppm** *Jedan sat nakon izrade kompozitne ploče,* ppm	**Std_{1h}**	**24 hours after composite panel manufacturing, ppm** *24 sata nakon izrade kompozitne ploče,* ppm	**Std_{24h}**
P1	0.28	0.03	0.08	0.01
P2	0.24	0.03	0.06	0.01
P3	0.26	0.03	0.06	0.01
P4	0.26	0.03	0.06	0.01
P5	0.22	0.03	0.04	0.01
P6	0.26	0.03	0.06	0.01
P7	0.25	0.03	0.05	0.01
P8	0.23	0.03	0.05	0.01
P9	0.23	0.03	0.05	0.01
P10	0.21	0.03	0.06	0.01
P11	0.17	0.03	0.03	0.01
P12	0.20	0.03	0.06	0.01

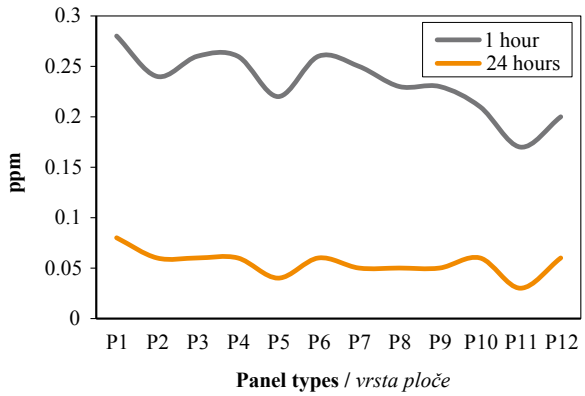

Figure 4 Formaldehyde emission results
Slika 4. Vrijednosti emisije formaldehida

ite panels made solely with the peanut husk P1 type composite panels.

Composite panels often have problems with satisfying board formaldehyde emission requirements of the El class, which stipulates a maximum emission of 0.1 ppm formaldehyde emission. The composite panels were tested 24 hours after the manufacturing process. According to the test results, all manufactured composite panels met the requirements of E1 board formaldehyde class. These composite panels may be suitable for indoor air quality conditions for green buildings. The coating of the composite panel and the low mole ratio of formaldehyde in adhesive may be further reduced to the FE in the manufactured panel.

4 CONCLUSIONS
4. ZAKLJUČAK

The manufactured composite panels were subjected to combustion and formaldehyde tests. The highest combustion temperatures of 187.00 °C, 406.67 °C and 145.00 °C were observed during CWF, CWOF and ECP, respectively, in P1 type composite panels. The lowest temperatures during of 313.67 °C, 147.67 °C and 99.67 °C during CWOF, CWF and ECP, respectively, were observed in P12 type composite panels.

The combustion temperatures of the composite panels produced with 100 % peanut husk additive (P1) were found highest. According to this, combustion temperatures of 187.00 °C were found in CWF stage, 406.67 °C in CWOF stage and 145 °C in ECP stage. It was observed that, when the peanut husk ratio decreased, the combustion temperatures also decreased. We have not found a relationship between adhesives and combustion temperatures.

During the first combustion stage, combustion with flame (CWF), the highest illuminance values were observed in composite panels P8 produced using 50 % peanut husk fibers and 50 % wood fibers, and 95 % UF and 5 % MF. During CWF, the lowest illuminance values were observed in composite panels P8 produced using 50 % peanut husk fibers and 50 % wood fibers, and 95 % UF and 5 % FF. According to these results, FF adhesive decreased illuminance values.

In terms of peanut additive ratio and adhesive type, the longest combustion time of 2098.89 seconds was detected in P12, while the shortest time of 1440.00 seconds, with a decrease of 31.33 %, was observed in P3 boards. It has been determined that the panels with more peanut husk additives burn faster and that the burning time is shorter than that of the boards with less additives. This could be explained by the fact that the peanut husk burned faster than wood fibers and the charring time was longer in wood fibers. As a result of the experiments, it was understood that when the peanut husk additive ratio increased, combustion time was reduced.

The total mass loss was measured as 46.50 % in P1 boards. As the peanut husk additive ratio decreased,

total mass loss also decreased and it was 23.97 % in P12 boards. Regarding the total mass losses, it has been determined that the peanut husk showed incineration faster at lower temperatures than wood fibers. As a result, it was determined that the total mass loss at the end of the combustion process increased as the peanut husk additive ratio increased. When the adhesive type is taken into consideration, it is seen that the FF additive ratio reduced the combustion time because of the characteristics of the adhesive.

According to the test results, all manufactured composite panels met the requirements of E1 board formaldehyde class. These composite panels may be suitable for indoor air quality conditions for green buildings. The coating of the composite panel and the low mole ratio of formaldehyde in adhesive may be further reduced to the FE in the manufactured panel. We found a negative relationship between wood fiber additive ratios and formaldehyde emissions. This can be explained by the lower bonding performance among the peanut husks. When the peanut husk additive ratio increased, formaldehyde emission values also increased.

Acknowledgements – Zahvala

This paper is a part of the PhD Thesis, prepared by Ersin ERCAN, Institute of Science and Technology, Gazi University, Ankara, Turkey.

5 REFERENCES
5. LITERATURA

1. Atılgan, A.; Peker, H., 2012: Some physical properties effects of various wood preservatives used in furniture and construction industry wood species. Artvin Coruh University Journal of Forestry Faculty, 13 (1): 67-78.
2. Bekalo, S. A.; Reinhardt, H. W., 2010: Fibers of coffee husk and hulls for the production of particleboard. Materials Science, 43: 1049-1060. https://doi.org/10.1617/s11527-009-9565
3. Buyuksari, U.; Ayrilmis, N.; Avci, E.; Koc, E., 2010: Evaluation of the physical, mechanical properties and formaldehyde emission of particleboard manufactured from waste stone pine cones. Bioresource Technology, 101 (1): 255-259. https://doi.org/10.1016/j.biortech.2009.08.038
4. Fiorelli, J.; Curtolo, D. D.; Barrero, N. G.; Savastano, H.; Pallone, E. M. J. A.; Johnson, R., 2012: Particulate composite based on coconut fiber and castor oil polyurethane adhesive: An eco-efficient product. Industrial Crops and Products, 40: 69-75. https://doi.org/ 10.1016/j.indcrop.2012. 02.033
5. Gurjar, R. M., 1993: Effect of different binders on properties of particleboard from cotton seed hulls with emphasis on water repellency. Bioresource Technology, 43 (2): 177-179. https://doi.org/10.1016/0960-8524(93)90179-F
6. Groah, W. J.; Bradfield, J.; Gramp, G.; Rudzinski, R.; Heroux, G., 1991: Comparative response of reconstituted wood products to European and North American test methods for determining formaldehyde emissions. Environmental Science & Technology, 25 (1): 117-122. https:// doi.org/10.1021/es00013a012
7. Fernandez, J., 2006: Material architecture: emergent materials for innovative buildings and ecological construction, Architectural Press: Elsevier, Boston, USA.
8. Fidan, M. S.; Yasar, S. S.; Yasar, M.; Atar, M.; Alkan, E., 2016: Characterization of the combustion parameters of impregnated and varnished cedar wood (*Cedrus libani* A. Rich). Forest Products Journal, 66 (5/6): 290-298.
9. Hulme, J.; Radford, N., 2010: Sustainable supply chains that support local economic development; prince's foundation for the built environment. United Kingdom, pp. 19-22.
10. Kadiroglu, A., 2018: Peanut Growing, West Mediterranean Research Institute, Antalya.
11. Keskin, H.; Kucuktuvek, M.; Guru, M., 2015: The potential of poppy (*Papaver somniferum* L.) husk for manufacturing wood-based particleboards. Construction and Building Materials, 95: 224-231. https://doi.org/10.1016/j.conbuildmat.2015.07.160
12. Kim, S.; Kim, J. A.; Kim, H. J.; Kim, S. D., 2006: Determination of formaldehyde and TVOC mission factor from wood based composites by small chamber method. Polymer Testing, 25 (5): 605-614. https://doi.org/10.1016/j.polymertesting.2006.04.008
13. Kim, S.; Kim, H. J., 2005: Comparison of standard methods and gas chromatography method in determination of formaldehyde emission from MDF bonded with formaldehyde-based resins. Bioresource Technolology, 96 (13): 1457-1464.https://doi.org/10.1016/j.biortech.2004.12.003
14. Nemli, G.; Kırcı, H.; Serdar, B.; Ay, N., 2007: Suitability of kiwi (*Actinidia sinensis* Planch) prunings for particleboard manufacturing, Industrial Crops and Products, 26 (3): 252-258. https://doi.org/10.1016/j.indcrop.2007.03.016
15. Nemli, G.; Aydin, A., 2007: Evaluation of the physical and mechanical properties of particleboard made from the needle litter of *Pinus pinaster* Ait. Industrial Crops and Products, 26 (3): 252-258. https://doi.org/10.1016/j.indcrop.2007.03.016
16. Ntalos, G. A.; Grigoriou, A. H., 2002: Characterization and utilization of vine prunings as a wood substitute for particleboard production. Industrial Crops and Products, 16 (1): 59-68. https://doi.org/10.1016/S0926-6690(02)00008-0
17. Pulselli, R. M.; Simoncini, E.; Pulselli, F. M.; Bastianoni, S., 2007: Energy analysis of building manufacturing, maintenance and use: Em-building indices to evaluate housing sustainability. Energy and Buildings, 39: 620-628. https://doi:10.1016/j.enbuild.2006.10. 004
18. Ries, R.; Bilec, M.; Gokhan, N. M.; Needy, K. L., 2006: The economic benefits of green buildings: a comprehensive case study. The Engineering Economist, 51 (3): 259-295. https://doi.org/ 10.1080/00137910600865469
19. Seyfang, G., 2010: Community action for sustainable housing: Building a low-carbon future. Energy Policy, 38 (12): 7624-7633. https://doi.org/10.1016/j.enpol.2009.10.027
20. Terzi, E., 2008: Characteristics burning of wood material impregnated with ammonium compounds, MSc Thesis, Istanbul University, Inst. of Nat. App. Sci., Department of Forestry Industry Engineering, Istanbul, pp. 106-109.
21. Ulker, O. C.; Ulker, O., 2019: Toxicity of formaldehyde, polybrominated diphenyl ethers (PBDEs) and phthalates in engineered wood products (EWPs) from the perspective of the green approach to materials: A review. BioResources, 14 (3): 7465-7493.

22. Ulker, O.; Burdurlu, E., 2015: Effects of some mineral wools and adhesives on burning characteristics of particleboard. BioResources, 10 (2): 3775-3789.
23. Ulker, O.; Burdurlu, E., 2016: Effect of glass wool and stone wool additives on some mechanical properties of wood composites. BioResources, 11 (3): 5974-5986.
24. Umar, U. A.; Khamidi, M. F.; Tukur, H., 2012: Sustaınable building material for green building construction, conservation and refurbishing. Conference: Management in Construction Research Association (MiCRA) Postgraduate Conference, pp. 5-6.
25. Yasar, S. S.; Fidan, M. S.; Yasar, M.; Atar, M.; Alkan, E., 2017: Combustion properties of impregnated spruce (*Picea orientalis* L.) wood. Construction and Building Materials, 143: 574-579. https://doi.org/10.1016/j.conbuildmat.2017.03.141
26. Yudelson, J., 2008: The green building revolution. Journal of Real Estate Literature, 16 (2): 253-255. https://www.jstor.org/stable/44105048
27. Venkatarama, R. B. V.; Jagadish, K. S., 2003: Embodied energy of common and alternative building materials and technologies. Energy and Buildings, 35 (2): 129-137. https://doi.org/ 10.1016/S0378-7788(01)00141-4
28. ***ASTM E 160-50, 1975: Standard test method for combustible properties of treated wood by the crib test.
29. ***EN 312, 2010: Wood-based panels: Particleboards specifications.
30. ***EN 717-1, 2004: Wood-based panels – Determination of formaldehyde release. Part 1: Formaldehyde emission by chamber method.

Corresponding address:

Assoc. Prof. MUSTAFA KUCUKTUVEK, PhD
İskenderun Technical University (ISTE), Faculty of Architecture, Department of Interior Architecture, Merkez Kampüs, 31200, İskenderun, Hatay, TURKEY, email: mustafa.kucuktuvek@iste.edu.tr

Igor Đukić[1], Miran Merhar[2], Juraj Jovanović[1], Darko Herceg[1]

Analysis of Circular Saw Tooth Marks Profile on Material Machined Surface After Filtering with Fast Fourier Transform (FFT)

Analiza profila kinematičkih tragova zubi lista kružne pile na obrađenoj površini materijala provedena filtriranjem na načelu brze Fourierove transformacije (FFT)

ORIGINAL SCIENTIFIC PAPER
Izvorni znanstveni rad
Received – prispjelo: 27. 1. 2022.
Accepted – prihvaćeno: 23. 3.2022.
UDK: 620.179.118; 621.934; 630*82
https://doi.org/10.5552/drvind.2022.0011

ABSTRACT • *The article presents theoretical analysis of machined surface roughness after sawing on circular saw and implementation of fast Fourier transform (FFT) as a possible simple filtering method for filtering out just the saw blade and saw tooth influence on the surface roughness. Surface roughness profile is represented as a signal that can be obtained as a sum of complex periodic signals that represent theoretical profile of tooth marks and lateral movement of tooth due to saw lateral movement and signals that represent structural roughness of wood combined with machining roughness, represented as a Gaussian noise. The application of FFT based filtering on such a signal can be effectively used to extract the main frequency components due to tool influence on total surface signal and the time domain of filtered signals display can then be obtained by use of the inverse Fourier transform. In order to test the theoretical assumptions, the machining tests in sawing of solid oak wood (Quercus robur L.) and medium density fiberboard (MDF) was conducted. Machined surface roughness was measured and analyzed in accordance with theoretical assumptions. It was concluded that a combination of discrete Fourier transform of surface roughness profile and standard roughness parameters can give a more complete representation of machined surface roughness after sawing with circular saws and that filtering of surface roughness profile signal with FFT filter can be used as a simple and effective method in quantifying tool influence on machined surface roughness after sawing on circular saw in varying machining conditions and on different workpiece material.*

KEYWORDS: *machined surface roughness; circular saw; solid wood; signal analysis; FFT*

SAŽETAK • *U radu je prikazana teorijska analiza hrapavosti obrađene površine nakon piljenja kružnom pilom i primjena brze Fourierove transformacije (FFT) kao moguće metode filtriranja profila hrapavosti radi jednostavnog načina kvantificiranja utjecaja bočnog pomaka lista pile i zubi na ukupnu hrapavost obrađene površine.*

[1] Authors are associate professor, PhD student and graduate student at Faculty of Forestry and Wood Technology, University of Zagreb, Croatia.
[2] Author is assistant professor at University of Ljubljana, Biotechnical Faculty, Department of Wood Science and Technology, Ljubljana, Slovenia.

Profil hrapavosti površine opisan je kao signal koji se može dobiti kao zbroj složenih periodičnih signala koji daju teorijski profil kinematičkih tragova zubi i njihova bočnog pomaka zbog lateralnoga gibanja lista pile te signala koji predočuje strukturnu hrapavost drva i hrapavost zbog obrade, a opisan je kao Gaussov šum. Primjena filtra utemeljenoga na FFT-u na takvom signalu može se učinkovito iskoristiti za izdvajanje glavnih frekvencijskih komponenata signala vezanih za utjecaj alata na ukupnu hrapavost, a prikaz filtriranog signala može se pritom dobiti primjenom inverzne Fourierove transformacije. Kako bi se provjerile teorijske pretpostavke, provedena su ispitivanja pri piljenju masivnog drva hrastovine (Quercus robur L.) i ploče vlaknatice srednje gustoće (MDF). Izmjerena je i analizirana hrapavost obrađene površine u skladu s teorijskim pretpostavkama. Zaključeno je da kombinacija diskretne Fourierove transformacije profila hrapavosti površine i standardnih parametara hrapavosti može dati potpuniji prikaz hrapavosti obrađene površine nakon piljenja kružnim pilama te da se filtriranje signala profila hrapavosti površine uz pomoć FFT filtra može primjenjivati kao jednostavna i učinkovita metoda za kvantificiranje utjecaja alata na hrapavost obrađene površine nakon piljenja kružnom pilom u različitim uvjetima obrade i na različitom materijalu uzorka.

KLJUČNE RIJEČI: *hrapavost obrađene površine; kružna pila; masivno drvo; analiza signala; FFT*

1 INTRODUCTION
1. UVOD

Theoretical profile of tooth marks on machined surfaces after sawing with circular saw can be determined from the analysis of an ideal interaction of tool and workpiece in the given machining conditions. Based on such analysis, the profile of kinematic traces of the tool tip on machined surface can be determined and the parameter that is usually derived as the representative parameter is the maximum height of those traces in given machining conditions (Zdenković, 1965; Šavar, 1990; Goglia, 1994; Gottlöber, 2014; Csanády, 2015). On the other hand, the parameters that are usually used in solid wood machining research as a representative parameters to quantify the surface roughness or waviness based on measurements are R_a (W_a), R_q (W_q) and R_z (W_z), which according to ISO 4287: 1997 represent the arithmetic mean of the absolute ordinate values within the sampling length, the root mean square value of the ordinate values within the sampling length and the average of the sum of height of the largest profile peak height and the largest profile valley absolute depth within a sampling length, respectively. Those parameters are used to determine the surface roughness which is the sum of the:

- structural roughness due to anatomical characteristics of wood, which is not a function of machining process,
- machining roughness caused by machining that cannot be represented as some periodic signals and
- kinematic roughness due to teeth marks and lateral movement of the saw blade, which can be represented as complex periodic signals.

The effect of structural roughness in solid wood machining can have a big impact on the overall surface roughness, depending on the wood species, and it can be hard to distinguish between structural roughness and roughness due to machining (Gottlöber, 2014). The possibility of removing or quantifying the impact of structural roughness from measured surface profiles has been a topic of research projects (Csiha, 2000; Magoss and Sitkei, 2003; Fujiwara *et al*. 2003; Hendarto *et al.* 2006; Gurau, 2006; Magoss, 2008; Thoma, 2015), but at present there is no single solution to this problem.

According to Goli (2005), in order to better evaluate the surface quality, the primary profile (*P*), which is the sum of all the deviations of the measured profile from the nominal profile, should be analyzed and it is used in some cases (Sandak *et al.* 2020). Also, the other standard profile parameters, like Abbott curve, R_{vk}, R_{pk}, R_k, are proposed for the assessment of surface roughness (Magoss, 2008; Gottlöber, 2014). Surface roughness is a key element in characterisation of surface quality and relation to human perception of that quality and some technological properties of those surfaces (Sinn *et al*., 2009). There are a lot of parameters introduced in order to quantify the relationship between measurable quantities associated with roughness and the end goal of such analysis (Sandak and Negri, 2005).

As can be seen from this short overview, the machined surface quality of solid wood is still hard to exactly define and connect to theoretical surface roughness, which can be calculated from the tool-workpiece interaction relations and there is no single best way to do it. On the other hand there is interest, even in circular sawing of solid wood, in using measurable roughness parameters to quantify the influence of different process parameters on machined surface quality (Budakçi *et al*., 2011; Kminiak and Gaff, 2015; Kminiak *et al*., 2015, Lee *et al*., 2017) or to optimize the sawing process based on measurable surface roughness or waviness parameters (among other influential quantities) (Nasir and Cool, 2019). According to authors' experience and based on the literature (Orlowski, 2010), common use of standard roughness parameters with standard filtering, which is usually used for analysis of machined surface roughness after sawing with

circular saws, can give misleading results. According to Brock (1983), better results can be obtained by combining standard parameters with Fourier analysis of surface roughness signal, which can give a nearly complete description of surface roughness.

Combining the ideas of using Fourier transform for roughness analysis and signal filtering based on Fourier transform, a procedure for separating part of the signal that should describe kinematic roughness and the rest of the signal remaining after filtering that should mainly describe structural and machining roughness can be made. After that, individual signals can be described by standard roughness parameters and the influence of individual components on the overall roughness can be easily quantified. In the rest of the article, this procedure is presented from the theoretical and experimental point of view.

1.1 Theoretical analysis of machined surface roughness after sawing on circular saws
1.1. Teorijska analiza hrapavosti obrađene površine nakon piljenja kružnim pilama

The circular saw in conventional sawing, with parameters relevant for the calculation of the tooth marks theoretical height on a machined surface, can be represented by Figure 1.

In order to calculate the theoretical roughness height (h_c), we can use Eq. 1

$$h_c = \delta \cdot tan\varepsilon \tag{1}$$

Where δ is chip thickness and ε is saw tooth radial side clearance angle.

As can be seen, the theoretical roughness height changes during one tooth pass and the maximum value is given by

$$\begin{aligned} h_{c_{max}} &= \delta_{max} \cdot tan\varepsilon \\ h_{c_{max}} &\approx f_z \cdot cos\varphi_2 \cdot tan\varepsilon \\ h_{c_{max}} &\approx f_z \cdot cos\left[sin^{-1}\left(\frac{D/2 - p}{D/2} \right) \right] \cdot tan\varepsilon \end{aligned} \tag{2}$$

Where D is circular saw blade diameter, f_z is feed per tooth and p is protrusion of the saw blade above worktable.

From the theoretical roughness profile after sawing with circular saw (Figure 1), it can be seen that, if the actual roughness profile was dominated by kinematic traces of saw teeth, the standard roughness parameter that would closely resemble the theoretical roughness is R_t, which represents the vertical height between the highest and lowest points of the profile within the evaluation length, and the distance between consecutive peaks (f_z) would be equal to the spacing distance RS_m.

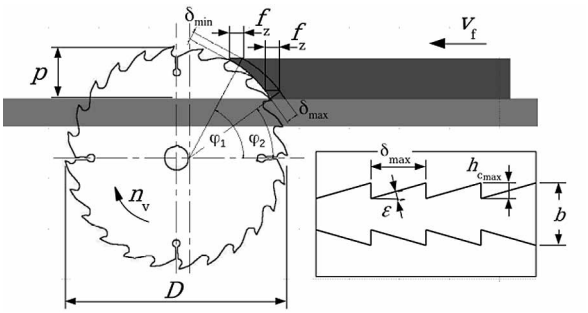

Figure 1 Circular saw in conventional sawing and theoretical profile of tooth marks on machined surface after sawing
Slika 1. Kružna pila u protusmjernom rezu i teoretski profil neravnina na obrađenoj površini nakon piljenja

In such an ideal case, and according to recommended feed per tooth ranges (Leitz Lexicon, 2020), the maximum theoretical roughness height would be (if we take that δ_{max} is roughly equal to f_z and side (radial) clearance angle for tungsten carbide (HW) tipped saw blade ε = 1°) in the range from 2 µm to 16 µm.

The real roughness profile is much more complicated and that is why all the different parameters, mostly R_a, R_q and R_z, are used. One of the reasons for this can be attributed to the difference between the actual and ideal tooth shape, which can be due to different reasons (lack of tooth symmetry, deviation from the center line, wrong cutting angles) and results in a flutter or washboarding (Orłowski and Wasielewski, 2006). On the other hand, circular saw blade lateral vibration due to cutting-induced vibration is identified as a main cause for washboarding. All of this lateral vibration is superimposed on the ideal tooth path in the workpiece. What is common to all these influences on lateral movement is that they can all be represented as complex periodic functions (Tian and Hutton, 2001). Structural roughness of wood also plays an important role in roughness profile.

1.2 Signal analysis of machined surface roughness profile
1.2. Analiza signala profila hrapavosti obrađene površine

Surface roughness profile can be thought of as a signal. Signals are usually modeled mathematically in order to make them unambiguous, precise and manipulable (Lee and Varaiya, 2002). Theoretical profile of tooth marks on machined surface after sawing with a circular saw can be represented as a saw-tooth signal (Figure 1) and Eq. 3 used to describe it (Weisstein, 2020) can be derived as follows:

$$h_i(x) = h_c \cdot \left(\frac{1}{2} - \frac{tan^{-1}\left(cot\left(\frac{x \cdot \pi}{f_z} \right) \right)}{\pi} \right) \tag{3}$$

Where h_i is instantaneous profile height as a function of position.

From a signal analysis perspective, it is more convenient to deal with functions of time, rather than position. Surface roughness profiles are mostly obtained by means of stylus, which traverses surface with speed (v_s) according to ISO 3274, and as a result of measurement, we get a finite set of points, which represent discrete signals that are separated by some constant distance (Δx). So, if the time difference is introduced between two samples (Δt_s)

$$\Delta t_s = \frac{\Delta x}{v_s} \tag{4}$$

then the time difference between two consecutive peaks of saw-tooth profile (Δt_z) is

$$\Delta t_z = \frac{f_z}{v_s} \tag{5}$$

Then the instantaneous profile height can be written as a function of time

$$h_i(t) = h_c \cdot \left(\frac{1}{2} - \frac{tan^{-1}\left(cot\left(\frac{t \cdot \pi}{\Delta t_z} \right) \right)}{\pi} \right) \tag{6}$$

According to Tian and Hutton (2001) the lateral movement of saw blade (y_i), if we assume that only one mode of vibration is excited, can be written as simple periodic function of time

$$y_i(t) = A_0 \cdot cos\left(2 \cdot \pi \cdot f_n \cdot t\right) \tag{7}$$

Where f_n is the resonant frequency of the saw blade and A_0 is the amplitude of sawtooth tip lateral movement.

If there are n teeth passing through the same horizontal line in the time period Δt, then the lateral displacement in the space domain - $y_z(x)$ is

$$y_z(x) = A_0 \cdot cos\left(2 \cdot \pi \cdot \left[\frac{f_t - f_n}{v_f} \right] \cdot x \right) \tag{8}$$

Where f_t is the tooth passing frequency and it can be expressed as

$$f_t = n_v \cdot z \tag{9}$$

Where z is the number of circular saw teeth and n_v is rotational frequency of the saw.

As can be seen from (8), the wavelength of the washboarding pattern (λ_x) can be expressed as

$$\lambda_x = \frac{v_f}{f_t - f_n} \tag{10}$$

This wavelength could represent a problem for roughness analysis with standard cut-off filters and evaluation lengths. In some cases this wavelength can be in the range close to 30 mm (Tian and Hutton, 2001) and because of its large values it could be filtered out as a form signal or inadequate length of signal could be sampled for reliable determination of washboarding pattern frequency and its influence on machined surface roughness.

If $y_z(x)$ signal is to be represented as a function of time, than λ_x can be converted to frequency (f_{fx})

$$f_{fx} = \frac{v_s}{\lambda_x} \tag{11}$$

If we assume that structural roughness of wood can be represented as a Gaussian noise (Lemaster and Taylor, 1999) and machining roughness can also be represented as a Gaussian noise and combined in one non-deterministic signal - $p(x)$, then the signal that represents all of these influences on resultant profile would be a sum of these signals $y_r(x) = h_i(x) + y_z(x) + p(x)$. It is assumed that form errors are filtered out and do not influence the final roughness profile (this assumption holds if standard roughness or waviness profiles, obtained with adequate cut-off filters in line with ISO 4288, are analyzed). From this resultant signal (y_r), standard roughness parameters can be calculated. If such a profile was measured with digital surface roughness meter, it would be represented by discrete signal and R_a parameter can be calculated as

$$R_a = \frac{1}{N} \cdot \sum_{i=1}^{N} \left| y_{ri} \right| \tag{12}$$

and R_q parameter can be calculated as

$$R_q = \sqrt{\frac{1}{N} \cdot \sum_{i=1}^{N} y_{ri}^2}, \tag{13}$$

Where N is the number of samples in measurement.

So, if one knew or measured all of the relevant parameters to quantify the $h_i(x)$ and $y_z(x)$, the calculation of tool influence on resulting surface roughness would be straightforward, but in practice that can be hard to accomplish and because much of the signal could be dominated by structural roughness, it can even lead to wrong conclusions (Brock, 1983).

According to Lemaster and Taylor (1999), low-pass filtering of roughness profile with different cut-off frequencies could be used for fuzziness or tear-out detection.

A combination of these methods can be used as a basis for filtering out most of the signal that represents the tool influence in measured surface roughness signal.

Any periodic signal can be represented by Fourier series (Kreyszig, 2011)

$$f(x) = a_0 + \sum_{n=1}^{\infty} \left(a_n \cdot cos\left(n \cdot x\right) + b_n \cdot sin\left(n \cdot x\right) \right) \tag{14}$$

Where a_0, a_n and b_n are known as Fourier coefficients and can be calculated as

$$a_0 = \frac{1}{2 \cdot \pi} \int_{-\pi}^{\pi} f(x)\,dx$$

$$a_n = \frac{1}{\pi} \int_{-\pi}^{\pi} f(x) \cdot cos(n \cdot x)\,dx \qquad n = 1,2,\ldots, \quad (15)$$

$$b_n = \frac{1}{\pi} \int_{-\pi}^{\pi} f(x) \cdot sin(n \cdot x)\,dx \qquad n = 1,2,\ldots,$$

showing that any periodic signal can be represented as a sum of sines and cosines of different amplitudes and frequencies. As in practice there are finite discrete signals that represent function $f(x)$, the discrete Fourier transform (DFT) is used, but the meaning of analysis is the same (Randall, 1987; Lee and Varaiya, 2002).

So, if all of the signals in the measured roughness profile that represent the tool and machine influence can be represented as a complex periodic and structural and machining roughness as noise, then if a DFT is made of that signal, the amplitude of the periodic part of the signal should stand out above the noise floor. Fourier series of a sawtooth signal that represents the theoretical profile of tooth marks - $h_t(x)$ is composed of many cosine terms with falling amplitudes (Kreyszig, 2011), so it is certain that components whose amplitudes are in line with noise floor cannot be distinguished. If there are no frequency components that stand out above the noise floor in the DFT of surface roughness signal, then the direct influence of tool and machine on surface roughness cannot be quantified by this method.

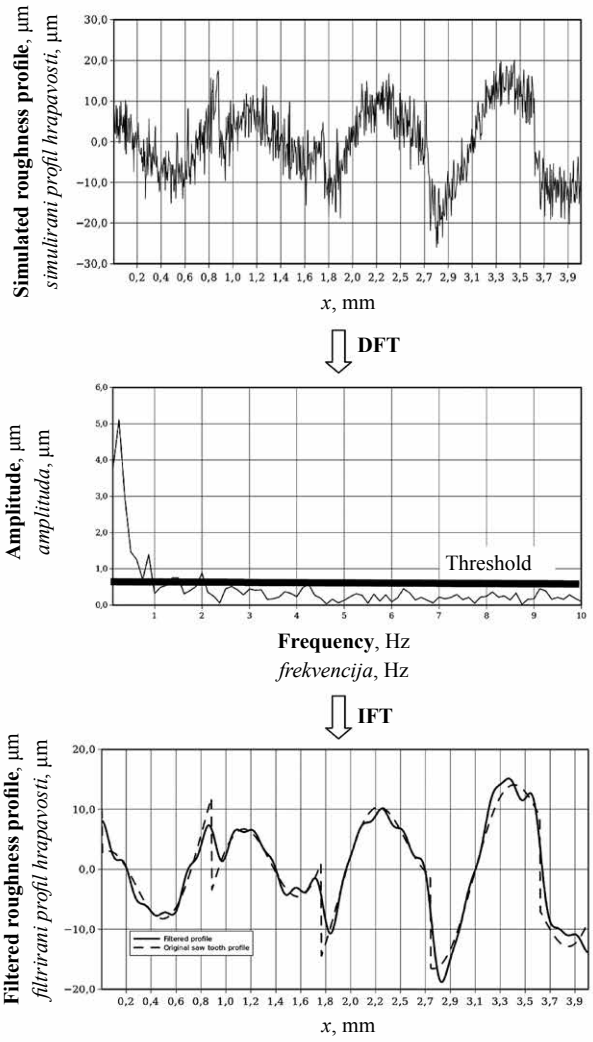

Figure 2 Block diagram representing the procedure of filtering a simulated roughness signal after sawing with circular saw with FFT based filter
Slika 2. Blok-dijagram postupka filtriranja simuliranog signala hrapavosti nakon piljenja kružnom pilom uz primjenu FFT filtra

In order to try to extract just the periodic signals associated with tool influence on the resultant profile, we can use the DFT data. From the plot of the DFT data, a threshold can be defined and it can be used to remove all of the data below that threshold value. After extraction, the amplitudes and frequencies are left and they should represent the periodic components of the signal. As the DFT is a computationally intensive task, fast Fourier transformation (FFT) algorithms are usually used.

Inverse Fourier transform (IFT) is performed on this extracted signal in order to get the estimated profile of tooth marks as a function of time or position (Figure 2). From this signal, R_a and R_q values, that should now mostly represent the influence of tooth marks on overall surface roughness, can be calculated.

This method should allow a simple and effective way for quantification of tool influence on machined surface roughness after sawing with circular saw.

2 MATERIALS AND METHODS
2. MATERIJALI I METODE

In order to test the proposed method for the roughness signal analysis after machining with circular saw, the experimental part of the research was conducted in the Laboratory for Mechanical Wood Processing, which is part of the Faculty of Forestry and Wood Technology in Zagreb. Medium density fiberboard (MDF) and solid oak wood (*Quercus robur* L.) were chosen as test materials. MDF was chosen because of its more uniform cross section so it could be used as a reference material to test the proposed signal analysis procedure, and oak wood because it is a ring porous type of wood and large pores tend to be problematic in surface roughness assessment. The moisture content of test specimens was 9 %. The average density of MDF boards was 685 kg/m^3 and of solid oak 695 kg/m^3. The average cutting height (material thickness) for MDF samples was h = 18 mm and for oak boards h = 24 mm.

For the sawing, cabinet table saw Bratstvo SC-10 was used and the sawing setup was as in Figure 1. The circular saw blade used for the experiment was a new standard saw blade for cutting solid wood along the grain, with tungsten carbide (HW) teeth. The saw di-

ameter was D = 300 mm with 24 teeth with straight tooth shape (FZ type), saw thickness a = 2.2 mm, cutting width b = 3.2 mm and radial side clearance angle ε was not equal on both sides of the saw teeth due to sharpening inaccuracies, so on one side it averaged 0.7° and on the other side 1.1°. Limit rotational frequency for the saw blade is 6500 min^{-1}. The saw blade was fastened to the main shaft by a flange with a diameter of d_f = 72 mm, so the clamping ratio was d_f/D = 72/300 = 0.24. Saw blade stiffness was measured by applying lateral force at tooth tip by means of weighing scale, and lateral displacement was measured with a dial indicator. The average calculated initial saw blade stiffness measured at tooth tip was k_t = 42 N/mm.

In order to be able to estimate if certain frequency components that were obtained from measured surface roughness are really due to lateral tooth movement and not some other factor, the circular saw vibration response to impact stimulus and frequency analysis of sound during idling and cutting was measured. The average electrical power required during sawing was also measured.

Before sawing, the resonant frequencies of the clamped saw blade were measured. The saw blade was lightly struck with a light hammer (impulse stimulus) and the response was measured with National Instruments NI USB-9162 with NI 9233 Signal IEPE Conditioning module and BSWA measurement microphone MPA 215 (Ser. No. 450051), which was positioned 1 meter from the saw blade. The whole measurement chain was calibrated before the measurement with Bruel & Kjaer pistonphone, Type 4230 (Ser. No. 656775). The sampling frequency was 50 kS/s. From the ten measurements of response signal, the average frequency response was measured and the dominant resonant frequencies were at 1.6 kHz and 3.6 kHz.

Rotational frequency of the saw blade was constant during measurements. During idling, it was measured with a laser tachometer and it was 3838 min^{-1}. The tooth passing frequency was f_t = 1535 s^{-1} and it was below the measured dominant resonant frequency of the clamped saw blade natural frequency. According to Tian and Hutton (2001), the largest unstable region of where washboarding can occur is associated with the case where the f_t is somewhat greater than the natural frequency of the saw. There was no evidence of self-excited vibrations during idling of the saw. During idling of the saw, the main frequency components measured were at 63 Hz, 100 Hz, 391 Hz and 1536 Hz. These frequency components can be attributed to rotational frequency of the saw, rotational frequency of the main electromotor and tooth passing frequency. During cutting, there was no noticeable change and the dominant frequency component was due to tooth passing frequency, which changed a little bit during cutting due to the change in the rotational speed of the saw blade because of the higher load on the main electromotor.

During the cutting experiment, the variables were workpiece material and feed speed. Feed movement was obtained by power feed system with rubber rollers attached to the table saw and due to limitations of test setup the feed speeds chosen for the experiment were v_f = (2, 4, 6.5 and 13) m/min. Corresponding feed per tooth was f_z = (0.02, 0.04, 0.07 and 0.14) mm and feed per one revolution of the saw blade f_o = (0.52, 1.04, 1.69 and 3.39) mm. These values are much lower than the values recommended for sawing solid wood along the grain, but this was not considered to be a problem for the purpose of the experiment. During cutting, the electrical power required for sawing was measured with Fluke Power Quality Analyzer 435-II (Ser. No. 462 13 102), which was connected to the main electromotor by standard three-phase delta connection for loads with no neutral wire.

After sawing, the machined surface roughness of MDF and solid oak test specimens was measured with surface roughness tester Mitutoyo SurfTest SJ-500 (Ser. No. B0007 1808), with an amplitude measurement range of 2 mm. The measurements were done in accordance with ISO 1997 and R profile was measured. The stylus tip radius was 10 μm and, in accordance with the recommendations of ISO 3274: 1996, the λ_s profile filter cutt-off was 25 μm and λ_c profile filter cut-off was 8 mm. Gaussian filter was used, but it must be kept in mind that this type of filter can introduce artifacts, such as very high peaks, when filtering the roughness profile. Evaluation length was 40 mm. Stylus traversing speed was set to v_s = 0.1 mm/s, which than corresponded to spatial resolution of 5 μm between two measurement points, which in the end was equal to sampling frequency of f_s = 20 Hz, so the maximum analyzed frequency component of the surface roughness signal was 10 Hz. Before the measurements, the roughness tester was calibrated with a working gauge that provides reference roughness profile with R_a = 2.97 μm (Mitutoyo, Ser. No. 393041807).

According to equation (5), the expected dominant frequency components due to feed per tooth or feed per one revolution were calculated as reciprocal values of Δt_z and Δt_o (time difference between two consecutive peaks due to saw tooth lateral movement for one revolution of the saw blade) and the values were f_{fz} = (4.6, 2.3, 1.4 and 0.7) Hz and f_{fo} = (0.19, 0.10, 0.06 and 0.03) Hz, respectively.

By visual examination of machined surfaces, it was determined that there were no repeating patterns with longer wavelengths that would be cut off by filtering, and that evaluation length was sufficient to sample a few cycles of the repeating pattern even in the worst case.

According to recommendations (Dagnall, 1998), in order to accurately determine the influence of the saw teeth on the surface roughness, the measurement stylus tip traversed the machined surface during measurement in the direction that corresponded to the direction of the feed movement vector and the position of subsequent measurements were chosen to provide the representative traces for later evaluation.

On every sawn surface of MDF and solid oak specimens machined with different feed speeds, five measurements of R profile data were obtained and exported to text (comma separated value) file. For the analysis of roughness profile signal data, a small script was written in Scilab (https://www.scilab.org). With this script, the original roughness profile signal was represented as a function of time and as such the discrete Fourier transform of that signal was obtained. The R_a and R_q values were calculated according to the equations (12) and (13). From the obtained spectrum plot of roughness signal, the threshold value was chosen by trial and error, because we were not able to determine some objective criterion for optimal determination of its value. The same value of threshold was used for all analyzed roughness signals, because in that case there was no need to change filter parameters due to changing machining conditions and the assumption that it can be used in this way was tested. In the next step, all values in the time domain signal that were below threshold were set to zero and that signal represented a filtered signal. The R_a and R_q values of the filtered signal were calculated, and the spectrum plot was also plotted for further analysis. For further analysis, only R_a value was used because it is more often used as a parameter, but R_q value shows the same trend.

3 RESULTS AND DISCUSSION
3. REZULTATI I RASPRAVA

The results of the obtained R_a values before and after filtering with FFT filter are presented in Figure 3.

Theoretical surface roughness h_{cmax} for the given sawing conditions is in the range from 0.3 µm to 1.7 µm and the corresponding value of R_a parameter, due to the fact that for saw-tooth waveform it can be easily calculated as $h_{cmax}/2$, is in the range from 0.15 µm to 0.85 µm. The measured values are much higher, even for the filtered signal.

As can be seen from the presented graphs, the roughness quantified by R_a parameter, as expected, shows a linear relationship with feed per tooth and is

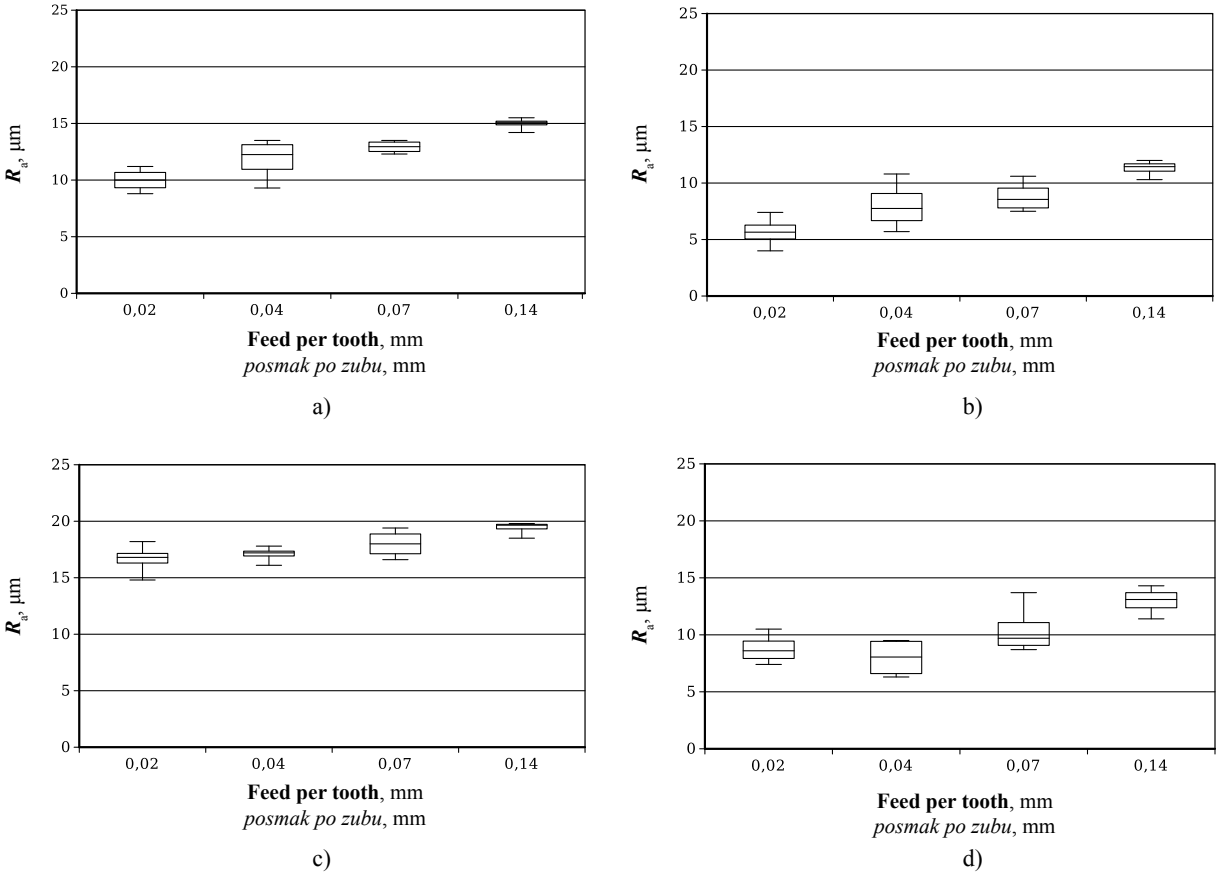

Figure 3 Machined surface roughness expressed through parameter R_a: a) after sawing solid oak, b) after sawing solid oak and filtering the roughness signal, c) after sawing MDF and d) after sawing MDF and filtering the roughness signal
Slika 3. Hrapavost obrađene površine izražena putem parametra R_a: a) nakon piljenja hrastovine, b) nakon piljenja hrastovine i filtriranja signala hrapavosti, c) nakon piljenja MDF-a, d) nakon piljenja MDF-a i filtriranja signala hrapavosti

consistent for unfiltered and filtered profiles (only the first sample in machining MDF at f_z = 0,02 mm does not fit into this trend and it was excluded from straight line fitting). The average difference between mean values of unfiltered and filtered R_a values on machined surface of solid oak wood was (4.0 ± 0.3) μm and on MDF it was (7.7 ± 1,1) μm. This difference should represent the average value of surface roughness components due to structural roughness of wood, chipped, raised grain, etc. and it was on average higher on machined surface of MDF, which was verified by tactile testing and was mainly attributed to raised fibers.

The average slope of fitted trend line for R_a values of filtered and unfiltered signals as a function of f_z was approximately 44 μm/mm, the only big difference

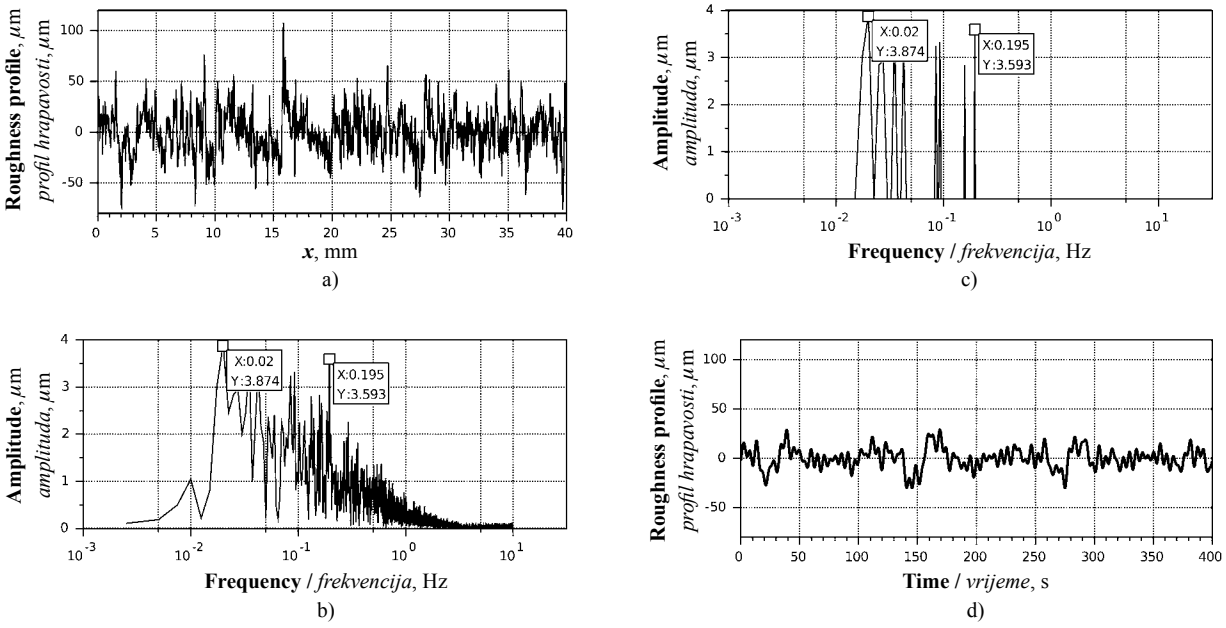

* analysis of machined surface roughness signals after sawing MDF with v_f = 2 m/min

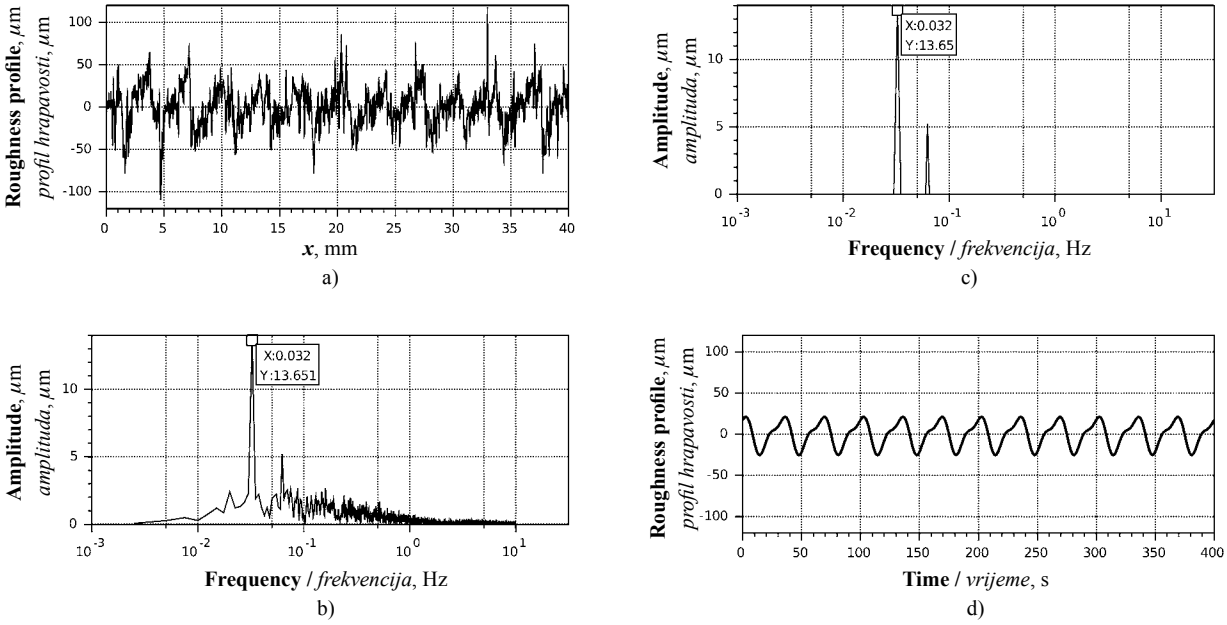

* analysis of machined surface roughness signals after sawing MDF with v_f = 13 m/min

Figure 4 Results of analysis of machined surface roughness signals: a) original surface roughness profile, b) frequency spectrum of the original roughness signal, c) frequency spectrum of the filtered roughness signal and d) surface roughness profile after filtering with FFT filter

Slika 4. Rezultati analize obrađenih signala hrapavosti površine: a) izvorni profil hrapavosti površine, b) frekvencijski spektar izvornog signala hrapavosti, c) frekvencijski spektar filtriranog signala hrapavosti, d) profil hrapavosti površine nakon filtriranja FFT filtrom

in the trend being in unfiltered signal of MDF machined surface where it was 23 μm/mm.

If the values of fitted straight line slopes obtained from the measured data is compared to the value of straight line slope from the calculated theoretical height of tooth marks as a function of f_z in given sawing conditions obtained with Eq. (2), which is approximately 12 μm/mm, it can easily be seen that not only the values of theoretical surface roughness in relation to the value of surface roughness parameters, but also the sensitivity of those parameters to change in f_z is quite different from the theoretically obtained values.

From the presented graphs and data, limited conclusions can be drawn. There is no clear indication if R_a values of filtered roughness signal are caused by tool

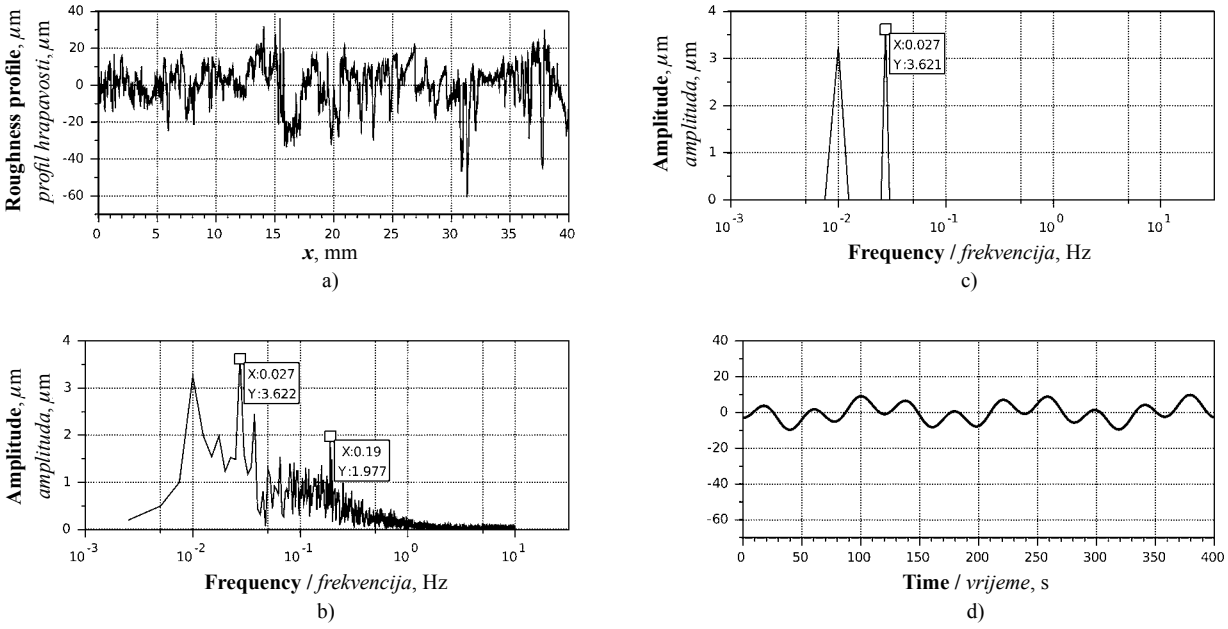

* analysis of machined surface roughness signals after sawing solid oak wood with v_f = 2 m/min

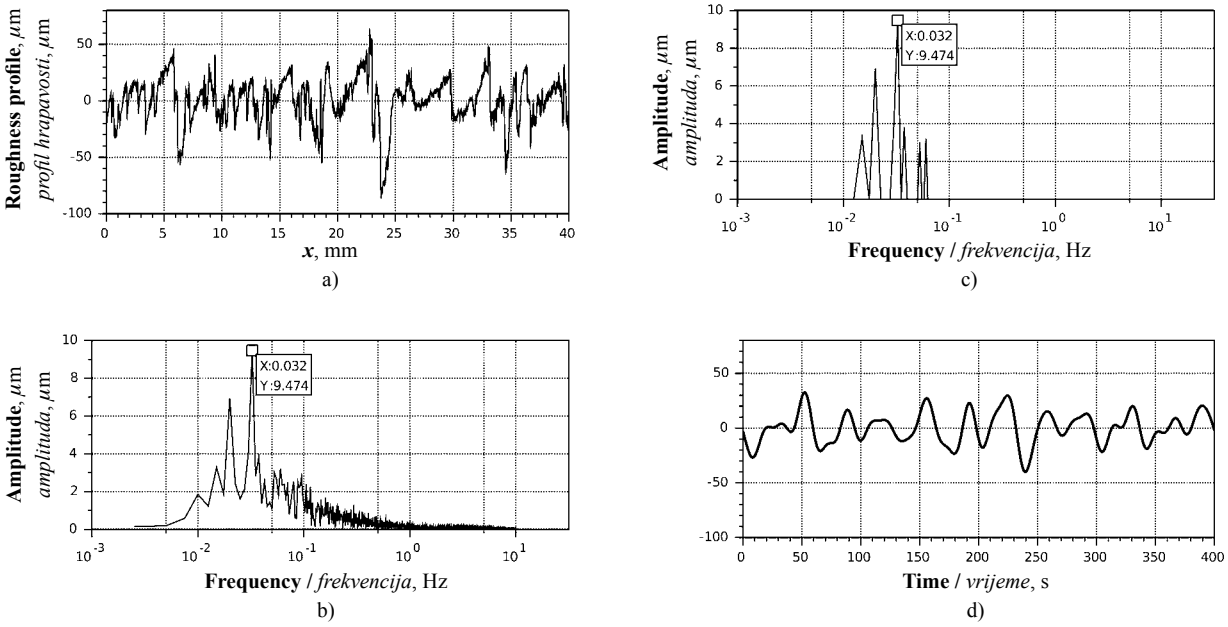

* analysis of machined surface roughness signals after sawing solid oak wood with v_f = 13 m/min

Figure 5 Results of analysis of machined surface roughness signals: a) original surface roughness profile, b) frequency spectrum of the original roughness signal, c) frequency spectrum of the filtered roughness signal and d) surface roughness profile after filtering with FFT filter

Slika 5. Rezultati analize obrađenih signala hrapavosti površine: a) izvorni profil hrapavosti površine, b) frekvencijski spektar izvornog signala hrapavosti, c) frekvencijski spektar filtriranog signala hrapavosti, d) profil hrapavosti površine nakon filtriranja FFT filtrom

influence or something else, and which component is the main contributor to the final estimated roughness.

In order to see how filtering of the original surface roughness signal by FFT filtering affects the signal and to better understand the main factors that contribute to calculated values of R_a, for every measurement the set of four graphs was produced.

As stated above, the frequency components expected due to feed per tooth and feed per revolution were calculated as f_{fz} = (4.6, 2.3, 1.4 and 0.7) Hz and f_{fo} = (0.19, 0.10, 0.06 and 0.03) Hz and, as can be seen from Figure 4, the surface roughness profile after machining MDF is dominated by lower-frequency components. The frequency component that would be expected due to feed per tooth component of the signal could not be distinguished. From the lower values of the feed speed range up to the higher values, it was evident that the frequency component of the roughness signal that could be associated with the values of feed per one revolution of the saw was becoming dominant and for the v_f = 13 m/min, it is evident from the frequency analysis of the filtered roughness signal that it is the main component that contributes to the overall roughness estimation of the filtered signal.

This component is also present for v_f = 2 m/min, but it is not dominant; the lower frequency components are more dominant and probably some structural or machining roughness components made their way through the filtering procedure. As cyclical components were more pronounced, FFT filtering with constant threshold value did a better job in extracting tool impact on the overall surface roughness. The same trend is evident in the analyzed data of roughness signal from sawing solid oak wood (Figure 5).

As can be seen from the presented figures, filtering the original signal with FFT filter made filtering out the surface roughness components due to tool influence straightforward, even with no change in any parameter of the filter for changing machining conditions and for different materials. The selected threshold value may not be optimal for all of the cases and there still remains the problem of optimal and automatic setting of that value, but the general concept looks promising as a simple and effective way for filtering out the tool impact on the overall surface roughness.

The results of frequency analysis clearly show that, in this case, the main driver of surface roughness is saw blade lateral deflection due to lateral forces on saw teeth, probably caused by uneven lateral bite of saw teeth. As the lateral force on the saw teeth could not be measured, it could only be approximated from the cutting force. The average cutting force (F_c) during sawing was calculated by dividing the average cutting power during sawing (P_c) with cutting speed v_c = 60 m/s. Cutting power was calculated as a difference between measured average electrical power during sawing (P_{tot}) and average electrical power during idling (P_0). The results are presented in Table 1.

Table 1 Calculated average cutting forces (F_c)
Tablica 1. Izračunane vrijednosti prosječne sile rezanja (*Fc*)

f_z, mm	F_c, N	
	Solid oak wood *masivno drvo hrasta*	MDF
0.02	12	3
0.04	19	5
0.07	22	6
0.14	34	10

If the calculated values of average cutting forces are compared with measured saw blade stiffness at tooth tip (k_t = 42 N/mm), it can be seen that lateral forces, even being a small percentage of the main cutting force, could cause measurable effect on the roughness of the machined surface. Combining this data and R_a values (Figure 3), it can be concluded that the lateral forces for the smallest feed speeds in sawing MDF were not strong enough to show significant difference in R_a values, but as soon as the lateral forces were strong enough, R_a values started to rise in line with values obtained on solid oak wood, where from the smallest values of feed speed the lateral forces were strong enough to show the change in R_a values with every change in feed speed.

There are still doubts about the values of measured R_a parameters after sawing solid oak wood and MDF, because if the main contribution to R_a values due to tool influence on the surface roughness is explained by lateral forces, the obtained values would be expected to be higher in value on machined surface of solid oak then on MDF. In our analysis, the result was the opposite. One possible explanation could be that, during sawing, the machined surface is produced by minor cutting edges with cutting angle of 90° and due to the fact that oak wood is harder than MDF for similar values of density, the oak wood has the necessary counterforce with less deformation compared to MDF, which in the end results in lower signal values due to structural and machining roughness (in this case it is mostly dominated by machining roughness and heavy deformation of material surface by saw teeth, as vessels characteristic of oak wood surface cannot be seen clearly from the measured signal).

As the main goal of this research was to implement FFT filter and to evaluate its usefulness in extraction of surface roughness components due to tooth marks and lateral movement of the saw, further analysis was not conducted, because the data analysis conducted so far has shown that the proposed method can be easy to implement and effective in quantifying the surface roughness components due to saw teeth marks and lateral movement of the saw blade.

4 CONCLUSIONS
4. ZAKLJUČAK

From the obtained research results, it can be concluded that the surface roughness profile of machined surface after sawing with circular saw can be adequately represented, for practical purposes, as a signal obtained as a sum of signals that represent theoretical profile of tooth marks, lateral movement of tooth due to saw vibration and structural roughness of wood, represented as a Gaussian noise. The combination of discrete Fourier transform of surface roughness profile and standard roughness parameters can give a more complete representation of machined surface roughness after sawing with circular saws. Filtering of surface roughness profile signal with FFT filter, even without changing the filter threshold value, can be a simple and effective method in quantifying the tool influence on machined surface roughness after sawing on circular saw in varying machining conditions and on different workpiece material. Appropriate choice of threshold value for FFT filtering is the main factor for adequate extraction of surface roughness component due to tool influence and it would be beneficial to have a method of automatic and objective determination of its level in given machining conditions, in order to eliminate the subjective trial and error method.

Acknowledgements – Zahvala

The authors would like to acknowledge the support of the European Structural and Investment Funds through financing the IRI project "Research in the company Spačva d.d. for the purpose of developing innovative massive doors made of Slavonian oak" - KK.01.2.1.01.0117.

5 REFERENCES
5. LITERATURA

1. Brock, M., 1983: Fourier analysis of surface roughness. Brüel & Kjær – Technical Review No. 3.
2. Budakçi, M.; Ilçe, A. C.; Korkut, D. S.; Gurleyen, T., 2011: Evaluating the surface roughness of heat-treated wood cut with different circular saws. BioResources, 6 (4): 4247-4258.
3. Csanády, E.; Magoss, E.; Tolvaj, J., 2015: Quality of machined wood surfaces. Springer International Publishing. http://dx.doi.org/10.1007/978-3-319-22419-0
4. Csiha, C.; Krisch, J., 2000: Vessel filtration – a method for analysing wood surface roughness of large porous species. Wood Research, 45 (1): 13-22.
5. Dagnall, H., 1998: Exploring surface texture. Taylor Hobson Ltd., Leicester, United Kingdom.
6. Fujiwara, Y.; Fujii, Y.; Okumura, S., 2003: Effect of removal of deep valleys on the evaluation of machined surfaces of wood. Forest Products Journal, 58-62.
7. Goglia, V., 1994: Woodworking machines and tools, Part I. University of Zagreb Faculty of Forestry, Zagreb (in Croatian).
8. Gottlöber, C., 2014: Machining of wood and wood-based materials. Fachbuchverlag Leipzig im Carl Hanser Verlag (in German).
9. Gurau, L.; Mansfield-Williams, H.; Irle, M., 2006: Filtering the roughness of a sanded wood surface. Holz als Roh- und Werkstoff. 64: 363-371. http://dx.doi.org/10.1007/s00107-005-0089-1
10. Goli, G.; Fioravanti, M.; Sodini, N.; Uzielli, L.; Taglia, A. D., 2005: Wood processing: a contribution to the interpretation of surface origin according to grain orientation. Paper presented in COST E35 Rosenheim Workshop. Stanzl-Tschegg, S. E.; Sinn, G. (eds.). BOKU – University of Natural Resources and Applied Life Sciences, Vienna.
11. Hendarto, B; Shayan, E.; Ozarska, B.; Carr, R., 2006: Analysis of roughness of a sanded wood surface. The International Journal of Advanced Manufacturing Technology, 28: 775-780. http://dx.doi.org/10.1007/s00170-004-2414-y
12. Kminiak, R.; Gaff, M., 2015: Roughness of surface created by transversal sawing of spruce, beech and oak wood. BioResources, 10 (2): 2873-2887. https://doi.org/10.15376/biores.10.2.2873-2887
13. Kminiak, R.; Gašparik, M.; Kvietkova, M., 2015: The dependence of surface quality on tool wear of circular saw blades during transversal sawing of beech wood. BioResources, 10 (4): 7123-7135. https://doi.org/10.15376/biores.10.4.7123-7135
14. Kreyszig, E., 2011: Advanced engineering mathematics. John Wiley & Sons, inc.
15. Leach, R., 2001: The measurement of surface texture using stylus instruments. National Physical Laboratory, Teddington, Middlesex, United Kingdom.
16. Lee, E. A.; Varaiya, P., 2002: Structure and interpretation of signals and systems, 1st ed. Addison-Wesley, Boston.
17. Lee, W.; Zhang, Z.; Peng, X.; Li, B., 2017: The influence of circular saw teeth of mic-zero-degree radial clearance angles on surface roughness in wood rip sawing. Annals of Forest Science, 74: 37. https://doi.org/10.1007/s13595-017-0632-3
18. Lehmann, B. F.; Hutton, S. G., 1997: The kinematics of washboarding of bandsaws and circular saws. In: Proceedings of the 13th International Wood Machining Seminar, Vancouver, Canada, pp. 205-216.
19. Lemaster, R. L.; Taylor, J. B., 1999: High Speed Surface Assessment of Wood and Wood-Based Composites. In: Proceedings of the 14th International Wood Machining Seminar, Epinal, France.
20. Magoss, E.; Sitkei, G., 2003: Optimum surface roughness of solid woods affected by internal structure and woodworking operations. In: Proceedings of the 16th International Wood Machining Seminar, pp. 366-371.
21. Magoss, E., 2008: General regularities of wood surface roughness. Acta Silvatica et Lignaria Hungarica, 4: 81-93.
22. Nasir, V.; Cool, J., 2019: Optimal power consumption and surface quality in the circular sawing process of Douglas-fir wood. European Journal of Wood and Wood Products, 77: 609-617. https://doi.org/10.1007/s00107-019-01412-z
23. Okai, R.; Kimura, S.; Yokochi, H., 1997. Dynamic characteristics of the bandsaw. 3. Effects of workpiece thickness and its position from the ground on self-excited vibration and washboarding during sawing. Mokuzai Gakkaishi, 43 (7): 551-557.
24. Orlowski, K.; Wasielewski, R., 2006. Study washboarding phenomenon in frame sawing machines. Holz als

Roh- und Werkstoff, 64 (1): 37-44. https://doi.org/10.1007ls00107-005-0037-0
25. Orlowski, K. A., 2010: The fundamentals of narrow-kerf sawing: the mechanics and quality of cutting. Technical University in Zvolen, Faculty of Wood Sciences and Technology.
26. Randall, R. B., 1987: Frequency analysis. Brüel & Kjær, Denmark.
27. Sandak, J.; Negri, M., 2005: Wood surface roughness – What is it? In: Proceedings of the 17th International Wood Machining Seminar, Rosenheim, Germany, 1: 242-250.
28. Sandak, J.; Orlowski, K. A.; Sandak, A.; Chuchala, D.; Taube, P., 2020: On-Line measurement of wood surface smoothness. Drvna industrija, 71 (2): 193-200. https://doi.org/10.5552/drvind.2020.1970
29. Sinn, G.; Sandak, J.; Ramananantoandro, T., 2009: Properties of wood surfaces – characterisation and measurement. A review COST Action E35 2004-2008: Wood machining – micromechanics and fracture. Holzforschung, 63: 196-203. https://doi.org/10.1515/HF.2009.016
30. Šavar, Š., 1990: Metal machining. Školska knjiga, Zagreb (in Croatian).
31. Tian, J, F.; Hutton, G., 2001: Cutting-induced vibration in circular saws. Journal of Sound and Vibration, 242 (5): 907-922. https://doi.org/10.1006ljsvi.2000.3397
32. Thoma, H.; Peri, L.; Lato, E., 2015: Evaluation of wood surface roughness depending on species characteristics. Maderas, Ciencia y tecnología, 17 (2): 285-292. https://doi.org/10.4067/S0718-221X2015005000027
33. Weisstein, E. W.: Sawtooth Wave. From MathWorld-A Wolfram Web Resource. https://mathworld.wolfram.com/SawtoothWave.html (Accessed Oct 5, 2020).
34. Zdenković, R., 1965: Metal machining. University of Zagreb Faculty of Mechanical Engineering and Naval Architecture (in Croatian).
35. ***2011: Exploring Surface Texture – A fundamental guide to the measurement of surface finish. Taylor Hobson, Leicester, England.
36. ***ISO 3274 (1996): Geometrical product specifications (GPS) – Surface texture: Profile method – Nominal characteristics of contact (stylus) instruments.
37. ***ISO 4287 (1997): Geometrical product specifications (GPS) – Surface texture: Profile method – Terms, definitions and surface texture parameters.
38. ***ISO 4288 (1996): Geometrical product specifications (GPS) – Surface texture: Profile method – Rules and procedures for the assessment of surface texture.
39. ***ISO 13565 (1996): Geometrical product specifications (GPS) – Surface texture: Profile method; Surface having stratified functional properties. Part 1: Filtering and general measurement conditions.
40. ***Leitz Lexicon – Sawing. https://www.leitz.org/en/news-downloads/leitz-lexicon/ (Accessed Jan 18, 2021).
41. ***Scilab Group: Signal Processing with Scilab. INRIA – Unité de recherche de Rocquencourt – Projet Meta2.

Corresponding address:

Assoc. Prof. IGOR ĐUKIĆ, PhD
University of Zagreb,˝Faculty of Forestry and Wood Technology, Svetošimunska cesta 23, 10000 Zagreb, CROATIA, e-mail: idukic@sumfak.unizg.hr

Kemal Hacıefendioğlu[1], Hasan Basri Başağa[1], Murat Emre Kartal[2], Mehmet Ceyhun Bulut[1]

Automatic Damage Detection on Traditional Wooden Structures with Deep Learning-Based Image Classification Method

Automatsko otkrivanje oštećenja na tradicionalnim drvenim konstrukcijama metodom klasifikacije slika utemeljenom na dubokom učenju

ORIGINAL SCIENTIFIC PAPER
Izvorni znanstveni rad
Received – prispjelo: 25. 2. 2021.
Accepted – prihvaćeno: 13. 12. 2021.
UDK: 624.011.1
https://doi.org/10.5552/drvind.2022.2108

ABSTRACT • *Wood has a long history of being used as a valuable resource when it comes to building materials. Due to various external factors, in particular the weather, wood is liable to progressive damage over time, which negatively impacts the endurance of wooden structures. Damage assessment is key in understanding, as well as in effectively mitigating, problems that wooden structures are likely to face. The use of a classification system, via deep learning, can potentially reduce the probability of damage in engineering projects reliant on wood. The present study employed a transfer learning technique, to achieve greater accuracy, and instead of training a model from scratch, to determine the likelihood of risks to wooden structures prior to project commencement. Pre-trained MobileNet_V2, Inception_V3, and ResNet_V2_50 models were used to customize and initialize weights. A separate set of images, not shown to the trained model, was used to examine the robustness of the models. The three models were compared in their abilities to assess the possibilities and types of damage. Results revealed that all three models achieve performance rates of similar reliability. However, when considering the loss ratios in regard to efficiency, it became apparent that the multi-layered MobileNet_V2 classifier stood out as the most effective of the pre-trained deep convolutional neural network (CNN) models.*

KEYWORDS: *deep learning method; convolutional neural networks; MobileNet_V2; Inception_V3; ResNet_V2_50; wooden structures*

SAŽETAK • *Drvo kao vrijedan građevni materijal ima dugu povijest uporabe u graditeljstvu. No zbog brojnih vanjskih čimbenika, posebice vremenskih utjecaja, drvo tijekom vremena postaje podložno progresivnom propadanju, što negativno utječe na izdržljivost drvenih konstrukcija. Procjena šteta na drvu ključna je za razumijevanje*

[1] Authors are researchers at Karadeniz Technical University, Department of Civil Engineering, Trabzon, Turkey.
[2] Author is researcher at İzmir Democracy University, Department of Civil Engineering, İzmir, Turkey.

problema koji će vjerojatno nastati na drvenim konstrukcijama, kao i za njihovo učinkovito ublažavanje. Primjena sustava klasifikacije uz pomoć dubokog učenja može potencijalno smanjiti vjerojatnost oštećenja u inženjerskim projektima koji se oslanjaju na drvo. U ovom je istraživanju primijenjena tehnika transfernog učenja kako bi se postigla veća točnost modela umjesto da se model za utvrđivanje vjerojatnosti rizika za drvene konstrukcije radi prije početka projekta. Za prilagodbu i inicijalizaciju težina primijenjeni su unaprijed osposobljeni modeli MobileNet_V2, Inception_V3 i ResNet_V2_50. Za ispitivanje robusnosti modela upotrijebljen je zaseban skup slika koji nije prikazan u osposobljenome modelu. Spomenuta tri modela uspoređena su s obzirom na njihove mogućnosti procjene vjerojatnosti i vrste oštećenja drvenih konstrukcija. Rezultati su otkrili da sva tri modela imaju sličnu pouzdanost. Međutim, kada se uzmu u obzir omjeri gubitaka u odnosu prema učinkovitosti, postalo je očito da se višeslojni MobileNet_V2 klasifikator istaknuo kao najučinkovitiji od unaprijed pripremljenih modela dubokih konvolucijskih neuronskih mreža (CNN).

KLJUČNE RIJEČI: *metoda dubokog učenja; konvolucijska neuronska mreža; MobileNet_V2; Inception_V3; ResNet_V2_50; drvene konstrukcije*

1 INTRODUCTION
1. UVOD

Wooden structures have a long and varied history in the realms of engineering. Indeed, throughout the world, and specifically in Turkey, a number of very old wooden structures have managed to survive. It is important for cultural posterity that these structures be protected, however, this can only be achieved with adequate resources, including the ability to predict potential risks in regard to damage, and how best to carry out repairs. Intensive studies regarding longevity estimation and evaluation methodologies have been carried out in recent years with a view to ensuring sustainability of older wooden structures, while also negotiating the environmental and economic impact of conservation. When evaluating the long-term performance of buildings and building materials, a key aim is to reduce the ecological and economic effects brought about by maintenance, repairs, and renewal, and thus use resources effectively (Jones *et al*., 2007). It is essential to know the environmental impact that building materials and elements can cause throughout the entire service life. An examination of the available research evidently showed that potential damage to building elements and materials are best examined through the preparation of a condition evaluation protocol and subsequent processing on a mapping system. This system, known as a damage map, is the sum of studies that show deterioration in various building elements via dimages, which can then be used to explain the causes of deterioration and the specific conditions that result in certain types of damage determining their degree, and provide environmentally and economically sustainable repair suggestions. Damage that may occur over time due to environmental factors in wooden building elements and materials are usually categorized as surface changes, color changes, fragmentation, cracks, and mechanical and biological degradations. In this study, the damage that occurs in the building elements of wooden structures are examined within three categories, namely wet rot damage, dry rot damage, and insect damage.

Dry rot damage is a wood-destroying fungus that causes timber rot by feeding wood cells and reducing their strength. This type of damage is a term used to describe any kind of decay that causes deterioration resulting in blackened, weakened, and cracked wood in buildings and ships caused by the fungus (Robinson, 2005). Dry rot damage is the most severe form of fungal rot. It attacks timber in buildings, and essentially digests parts of the wood, weakenng it severely over time. The scientific name of the fungus that creates dry rot is *Serpula Lacrymans*. Since wood can produce moisture through digestion, it can spread without any source of moisture. When dry rot damage spreads, it can seriously damage the structural integrity of the building. If dry rot damage is not immediately detected and treated, all affected timber may need to be removed and replaced. Spores of the fungus that create dry rot are found in the atmosphere; however, the right conditions for germination are needed for the fungus to take hold. These conditions include moist timber with a moisture content of about 20 %, which is freely accessible to the air (Jones *et al*., 2007). Wet rot damage is caused by a fungus that affects timber in very humid environments. High humidity creates rot by attracting spores that produce excess moisture. Compared to dry rot damage, wet rot damage is less destructive because wet rot damage remains limited to wet areas. However, it must still be treated effectively so as not to erode the structural integrity of wooden buildings (Jones *et al*., 2007). Wet rot damage can cause significant structural damage if left to grow uncontrollably because it will weaken timber over time. Wet rot is a general term for several fungi types, the most common being *Coniophora Puteana*, also known as cellar fungus. Wet rot damage is formed when the lumber is exposed to excessive moisture over longer periods of time. The wet timber will continue to soften as it absorbs more and more moisture thus leading to significant damage (Jones *et al*., 2007). This type of damage is often found in cellars, roofs, and window casings. The danger of wet rot damage when left untreated is the potential significant erosion of a wooden structure strength.

Insect damage can also be a common problem that affects wooden structures. Damage is typically caused by termites, carpenter ants, and powder insects. Although termites usually cause the most significant damage, carpenter ants and powder insects must also be accounted for. Like termites, carpenter ants carve channels through wood, however, unlike their counterparts, the grooves of carpenter ants have a smooth and clean appearance (Robinson, 2005). Although damage inflicted by carpenter ants is typically not as severe as the damage caused by termites, carpenter anthills can cause significant damage if left untreated over the years. As the number of individuals in a colony increases, they will continue to break down the wood, causing further damage (Jones *et al*., 2007). The larvae of powdered insects feed on cellulose in wood and cause significant structural damage over a period of one to five years. As the insects feed, a fine powder in the cavities under the wooden surface is produced. They typically inhabit soft woods and are therefore less likely to be the cause of substantial structural problems (Robinson, 2005), however, their effects should not be discounted.

With the development of technology in civil engineering, many preliminary examinations such as damage inspection, detection of defects, and determination of material strengths are now carried out with computers to evaluate structural performance against external influences. In wooden structures, it is essential to detect any damage or defects of wooden materials and, in light of this, a number of studies have been carried out over the last few decades. One of the first of these kinds of studies is the detection and classification of wood defects using artificial intelligence performed by Cavalin *et al*. (2006). They attempted to detect wood defects using features determined from grayscale images. They defined features according to smoothness, coarseness, and regularity. In experimental studies, neural networks and support vector machines with two different learning paradigms were taken into account, as well as a feature selection algorithm based on multi-objective genetic algorithms. The experimental results indicate that after feature selection the grayscale image-based feature set accomplishes superior wood defect detection performance than color image-based features. In a study carried out by Jabo (2011), image analysis and classification methods were proposed. These methods cover the sorting of defects, including "wood decay", "blue stain", and "shake". A supervised classifier was first trained with Adaboost, and used to extract colors of stain-type defects and methods such as an integral image. Sioma (2015) presented the analysis and use of 3D images to detect and locate defects on wood surfaces automatically. In the study, defects occurring on wood surfaces were explained in detail, and examples were presented of the most common defects recorded in wood industry production lines. A method was applied to create a 3D image of the surface using the laser triangulation method (LTM). For selected defects, measurement algorithms that can detect a parametric description of the defect and its location on the surface were presented. Wenshu *et al*. (2015) aimed to identify the location and size of defects on wood quickly and accurately by using a computer and artificial neural network (ANN) technology. In their work, the location and size of the defects in the wood were determined by taking images with a CCD (charged coupling devices) camera, and processing said images using the MATLAB program. Additionally, ANN was created to recognize defects with results showing that the wood defect identification rate is ascertainable up to 86.67 %. Urbonas *et al*. (2019) proposed an automatic visual inspection system for the location and classification of defects on wooden surfaces. A faster region-based CNN (Faster R-CNN) method was used to identify defects in wood veneer surfaces. Pre-trained AlexNet, VGG16, BNInception and ResNet152 neural network models were used for transfer learning to improve the results. In their study, Li *et al*. (2019) proposed a new methodology, including the application of machine learning algorithms, to cope with damage accumulation effects in wood. The proposed algorithm takes into account a multi-objective optimization process with a combination of goodness of fit and complexity.

Researchers have used long-term experimental data of typical wood species to develop damage accumulation models based on machine learning. He *et al*. (2019) and (2 proposed a diverse, fully convolutional neural network (Mix-FCN) to locate wood defects and automatically classify defect types in wood surface images. The images were first collected with a data acquisition device developed in the laboratory. They then utilized TensorFlow and Python language (Van Rossum and Drake Jr, 1995) to create a VGG16 model. They used two types of data sets (dataset 1 and dataset 2) to maximize the data, which was collected on a limited basis, to ensure that the Mix-FCN merges quickly during training. The proposed models were trained, validated, and tested by dataset 2. In order to classify lumber images, Hu *et al*. (2019) explored varieties of deep learning strategies based on ResNet18. Their study four datasets were manually marked as lumber defects, wood textures, and lumbers by experts. In the study, they used transfer learning in CNN with a classifier layer that provides training with a small amount of training data. The accuracy rate was clearly upgraded by expanding unbalanced samples. He *et al*. (2020) suggested a learning method to perceive wood defects as well as automatically categorize imperfections in wood images obtained using a laser scanner via a deep convolutional neural

network (DCNN). They implemented TensorFlow to train the network composed of an input layer, four convolutional layers, four maximum pooling layers, three fully connected layers, a softmax layer, and an output layer. Results indicated that the DCNN model could identify wood defects more accurately and effectively than traditional methods.

Turkey, particularly the Anatolian region, has relied on the use of local materials, including wood, stone, and adobe, for much of its history to this day. Wood is used in a multitude of ways as follows: as a carrier element, for exterior cladding, joinery, flooring, and roofing material in various buildings from past to present. Although foundation and basement walls are typically made of stone along the coastline of Turkey, the upper floors are typically constructed of wooden masonry or have a wooden frame system. Serenders are the most common structures in which wooden masonry and a carcass system are jointly used. Serenders are warehouses where various food items are placed. Unlike dwellings, although the lower floor is carcass with buttress poles, the upper floor is wooden masonry. Regardless of the materials used for a building exterior walls, the interior walls, floors, and ceilings are made of wood (Özgel Felek, 2020).

Object recognition is conducted by looking at the attributes associated with an object and identifying criteria that can determine appropriate labeling. Recognition comes from experience, education, and training. Deep learning methods allow programs to quickly recognize and classify an object while taking into account features that the human eye cannot distinguish. The deep learning-based classification methods used in the present study are designed for the visual identification of types of damage. Typically, dry damage and insect damage are difficult to distinguish with the human eye as they often appear similar in texture. While the human eye can certainly detect specific classifications of damage, deep learning allows for classification involving more complex features, and the ability to do so with greater speed and practicality.

2 AIM OF STUDY
2. CILJ ISTRAŽIVANJA

The present study sought to make use of CNN based on the deep learning method, to better automate the assessment of traditional wooden structures in Turkey. The primary focus was the automatic detection and localization of actual damage caused by environmental influences on structural wooden elements via the use of images processed through deep learning techniques. It is important to note that, as this was the first attempt at such an assessment, there were a few limitations. Firstly, more than one type of damage was not taken into account at the same time, which means that the images used by the model belong only to one category. Secondly, only images with visible damage were taken into account. Thirdly, excessive or low illumination affecting the brightness of images as well as the orientation of the images needed to be accounted for.

The aim of the present study is to automatically detect partial damage in wooden structures, which are widely used in Turkey, by using image classification methods based on deep learning. For this purpose, a partially damaged selender structure was used as the example structure.

3 DEEP LEARNING METHOD
3. METODA DUBOKOG UČENJA

Deep learning is a machine learning technique that identifies features and tasks directly from data. Data typically consists of sounds, images, or text. Deep learning is a systematic subset of artificial intelligence and machine learning, and is the most popular artificial intelligence application approach. Studies can be referred to as data interpretation when it comes to the generalization of deep learning (LeCun *et al*., 2015). Deep learning algorithms take all the pixels on the pattern as input data when learning through a tagged pattern. The input data varies depending on whether the pattern is gray or colored. When a color image is given as input to the model, whereby red, green, and blue frequencies are used, the current pixel is used three times as input data. In a grayscale image, the input data is the number of pixels. Primarily, convolution layers, ReLu (Rectified Linear Unit) layers, and pooling layers are applied in order to draw the feature map on the image. After the feature map is drawn, fully linked layers and unique classification layers of Softmax come into play. At this stage, each pixel has probability values for each class. These values are determined by Softmax, which identifies the class of the pixels (Hassaballah and Awad, 2020).

3.1 Convolutional neural networks
3.1. Konvolucijska neuronska mreža

Artificial neural networks are models created based on the functioning of the human brain. The system aims to realize the learning process through the interpretation of these teachings with the system then making decisions autonomously due to this interpretation. This structure consists of three layers. Observations are transferred to the system in the input layer. The number of nodes in this layer is equal to the number of features that will best represent the observation. Values can be copied and sent to more than one layer in the input layer. The hidden layer applies transformations to the values from the input layer by multiplying

them with specific coefficients. There can be more than one node in this layer. By using certain threshold conditions at these nodes, a value as much as the output number can be obtained after the hidden layer is the output layer. The system makes predictions according to the value obtained.

CNN is a class of deep neural networks used in image recognition problems (Salman *et al*., 2018)such as Dynamic Movement Primitives (DMPs. According to CNN working principle, the pictures given as input must be recognized by computers and converted into an operable format. For this reason, images are first converted to matrix format.

CNNs are structures designed to take images as inputs and are thus used effectively in computer vision. CNN consists of one or more complex layers and fully bonded layers, such as a standard multilayer neural network (LeCun *et al*., 2015). CNN architecture consists of convolution, pooling, flattened and fully connected layers dropout and classification as shown in Figure 1. If the CNN architecture is considered as two separate sections, and feature extraction for the unit where convolution and pooling layers are used, the unit, where flattening and a fully bonded layer is used, is regarded as the classification. The section after the flattening layer has the same structure as standard neural networks.

Convolution layers are the central part in which the object recognition problem calculations are the most intense. Raw data is given as input to this unit. In this layer, many convolution layers are interconnected to perform a series of convolution operations. Each convolution layer represents a series of feature maps with organized neuron cells. In other words, the attributes of the image given in input are extracted in these layers. The parameters of the layers are a set of learnable filter coefficients. As the convolution layers progress from input to output, features, from simple to complex, are extracted.

The convolutional layers create feature maps with linear filters followed by linear functions (rectifier, sigmoid, tanh, etc.). The feature map can be calculated using Eq. 1:

$$f_{i,j,k} = max(w_k^T x_{i,j} + b_k, 0)$$

Where (i, j) defines the spatial location on feature maps, k is the feature map index, $x_{i,j}$ denotes the input patch centered at (i, j) and w_k^T, b_k are the filter coefficient vector and bias of the k_{th} feature map, respectively. In CNN architecture, a pooling layer is commonly added between the convolution layers periodically. This layer function gradually decreases the notation spatial dimension to reduce the network's number of parameters and calculations, which controls excessive compliance. This is known as a sub-sampling. The

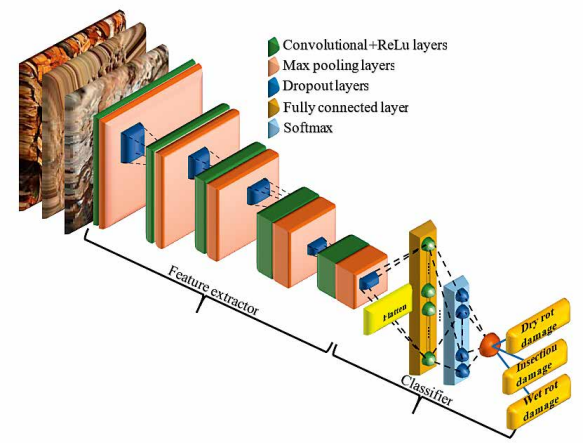

Figure 1 Typical convolutional neural network
Slika 1. Tipična konvolucijska neuronska mreža

pooling layer makes the sample by lowering the feature map height and width although the depth remains the same. Spatial pooling has types such as maximum pooling, average pooling, and total pooling. The most used technique is maximum pooling. Maximum pooling takes the largest item in the corrected feature map. The size of the feature map is halved after pooling.

Neurons in a fully-connected layer, as in regular neural networks, have full connections with all activations in the previous layer. It is the last and most crucial layer of CNN. It is identified as fully connected because every neuron in the previous layer is connected to each neuron in the next layer. The fully-connected layer aims to use high-level features to classify the input image into different classes. As seen in Figure 4, there are four networks in the fully connected layer. Each of these neurons represents a class (e.g. house, boat, tree, cat, etc.). By looking at the convolutional network attributes, it detects which class the input data is closer to and ultimately returns a class (Schmidhuber, 2015).

3.2 Transfer learning
3.2. Transferno učenje

Transfer learning uses deep learning methods to hide the information obtained while solving a problem and then uses that information when faced with another problem. When it comes to the transfer of learning, models that result in higher success rates and via faster learning with less training data, are typically obtained by using previous knowledge. It is typical for a separate 'learning from scratch' to be performed for each task in deep learning. Since it is possible and advantageous to use information learned from some tasks in other tasks, the source task information is used to solve the target task. Features, weights, etc., are obtained from previously trained models with transfer learning used for a new task. For this method to work, the information transferred needs to be general information.

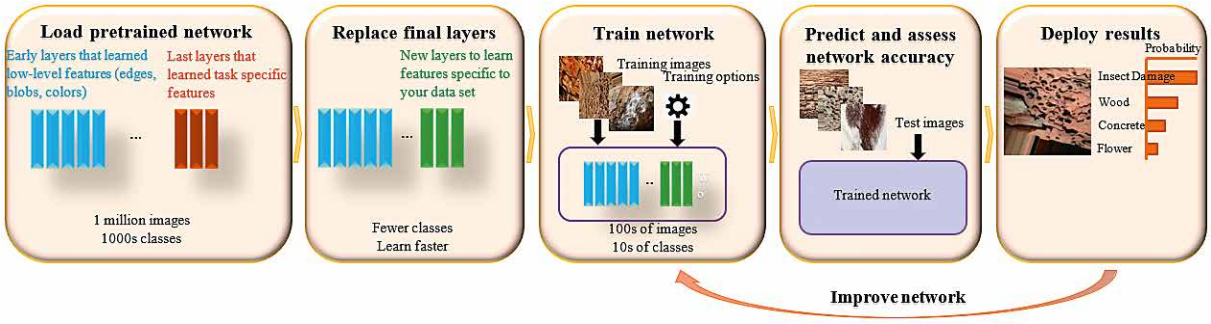

Figure 2 Reuse of pre-trained network
Slika 2. Ponovna uporaba unaprijed osposobljene mreže

Appropriate information for both the source and target tasks is transmitted instead of specific to the source task. It is common practice to purchase and use ready-trained models such as VGG-16, VGG-19, ResNet, Inception, and Xception with Keras library. Pan and Yang (2010) provide a comprehensive review of transfer learning. The reuse of pre-trained network is shown in Figure 2. In this study, Resnet-50, VGG-19, and Inception-V3 models were utilized to localize landslide regions, where wooden structures are particularly liable to damage.

3.2.1 Trained convolutional neural networks
3.2.1. Osposobljena konvolucijska neuronska mreža

The present study used three pre-trained convolutional neural network models -MobileNet_V2, Inception_V3, and ResNet_V2_50, to perform classification on a new collection of images.

3.2.1.1 MobileNet_V2 model
3.2.1.1. Model MobileNet_V2

MobileNet_V2 consists of two types of blocks as shown in Figure 3. The first is a residual block with a stride of 1 and the second is a block with a stride of 2 for downsizing. Three layers are defined for both block types. The first layer is 1×1 convolution with ReLU6. The second layer is representative of the depthwise convolution. The third layer is 1×1 convolution but has non-linearity. In the case of ReLU, the deep networks have a linear classifier power only in the non-zero volume portion of the output domain. There is an expansion factor t, and t=6 for all primary experiments. If the input had 64 channels, for example, the internal output would have 64×t=64×6=384 channels (Sandler *et al.*, 2018). For this model, the input images sizes were fixed at a height x width = 224 × 224 pixels.

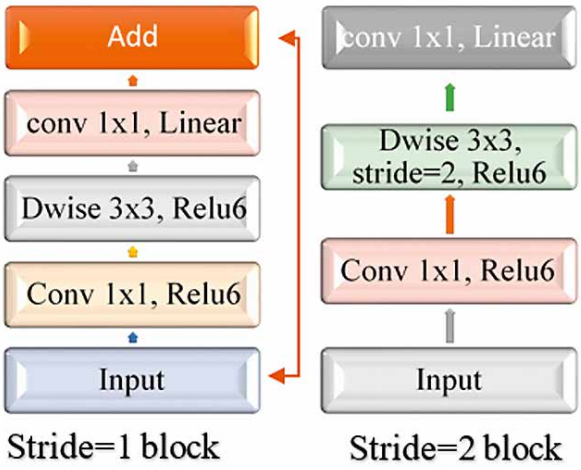

Figure 3 MobileNet_V2 convolutional blocks
Slika 3. Konvolucijski blokovi modela MobileNet_V2

3.2.1.2 Inception_V3 model
3.2.1.2. Model Inception_V3

The inception network model consists of various modules. Different sizes of convolution and maximum partnering are carried out in each of these modules. GoogLeNet is also known as Inception_V1 in the literature (Szegedy *et al.*, 2015). Versions later called Inception_V2 (Szegedy *et al.*, 2016), Inception_V3 (Szegedy *et al.*, 2016), and Inception_V4 (Szegedy *et al.*, 2017) have also been developed. Inception_V3 consists of two parts: feature extraction and classification. The feature extraction section involves the convolutional neural network. Inception_V3 is a familiar architecture, and the input of the network should be an image of 299×299 pixels. Moreover, the classification section is wholly connected and contains Softmax layers. All layers specified in Inception_V3 are depicted in Figure 4.

3.2.1.3 ResNet_V2_50 model
3.2.1.3. Model ResNet_V2_50

ResNet_V2_50 (He *et al.*, 2015) is a convolutional neural network that is 50 layers deep with a pre-trained version of the network trained on more than one million images from the ImageNet database. The pre-trained network can classify images into 1000 object categories (e.g. keyboard, computer mouse, pencil, animal, etc.). As a result, the network has learned rich feature representations for a wide range of images. The network has an image input size of 224×224. The architecture of ResNet_V2_50 is shown in Figure 5.

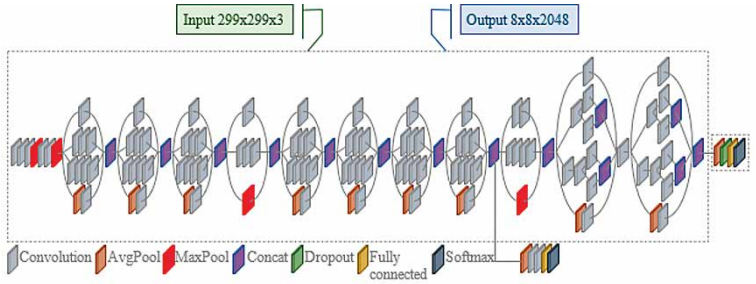

Figure 4 Architecture of inception_V3
Slika 4. Arhitektura modela Inception_V3

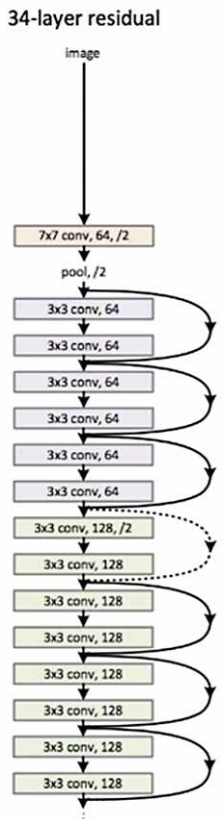

Figure 5 Architecture of ResNet_V2_50 (He *et al*., 2015)
Slika 5. Arhitektura modela ResNet_V2_50 (He *et al*., 2015.)

3.2.2 Fine-tuning
3.2.2. Fino podešavanje

A wide breadth of information can be found in the weights in pre-trained models. This allows for fine-tuning to be carried out and the new model can be trained faster using this information. High achievement can be succeeded in the 2–4 epoch by using learning transfer, even for some problems. The requirement of a large-scale dataset for education purposes is arguably the most significant disadvantage when it comes to models created from scratch, as creating these datasets is very time consuming. The use of pre-trained models and fine-tuning them can give results with less data but still maintain high performance parameters. The simple operation of adding a new fully linked layer(s) to pre-trained models improves success. Fine-tuning, on the other hand, requires the CNN architecture to not only be updated but also re-trained in order to learn new object classes.

In the transfer learning method, the existing layers in the pre-trained models are frozen while the learning is performed; in other words, the weights in these layers should not change. During the training process, random weights associated with the newly added layers are changed. This process is called fine-tuning. Figure 6 illustrates the fine-tuning method in transfer learning.

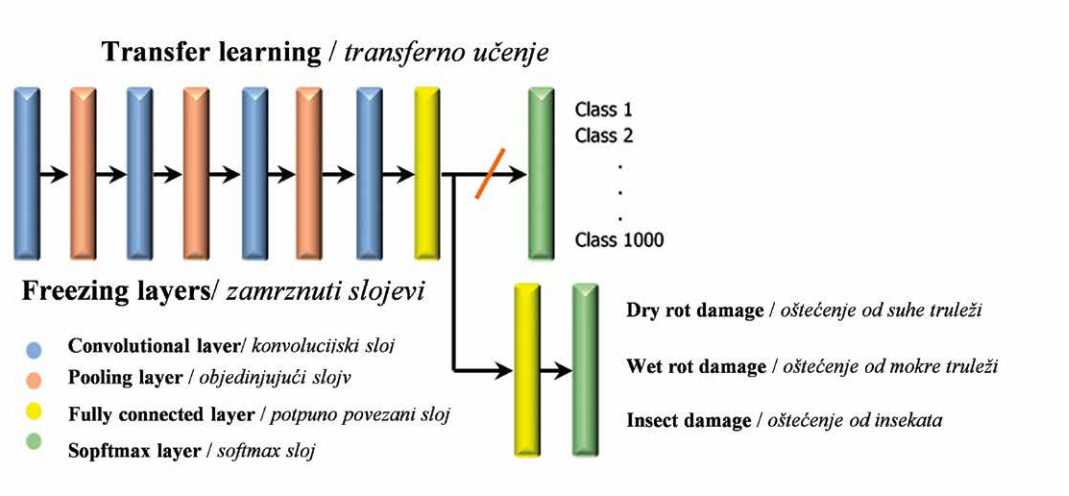

Figure 6 Fine-tuning in transfer learning
Slika 6. Fino podešavanje u transfernom učenju

4 METHODOLOGY
4. METODOLOGIJA

This study aimed to identify damaged areas in traditional wooden structures using a deep classification system based on the classification method. In this study, three types of damage found in wooden structures were considered: dry rot, wet rot, and insect damage. Initially, images depicting these types of damage were collected from various, primarily online, sources. The images were then cropped appropriately and resized to create the dataset used to train the model. A transfer learning technique was used to achieve higher accuracy, instead of training a model from scratch. A selender sample, which is one of the traditional wooden structures found in the region of Trabzon, Turkey, was selected for the experimental study. The analysis of MobileNet_V2, Inception_V3 and ResNet_V2_50 models were performed to determine damaged areas on the serender structure, and results were compared to determine the most reliable and robust pre-trained model. Pre-trained MobileNet_V2, Inception_V3, ResNet_V2_50 are the convolutional neural networks commonly used for an image classification task. The three pre-trained networks were analyzed following the framework as seen in Figure 6. The idea behind MobileNet is to use depthwise separable convolutions to build lighter deep neural networks. Inception was developed with the aim of reducing the computational load of deep neural networks while achieving state-of-the-art performance. While Inception focuses on computational cost, ResNet focuses on computational accuracy and was implemented to increase said accuracy. Due to the phenomena described above, these three networks, which are most commonly used, were deemed the best choices for the experimental study.

Typical input image sizes for MobileNet_V2 , Inception_V3, ResNet_V2_50 are 224×224, 299×299 and 224×224, respectively. A separate set of images not used by the pre-trained model was used for verification to examine the robustness of the models. The three pre-trained neural networks were trained on a data set by using 9140 images; as a result. the algorithms developed can classify new images into 1,000 different object categories. Via deep learning, each network can detect images based on unique features representative of a particular category. By replacing the last fully connected layer, as shown in Figure 7, and retraining (the fine-tuning of deeper layers) the neural network with the new dataset, the neural network is then able to detect specific types of wood damage.

TensorFlow Hub (Abadi *et al*., 2016) and Keras (Ketkar, 2017) were used in all analyses. Tensorflow is an open source machine learning platform used to perform high-performance numerical calculations. It provides excellent architecture support by enabling easy deployment of computations across a variety of platforms, from desktops to server clusters, mobile devices, and edge devices. The remainder of the imports consists of additional helper functions, followed by NumPy for numerical processing and cv2 for OpenCV bindings.

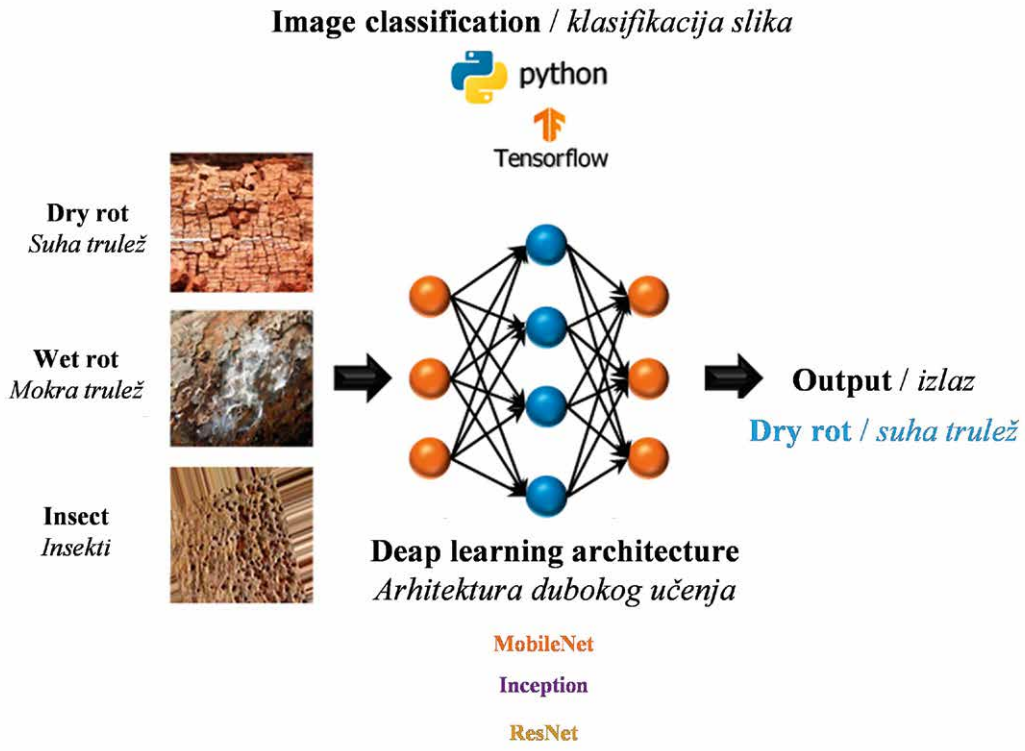

Figure 7 Framework for wood damage detection using pre-trained neural network
Slika 7. Okvir za otkrivanje oštećenja drva uz pomoć unaprijed osposobljene neuronske mreže

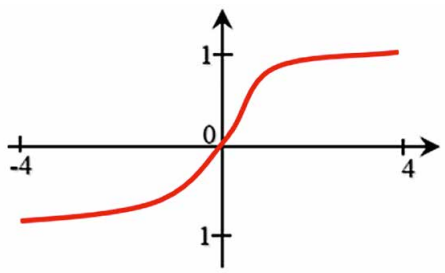

Figure 8 Softmax classification function (Nwankpa *et al*., 2018)
Slika 8. Funkcija klasifikacije *Softmax* (Nwankpa *et al*., 2018.)

There are two types of regularization methods, the L1 and L2, to regulate neural networks. However, the L2 regularization technique is used more often in deep neural networks as it is more advantageous in terms of computational efficiency. The present study used the Softmax classification function (Figure 8), which is used for multiclass classification. The softmax step can be seen as a generalized logistic function that takes a vector of $x \in R^n$ scores as input and creates the probability vector $p \in R^n$ output from the softmax function at the end of the architecture. It is defined as follows:

$$p = \begin{pmatrix} p_1 \\ \vdots \\ p_n \end{pmatrix} \text{ whereas } P_i = \frac{e^{x_i}}{\sum_{j=1}^{n} e^{x_j}}$$

4.1 Dataset
4.1. Skup podataka

Images of different sizes and with a variety of different resolutions were obtained from many sources, including photos taken by mobile phones and copyright-free images obtained from the web, for three types of wood element damage. These images amounted to a total of 9140 pictures, and data augmentation methods were used to increase the dataset size. The data are divided into three main categories: dry rot damage (3245 images), wet rot damage (2877 images) and insect damage (3018 images). For the classification experiments, the dataset was randomly split into 80 % - 20 %, where 80 % was used for training and 20 % was used for testing and validation. The total number of images used as training data amounted to 7312: dry rot damage (2596 images), wet rot damage (2302 images), and insect damage (2414 images). A wide variety of image magnifications have been applied to the training set, including rescaling, rotation, height and width shifts, and horizontal and vertical flips in order to avoid over-fitting and better generalization. The remaining 1828 images of the original 9140 were used as testing data. Samples of the images used are shown in Figure 9.

4.2 Verification of models
4.2. Verifikacija modela

4.2.1 Loss function
4.2.1. Funkcija gubitka

The categorical cross-entropy loss function, which is common in multi-class classification tasks, was used in the study. Cross-entropy generally calculates the difference between two probability distributions for a given random variable/event set.

The categorical cross-entropy loss function calculates the loss of a sample using Eq. 3:

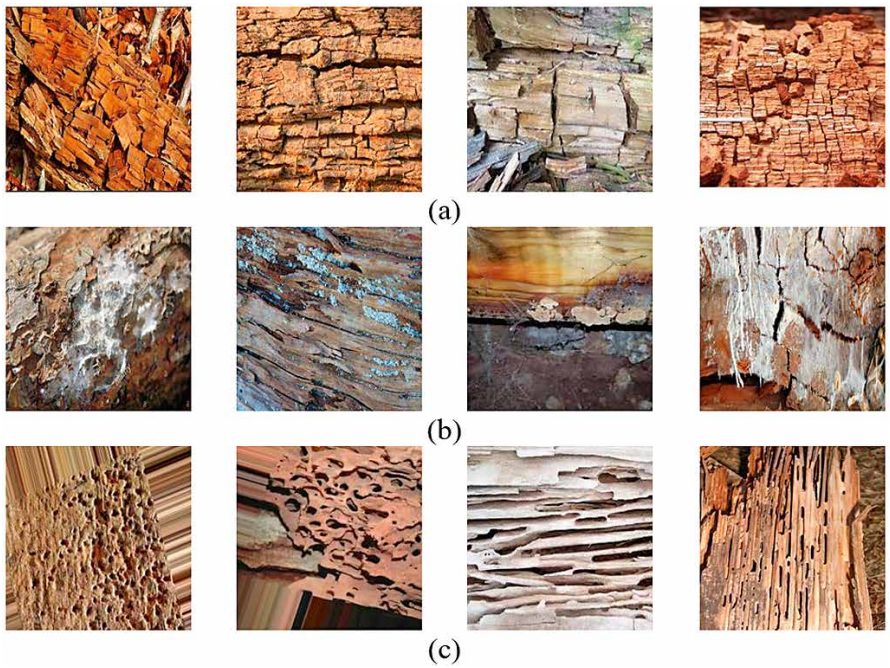

Figure 9 Image samples for (a) dry rot damage, (b) wet rot damage, and (c) insect damage
Slika 9. Uzorci slika za (a) oštećenja od suhe truleži, (b) oštećenja od mokre truleži i (c) oštećenja od insekata

$$Loss = -\sum_{i=1}^{output\ size} y_i \cdot log\ \hat{y}_i \quad (3)$$

Where defines the *i*-th scalar value in the model output, denotes the corresponding target value, and is the number of scalar values in the model output.

The network was trained to more than 30 epochs using a batch size of 32. The sizes of the input images are fixed to height x width = 224 × 224, 299 × 299 and = 224 × 224 for MobileNet_V2, Inception_V3 and ResNet_V2_50 per epoch, respectively. The final accuracy recorded at the end of the 30th epoch for MobileNet_V2, Inception_V3 and ResNet_V2_50 models was 96.38 %, 96.49 %, and 95.39 % for the training, respectively, and with validation values close to the training. The final loss values for MobileNet_V2, Inception_V3 and ResNet_V2_50 models were 0.13, 0.31 and 0.34 for training, respectively, and with validation sets close to the training. In general, the classification ability of loss values below 0.2 is highly acceptable (Fei *et al*., 2020). Accuracy and loss graphs of training and validation for the three network models are given in Figure 10a-c.

The graphs of accuracy for the three models in Figure 10 illustrate the success of the training although the trend for accuracy on both validations and training datasets continued to slightly increase for the last few epochs. It is clear that the models do not over-learn from the training and datasets, and that the validation curves still show a slight increase. However, since the validation curves are adjacent to the training curves and do not diverge from the training curves, none of the models had overfitting problems during training. When these three models are examined, it is evident that MobileNet_V2 is the most robust model in both accuracy and loss of graphic values. In light of this evidence, this model was used for all subsequent analyses.

The models were evaluated to test their robustness, which included a prediction test performed on new images. Upon completion of the test, the accuracy rate for all three models was over 95 %. A sample study of the correct classification of different types of damage images is provided in Figure 11.

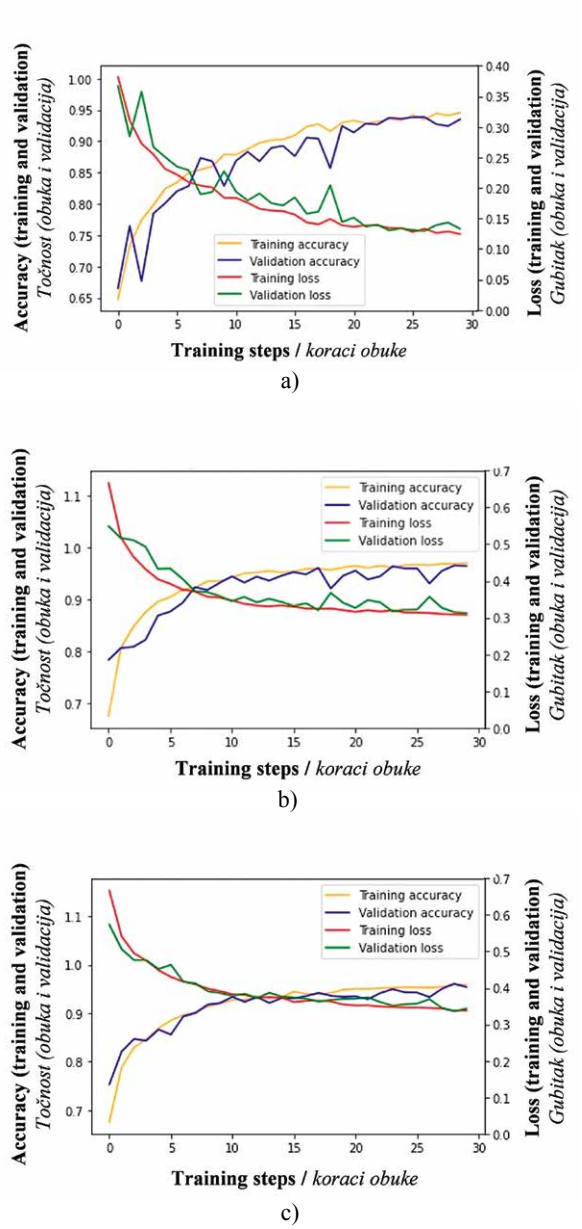

Figure 10 Comparative model accuracy and loss diagram. In sub-figure a) MobileNet_V2, (b) Inception_V3 and (c) ResNet_V2_50 models
Slika 10. Usporedna točnost modela i dijagrami gubitaka: a) model MobileNet_V2, b) model Inception_V3, c) model ResNet_V2_50

5 RESULTS
5. REZULTATI

According to the class of damage previously determined using the image data, all the selected structure regions were photographed to identify the location of damaged areas on a real building model. These critical locations are numbered numerically on the selender photos (Figure 12). The MobileNet_V2 model, identified as the most robust model as previously stated, was used to estimate the class of damage type if found to be present in a given image. As seen in the images in Figure 12, representative images showing different damage types were accurately localized using this method. Figure 12 shows predicted damage in yellow and incorrectly estimated damage in blue.

The pictures obtained from the analyses, the types of damage, and their accuracy rates are labeled on the photo by the computer. As a result of the photos taken, it was observed that these wooden selender structural elements were exposed to all three types of damage that the model was trained on. However, as observed in Figure 12, structural elements were mostly

Figure 11 Dataset used in this study for (a) MobileNet_V2, (b) Inception_V3 and (c) ResNet_V2_50 models
Slika 11. Skup podataka upotrijebljenih u ovoj studiji za modele: a) MobileNet_V2, b) Inception_V3, c) ResNet_V2_50

exposed to insect damage with only one selender exposed to wet rot damge and one selender to dry rot damage. When the predicted accuracy rates were taken into consideration, it was observed that all damage estimates were equal to 100 % and over 99 %.

As seen in Figure 12 (a), where photos obtained for some parts of the sample wooden structure were evaluated, an incorrect classification was made. Insect damage was estimated to exist in all of these classifications. When D11 damage is evaluated with human eyes in Figure 12 (a), it is possible to view this damage as both insect damage and dry rot damage. However, since double or multiple classifications were not made during the training phase, it was estimated that this damage was in fact only insect damage as identified by the model's superior vision. It is important to note that, in the evaluation of D11, 12, D13, and D14 images, there were false predictions, with the model identifying damage when there was none. The issue appears to have been the photo texture, which is similar in appearance to the images of insect damage used in training.

6 DISCUSSION AND SUGGESTIONS FOR FUTURE RESEARCH
6. RASPRAVA I PRIJEDLOZI ZA BUDUĆA ISTRAŽIVANJA

In civil engineering, it is essential to determine the potential damage that can occur in structures, estimate the structure behavior under the influence of external loads, and repair and strengthen said structures with this information in mind. For this reason, in this study, a traditional wooden structure found in Turkey, known as a selender, was chosen as an example, and damage assessment studies based on the deep learning method were carried out. Learning transfer strategies, a state-of-the-art method, have been used to detect damage to wood that occurs in building elements that make wooden structures. The data, classified by damage type, was determined with pre-trained deep convolutional neural network models (MobileNet_V2, Inception_V3, ResNet_V2_50). The deep learning methods used were then compared, and the possibility and type

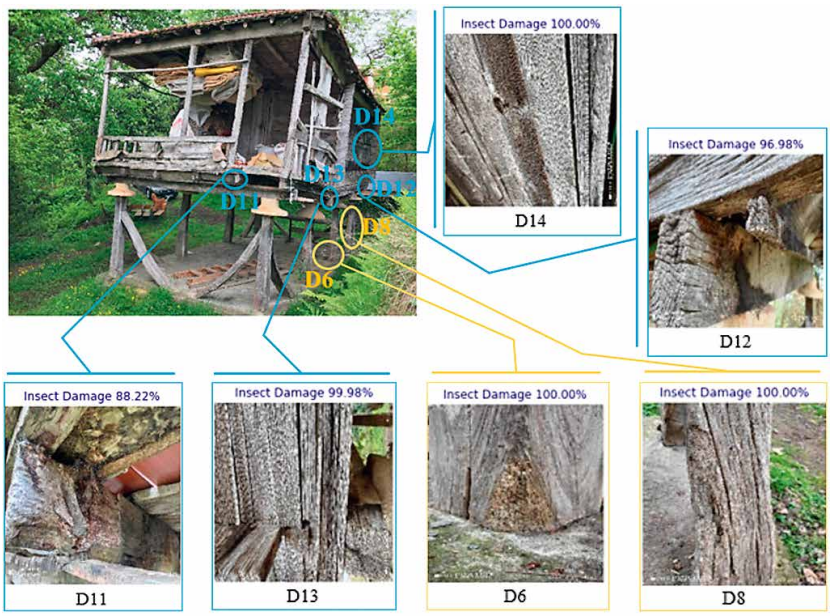

a)

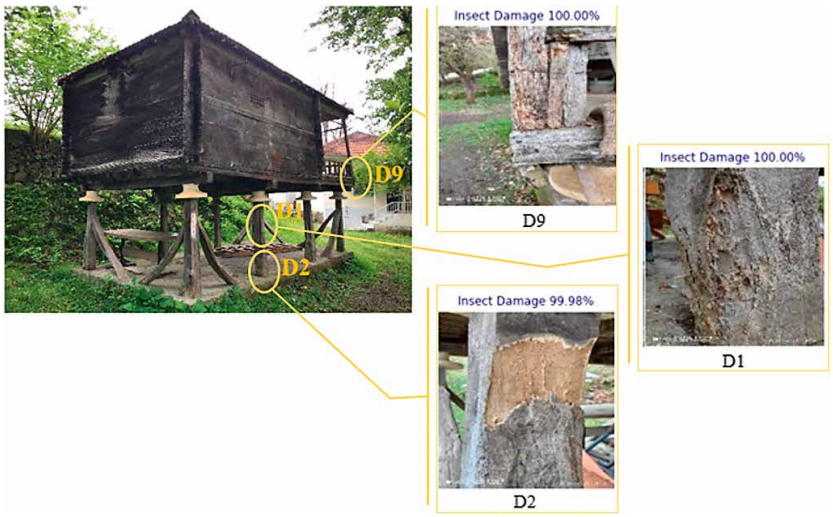

b)

c)

Figure 12 Examples of application images classified as "Insect Damage" classes with MobileNet_V2
Slika 12. Primjeri slika aplikacija klasificiranih kao klase „oštećenja od insekata" u modelu MobileNet_V2

of damage faced by the chosen structure were obtained using the most appropriate method.

Images of different sizes and resolutions were obtained from various sources, including photographs taken with a mobile phone and copyright-free images from the web, as representative of three specific types of wood element damage. These images were increased in number by applying the data augmentation method to the data set. Features obtained using pre-trained models and their labels are divided into training and test sets at 80 % and 20 %. These features are given as input to various classifiers and their labels. Analysis revealed that the lowest loss ratio from these classifiers came from the Multilayer Sensor MobileNet_V2 with 0.13, while the second-lowest loss ratio came from the Inception_V3 classifier with 0.31. The third lowest loss ratio was obtained with the ResNet_V2_50 classifier with 0.34. The accuracy rates of MobileNet_V2, (b) Inception_V3 and (c) ResNet_V2_50 models were identified as 96.38 %, 96.49 %, and 95.39 %, respectively. The accuracy points obtained via these three models are of similar significance. However, when considering the loss ratios, it is apparent that in terms of efficiency and accuracy rates the multi-layer MobileNet_V2 classifier is the most robust.

Three data sets were used in the present study; however, future research can expand on this by using more data sets. Due to the low number of labeled wood element damage data sets available in the literature, it is possible to decrease the ratio of false estimation based on the class by increasing and /or improving the class of wood damage images. The number of images used for training, as well as the correct classification of images, will increase the accuracy of prediction rates of CNN models. The present study identified the damage detection rate of the models used as being over 95 %. This is persuasive evidence of the viability of these models in the classification of types of wood damage.

The ability to accurately identify features of a given object is a direct result of having knowledge and experience of other objects, which varies from person to person. Object recognition in computer science requires the translation of these features into a numerical form. These property values are then processed in a decision making program called a classifier. In this way, each attribute can be associated with a class label. In this way, even a person who does not have any experience with wood damage can easily understand the type of damage, the risk to the structure, and how best to ameliorate the problem.

In future studies, it is considered to identify additional types of damage using various pre-trained models, and to predict which elements in wooden structures cause strength reduction and to what extent. It will also be necessary to take into account the estimation of the dynamic behavior of wooden structures under dynamic loads, such as earthquakes and strong winds, to better calculate potential risks and successfully account for them.

Data availability statement
– Izjava o dostupnosti podataka

Data, models, or codes that support this study's findings are available from the corresponding author upon reasonable request.

5 REFERENCES
5. LITERATURA

1. Abadi, M.; Barham, P.; Chen, J.; Chen, Z.; Davis, A.; Dean, J.; Devin, M.; Ghemawat, S.; Irving, G.; Isard, M.; Kudlur, M.; Levenberg, J.; Monga, R.; Moore, S.; Murray, D. G.; Steiner, B.; Tucker, P.; Vasudevan, V.; Warden, P.; Wicke, M.; Yu, Y.; Zheng, X., 2016: TensorFlow: A System for Large-Scale Machine Learning, Business Opp.
2. Cavalin, P.; Oliveira, L. S.; Koerich, A. L.; Britto, A. S., 2006: Wood defect detection using grayscale images and an optimized feature set. IECON 2006 – 32nd Annual Conference on IEEE Industrial Electronics, 3408-3412. https://doi.org/10.1109/IECON.2006.347618
3. Fei, R.; Yao, Q.; Zhu, Y.; Xu, Q.; Li, A.; Wu, H.; Hu, B., 2020: Deep learning structure for cross-domain sentiment classification based on improved cross entropy and weight. Scientific Programming, 2020, 3810261. https://doi.org/10.1155/2020/3810261
4. Hassaballah, M.; Awad, A. I.; 2020: Deep learning in computer vision: Principles and applications, 1st ed. CRC Press, Qena, Egypt.
5. He, K.; Zhang, X.; Ren, S.; Sun, J., 2015: Deep residual learning for image recognition. In: Proceedings of the IEEE Computer Society Conference on Computer Vision and Pattern Recognition. IEEE Computer Society, pp. 770-778. https://doi.org/10.1109/CVPR.2016.90
6. He, T.; Liu, Y.; Xu, C.; Zhou, X.; Hu, Z.; Fan, J., 2019: A fully convolutional neural network for wood defect location and identification. IEEE Access, 7: 123453-123462. https://doi.org/10.1109/ACCESS.2019.2937461
7. He, T.; Liu, Y.; Yu, Y.; Zhao, Q.; Hu, Z., 2020: Application of deep convolutional neural network on feature extraction and detection of wood defects. Measurement, 152, 107357. https://doi.org/10.1016/j.measurement.2019.107357
8. Hu, J.; Song, W.; Zhang, W.; Zhao, Y.; Yilmaz, A., 2019: Deep learning for use in lumber classification tasks. Wood Science and Technology, 53: 505-517. https://doi.org/10.1007/s00226-019-01086-z
9. Jabo, S., 2011: Machine vision for wood defect detection and classification. MSc Thesis, Department of Signals and Systems, Chalmers University of Technology, Göteborg.
10. Jones, S.; Kick-Rack, J.; Pound, W., 2007: Wood-Destroying Insect Diagnostic Inspection. Ohio, USA.
11. Ketkar, N., 2017: Introduction to Keras. In: Deep Learning with Python. Apress, Berkeley, CA. https://doi.org/10.1007/978-1-4842-2766-4_7
12. LeCun, Y.; Bengio, Y.; Hinton, G., 2015: Deep learning. Nature, 521: 436-444. https://doi.org/10.1038/nature14539

13. Nwankpa, C.; Ijomah, W.; Gachagan, A.; Marshall, S., 2018: Activation functions: comparison of trends in practice and research for deep learning. In: Proceedings of 2nd International Conference on Computational and Technology (INCCST 20), MUET Jamshoro.
14. Özgel Felek, S., 2020: Doğu karadeniz yerel mimariye ait serender ve dünya'dan benzer yapılar. Karadeniz İncelemeleri Dergisi, 28: 525-546.
15. Pan, S. J.; Yang, Q., 2010: A survey on transfer learning. IEEE Transactions on Knowledge and Data Engineering, 22 (10): 1345-1359. https://doi.org/10.1109/TKDE.2009.191
16. Robinson, W. H., 2005: Urban insects and arachnids: A handbook of urban entomology. 1st ed. Cambridge University Press. https://doi.org/10.1017/CBO9780511542718
17. Salman, H.; Grover, J.; Shankar, T., 2018: Hierarchical reinforcement learning for sequencing behaviors. arXiv:1803.01446v1 [cs.RO]. https://doi.org/10.48550/arXiv.1803.01446
18. Sandler, M.; Howard, A.; Zhu, M.; Zhmoginov, A.; Chen, L.-C., 2018: MobileNetV2: Inverted residuals and linear bottlenecks. In: Proceedings of the IEEE Conference on Computer Vision and Pattern Recognition (CVPR), pp. 4510-4520.
19. Schmidhuber, J., 2015: Deep learning in neural networks: An overview. Neural Networks, 61: 85-117. https://doi.org/10.1016/j.neunet.2014.09.003
20. Sioma, A., 2015: Assessment of wood surface defects based on 3D image analysis. Wood Research, 60 (3): 339-350.
21. Szegedy, C.; Ioffe, S.; Vanhoucke, V.; Alemi, A. A., 2017: Inception-v4, inception-ResNet and the impact of residual connections on learning. In: Proceedings of 31st AAAI Conference on Artificial Intelligence, pp. 4278-4284.
22. Szegedy, C.; Liu, W.; Jia, Y.; Sermanet, P.; Reed, S.; Anguelov, D.; Erhan, D.; Vanhoucke, V.; Rabinovich, A., 2015: Going deeper with convolutions. In: Proceedings of the IEEE Computer Society Conference on Computer Vision and Pattern Recognition, pp. 1-9. https://doi.org/10.1109/CVPR.2015.7298594
23. Szegedy, C.; Vanhoucke, V.; Ioffe, S.; Shlens, J.; Wojna, Z., 2016: Rethinking the inception architecture for computer vision. In: Proceedings of the IEEE Computer Society Conference on Computer Vision and Pattern Recognition, pp. 2818-2826. https://doi.org/10.1109/CVPR.2016.308
24. Urbonas, A.; Raudonis, V.; Maskeliunas, R.; Damaševičius, R., 2019: Automated identification of wood veneer surface defects using faster region-based convolutional neural network with data augmentation and transfer learning. Applied Sciences, 9, 4898. https://doi.org/10.3390/app9224898
25. van Rossum, G.; Drake, F. L. Jr., 1995: Python reference manual. Centrum voor Wiskunde en Informatica Amsterdam, Computer Science Department of Algorithmics and Architectur, Report, CS-R9525.
26. Wenshu, L.; Lijun, S.; Jinzhuo, W., 2015: Study on wood board defect detection based on artificial neural network. The Open Automation and Control Systems Journal, 7: 290-295. https://doi.org/10.2174/1874444301507010290

Corresponding address:

KEMAL HACIEFENDIOĞLU
Karadeniz Technical University, Department of Civil Engineering, 61080, Trabzon, TURKEY,
e-mail: kemalhaciefendioglu@ktu.edu.tr

Vasiliki Kamperidou[1], Efstratios Aidinidis[2], Ioannis Barboutis[1]

Surface Roughness of Sliced Veneers in Terms of Defects and Wood Structure Variability – Impact of Mild Hydrothermal Treatment

Hrapavost površine rezanog furnira u smislu nedostataka i varijabilnosti strukture drva – utjecaj blage hidrotermičke obrade

ORIGINAL SCIENTIFIC PAPER
Izvorni znanstveni rad
Received – prispjelo: 1. 7. 2021.
Accepted – prihvaćeno: 13. 12. 2021.
UDK: 620.179.118; 691.116
https://doi.org/10.5552/drvind.2022.2129

ABSTRACT • *This study deals with the surface roughness and quality of oak sliced veneers and how these characteristics are influenced by the presence of knots, and other defects associated to knots. The variability of roughness is thoroughly examined along the oak stem, exploring also how it differentiates going from one veneer to the adjacent one, cut in different wood depths of the same sawn wood piece in defect and non-defect areas. The expected vertical variability of morphological characteristics did not influence significantly the surface roughness along the stem, which favors the sliced veneers application and performance. The veneers obtained from the edges of the veneer package presented surfaces of high roughness. The smoothest surfaces were recorded in some of the areas on or peripherally of the living intergrown knots. Apart from the cases of large or dead knots that break and result in detrimental cavities, the small live knots do not influence negatively the roughness and therefore, neither the veneer processing demands, nor the overall quality of the final veneer-based product. In order to improve the surface quality of oak sliced veneers and to investigate the response of both defect- and non-defect areas to the hydrothermal modification, two mild and short-term hydrothermal treatments were applied. Among these treatments, only the mildest one (110 °C) managed to improve significantly the surface quality, concerning both the defect and non-defect areas, while the treatment at 130 °C did not reveal a significant change of the surface roughness of veneers.*

KEYWORDS: *knot; modification; quality; surface property; texture; veneer*

SAŽETAK • *U radu je istraživana hrapavost površine i kvaliteta rezanoga hrastova furnira te utjecaj kvrga i drugih nedostataka povezanih s kvrgama na hrapavost površine i kvalitetu tog furnira. Varijabilnost hrapavosti temeljito je ispitana duž hrastova debla te među susjednim furnirima rezanim na različitim dubinama istog debla u područjima s greškama i bez njih. Očekivana vertikalna varijabilnost morfoloških obilježja drva duž debla nije značajno utjecala na hrapavost površine furnira, što pogoduje primjeni i svojstvima rezanog furnira. Površina furnira uzetih s rubova paketa bila je vrlo hrapava. Površine s najmanjom hrapavošću bile su one s područja zdravih*

[1] Authors are researchers at Aristotle University of Thessaloniki, Department of Harvesting and Technology of Forest Products, Thessaloniki, Greece.
[2] Author is researcher at Agricultural University of Athens, Department of Forestry and Natural Environment Management, Athens, Greece.

uraslih kvrga ili periferno od njih. Osim velikih ili mrtvih kvrga, koje pucaju i rezultiraju štetnim šupljinama, male zdrave kvrge ne povećavaju hrapavost površine furnira, a time ne utječu na zahtjeve obrade furnira ni na kvalitetu proizvoda od njih. Kako bi se poboljšala kvaliteta površine hrastovih rezanih furnira i istražio utjecaj područja s greškama i bez njih na hidrotermičku modifikaciju, primijenjena su dva blaga i kratkotrajna hidrotermička tretmana. Od tih tretmana samo je blaži (110 °C) uspio znatnije poboljšati kvalitetu površine, kako područja s greškama, tako i područja bez grešaka, dok tretman pri 130 °C nije bitno utjecao na promjenu hrapavosti površine furnira.

KLJUČNE RIJEČI: *kvrga; modifikacija; kvaliteta; svojstvo površine; tekstura; furnir*

1 INTRODUCTION
1. UVOD

Wood is a polymeric lignocellulosic, anisotropic, complex material, of a distinct morphology, the structure of which depends on the way of biosynthesis and composition of its cells in the wood tissue. The texture is strongly related to the size (diameter) of the structural elements (cells) of wood, to cells type and distribution within the growth rings, differences in density and structure between early and late wood, earlywood and latewood ratio, with latewood to be much smoother than earlywood (Pinkowski *et al*., 2016), juvenility/maturity of wood, number and distribution of tracheid and vessel elements, etc. As a result, the surface properties of wood depend on the size and distribution of the micro-geometric deviations characterized by the small peaks and valleys of the relief, which constitute the wood surface topography. The surface roughness of wood constitutes a crucial characteristic for its utilization potential in numerous final applications (window frames, furniture manufacturing, benches, table tops, floors, etc.), affecting strongly the structures texture, appearance, surface touch feeling and the subsequent impact on the user's phycology, the manufacturing possibilities, finishing and sanding processes demands, adhesive quantity demands for the achievement of adequate wettability and bonding, wood surfaces bonding strength (Coelho *et al*., 2008; Li *et al*., 2010; Vassiliou *et al*., 2016; Bao *et al*., 2016; Sandak *et al*., 2020). Usually, the rough wood surfaces result in limited contact between the two wood surfaces, poor internal adhesion strength between adhered wood surfaces and consequently, lower mechanical performance of the whole structure (Coelho *et al*., 2008; Bao *et al*., 2016; Kamperidou *et al*., 2020). Furthermore, the phenomenon of adhesive bleeding through the face veneer is much limited in veneers of smooth surfaces (Dundar *et al*., 2008; Bekhta *et al*., 2009). Additionally, the importance of the surface quality in constructions is also proven by the fact that the perfection of the surface manufacturing/machining process and subsequent treatments (finishing, polishing processes) increase the service life of the product (Sandak *et al*., 2020). Excessive roughness tends to create rapid wear and dimensional changes, while surface irregularities, even tiny scratches or grooves, cause stress concentrations, which are the cause of cracks or the onset of fracture (Tsoumis, 2002).

Therefore, surface roughness has received much attention in the previous years. Several studies have been implemented so far, dealing with the surface roughness of wood products, revealing that it is highly influenced by factors, such as the wood species, wood structure, density, moisture content, anisotropy, growth rings width, early to latewood transition, work piece hardness, chemical composition, etc.

The material properties of the tool, concerning the cutting conditions, cutting means, tool wear, angle of knife, number of cutting teeth, cutting speed, cutting depth, feed rate, grain angle, etc., highly influence the surface roughness (Aydin *et al*., 2006; Csanády, 2015; Dobrzynski *et al*., 2018). Another crucial processing treatment, applied aiming to achieve the reduction of surface roughness and increase of sliced veneers quality, is the steaming process that precedes the slicing process of veneers to facilitate the veneer cutting process (Tanritanir *et al*., 2006).

The steaming pre-treatment method strengthens the toughness of wood, reduces the cutting resistance during slicing and therefore decreases the use of energy, damage to cell walls and color variations, improving the overall quality of sliced wood veneer (Aydin *et al*., 2006; Li *et al*., 2015). Additionally, the sanding process that follows the veneers slicing, contributes to the smoothness of wood surface, which depends on the grit number of the sandpaper used (Faust, 1987). The main sanding process of veneer is applied during the veneer-based panels production, using sandpapers of high grit numbers (>180). Other veneer quality criteria, except for the surface roughness, are the veneer thickness (average and variation), and lathe checks presence (depth and frequency) (Wang *et al*., 2006).

Unfortunately, the supply of high-quality wood has become increasingly scarce and therefore the contradiction between wood supply and demand has become increasingly prominent. As a result, research and industrial world recently attempt to evaluate the potential use of low-quality wood species, characterized by a high number of defects, for the preparation of various wood-based panels to meet the urgent needs of the immensely rising population concerning wood material (Yu *et al*., 2020). Defects such as dead (encased) knots,

veneers joint zones, holes and cracks on the surface of the wood veneer adversely affect the strength, appearance, and quality class of the product. They make the veneers less attractive to be applied in front face-side surfaces of structures (Bao *et al*., 2016; Kamperidou *et al*., 2020) and determine wood quality classification, as well as to evaluate and determine the cost of manufactured veneer-based products (Sandak *et al*., 2020).

Recently, Sandak *et al*. (2020) tested optimal sensors for refined and accurate enough scanning of the wood surface topography in an industrial environment in-line and on-line, proving their usability and success to access the surfaces of diverse quality and finishing state. The literature review showed a great lack of information as regards the way in which the defects (knots, decay, tensile wood, spiral grain, etc.) affect the smoothness and surface quality of sliced veneer sheets and. subsequently, the quality of veneer-based composites. Furthermore, no data have been found in literature concerning the roughness and surface quality of oak, a species whose veneers are in particular demand in the market, especially the "rustic" oak veneer. This particular type of oak veneer is known and appreciated for its unique appearance characterized by the presence of numerous small live knots and is being sold in the market at higher prices than the typical oak veneers.

Some preservation treatments have been applied so far to rotary cut veneer surfaces, aiming to improve the surface properties of wood, to increase surface activation and enhance the bondability of wood veneers (Kamperidou *et al*., 2012), such as chemical treatments with activating agents, hydrogen peroxide, aluminium persulfate, acetic acid, sodium carbonate, etc. (Bekhta *et al*., 2015) and compression treatments among others. Dudik *et al*. (2020) investigated the surface properties of birch wood rotary cut veneers after heat treatment (170-200 ºC, 1-5 h), namely color, hardness, roughness and wetting, and, in particular, the marketing evaluation of the attractiveness of colored birch wood. The applied heat treatments did not cause any significant changes in a positive or negative direction concerning the surface properties and roughness. As for sawn wood, a variety of results for the surface roughness of thermally modified wood has been demonstrated (Pinkowski *et al*., 2016), depending on many different factors including wood properties and thermal treatment parameters. Budakçı *et al*. (2013) outlined that surface roughness of several soft- and hard-wood species was not at all affected by heat treatment, whereas Gűndűz *et al*. (2008) recorded a lower surface roughness after the modification of black pine wood. Generally, commercial processes tend to first treat and then machine the wood (Gurau *et al*., 2017), and as a result, only few studies and limited information can be found in literature concerning the treatment of already cut (sliced or rotary) veneers. In parallel, there is a lack of information concerning the thermal, hydrothermal or chemical treatment of sliced (decorative) veneers.

Yu *et al*. (2020) investigated the potential of impregnated sliced veneers of poplar with glycidyl methacrylate and ethyleneglycol dimethacrylate, combined with maleic anhydride, as a reactive catalyst and in-situ polymerized and bonded monomers in their mass, through hot pressing method, revealing an impressive increase in bending strength, abrasion resistance, surface bonding strength and smoothness. Peng and Zhang (2019) treated five kinds of typical natural precious decorative veneer (rosewood, teak, black walnut, northeast China ash and red oak) by plasma at different discharge powers and speeds and among other findings, revealed improved surface wettability and increased surface roughness. However, no information or research data have been found concerning the potential of hydrothermal treatment to enhance the sliced veneer surface quality in terms of roughness or decrease of defects presence with an impact on the surface quality.

Therefore, the aim of this study is to examine the surface quality of oak sliced veneers, so that the roughness influenced by the presence of various structural defects (knots, and defects related to knots such as spiral grain, decay and tensile wood around the knots), is compared to non-defect areas of veneer surfaces. The vertical variability of roughness is thoroughly examined along the entire log, while it is also investigated how the surface roughness differentiates among the successively cut veneer sheets from the same batch of material, on different wood depths. In an attempt to improve the surface quality of oak cut (sliced) veneers and to investigate the response of both, defect- and non-defect- areas, to the hydrothermal modification, two mild and short-term hydrothermal treatments were applied.

2 MATERIALS AND METHODS
2. MATERIJALI I METODE

2.1 Collection of veneers and preparation of samples
2.1. Odabir furnira i priprema uzoraka

For the purposes of this experimental work, a package of 17 continuously sliced veneers of European oak (*Quercus robur* L.) wood was obtained from the market. The veneer package was of Balkan region origin (Croatia), produced by one of the most significant manufacturers of sliced veneers in Croatia and was imported to the Greek market, intended to be typically used as raw decorative veneers, applied on particleboards, plywood panels, door frames, etc. The specific company merchandises packages of 17 veneers in the market, which is the reason why we purchased the whole package of 17 veneers. Oak was selected as raw material to be characterized in this study, mainly be-

cause it is a significant species typically used in sliced veneers production in the Balkan region, among other species, and as a ring-porous, deciduous species bearing wide rays and vessels (often 3 times wider than adjacent fibers), which can be considered to be more of a rough texture (Zhao *et al*., 2020).

According to the information gathered through the communications with the specific veneer production industry, the tree log used for the production of the specific sliced veneers was of large diameter and approximately at the age of 72 years. It was industrially converted into decorative veneer sheets, using the slicing method, applied in the infrastructures of the abovementioned industry of sliced veneer production, so that the pre-treatment processes, steaming, mechanical processing conditions, cutting tools, slicing method applied, etc. would be based on industrial conditions and certified practices. The sliced veneer production met the requirements of the industrial sliced veneer production standards applied in this certified industrial unit, in terms of defects elimination, thickness similarity, avoidance of irregularities attributed to mechanical processing errors, such as burning and injuries, among others (stated by the veneer production industry and the collaborating market stores). Prior to the slicing process of veneers, the oak log was initially debarked, naturally dried and exposed to steaming. The slicing device used for the preparation of these decorative flat-cut veneers was of horizontal operation, appropriate for slicing hardwood veneer.

The veneers were sliced in radial direction and there was no visible color difference between heartwood and sapwood and therefore the percentage of sapwood/heartwood has not been considered in the measurements of this study. The growth rings were clearly visible, as expected in a typical ring-porous species, in which there is a clear transition from early- to late-wood. The phenomenon of oak to present the effect of chrysalis in radial section is not so easily seen with the naked eye in the wood veneers examined in the present research. The conical shape of stem is not intense, which may indicate that the tree probably grew in a closed cluster or that pruning had been applied, among other factors. As a tree of medium to high age, with mature wood, it is expected not to present conical shape, since this is a typical characteristic of younger stems (Tsoumis, 2002). The fact that the tree may have grown in narrow space or at a considerably low distance from other trees, is consistent with its narrow growth rings. Of course, the growth rings width depends on various factors, such as age, growing conditions (soil, moisture, sun) and heredity (Tsoumis, 2002).

The package of the continuously sliced veneers (continuous in a row and successively cut) was selected to be characterized (Figure 1), aiming to observe the evolution of the whole defects (mainly knots) as they are encountered in the log mass. The veneers were of (0.53±0.1) mm thickness, cut mainly from the logs heartwood, in dimensions (3130 mm length × 250 mm width), and were left to be conditioned at (20±2) ºC and (65±5) % relative humidity, till constant weight. All veneer sheet samples were conditioned to equilibrium moisture content (EMC), and stayed there until the measurement of roughness. Each roughness measurement area corresponded to a surface of approximately 30 mm × 30 mm. These areas were selected and marked on the surface of veneer samples, so that each of them was in a close proximity to the respective knot/defect examined (Figure 1). Much attention has been paid to ensure the representativeness of the measurements, trying to distribute the 30 mm × 30 mm measurement areas on the whole surface of each veneer to depict the quality of the whole veneer, based also on the distribution pattern of knots. As regards the estima-

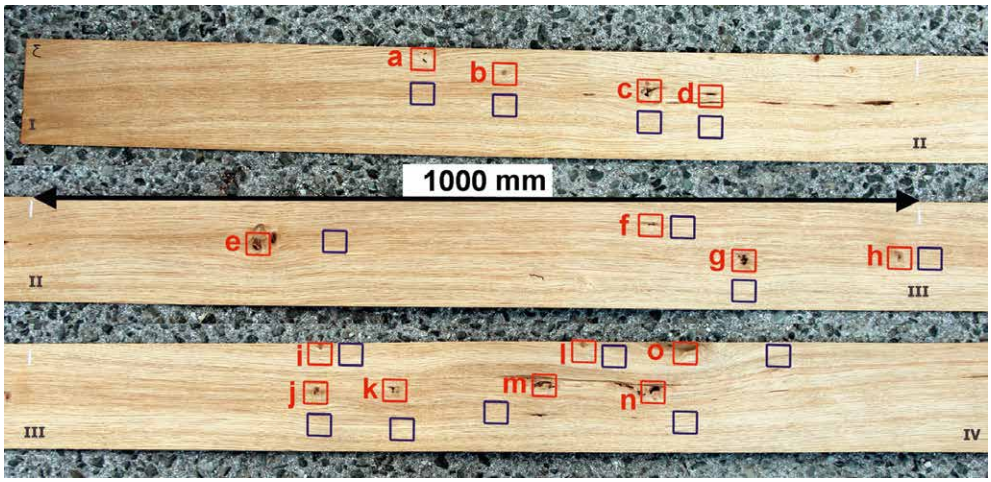

Figure 1 Distribution of 15 studied knots (a-o) on the surface of veneer sample and configuration of roughness measurement areas (30 mm × 30 mm) concerning 15 knot areas (red squares), and respective non-defect areas (blue squares)
Slika 1. Raspodjela 15 proučavanih kvrga (od a do o) na površini uzorka furnira i konfiguracija područja mjerenja hrapavosti (30 × 30 mm) s obzirom na područja od 15 kvrga (crveni kvadrati) i područja bez grešaka (plavi kvadrati)

tion of roughness on the knot areas, several measurements were implemented within surface areas of 30 mm × 30 mm (applying the stylus method in several directions, perpendicular to the veneer length, from circumference of knot to its center and vice versa, etc.), on the knots (when possible), where the orientation of the tissue is perpendicular to the surface, and also, around the examined knots, in their peripheral area, within a radius of 10–20 mm around the knot, including in this way the transition zone from the knot to defect-free wood. In this case, the orientation of the tissue is arbitrarily between 0 and 90 ° and this could influence the surface roughness.

2.2 Roughness measurement
2.2. Mjerenje hrapavosti

In case of areas without defects, the measurements were implemented on an axis perpendicular to the grain (on both directions), recording different growth rings, as encountered on wood surface. This was based on methodology proposed in the respective standard of roughness measurement ISO 4287:1997, as well as the manual instructions of the profilometer used and the practice followed in previous studies (Budakci *et al*., 2013; Kamperidou and Barboutis, 2017; Li *et al*., 2018), aiming to ensure comparability of results. Given the uniqueness of each defect and each knot, it is easily comprehended that some of them constitute live or dead knots, knots accompanied by traces of decay, cavities or deviations of fibers orientation from the stem axis direction, etc. (Figure 2). Although, almost all knots can be considered to be of relatively small dimensions (based on the market considerations and authors' experience), the knots of slightly higher diameter/dimensions were found near the base of the tree, while going towards the canopy, only small knots were detected.

At least 12-15 measurements were implemented on the areas of these 15 knots that were detected on the surface of the veneers (symbolized as knots a-o, going from the canopy to the base of the tree). These roughness measurements were implemented on the differentiated wood structure of knot area, and separately to a respective non-defect area located close to each knot. This approach of clean/defect wood structure pair-points of measurement was applied in order to eliminate the interactive influence of other factors on the surface roughness on different stem heights (the potential of not apparent presence of small injuries/infection/mechanical processing difference, or other cell biosynthesis factors, etc.), allowing the comparison between the roughness values of knot areas and non-defect areas.

All the 17 veneers could not be thoroughly measured (one by one), with such a detailed characterization, examining the 15 knot areas and 15 non-defect areas (x15 measurements on each area of 30 mm × 30 mm). Therefore, some initial measurements had been implemented on all of the 17 veneers to obtain a general idea on the veneers quality and roughness, and finally, we determined to measure thoroughly (as mentioned above) the 1st, 6th, 12th and 17th veneer collectively, in order to provide a representative image of the surface roughness of the whole package of these sliced veneers. In this way, the potential differentiation of roughness as a function of different wood depths on the areas of knot development was investigated. In parallel, attention has been paid to ensure the representativeness of the measurements and therefore the reliability of the results.

The surface roughness of the sliced veneers was examined applying a contact method over the object surface, using a "Mitutoyo Surftest SJ-301" fine stylus

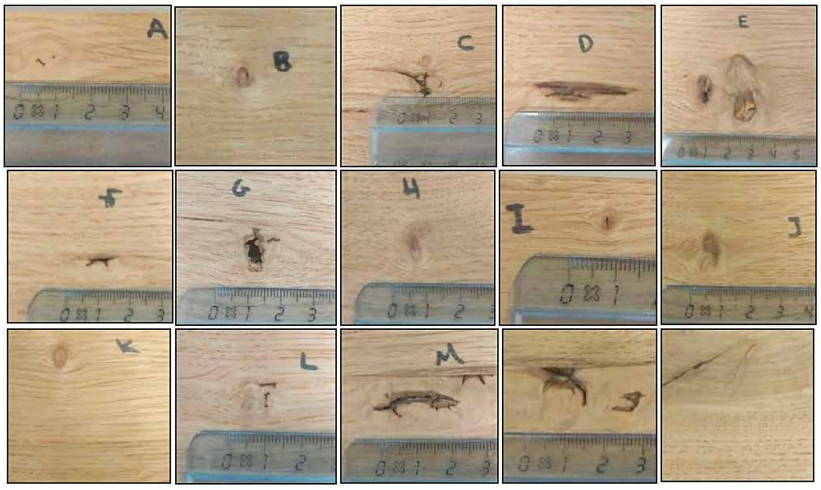

Figure 2 Configuration of 15 knots (a-o) detected on the surface of examined oak decorative veneers, going from canopy to tree base
Slika 2. Konfiguracija 15 kvrga (od a do o) otkrivenih na površini ispitivanih hrastovih dekorativnih furnira, dobivenih s područja od krošnje do baze debla

(a)

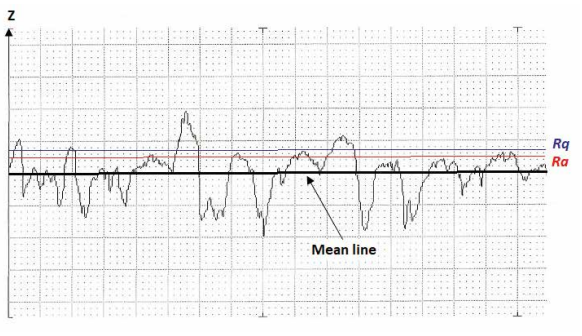

(b)

Figure 3 Surface roughness characterization using a stylus-type profilometer instrument (a) and surface roughness parameters defined (b)
Slika 3. (a) Karakterizacija hrapavosti površine uz pomoć profilometra s trnom i (b) definirani parametri hrapavosti površine

type profilometer (Figure 3a) according to the standard ISO 4287:1997. This method was chosen as convenient, as it provids accurate results. The measuring speed, the diameter of the pin and the upper angle of the pin tool were 10 mm / min, 4 μm, and 90 °, respectively. The sampling length was of 2.5 mm, and the measurements were implemented in a direction perpendicular to the direction of grain orientation (in areas of clean wood structure).

Three roughness parameters, the mean arithmetic deviation of profile (*Ra*), the mean peak to valley height (*Rz*), and the maximum defect height indicator within the assessed profile, in other words the maximum roughness (*Rq*), were evaluated (Figure 3b). These 3 parameters have been previously used in literature (Budakci *et al*., 2013; Kamperidou and Barboutis, 2017; Li *et al*., 2018), as well employed in veneers roughness assessment (Mummery, 1993), and other wood-based composites. They are specified by the relevant standard ISO 4287:1997. Calibration was a necessary step, implemented before the operation of the profilometer using the calibration standard plate of the device (Mitutoyo 178-601 surface roughness standard), while the measurements were carried out at ambient conditions of (20±2) ºC) (Korkut *et al*., 2008; Korkut and Budakci, 2010).

2.3 Moisture content, density and growth rings width
2.3. Sadržaj vode, gustoća i širina goda

At the end of the measurements of each veneer, 6 specimens of dimensions 20 mm × 20 mm were cut from the edges of each studied veneer (defect-free structure of wood) to measure the veneer moisture content by applying the drying method of the veneer samples according to the respective methodology (ISO 13061-1:2014). The mean value of moisture content of the studied veneers at the time of measurements, which corresponds to the EMC value, was measured to be (9.8 ±0.4) %. For the dry mass measurement, a scale of high accuracy (4 decimals) was used, and for the volume determination, a digital caliper (Mitutoyo 500-196-30) of 0.0005”/0.01 mm resolution was used. On the above specimens, prepared for the moisture content measurement, the mean density of oak wood of 0.721 (± 0.09) g/cm3 was measured based on the respective standard methodology (ISO 13061-2:2014). The mean growth ring width of the examined sliced veneers was found to be (1.2±0.08) mm. This value corresponds to the mean value of measurements in three different points/heights of each veneer (in the middle of veneer length and in the 2 edges of each veneer). Afterwards, using a stereoscope (Nikon SMZ800, Nikon Instruments Inc., NY, USA), the abovementioned examined areas were magnified (X16) and then the growth rings width was recorded using the digital caliper.

2.4 Veneers heat treatment
2.4. Toplinska obrada furnira

After the implementation of the roughness measurements, the four studied veneers were cut in their middle, providing 2 pieces of smaller length (around 1530 mm). They were exposed to heat treatment at 110 ºC (Veneers V6 and V17 – one from the middle and one from the edge of package) and at 130 ºC (V1 and V12– one from the middle and one from the edge of package), in an atmosphere saturated with steam, at a pressure of around 1.5 atm (custom-made chamber, AUTh, Thessaloniki, Greece), for 2 hours from the moment of reaching the final conditions (maximum temperature/pressure). It took approximately 15 min to reach the final conditions inside the chamber at the beginning of the treatment, while at the end of the treatment, the veneer samples were kept for 15 min inside the chamber till the gradual decrease of temperature. Then, the veneers were conditioned till constant weight to EMC, and remained in the conditioning room till the time of roughness measurements (for around 2 weeks).

Both treatments had to be short and mild in order to try to improve the surface quality of these veneers and at the same time to avoid the intensive chemical changes that may take place due to thermal degradation

(hemicelluloses, cellulose and lignin depolymerization) (Gonultas and Candan, 2018; Kamperidou, 2019), and the subsequent mechanical strength loss. After the implementation of these short-term hydrothermal treatments and a 2-week conditioning process of the treated veneers, the measurements of surface roughness were conducted again, on the same marked surface areas (30 mm × 30 mm) concerning both defect and non-defect areas, under the same conditions, following exactly the same methodology, in order to get comparable results.

2.5 Statistical analysis
2.5. Statistička analiza

For the statistical analysis of the results, the statistical package SPSS Statistics 25 was used to determine the variability of the mean values of roughness parameters, and the effect of two different independent variables, "Veneers" (referring to the different veneers from V1 to V17), and "Structure" (referring to the defect and non-defect area of wood), and the potential interaction of these two factors upon the dependent variable of roughness parameter *Ra,* chosen as the most commonly used in literature to assess surface quality (Gurau *et al*., 2017), using two way analysis of variance (ANOVA) with a significance level of 0.05 ($p < 0.05$). The homogeneity of variances of the results was tested by means of "Levene´s test of Equality of Error Variance" (the null hypothesis) (Levene, 1960).

3 RESULTS AND DISCUSSION
3. REZULTATI I RASPRAVA

The progress of roughness parameters (*Ra, Rz* and *Rq*) along the stem, measured following a direction from the canopy to the tree base, concerning areas of defect-free wood structure of the four examined veneers (V1, V6, V12, V17), is presented in Figure 4, 5 and 6.

As regards the roughness parameters along the stem measured on non-defect areas, from the canopy (a) to the tree base (o), even though some statistically significant differences were recorded from point to point among a-o points, a clear tendency of roughness increase or decrease was not depicted along the veneer from the canopy to the tree-base. This is a similar trend as reported for all the examined veneers (V1, V6, V12, V17). Therefore, despite the expected vertical wood structure variability, usually detected along the stems, and the fact that the vessel size may increase by a factor of 3 within the same oak stem (Leal *et al*., 2007),

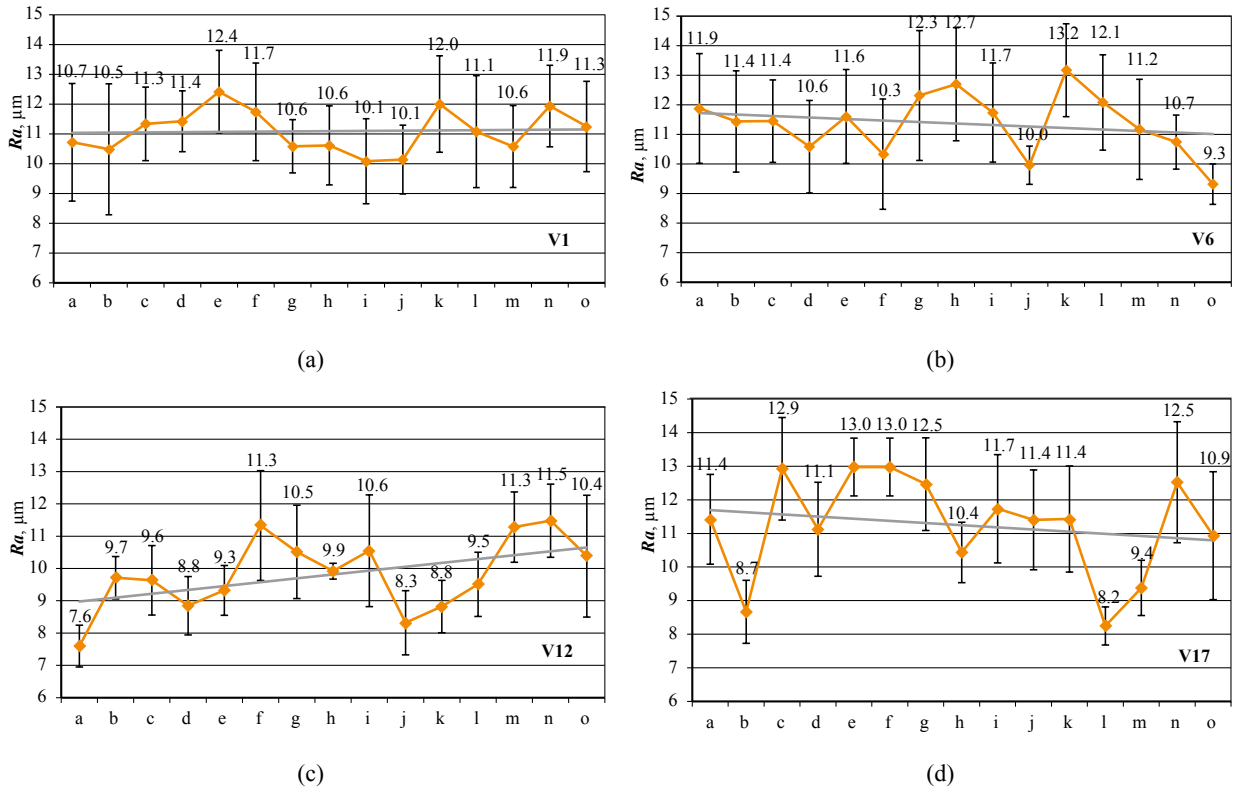

Figure 4 Progress of *Ra* roughness parameter (µm) along the stem, measured on typical structure areas, from the canopy to the lowest part of the tree base, on veneers of (a) V1, (b) V6, (c) V12 and (d) V17. The linear trend line is displayed in gray color.

Slika 4. Povećavanje parametra hrapavosti *Ra* i (µm) duž debla, mjereno na tipičnim strukturnim područjima, od krošnje do najnižeg dijela baze debla, na furnirima (a) V1, (b) V6, (c) V12 i (d) V17. Linija linearnog trenda prikazana je sivom bojom.

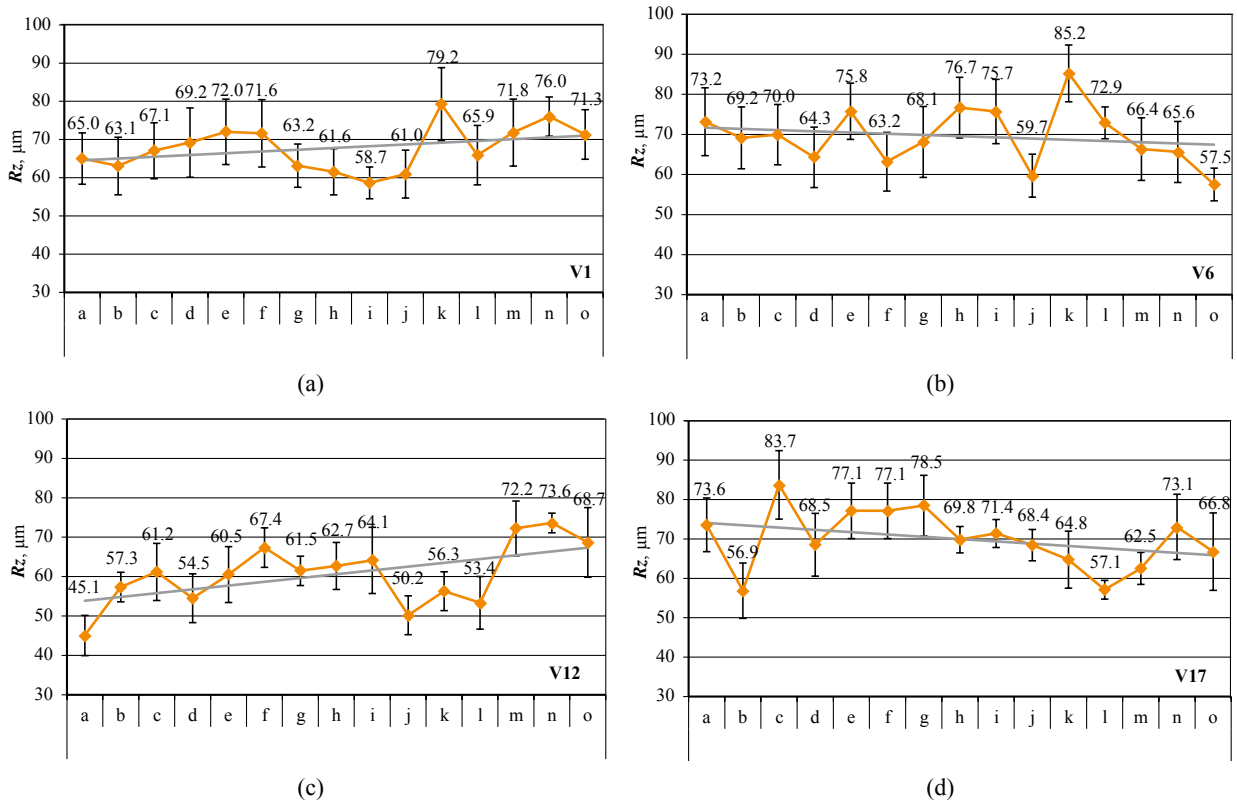

Figure 5 Progress of *Rz* roughness parameter (μm) along the stem, measured on typical wood structure areas, from the canopy to the lowest part of the tree base, on veneers of (a) V1, (b) V6, (c) V12 and (d) V17. The linear trend line is displayed in gray color.

Slika 5. Povećavanje parametra hrapavosti *Rz* i (μm) duž debla, mjereno na tipičnim strukturnim područjima, od krošnje do najnižeg dijela baze debla, na furnirima (a) V1, (b) V6, (c) V12 i (d) V17. Linija linearnog trenda prikazana je sivom bojom.

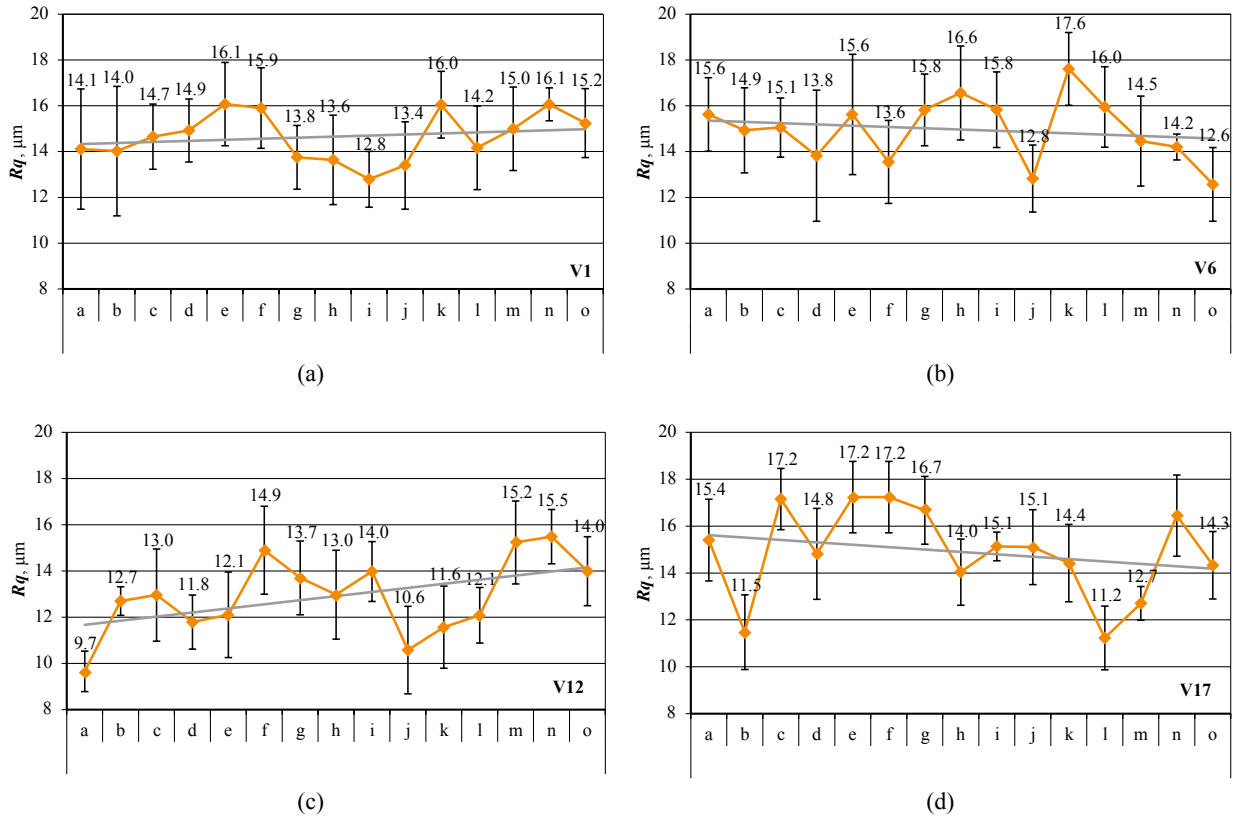

Figure 6 Progress of *Rq* roughness parameter (μm) along the stem, measured on typical structure areas, from the canopy to the lowest part of the tree base, on veneers of (a) V1, (b) V6, (c) V12 and (d) V17. The linear trend line is displayed in gray color.

Slika 6. Povećavanje parametra hrapavosti *Rq* (μm) duž debla, mjereno na tipičnim strukturnim područjima, od krošnje (a) do najnižeg dijela baze debla, na furnirima (a) V1, (b) V6, (c) V12 i (d) V17. Linija linearnog trenda prikazana je sivom bojom.

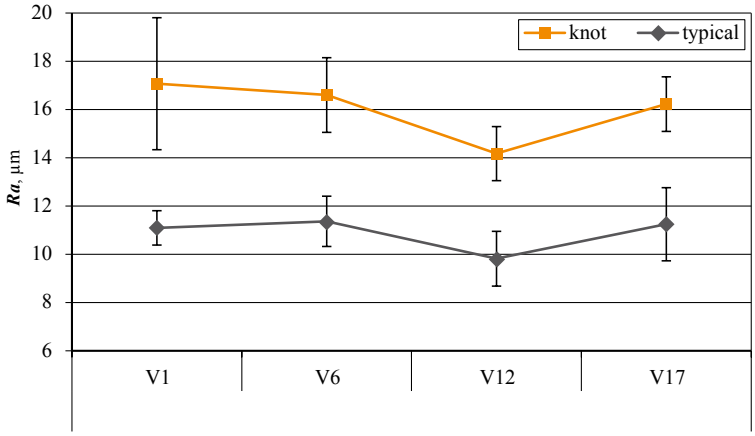

Figure 7 Mean values (μm) of roughness parameter (*Ra*) measured on 15 different points (a-o) along the stem of the examined veneers V1, V6, V12 and V17
Slika 7. Srednje vrijednosti (μm) parametra hrapavosti (*Ra*) izmjerene na 15 različitih točaka (a – o) duž debla, za ispitivane furnire V1, V6, V12 i V17

also increasing the surface roughness, similar surface quality and roughness was recorded along the veneer and the stem. This indicates that the variability of morphological characteristics usually detected on different stem heights was not sufficient to influence the roughness of the surfaces. This characteristic of roughness and quality uniformity in the surface of veneers could highly favor their performance and utilization.

Nevertheless, statistically significant differences were recorded between V12 and the other values of veneer roughness, with V12 to record the lowest surface roughness value, both on non-defect wood surfaces and knot areas (Figure 7) and the lowest standard deviation values compared to the rest of examined veneers. Veneer sheet V1 presented the highest roughness values. V1 and V17 were the first and last veneers of the package, respectively, and therefore their higher surface roughness could be partly attributed to the fact that they may have experienced some intensive changes of moisture content, during an earlier stage that preceded the experimental work, during their transfer or storage, that may have resulted in dimensional changes, which could have led to fibers detachment and to wilder/rougher surfaces.

According to Figures 8 and 9 that present the percentage of differences between roughness parameters *Ra, Rz* and *Rq* of defect-free wood structure veneer surfaces and defect-wood structure areas on/around the knots (a-o), it is obvious that concerning all the veneers and 14 out of 15 cases of knots examined, the surface roughness parameters were significantly lower, from a statistical point of view, than the respective values measured on defect-free wood structure surfaces very close to knot areas. This finding of lower roughness around the knots could be attributed mainly to the fact that in hardwoods, in the lower part of the knot, tensile wood usually appears. It can be recognized by its lighter color and higher gloss, a slightly higher axial shedding (up to 1.5 %), with more cells of smaller diameters, resulting in 2-20 % higher density of wood in these areas (Tsoumis, 2002; Dundar *et al*., 2008). Another factor contributing to the lower roughness, could be the fact that in these areas the fibers usually bear a gelatinous layer inside the fiber walls, which is rich in cellulose and of a high crystallinity degree. **Tensile** wood bears more fibers, and smaller and fewer vessels, as well as more rays. Therefore, the differences in density and structure of tensile wood areas may have a high impact on surface roughness (Tsoumis, 2002).

Another reason could be the presence, number and size of vessels found in defect-free wood structure surfaces of such a ring-porous species. Since the roughness measurements in the non-defect areas were conducted on an axis perpendicular to the grain, at least 2 growth rings were scanned by the stylus of the profilometer, taking into account the area of vessels. Lower roughness was also recorded in areas around the knot (till 20 mm), in the transition zone from knot to defect-free wood areas, where irregularities of annual rings or spiral grain phenomena were also present. This is of great importance for the performance of oak sliced veneer in various applications, since evidently these areas of spiral grain (surrounding the knot) are usually of a larger area than the knot itself.

It is observed that in V12, not only the lowest roughness parameters values were recorded on non-defect wood surface, but at the same time the highest difference between the surface roughness of the areas around the knots and the respective non-defect areas was detected (table 1). In V6 and V17, high differences of roughness were recorded between wood structure of non-defect areas and different wood structures on and around the knots areas, with knots (especially the small live knots) to constitute smoother areas compared to defect-free wood surfaces. Of course, in some cases of firm or loose knots (c, d, g, m, n), where a cavity had

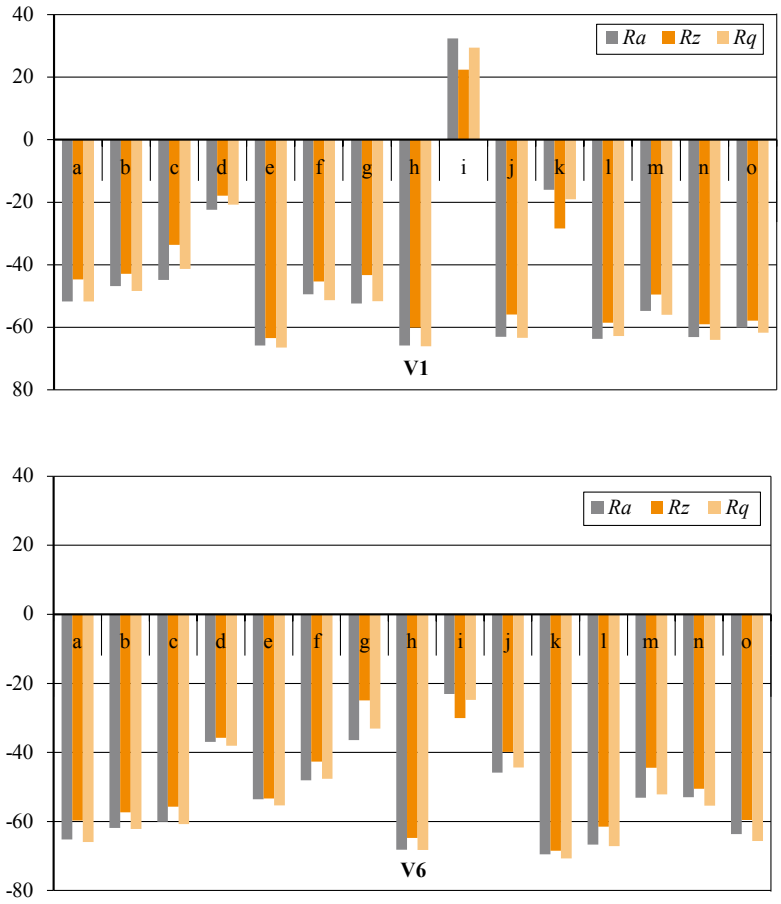

Figure 8 Percentage values depicting the decrease of roughness parameters (*Ra, Rz, Rq*) recorded on knot areas (a-o), compared to corresponding areas of non-defect surfaces in veneer V1 and V6
Slika 8. Postotne vrijednosti koje pokazuju smanjenje parametara hrapavosti (*Ra, Rz, Rq*) zabilježene na područjima s kvrgama (a – o) u usporedbi s odgovarajućim područjima bez kvrga na furniru V1 i V6

been generated because of a breaking knot or decay, especially in the case of large or dead knots, the resultant wood tissue discontinuity is proven detrimental to the surface quality, and the veneer requires special pretreatment, use of resin or substitution of the knot part with a non-defect veneer piece and sanding, thus also increasing the use of energy and cost of production. In case of veneer V1, as regards the defect-free wood structure surfaces, the highest surface roughness values were observed, even though without marking statistically significant difference, as well as the lowest roughness parameters difference values between defect-free wood structure and defect-wood structure (knot areas). This may be partly attributed to the potential frequent changes of relative humidity and the subsequent moisture absorption-desorption of wood during transport or storage that could deteriorate the surface quality of veneers, increasing the demands of sanding or the need of higher amounts of finishing, painting or adhesive agents applied to the surfaces. In this case, the necessity to protect the sliced veneers from frequent changes of climatic conditions would be highlighted.

The results of Levene's test (table based on two-way analysis of ANOVA, SPSS) showed that the null hypothesis cannot be rejected in a significance level of 0.05 (*p* value 0.213), and therefore the 6th requirement of ANOVA is fulfilled. The factor "Veneers" presented a statistically significant effect on surface roughness parameters, affecting their variability by 13 % (sig. 0.001). The factor of "Structure", referring to defect-free wood structure of non-defect areas or knot areas of different wood structure, demonstrated the statistically significant effect on roughness, marking an influence of 80.1 % on roughness variability (sig. 0.000). The interaction between these two factors, veneers and

Table 1 Mean percentage values depicting the decrease of roughness parameters *Ra, Rz* and *Rq* of defect areas, compared to respective non-defect wood structure veneer surfaces, recorded on examined veneers
Tablica 1. Srednje postotne vrijednosti koje pokazuju smanjenje parametara hrapavosti *Ra, Rz i Rq* na područjima s greškama u usporedbi s odgovarajućim područjima furnira bez grešaka strukture drva zabilježene na ispitivanim furnirima

Veneer / *Furnir*	***Ra***	***Rz***	***Rq***
V1	-45.82	-42.53	-46.33
V6	-53.67	-49.90	-54.08
V12	-55.50	-50.97	-55.62
V17	-54.90	-52.27	-56.02

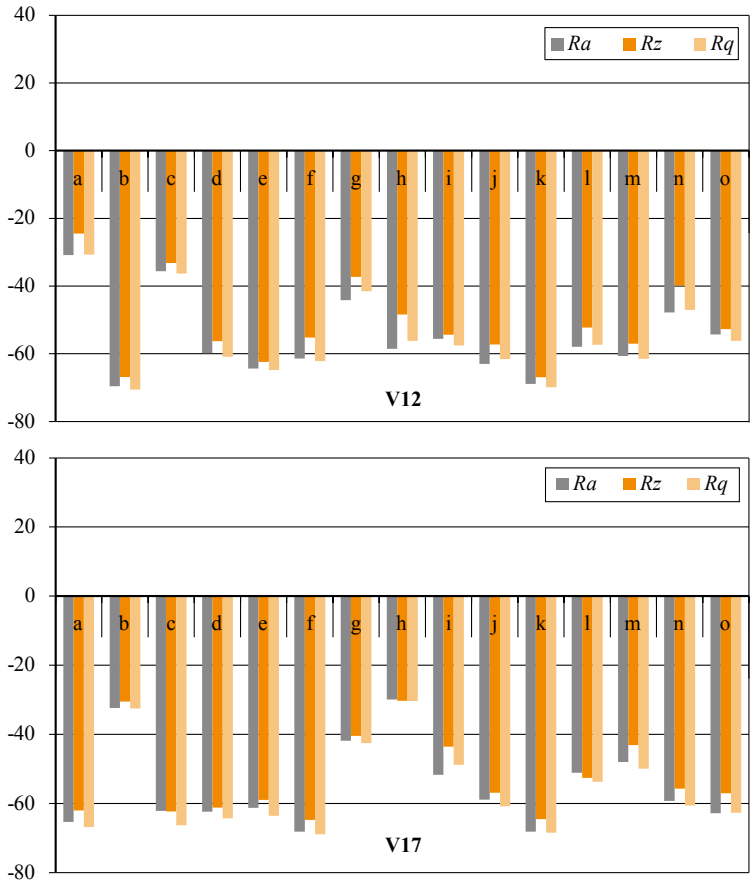

Figure 9 Percentage values depicting the decrease of roughness parameters (*Ra, Rz, Rq*) recorded on knot areas (a-o), compared to corresponding areas of non-defect surfaces in veneer V12 and V17
Slika 9. Postotne vrijednosti koje predočuju smanjenje parametara hrapavosti (*Ra, Rz, Rq*) zabilježene na područjima s kvrgama (a – o) u usporedbi s odgovarajućim područjima bez kvrga na furniru V12 i V17

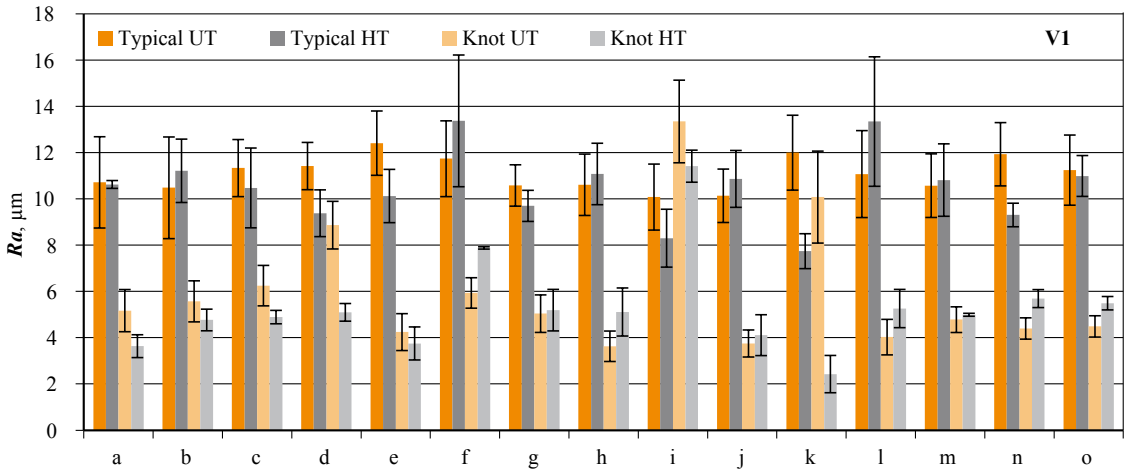

Figure 10 Mean values (µm) and respective standard deviation values of roughness parameter (*Ra*) measured on 15 different points (a-o) along the stem, concerning both knot areas and defect-free areas, on the surface of veneer V1, before (UT- untreated) and after (HT – treated) hydrothermal treatment (130 ºC-2h)
Slika 10. Srednje vrijednosti (µm) i odgovarajuće vrijednosti standardne devijacije parametra hrapavosti (*Ra*) izmjerene na 15 različitih točaka (a – o) duž debla, koje se odnose na područje s kvrgama i na područje bez grešaka, na površini furnira V1, prije hidrotermičke obrade (130 ºC, 2h) (UT – neobrađeno) i nakon obrade (HT – obrađeno)

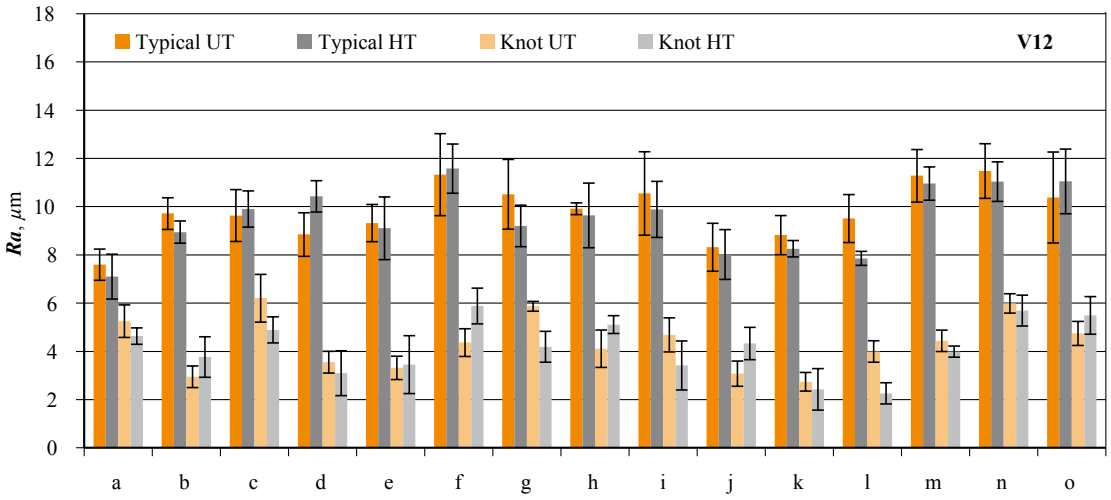

Figure 11 Mean values (μm) and respective standard deviation values of roughness parameter (*Ra*) measured on 15 different points (a-o) along the stem, concerning both knot areas and defect-free areas, on the surface of veneer V12, before (UT- untreated) and after (HT – treated) hydrothermal treatment (130 ºC-2h)
Slika 11. Srednje vrijednosti (μm) i odgovarajuće vrijednosti standardne devijacije parametra hrapavosti (*Ra*) izmjerene na 15 različitih točaka (a – o) duž debla, koje se odnose na područje s kvrgama i na područje bez grešaka, na površini furnira V12 prije hidrotermičke obrade (130 ºC, 2h) (UT – neobrađeno) i nakon hidrotermičke hidrotermičke obrade (HT – obrađeno)

structure, did not record a statistically significant impact on roughness parameters.

In an attempt to improve the surface quality of the oak sliced veneers and to investigate the response of both, defect-free wood structure areas and defect-areas, to the hydrothermal modification process, two short-term treatments were performed (max. temperature of 110 ºC and 130 ºC). According to the results, the hydrothermal treatment of 130 ºC did not show a clear tendency of impact (a negative or positive one) on the surface roughness of wood veneers, and in most of the cases, the recorded differences were not statistically significant, as demonstrated in Figures 10 and 11 for the veneers V1 and V12. It can be observed that in most of the cases, concerning both the non-defect and the defect-areas, the roughness of heat treated veneers was not found to differ significantly from the roughness values of the corresponding areas of untreated veneers.

The slightly milder hydrothermal treatment of 110 ºC, more favorable to the surface quality improvement of sliced veneers, was found in most of the study areas marking a statistically significant decrease of surface roughness in both wood structure of non-defect areas and defect areas, as presented in Figures 12 and 13 for veneers V6 and V17, respectively. This indicates that the hydrothermal modification could act beneficially on the surface quality (smoothness) of oak sliced veneers, only if it is applied at quite low temperatures (100-110 ºC) for short durations. This could be explained by the geometry and dimensions. To be specific, the very low thickness of the sliced veneers allows the entire cross-section to reach faster the temperature of the medium and therefore leaves the wood tissue vulnerable to thermo-degradation phenomenon and oxidative reactions. Treatments of higher intensity (higher temperatures or durations) can cause the loss of volatile extractives, generation of new extractives from the hydrolysis of polysaccharides or polymerization of some extractives, partial depolymerization of hemicelluloses and amorphous parts of cellulose, etc. also affecting the structure and surface properties of wood (Filipou, 2014; Kamperidou, 2019). However, according to the findings of Dudík *et al*. (2020), the heat treatment of birch wood veneers at 170 ºC, 190 ºC and 200 ºC (much higher temperatures than those applied in the present study), and duration of 1, 3, 5 hours, did not cause any significant negative or positive impact on the surface roughness of the veneers, but this different response could be probably attributed to the fact that the veneers were not sliced cut, but rotary cut, and were of different dimensions (500 mm x 500 mm, with thickness of 1.5 mm) than those of the present study. Concerning the surface roughness of thermally treated sawn wood/timber (assessed on samples of higher dimensions), most of the studies have revealed a decrease in surface roughness of wood after its exposure to heat treatment (Korkut and Budakci, 2010; Baysal *et al*., 2014).

Thermal or hydrothermal modification process is made of cost-effective and environmentally-friendly treatments that provide many benefits to wood and wood-based products (veneers and others), such as improved dimensional stability, lower moisture absorption, increased biological durability, higher color homogeneity, etc. (Kamperidou, 2019). As regards the aesthetics of wood material, these treatments tend to darken wood and confer a reddish color that helps it to imitate more expensive exotic species. Concerning the

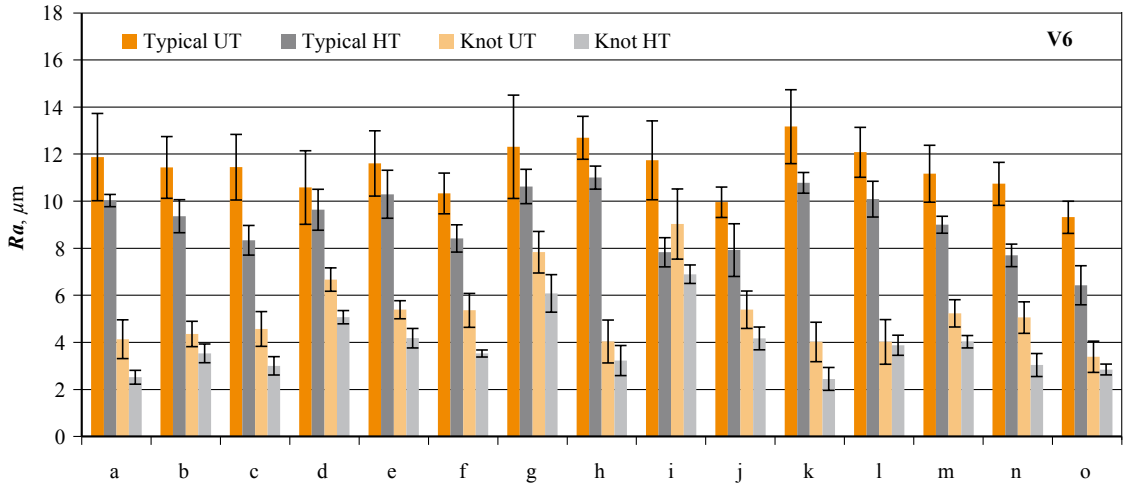

Figure 12 Mean values (μm) and respective standard deviation values of roughness parameter (*Ra*) measured on 15 different points (a-o) along the stem, concerning both knot areas and defect-free areas, on the surface of veneer V6, before (UT- untreated) and after (HT – treated) hydrothermal treatment (110 ºC-2h)
Slika 12. Srednje vrijednosti (μm) i odgovarajuće vrijednosti standardne devijacije parametra hrapavosti (*Ra*) izmjerene na 15 različitih točaka (a – o) duž debla, koje se odnose na područje s kvrgama i na područje bez grešaka, na površini furnira V6 prije hidrotermičke obrade (110 ºC, 2h) (UT - neobrađeno) i nakon hidrotermičke obrade (HT – obrađeno)

surface quality of wood, these treatments seem to enhance the smoothness of its surfaces (Korkut and Budakci, 2010; Baysal *et al*., 2014), even though the response of very thin sheets of wood, such as the sliced veneers, is not very clear. According to the findings of this experimental work, a mild hydrothermal treatment (around 100-110 ºC, for 2h) could improve significantly the surface quality of oak sliced veneers, decreasing the surface roughness of veneers, concerning both the wood structure of defect-free areas and the wood of defect areas. This response of the oak sliced veneers to hydrothermal treatment, presenting an enhanced smoothness in combination with the darkening of the surface color, could highly increase the range of applications of these products, allowing them to compete with other hardwoods of higher quality (mainly exotic) that have been preferably applied so far. Therefore, the issue of optimization of the hydrothermal treatment conditions, aiming to improve even more the surface quality of sliced veneers, is expected to attract high research interest and will be investigated thoroughly in the coming years. This paper provides the preliminary

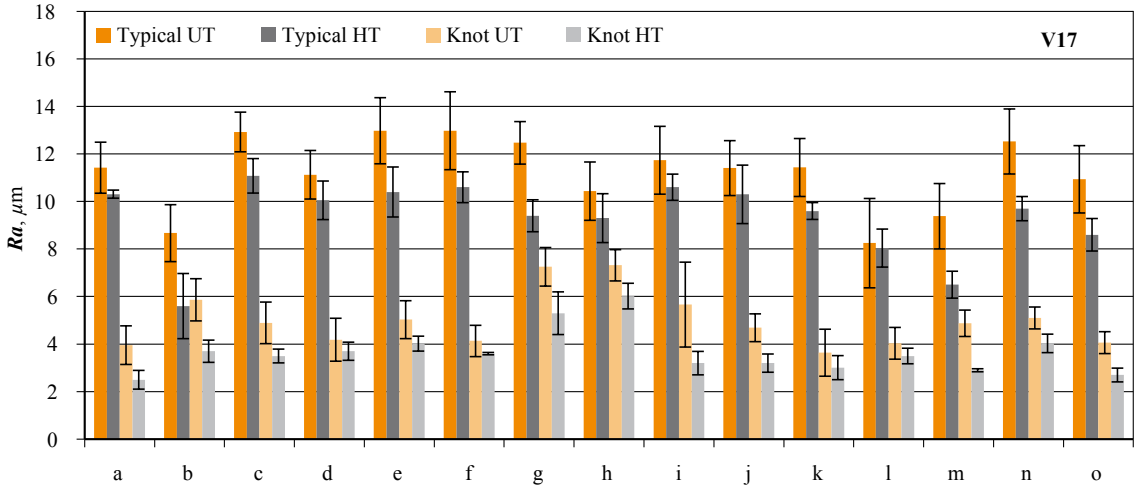

Figure 13 Mean values (μm) and respective standard deviation values of roughness parameter (*Ra*) measured on 15 different points (a-o) along the stem, concerning both knot areas and defect-free areas, on the surface of veneer V17, before (UT- untreated) and after (HT – treated) hydrothermal treatment (110 ºC-2h)
Slika 13. Srednje vrijednosti (μm) i odgovarajuće vrijednosti standardne devijacije parametra hrapavosti (*Ra*) izmjerene na 15 različitih točaka (a – o) duž debla, koje se odnose na područje s kvrgama i na područje bez grešaka, na površini furnira V17, prije hidrotermičke obrade (110 ºC, 2h) (UT – neobrađeno) i nakon hidrotermičke obrade (HT – obrađeno)

results of a more extensive experimental work as part of a research project intended to be implemented in the years to come. The specific data provided will be expanded, taking into consideration all the mentioned approaches, and correlated to other crucial properties assessed (color, density, etc.). A more thorough analysis of the structure will also be made.

4 CONCLUSIONS
4. ZAKLJUČAK

Similar surface quality and roughness was found along the oak veneers and stem. This roughness uniformity highly favors their performance and utilization potential.

The significantly lowest surface roughness, referring both to non-defect areas and knot areas were recorded by veneer V12, obtained from the middle of the package, while the edge veneers of the package presented the highest roughness, highlighting the necessity of the sliced veneers to be protected from frequent changes of climatic conditions, from the production time till the final application. Smoothness was recorded in areas on and around the knots, as well as other defects relevant to knots, possibly attributed to the presence of tensile wood, higher density and wider growth rings. This reveals that the wood structure differences in the area of live knots, as well as in the transition zone from knot to defect-free wood areas, do not influence negatively the surface quality. Therefore, the veneers processing is not more demanding because of such defects. The required energy and the cost of veneer production do not increase, while the overall quality of the final products and productivity is not deteriorated. Therefore, veneers bearing several small/live knots or other defects could be considered as candidate material of high potential to be utilized in a wide range of applications, e.g. as table-tops, benches, floors, cupboards, wardrobe back side or front side surface, highlighting the unique natural appearance of wood in the structures.

A short hydrothermal treatment at low temperatures (100-110 ºC) significantly favors the surface quality of oak sliced veneers, providing smoother surfaces concerning both defect-free areas and defect-areas of veneers. This could further increase the utilization potential of this product in applications where other exotic hardwoods have been traditionally used so far. Further research is highly recommended to comprehend thoroughly the impact of different defects on the surface properties of sliced veneers, to optimize the hydrothermal treatment conditions, as well as other surface modification methods, and to improve even more the surface quality, bonding strength and performance of the sliced veneers, and veneer-based composites.

5 REFERENCES
5. LITERATURA

1. Aydin, I.; Colakoglu, G.; Hiziroglu, S., 2006: Surface characteristics of spruce veneers and shear strength of plywood as a function of log temperature in peeling process. International Journal of Solids and Structures, 43 (20): 6140-6147. https://doi.org/10.1016/j.ijsolstr.2005.05.034
2. Bao, M.; Huang, X.; Zhang, Y.; Yu, W.; Yu, Y., 2016: Effect of density on the hygroscopicity and surface characteristics of hybrid poplar compreg. Wood Science and Technology, 62: 441-451. https://doi.org/10.1007/s10086-016-1573-4
3. Baysal, E.; Kart, S.; Toker, H.; Degirmentepe, S., 2014: Some physical characteristics of thermally modified Oriental-Beech wood. Maderas. Ciencia y tecnología, 16 (3): 291-298. DOI:10.4067/S0718-221X2014005000022
4. Bekhta, P.; Hiziroglu, S.; Shepelyuk, O., 2009: Properties of plywood manufactured from compressed veneer as building material. Materials & Design, 30 (4): 947-953. https://doi.org/10.1016/j.matdes.2008.07.001
5. Bekhta, P.; Sedliačik, J.; Tymyk, D., 2015: The effect of chemical treatment of wood veneer surfaces on their bondability. Acta Facultatis Xylologiae Zvolen, 57 (2): 71-79. https://doi.org/10.17423/afx.2015.57.2.07
6. Budakci, M.; Cemil Ilce, A.; Gurleyen, T.; Uter, M., 2013: Determination of the surface roughness of Heat-treated wood materials planed by the cutters of the horizontal milling machine. BioResources, 8: 3189-3199.
7. Coelho, C. L.; Carvalho, L. M. H.; Martins, J. M.; Costa, C. A. V.; Masson, D.; Meausoone, P. J., 2008: Method for evaluating the influence of wood machining conditions on the objective characterization and subjective perception of a finished surface. Wood Science and Technology, 42, 181-195. https://doi.org/10.1007/s00226-007-0166-1
8. Csanády, E.; Magoss, E.; Tolvaj, L., 2015: Surface roughness of wood. in quality of machined wood surfaces. Springer International Publishing: Cham, Switzerland, 2015; pp. 183-236. ISBN 978-319-22418-3
9. Dobrzynski, M.; Orlowski, K.; Biskup, M., 2018: Comparison of surface quality and tool-life of glulam window elements after planing. Drvna industrija, 70 (1): 7-18. https://doi.org/10.5552/drvind.2019.1741
10. Dudík, R.; Boruvka, V.; Zeidler, A.; Holecek, T.; Riedl, M., 2020: Influence of site conditions and quality of birch wood on its properties and utilization after heat treatment. Part II: Surface properties and marketing evaluation of the effect of the treatment on final usage of such wood. Forests, 11: 556. https://doi.org/10.3390/f11050556
11. Dundar, T.; Akbulut, T.; Korkut, S., 2008: The effects of some manufacturing factors on surface roughness of sliced Makoré (*Tieghemella heckelii Pierre* Ex A. Chev.) and rotary-cut beech (*Fagus orientalis* L.) veneers. Building and Environment, 43 (4): 469-474. https://doi.org/10.1016/j.buildenv.2007.01.002
12. Faust, T. D., 1987: Real time measurement of veneer surface roughness by image analysis. Forest Products Journal, 37: 34-40.
13. Gonultas, O.; Candan, Z., 2018: Chemical characterization and FTIR spectroscopy of thermally compressed eucalyptus wood panels. Maderas. Ciencia y tecnología, 20 (3): 431-442. http://dx.doi.org/10.4067/S0718-221X2018005031301
14. Gűndűz, G.; Korkut, S.; Korkut, D. S., 2008: The effects of heat treatment on physical and technological proper-

ties and surface roughness of Camiyanı Black Pine (*Pinus nigra* Arn. subsp. pallasiana var. pallasiana) wood. Bioresource Technology, 99: 2275-2280. https://doi.org/10.1016/j.biortech.2007.05.015
15. Gurau, L.; Irle, M.; Campean, M.; Ispas, M.; Buchner, J., 2017: Surface quality of planed beech wood (*Fagus sylvatica* L.) thermally treated for different durations of time. BioResources, 12 (2): 4283-4301. https://doi.org/10.15376/biores.12.2.4283-4301
16. Small ClearWood Specimens. Part 2: Determination of Density for Physical and Mechanical Tests; ISO: Geneva, Switzerland.
17. ***ISO 4287: 1997: Geometrical Product Specifications (GPS) – Surface Texture: Profile Method-Terms, Definitions and Surface Texture Parameters; ISO: Geneva, Switzerland.
18. Kamperidou, V.; Aidinidis, E.; Barboutis, I., 2020: Impact of structural defects on the surface quality of hardwood species sliced veneers. Applied Sciences, 10 (18): 6265. https://doi.org/10.3390/app10186265
19. Kamperidou, V., 2019: Biological durability of thermally and chemically modified black pine and poplar wood against basidiomycetes and mold action. Forests, 10 (12):1-18. https://doi.org/10.3390/f10121111
20. Kamperidou, V.; Barboutis, I.; Vasileiou, V., 2012: Effect of thermal treatment on colour and hygroscopic properties of poplar wood. In: Proceedings of 23rd International Scientific Conference: Wood is Good – With Knowledge and Technology to a Competitive Forestry and Wood Technology Sector, Proceedings, Zagreb, Croatia, pp. 59-67.
21. Kamperidou, V.; Barboutis, I., 2017: Mechanical strength and surface roughness of thermally modified poplar wood. PRO Ligno, 13: 107-114. (online). http://www.proligno.ro/en/articles/2017/201704.htm (Accessed Dec. 30, 2017)
22. Korkut, D. S.; Korkut, S.; Bekar, I.; Budakçı, M.; Dilik, T.; Çakıcıer, N., 2008: The effects of heat treatment on the physical properties and surface roughness of turkish hazel (*Corylus colurna* L.) wood. International Journal of Molecular Sciences, 9 (9): 1772-1783. ttps://doi.org/10.3390/ijms9091772
23. Korkut, S.; Budakci, M., 2010: The effects of high-temperature heat-treatment on physical properties and surface roughness of Rowan (*Sorbus aucuparia* L.) wood. Wood Research, 55: 67-78. (online9. http://www.woodresearch.sk/wr/201001/08.pdf (Accessed Oct. 30, 2010)
24. Leal, S.; Sousa, V. B.; Pereira, H., 2007: Radial variation of vessel size and distribution in cork oak wood (*Quercus suber* L.). Wood Science and Technology, 41 (4): 339. https://doi.org/10.1007/s00226-006-0112-7
25. Levene, H., 1960: Robust tests for equality of variances. In: Ingram Olkin; Harold Hotelling *et al*. (eds.). Contributions to Probability and Statistics: Essays in Honor of Harold Hotelling. Stanford University Press. pp. 278-292.
26. Li, G.; Lv, Z.; Liu, Z., 2015: A preliminary study on the main mechanical properties of the high moisture content wood after finger-jointed. Journal of Northwest University, 30: 224-227.
27. Li, G.; Wu, Q.; He, Y.; Liu, Z., 2018: Surface roughness of thin wood veneers sliced from laminated green wood lumber. Maderas. Ciencia y tecnología, 20 (1): 3-10. http://dx.doi.org/10.4067/S0718-221X2018005001101
28. Li, X.; Liu, Y.; Yu, H.; Li, J., 2010: Evaluation of the surface roughness of wood-based environmental materials and its impact on human psychology and physiology. Advanced Materials Research, 113-116. https://doi.org/10.4028/www.scientific.net/AMR.113-116.932
29. Mummery, L., 1993: Surface texture analysis; Hommelwerke: Muhlhausen, Germany, pp. 106.
30. Peng, X.; Zhang, Z., 2019: Surface properties of different natural precious decorative veneers by plasma modification. European Journal of Wood and Wood Products, 77: 125-137. https://doi.org/10.1007/s00107-018-1355-3
31. Pinkowski, G.; Krauss, A.; Piernik, M.; Szymański, W., 2016: Effect of thermal treatment on the surface roughness of scots pine (*Pinus sylvestris* L.) wood after plane milling. BioResources, 11 (2): 5181-5189. https://doi.org/10.15376/biores.11.2.5181-5189
32. Sandak, J.; Orlowski, K.; Sandak, A.; Chuchala, D.; Taube, P., 2020: On-Line measurement of wood surface smoothness. Drvna industrija, 71 (2): 193-200. https://doi.org/10.5552/drvind.2020.1970
33. Tanritanir, E.; Hiziroglu, S.; As, N., 2006: Effect of steaming time on surface roughness of beech veneer. Building and Environment, 41 (1): 1494-1497. https://doi.org/10.1016/j.buildenv.2005.05.038
34. Tsoumis, G., 2002: Wood Science and Technology, Wood Structure and Properties. Aristotle University of Thessaloniki. AUTh, Thessaloniki, pp.346.
35. Vassiliou, V.; Barboutis, I.; Kamperidou, V., 2016: Strength of corner and middle joints of upholstered furniture frames constructed with black locust and beech wood. Wood Research, 61 (3): 495-504.
36. Wang, B.; Chunping, D.; Ellis, S., 2006: Veneer surface roughness and compressibility pertaining to plywood/LVL manufacturing. Part I: Experimentation and implication. Wood and Fiber Science, 38 (3): 535-545.
37. Yu, X.; Xu, D.; Sun, Y.; Geng, Y.; Fan, J.; Dai, X.; He, Z.; Dong, Y.; Li, Y., 2020: Preparation of wood-based panel composites with poplar veneer as the surface layer modified by In-Situ polymerization of active monomers. Forests, 11 (8): 893. https://doi.org/10.3390/f11080893
38. Zhao, X.; Guo, P.; Zhang, Z.; Yang, Y.; Zhao, P., 2020: Wood density, anatomical characteristics, and chemical components of alnus sibirica used for industrial applications. Forest Products Journal, 70 (3): 356-363. https://doi.org/10.13073/FPJ-D-20-00006
39. ***ISO 13061-1, 2014: Physical and Mechanical Properties of Wood – Test Methods for Small ClearWood Specimens. Part 1: Determination of Moisture Content for Physical and Mechanical Tests; ISO: Geneva, Switzerland.
40. ***ISO 13061-2, 2014: Physical and Mechanical Properties of Wood – Test Methods for small clear wood specimens — Part 2: Determination of Density for Physical and Mechanical Tests; ISO: Geneva, Switzerland.

Corresponding address:

VASILIKI KAMPERIDOU
Aristotle University of Thessaloniki, Department of Harvesting and Technology of Forest Products,
54124 Thessaloniki, GREECE, e-mail: vkamperi@for.auth.gr

Hüseyin Sivrikaya[1], Ahmet Can[1]

Physical and Mechanical Properties and Decay Resistance of Poplar Modified with mDMDHEU

Fizička i mehanička svojstva te otpornost na propadanje topolovine modificirane mDMDHEU-om

ORIGINAL SCIENTIFIC PAPER
Izvorni znanstveni rad
Received – prispjelo: 21. 4. 2021.
Accepted – prihvaćeno: 13. 12. 2021.
UDK: 582.681.82; 630*84
https://doi.org/10.5552/drvind.2022.2118

ABSTRACT • *Chemical modification as a non-biocidal treatment is an effective method to improve physical and biological properties of wood. Poplar is a fast growing species but has poor dimensional stability and durability in addition to low mechanical properties. Low molecular weight Dimethylol dihydroxyethyleneurea (mDMDHEU) was used to improve the properties of poplar mainly dimensional stability and decay resistance. Results indicated high anti-swelling efficiency (ASE), but low variation between both concentrations of mDMDHEU. Tangential swelling was greatly reduced by mDMDHEU treatment during the water immersion period. Untreated poplar samples were severely decayed as compared to modified samples. Modified samples showed lower bending strength unlike to compression strength. Ester peak at 1720 cm^{-1} revealed chemical reaction between chemical reagent and wood cell wall components. Control samples exhibited considerably higher thermal degradation when compared to the samples modified with mDMDHEU.*

KEYWORDS: *wood modification; mDMDHEU; dimensional stability; MOR; FTIR; TGA; decay resistance*

SAŽETAK • *Kemijska modifikacija kao postupak bez biocida učinkovita je metoda za poboljšanje fizičkih i bioloških svojstava drva. Topolovina je drvo vrste koja brzo raste, ali ima slabu dimenzijsku stabilnost i prirodnu trajnost te slaba mehanička svojstva. Za poboljšanje svojstava topolovine, prije svega dimenzijske stabilnosti i otpornosti na propadanje, upotrijebljena je dimetilol dihidroksietilenurea male molekularne mase (mDMDHEU). Rezultati su pokazali visoku učinkovitost kemijske modifikacije u smislu sprječavanja bubrenja topolovine (ASE), ali s malom varijacijom među dvjema primijenjenim koncentracijama mDMDHEU-a. Tangencijalno bubrenje uzoraka topolovine tijekom uranjanja u vodu uvelike je smanjeno mDMDHEU modifikacijom. Nemodificirani uzorci topolovine bili su vrlo truli u usporedbi s modificiranima. Modificirani su uzorci, pak, pokazali manju čvrstoću na savijanje u usporedbi s tlačnom čvrstoćom. Vrh vrpce na 1720 cm^{-1} otkrio je kemijsku reakciju između kemijskog reagensa i spojeva u staničnoj stijenci drva. Na kontrolnim je uzorcima nastala znatno veća toplinska degradacija nego na uzorcima modificiranima mDMDHEU-om.*

KLJUČNE RIJEČI: *modifikacija drva; mDMDHEU; dimenzijska stabilnost; MOR; FTIR; TGA; otpornost na propadanje*

[1] Authors are researchers at Bartın University, Department of Forest Industrial Engineering, Bartin, Turkey. https://orcid.org/0000-0002-9052-9543, https://orcid.org/0000-0001-5926-6039

1 INTRODUCTION
1. UVOD

Numerous studies have been performed to improve dimensional stability, decay and insect resistance of wood. This can be done by modifying the reactive sites of cell wall components in wood (Militz, 1993). Nowadays, wood properties such as low dimensional stability and biological durability are improved by various non-biocidal treatments, e.g. thermal or chemical, and such methods extend the service life of the modified wood. These methods present environmentally friendly processes that have no toxic effects on nature and do not cause disposal problem after service life.

Chemical modification of wood is described as a reaction between wood cell wall components (cellulose, hemicelluloses and lignin) and chemical reagent, resulting in the formation of a stable chemical bond (Rowell, 1983; Hill, 2006; Sandberg *et al*., 2017). A wide range of chemical reagents such as acetic anhydride, carboxylic acids, isocyanates, epoxides, aldehydes were studied for chemical modification of wood; phenol formaldehyde, dimethylol dihydroxyethyleneurea (DMDHEU), furfuryl alcohol and silicon-containing compounds were used for impregnation modification (Hill, 2006). However, acetylation, heat treatments, furfurylation and DMDHEU have been introduced to the market since these methods were found to be successful (Militz and Lande, 2009). Although modifications of wood and veneers with DMDHEU were developed on a pilot scale, modified products with the first generation of DMDHEU have not been in the market. However, modified wood based on the second generation of DMDHEU is underway due to little or lack of formaldehyde (Brischke, 2018).

1,3-dimethylol-4,5-dihydroxyethyleneurea (DMDHEU) is a water-soluble glyoxal resin, acting as cross-linking agent and mostly used in textile industry for wrinkle resistance; it also found application in the field of wood modification (Emmerich *et al*., 2019). DMDHEU can make crosslinking with the wood cell wall polymers by reacting with the hydroxyl groups, and also can deposit within the cell walls leading to bulking of the cell wall (Xie *et al*., 2010). Magnesium chloride and zinc nitrate are the most commonly used catalysts for accelerating the cross-linking reaction of DMDHEU (Schindler and Hauser, 2004). In an early study on DMDHEU modification with different catalysts, like citric or tartaric acid, Militz (1993) improved anti shrink efficiency (ASE) up to 75 % and improved decay resistance with beech wood. Weight percentage gain (WPG) affects the performance of DMDHEU treated wood. Mass loss below 3 % against decay fungi was obtained with 15 % WPG in beech and 10 % WPG in pine against decay fungi (Verma *et al*., 2009). Differential scanning calorimetry (DSC) demonstrated that DMDHEU reduced the pore size in wood by filling the void space in the cell wall (Dieste *et al*., 2009). Infrared spectroscopy and scanning electron microscopy analyses showed that high WPG (48 %) stabilized lignin to some extent in wood veneers modified with DMDHEU, which effectively prevented the degradation of the wood cell wall during artificial weathering (Xie *et al*., 2005). Despite the improvements in physical and biological properties by DMDHEU modification, some mechanical properties are decreased. The loss in bending strength of DMDHEU modified wood was previously reported by some authors (Nicholas and Williams, 1987; Ashaari *et al*., 1990). Modification with mDMDHEU decreased the abrasion resistance in Scots pine (Brischke *et al*., 2019). According to Bollmus *et al*. (2020), DMDHEU increases the decay resistance, dimensional stability, compressive strength, and hardness, whereas it reduces the tensile and impact bending strength in modified wood. Pore size in wood was reduced by the filling effect of DMDHEU, resulting in the mechanical support to the cell wall that led to the preventing of strength loss in treated wood at lower curing temperatures, e.g. 90 ˚C. However, when curing was performed at the temperature as high as 150 °C, the bending strength of DMDHEU-treated wood greatly decreased (Yuan *et al*., 2013). Impact strength was decreased by DMDHEU treatment, while hardness and compression strength parallel and perpendicular to grain increased (Jiang *et al*., 2014).

Many studies related to chemical modification of DMDHEU have been carried out with Scots pine and beech, since both species displayed improved material properties. Then, various authors gave particular focus on permeable wood species such as Rubber wood, Slash pine, Radiata pine, Albizzia hardwood, Ponderosa pine, Maritime pine and Balsam poplar (Emmerich *et al*., 2019).

Poplar is a fast growing species, but has poor physical and durability properties. However, Poplar wood can be used in various places depending on the market and industrial technology. It is generally used for the production of wood based boards, packaging, pulp and biomass for energy (Castro and Zanuttini, 1991). In addition, modified poplar is produced according to thermal modification process, which improves the dimensional stability and decay resistance of wood. On the other hand, poplar is a proper species for impregnation modification as it shows good permeability. The treatability of poplar sapwood is classified as 1, which indicates that it can be easily treated according to EN 350-2 standard. However, natural resistance of poplar wood against decay fungi is classified as 5, which means that it is not durable according to that standard.

The objective of this study is to impregnate poplar wood by mDMDHEU with low molecular weight to improve dimensional stability and decay resistance. There is little research on poplar modification with DMDHEU compared to other wood species. In addition, modified DMDHEU with low molecular weight was used in this study at the curing temperature that was a bit higher than in a wide range of studies dealing with DMDHEU.

2 MATERIALS AND METHODS
2. MATERIJALI I METODE

Poplar (*Populus euramericana*) with 28 cm in diameter was provided from the sawmill producing wooden pallets in the Bartin province. The logs were cut vertically in four pieces and were left to the air drying before sizing of the specimens. Specimens were prepared from the sapwood section according to the dimensions specified in the experiments. All of the samples were oven dried at 103 °C before treatment.

Modified DMDHEU with low molecular weight (130 g/mol) was provided from Latro Chemistry (Istanbul, Turkey). It was diluted with distilled water to the concentrations of 15 % and 30 % (w/w), respectively. Magnesium chloride ($MgCl_2$) was added as a catalyst at a rate of 5 % of the total solution amount. Impregnation was carried out according to full cell process with 30 min vacuum (0.08 MPa) and 1 h air pressure (0.5 MPa), subsequently one-week air conditioning and curing at 130 °C for 48 h. Weight change in the samples after the modification was calculated as the percentage according to Eq. 1:

$$WPG(\%) = \left[\frac{M_m - M_u}{M_u}\right] \cdot 100 \quad (1)$$

Where M_m is the oven-dry mass of modified wood, M_u is the oven-dry mass of unmodified wood.

2.1 Physical tests
2.1. Ispitivanje fizičkih svojstava

Samples with dimensions of 20 mm × 20 mm × 10 mm (tangential × radial × longitudinal) were prepared for water related properties with six replicates. Oven-dry weight of the modified and unmodified samples was recorded and the lengths in the longitudinal, radial and tangential directions were measured by digital calliper for measuring the volumetric change. All samples were immersed in distilled water for 2, 4, 6, 24, 48, 72 h, 240 h and 360 h.

Leaching rate (*LR*) was obtained based on the oven dried weights after modification and water immersion as given below:

$$LR(\%) = \left[\frac{M_0 - M_1}{M_0}\right] \cdot 100 \quad (2)$$

Where M_0 is the oven dried weight of wood before immersion and M_1 is the oven dried weight of wood after immersion.

Bulking coefficient (*BC*), swelling coefficient (*S*), anti-swelling efficiency (*ASE*), tangential swelling (*TS*) were calculated as follows:

$$BC(\%) = \left[\frac{V_m - V_u}{V_u}\right] \cdot 100 \quad (3)$$

Where V_u is the volume of the unmodified wood sample and V_m is the volume of the modified wood sample

$$S(\%) = \left[\frac{V_{ws} - V_{od}}{V_{od}}\right] \cdot 100 \quad (4)$$

Where V_{ws} is the water-swollen volume of the wood sample and V_{od} is the oven-dry volume of the wood sample

$$ASE(\%) = \left[\frac{S_u - S_m}{S_u}\right] \cdot 100 \quad (5)$$

Where S_u is the swelling coefficient of unmodified wood and S_m is the swelling coefficient of modified wood

$$TS(\%) = \left[\frac{T_1 - T_0}{T_0}\right] \cdot 100 \quad (6)$$

T_0 and T_1 is the tangential length for oven dried wood and water-swollen wood, respectively.

2.2 Mechanical tests
2.2. Ispitivanje mehaničkih svojstava

Bending strength and modulus of elasticity, as well as compression strength, were performed on the control and modified samples. Three points bending measurements were performed according to TS 2474. Bending samples with 10 mm × 10 mm × 200 mm (tangential × radial × fibers direction) in size were used for each treatment with 15 replicates. The samples were air-conditioned for an equal moisture content level prior to the bending experiment.

Bending strength (*MOR*) was determined according to Eq. 7:

$$MOR = \frac{3 \cdot P_{max} \cdot L}{2 \cdot b \cdot h^2} \quad \left(\frac{N}{mm^2}\right) \quad (7)$$

Where P_{max} is the maximum load at failure of the samples, *L* is the span, *b* and *h* are the width and height of the specimen.

Modulus of elasticity (*MOE*) was determined according to Eq. 8:

$$MOE = \frac{\Delta F \cdot L^3}{\Delta f \cdot 4 \cdot b \cdot h^3} \quad \left(\frac{N}{mm^2}\right) \quad (8)$$

Where ΔF is the difference in load in the elastic deformation area, Δf is the deflection in the bending area, *L* is the span, *b* and h are the width and height of the specimen.

For the compression strength parallel to the fibers, wood samples were prepared in the dimensions of 20 mm × 20 mm × 30 mm (tangent × radial × fiber direction) according to TS 2595. Compression strength was determined according to Eq. 9:

$$\sigma\beta = \frac{F_{max}}{A} \quad (\frac{N}{mm^2}) \tag{9}$$

Where F_{max} is the maximum compressive force and A is surface area.

2.3 Fourier transform infrared spectroscopy (FTIR)
2.3. Fourierova transformacijska infracrvena spektroskopija (FTIR)

Measurements were carried out using the Shimadzu IR Affinity-1 FTIR spectrophotometer device equipped with an attenuated total reflectance probe (Shimadzu Corp., Kyoto Japan). Using the Pike ATR Diamond/ZnSe accessory compatible with the Shimadzu model, measurements were taken from the surface without causing any damage to the samples. The spectra of each sample were at a resolution of 4 cm^{-1} and a wavenumber range of 700-4000 cm^{-1}. 32 scans were obtained on the surface of untreated control and modified samples.

2.4 Thermogravimetric analysis (TGA)
2.4. Termogravimetrijska analiza (TGA)

Thermogravimetric analysis (TGA) of the samples was performed using a Netzsch TG 209 F1 Iris instrument (NETZSCH Group Selb, Germany). A sample of about 2 mg of wood was placed on an alumina crucible bowl (17 mm diameter), then heated from 25 °C to 500 °C at a heating rate of 20 °C (min^{-1}) per minute under nitrogen atmosphere.

2.5 Decay test
2.5. Ispitivanje propadanja

White rot fungus *Trametes versicolor* was selected for decay test for the mini-block samples of 30 mm × 15 mm × 5 mm in size used for each treatment with 10 replicates. For growth culture, 48 g of Malt extract agar (Merck) was diluted with 1 liter of distilled water, sterilized in the autoclave at 121 °C for 10 min. Control and treated samples were placed in the petri dishes completed with mycelium development and subjected to decay test for 8 weeks at 25 °C and 80 % of relative humidity. At the end of the decay test, the samples were taken from the petri dishes and the micelles on the surface were cleaned by brush and kept in the oven until the constant weight at 103 °C. Mass loss was calculated based on the weight differences at oven-dried state before and after decay test.

2.6 Statistical analysis
2.6. Statistička analiza

A descriptive analysis was developed (mean and standard deviation) for samples. ANOVA was applied to verify the effect of treatment with the mDMDHEU. Duncan's test was set at 99 % confidence level to determine the statistical difference between the means.

3 RESULTS AND DISCUSSION
3. REZULTATI I RASPRAVA

3.1 Weight percentage gain (*WPG* %)
3.1. Postotak povećanja mase (*WPG* %)

Weight percentage gain (*WPG* %) of the modified samples was calculated after curing at 130 °C for 48 hours on the water uptake, decay test, bending strength and compression strength samples (Table 1). The calculation was based on difference of oven-dry weights of the samples before and after impregnation.

Table 1 indicates that *WPG* results varied according to the concentration of mDMDHEU, and type of experiment, since samples were of different size in each experiment. Impregnation with 30 % of mDMDHEU resulted in approximately twofold *WPG* compared to those with15 %. This was due to the higher amount of mDMDHEU.

Generally, *WPG* values ranged from 15 % to 30 % in all experiments. The reasons for the differences in weight increase rates can be explained in two ways: The first and main reason is the difference in dimensions according to the radial, tangential and longitudinal directions of the samples for each experiment and the probability of the evaporation of some resins during the curing process at 130 °C. Our results on *WPG* are consistent with the findings of Yuan *et al*. (2013) who found the values of more than 15 % and lower than 25 % when the curing process was performed at 120 °C for DMDHEU treatment. Similarly, Li *et al*. (2019) obtained the WPG between 17.9 % to 29.3 % after modification of Masson and Camphor pine with 50 % DMDHEU catalyzed by acrylic acid. However, Li *et al*. (2020) found the highest WPG as 9.5 % with the bamboo modified with 50 % DMDHEU under cur-

Table 1 *WPG* values of wood samples impregnated with mDMDHEU
Tablica 1. *WPG* vrijednosti uzoraka drva impregniranoga mDMDHEU-om

Experiments *Istraživanje*	**mDMDHEU**	***WPG*, %**
Water uptake *primitak vode*	% 15	$15.22^{a} \pm 0.46$
	% 30	$29.1^{b} \pm 2.44$
Decay test *ispitivanje propadanja*	% 15	$25.18^{a} \pm 3.51$
	% 30	$30.87^{a} \pm 3.80$
Bending strength *čvrstoća na savijanje*	% 15	$15.63^{a} \pm 2.09$
	% 30	$28.92^{b} \pm 3.08$
Compression strength *čvrstoća na tlak*	% 15	$16.58^{a} \pm 0.96$
	% 30	$25.95^{b} \pm 0.65$

[a]The letters indicate Duncan's homogeneity groups in the column.
[a]*Slova označavaju Duncanove grupe homogenosti unutar stupca.*

Table 2 Weight and volumetric changes of wood samples due to water soaking
Tablica 2. Promjena mase i volumena uzoraka drva zbog namakanja u vodi

Treatment *Tretman*	**Density, g/cm³** *Gustoća,* g/cm³	***LR*, %**	***BC*, %**	***S*, %**	***ASE*, %**
Control / *kontrolni uzorci*	0.35^{a}±0.00	0.68^{a} ± 0.43	-	16.81^{c} ± 0.80	-
15% mDMDHEU	0.38^{b}±0.00	9.34^{b} ± 0.27	4.08^{a} ± 0.51	6.53^{b} ± 0.34	61.16^{a} ± 2.01
30 % mDMDHEU	0.43^{c}±0.02	11.13^{c} ± 0.80	6.44^{b} ± 0.29	5.74^{a} ± 0.38	65.88^{ab} ± 2.27

[a]The letters indicate Duncan's homogeneity groups in the column
[a]*Slova označavaju Duncanove grupe homogenosti unutar stupca.*

ing at 95 °C for 3 h. Poplar modified with 10 % DMDHEU resulted in 16.50 % *WPG* in another study (Cai *et al*., 2018).

3.2 Dimensional stability
3.2. Dimenzijska stabilnost

After two weeks of water soaking, bulking value of the samples due to the impregnation (ΔV %), Leaching rate (*LR* %), maximum swelling (S_{max} %) and anti-swelling efficiency (*ASE* %) are given in Table 2.

According to Table 2, impregnation with mDMDHEU increased the bulking coefficient of the wood samples. As expected, this value was increased by the increasing of the resin concentration.

Xie *et al*. (2010) referred that the positive relationship between *WPG* and bulking, meaning high *WPG,* may increase the bulking effects due to the deposition of DMDHEU in the cell walls by reducing the space within the cell walls where the water molecules enter.

At the end of the soaking experiment, the samples treated with 30 % of mDMDHEU showed slightly higher *LR* than 15 % of mDMDHEU due to water leaching.

Table 2 indicates that control samples displayed very high swelling compared to the treated samples. The difference in swelling was found to be low between the concentrations of the resin treatments. The similar result was obtained with the *ASE*, which slightly increased with the increasing of the resin amount. Cai *et al*. (2018) reported lower swelling (3.29 %) and lower *ASE* (52.45 %) than our results when poplar wood was modified with 10 % DMDHEU.

In an early report on DMDHEU, it was reported that permanent *ASE* was achieved up to 70 % as a function of wood species, chemical reagent, applied concentration (*WPG*), catalyst and hardening temperature (Militz, 1993).

In the industrial scale production (superheated steam process) with suitable concentrations (30 % DMDHEU, catalyst $MgCl_2$), 45-50 % of *ASE* in Scots pine (Schaffert, 2006) and 30-35 % in beech were reported (Bollmus, 2011). According to Van der Zee *et al*. (1998), catalysts added to the reagent significantly improved the dimensional stability of the modified wood. In our experiments, $MgCl_2$ as a catalyst at 5 % was used to increase the *ASE*. $MgCl_2$ was proposed as the most suitable catalyst for wood applications in terms of high fixation of DMDHEU, high dimensional stability and resistance to decay fungi. In addition, optimized concentration of $MgCl_2$ is suggested to be 5 % (Emmerich *et al*., 2019).

Volumetric ASE was found to be 47.8 % for Masson pine and 51.2 % for Camphor pine, respectively, as a result of DMDHEU modification catalyzed by acrylic acid (Li *et al*., 2019). It varied between 18 - 42 % in bamboo modified with DMDHEU catalyzed by maleic anhydride (Li *et al*., 2020).

Based on Table 2, it can be said that mDMDHEU improved the dimensional stability of poplar wood. However, there was little difference between the concentrations of 15 % and 30 % of mDMDHEU with regard to *ASE*, although there was a marked difference between the mDMDHEU treatments in relation to WPG. This may be due to the evaporation of mDMDHEU at high temperature or due to the interaction of mDMDHEU with cell wall. Some authors stated that the reaction mechanism between wood cell wall and DMDHEU is still not clear (Hill, 2006; Larsson-Brelid, 2013).

Tangential swelling of the control and modified samples during the two-week period is given in Figure 1.

Figure 1 shows that tangential swelling values of the control samples considerably increased during the water uptake. However, impregnation with mDMDHEU exhibited a great reduction in tangential swelling. When comparing rates of mDMDHEU, both concentrations showed almost similar behavior in tangential swelling. For control samples, swelling increased particularly between 2 h and 24 h of soaking, followed by a relatively stabilized period, and reached over 10 %. Swelling behavior of the samples treated with mDMDHEU showed increasing over 4 % for 2 h, but then remained at approximately the same level for later periods.

3.3 Mechanical properties
3.3. Mehanička svojstva

Impregnation of poplar with mDMDHEU significantly reduced the *MOR* compared to control samples as shown in Table 3.

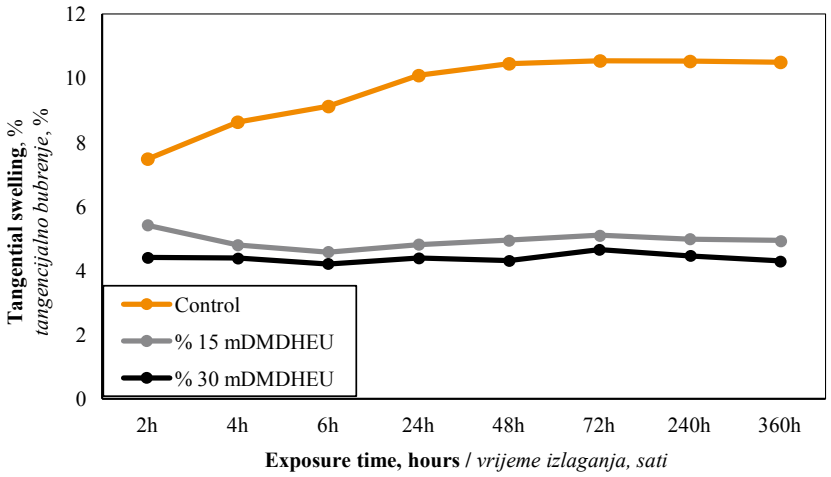

Figure 1 Tangential swelling of control and mDMDHEU modified samples depending on exposure time
Slika 1. Tangencijalno bubrenje kontrolnih uzoraka i uzoraka modificiranih mDMDHEU-om ovisno o vremenu izlaganja

Table 3 Strength values of control and modified samples
Tablica 3. Vrijednosti čvrstoće kontrolnih i modificiranih uzoraka

Modification *Modifikacija*	***MOR*, N/mm²**	**Change in *MOR*, %** *Promjena MOR-a, %*	***MOE*, N/mm²**	**Change in *MOE*, %** *Promjena MOE-a, %*	**Compression strength (*CS*), N/mm²** *Čvrstoća na tlak (CS), N/mm²*	**Change in *CS*, %** *Promjena čvrstoće na tlak, %*
Control / *kontrolni uzorci*	59.7 ± 3.9	-	4791 ± 477	-	31.2 ± 1.5	-
mDMDHEU (15 %)	40.4 ± 6.3	-32	4686 ± 377	-2	30.6 ± 2.9	-2
mDMDHEU (30 %)	39.9 ± 9.2	-33	4513 ± 615	-6	37.2 ± 2.3	19

On the other hand, there was no significant difference between the *MOR* values of the samples impregnated at 15 % concentration and at 30 %. This means that increasing in the concentration of resin had no apparent impact on the *MOR*.

MOE was found to be the highest in the control samples, followed by 15 % mDMDHEU and 30 % mDMDHEU, respectively. However, *MOE* results showed less difference.

In contrast to the *MOR*, the reduction in *MOE* in treated samples was not considerably lower than that of control.

Reduction in strength properties with regard to DMDHEU modification was previously reported by some authors. According to Yuan *et al*. (2013), decreasing in bending strength may be due to the hydrolysis effect of the catalyst, which accelerates the degradation of wood, and this effect would be different according to the type of catalyst.

Jiang (2014) found that DMDHEU with the concentration of 30 % improved the MOE, but decreased the *MOR*, the concentration being associated with the *WPG*. Lopes *et al*. (2013) reported the reduction in *MOR* up to 25 % in maritime pine regardless of the level of modification with DMDHEU. The variation in bending strength due to the DMDHEU modification varies depending on the wood species. DMDHEU increased the *MOR* at a rate of 2.8 % in Masson pine, whereas it decreased 25 % in Camphor pine compared to untreated wood (Li *et al.* 2019). It was stated that *MOR* of untreated bamboo was 145.6 MPa, whereas that of DMDHEU-modified bamboo ranged between 94.5 - 121.5 MPa. 30 % DMDHEU cured at 105 °C for 5h exhibited the lower impact on *MOR* of bamboo. In addition, modulus elasticity of modified bamboo changed less (Li *et al*., 2020).

The notable result in the mechanical properties was that the compression strength was not affected by chemical modification. Poplar samples modified with mDMDHEU at 30 % concentration was even remarkably higher than that of the control samples. This confirms that there is a positive relationship between *WPG* and compression strength.

Table 3 indicates that no significant difference was found between the control samples and the samples modified with 15 % of mDMDHEU. Increase in compression strength by DMDHEU modification was reported by previous authors (Schaffert, 2006; Bollmus, 2011; Derham *et al*., 2017). Winandy and Rowell (2005) reported 65 % increase in compression strength in DMDHEU-modified beech wood catalyzed by $MgCl_2$. Li *et al*. (2020) achieved the highest compression strength in bamboo modified with 50 % DMDHEU, cured at 95 °C for 5h.

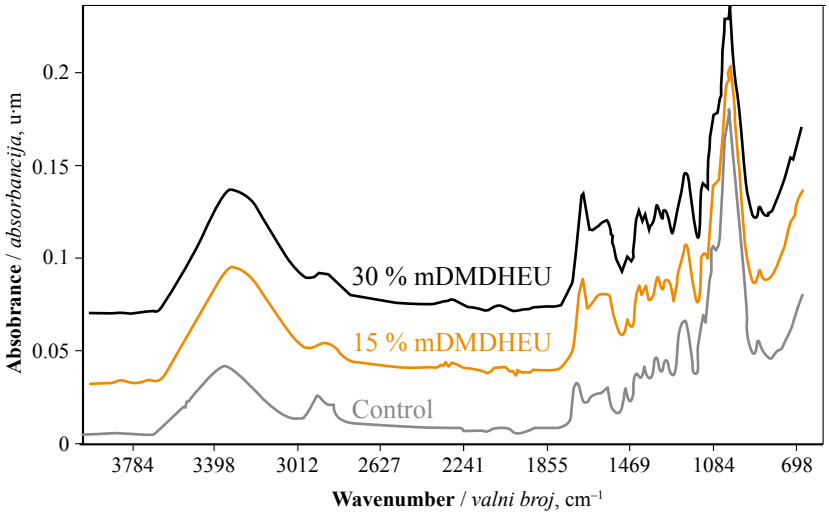

Figure 2 FTIR spectra of control and treated samples at different mDMDHEU level
Slika 2. FTIR spektri kontrolnih uzoraka i uzoraka tretiranih mDMDHEU-om različitih koncentracija

3.4 FTIR analysis
3.4. FTIR analiza

Change in the FTIR spectra of untreated control and treated samples is displayed in Figure 2 depending on the wavelength on the x-axis.

As can be seen in Figure 2, a broad peak around 3300 cm^{-1} shows the increasing of OH groups in samples modified with mDMDHEU. This can be attributed to the OH content in mDMDHEU. In this band region, OH stretching vibration was reported by previous authors (Pandey, 1999; González-Peña and Hale, 2011; Chen *et al*., 2017).

Ester peak due to the carbonyl content was revealed at 1720 cm^{-1}, which confirms the chemical reaction between wood cell wall components and mDMDHEU. A similar result was found by Xie *et al.* (2005), who reported that, as the WPG of DMDHEU increased, the carbonyl content increased (1707 - 1733 cm^{-1}), this increase in absorption resulting from the carbonyl groups in DMDHEU. Correspondingly, the increase in the carbonyl content (1709 and 1726 cm^{-1}) was attributed to the carbonyl groups in DMDHEU (Pfeffer *et al*., 2012).

The peak of 750 cm^{-1} demonstrated the cis occurring, increasing of crystallinity, and resulting in more regular formation for molecules.

Ether peaks are shown at the bands of 1030, 1060, 1100 and 1240 cm^{-1}, the large breaking in ether peaks in treated samples occurred between 1030 and 1060 cm^{-1}. Control samples displayed the strongest peak in this region due to the high ether content. Yuan *et al*. (2013) obtained the highest band at 1050 cm^{-1} and stated that this resulted from the reaction between cellulose and DMDHEU. In addition, absorbance maxima at 1475 cm^{-1} and 1236 cm^{-1} corresponded to CH_2 deformation and C-O stretch vibration, respectively.

Breaking of long chain ether peaks increased the ratio of short chain ether peaks, which was shown at 1230 cm^{-1}. According to Pfeffer *et al*. (2012), absorbance maxima at 1237 cm^{-1} and 1232 cm^{-1} for Scots pine and beech, respectively, were associated with the C–O stretch vibration in the N-methylol group of DMDHEU.

3.5 Thermogravimetric analysis
3.5. Termogravimetrijska analiza

Figure 3 shows the weight changes due to the increased temperature in untreated and treated samples by thermogravimetric analysis.

According to the results obtained from the TG curve, the weight loss in control samples between 30 °C and 200 °C was 7 %, while it was 12 % for 15 % of mDMDHEU and 13 % for 30 % of mDMDHEU, respectively. Evaporation of moisture and initial decomposition of cellulose and hemicellulose up to 200 °C were associated with the initial weight loss (Doh *et al*., 2005). Shebani *et al*. (2008) referred the low weight loss below 100 °C to the evaporation of water, the apparent distinct loss between 200 and 400 °C, and approximately 75 % weight loss at 400 °C. They reported that the degradation between 218 °C and 260 °C, which was responsible for the decomposition of hemicelluloses and the slower decomposition of lignin, while the degradation above 350 °C was responsible for the degradation of cellulose.

Hydrolysis process, determined from room temperature up to 223 °C, indicates the releasing of non-combustible products, traces of inorganic compounds and water vapor and dehydration reaction of hemicelluloses as a result of destruction of hydroxyl groups (Shen *et al*., 2010; Okon *et al*., 2018).

In the present study, decreasing in weight loss was more apparent especially over 200 °C. Control

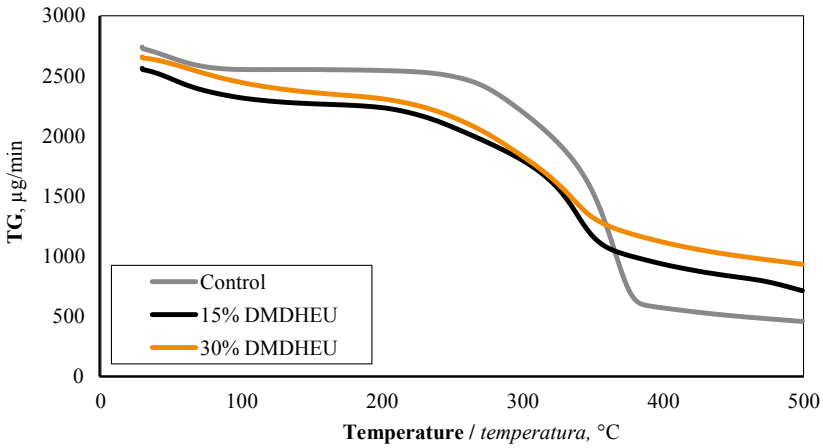

Figure 3 TG curve of control and modified samples at different temperatures
Slika 3. TG krivulja kontrolnih i modificiranih uzoraka pri različitim temperaturama

samples lost 65 % of their weight between 200 °C and 370 °C, while the weight loss was 54 % in the samples treated with 15 % of mDMDHEU and 48 % in samples with 30 % of mDMDHEU, respectively, in this temperature range.

According to Doh *et al*. (2005), cellulose and hemicellulose are major components, decomposed in the temperature range of 200 and 400 °C, and lignin causes the charring over 400 °C. In the last stage of TGA in our study, involving the temperatures range from 370 to 498 °C, weight loss in control samples was 48 %, whereas it was found to be 30 % and 23 % for mDMDHEU (15 and 30 %) treated samples. It was reported that in the last stage of thermal degradation up to 489 °C, decomposition of cellulose is around 80 % (Popescu *et al*., 2013; Okon *et al*., 2018).

It is concluded from Figure 4 that the treatment with mDMDHEU combined with magnesium chloride as a catalyst increased the thermal stability of poplar when compared to control samples. On the other hand, the increase in the *WPG* somewhat lowered the thermal decomposition. Magnesium chloride may have contributed to the improving of thermal stability.

The DTG curve shows the temperature at which the highest mass loss (maximum) occurs per minute for control and treated samples (Figure 4).

According to the DTG curve, the highest weight losses occurred at 366 °C in control samples, at 339 ° C in the samples impregnated with 15% of mDMDHEU, and at 335 °C in the samples with 30 % of mDMDHEU.

Results indicate that control samples were degraded at higher temperature than impregnated samples but resulted in greater weight loss as well. Although modified samples decompose at lower temperatures, their weight losses were less than those of control samples. It was reported that medium or higher concentration of DMDHEU improved the TGA of bamboo (Li *et al*., 2020).

Mass loss at approximately 330-340 °C was found higher in samples treated with 15 % mDMDHEU than with 30 %. Maximum weight loss was observed to be 383 µg in control samples, while it was 194 µg in treated samples with 15 % mDMDHEU and 132 µg with 30 % of mDMDHEU.

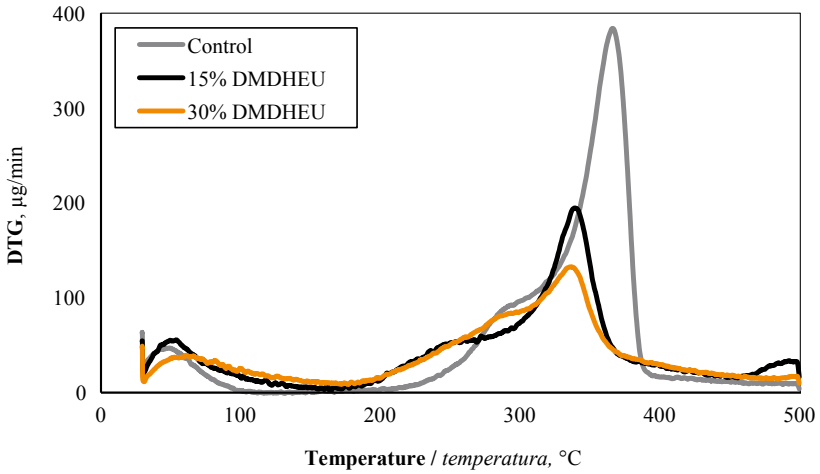

Figure 4 DTG curve of control and modified samples depending on temperature
Slika 4. DTG krivulja kontrolnih i modificiranih uzoraka u ovisnosti o temperaturi

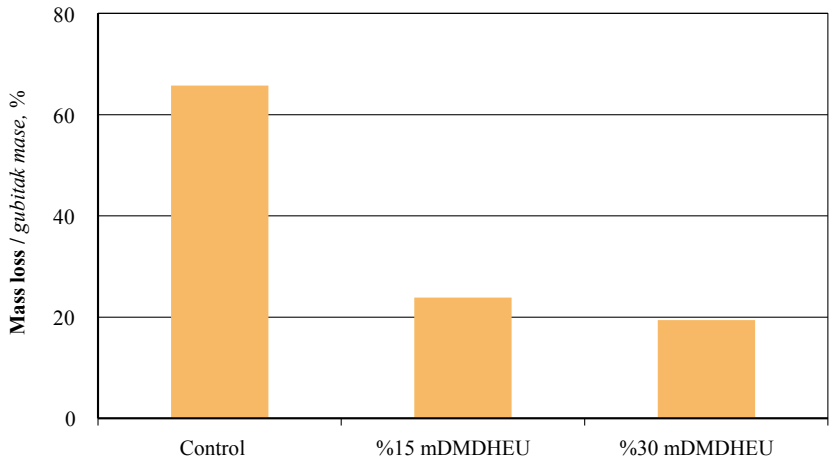

Figure 5 Mass loss of untreated (control) and mDMDHEU treated mini-blocks after 8 weeks of fungal incubation (*T. versicolor*)
Slika 5. Gubitak mase netretiranih (kontrolnih) blokova i miniblokova tretiranih mDMDHEU-om nakon osam tjedana inkubacije gljivom (*T. versicolor*)

3.6 Decay resistance
3.6. Otpornost prema propadanju

Durability of the untreated and treated samples against *T. versicolor* on malt-agar media is displayed in Figure 5.

Figure 5 indicates considerably higher mass loss in control samples than samples modified with mDMDHEU due to the activity of the decay fungus *T. versicolor*. Mass loss in control samples was about three times higher than in the samples treated with 30 % of mDMDHEU.

Mass loss was found lower with 30 % of mDMDHEU than 15 % in the poplar samples. Results reveal that increasing in the concentration of mDMDHEU moderately enhanced the decay resistance. The results of decay resistance was also in accordance with the WPG values of the 15 % mDMDHEU (25.18 % *WPG*) and 30 % mDMDHEU (30.87 % WPG).

Although the decay resistance of the samples treated with mDMDHEU was higher than that of the untreated samples, the mass loss of the treated samples was still above the expected value. It might be assumed that a reason for the loss of weight lies in the fact that some of the chemical reagent leached out during the incubation period. According to Emmerich *et al*. (2021), significant amounts of non-fixated chemicals were removed from the wood treated with DMDHEU and its derivatives when subjected to water leaching that may have affected the mass loss due to the fungal exposure.

In the earlier studies, good protection was achieved by wood modified with DMDHEU at about 10 % *WPG* against decay fungus *Coniophora puteana* in spite of the number of water-leaching cycles (Videlov, 1989). Van Acker *et al*. (1999) found significant reduction in weight loss depending on the treatment parameters rather than retention in their research involving the DMDHEU modification with pine and beech based on the EN113 and ENV807 tests. Verma *et al*. (2009) obtained good results with lower *WPG*, for example 15 % of *WPG* in beech and 10 % in pine, indicating that increasing in *WPG* increased the decay resistance to *T. versicolor* and *C. puteana*.

4 CONCLUSIONS
4. ZAKLJUČAK

Modification of poplar with mDMDHEU considerably improved the dimensional stability and reduced the tangential swelling. Compression strength was not affected by the modification process, even though it was improved with the increasing of mDMDHEU level, despite the decrease in bending strength. FTIR confirmed the chemical modification in the impregnated wood samples. Samples modified with mDMDHEU initially showed higher thermal degradation; however, at higher temperatures above 300 °C they gained thermal stability as compared to control samples. Modified samples showed substantially lower mass loss due to the decay by *T. Versicolor* in comparison to the unmodified wood samples.

Acknowledgements – Zahvala

This study was supported by Bartın University Scientific Research Projects Commission (Project No: 2018-FEN-A-007). The authors gratefully acknowledge the Latro Chemistry (Istanbul, Turkey) for providing chemicals.

5 REFERENCES
5. LITERATURA

1. Ashaari, Z.; Barnes, H. M.; Vasishth, R. C.; Nicholas, D. D.; Lyon, D. E., 1990: Effect of aqueous polymer treatments on wood properties. Part II: Mechanical proper-

ties, Doc. No. IRG/WP3611. International Research Group on Wood Preservation, Stockholm, Sweden.
2. Bollmus, S., 2011: Biologische und technologische Eigenschaften von Buchenholz nach einer Modifizierung mit 1,3-dimethylol-4,5-dihydroxyethyleneurea (DMDHEU) [Biological and technological properties of beech wood after modification with 1.3-dimethylol-4.5-dihydroxyethylurea (DMDHEU)]. PhD Thessis, University of Goettingen, Faculty of Forest Sciences and Forest Ecology, Goettingen.
3. Bollmus, S.; Beeretz, C.; Militz, H., 2020: Tensile and impact bending properties of chemically modified scots pine. Forests, 11 (1): 84. https://doi.org/10.3390/f11010084
4. Brischke, C., 2018: Timber. In: Ghiassi, B., Lourenço, P. B. (eds.), Long-term performance and durability of masonry structures: Degradation Mechanisms, Health Monitoring and Service Life Design. Woodhead Publishing.
5. Brischke, C.; Ziegeler, N.; Bollmus, S., 2019: Abrasion resistance of thermally and chemically modified timber. Drvna industrija, 70 (1): 71-76. https://doi.org/10.5552/drvind.2019.1813
6. Cai, M.; Fu, Z.; Cai, Y.; Li, Z.; Xu, C.; Xu, C.; Li, S., 2018: Effect of impregnation with maltodextrin and 1,3-dimethylol-4,5-dihydroxyethyleneurea on Poplar wood. Forests, 9 (11): 676. https://doi.org/10.3390/f9110676
7. Castro, G. L.; Fragnelli, G., 2006: New technologies and alternative uses for poplar wood. Boletín Informativo CIDEU, 2: 27-36.
8. Chen, F.; Li, Q.; Gao, X.; Han, G.; Cheng, W., 2017: Impulse-cyclone drying treatment of poplar wood fibers and its effect on composite material's properties. BioResources, 12 (2): 3948-3964.
9. Derham, B. R.; Singh, T.; Militz, H., 2017: Commercialisation of DMDHEU modified wood in Australasia. The International Research Group on Wood Protection, IRG/WP/17-40772.
10. Dieste, A.; Krause, A.; Mai, C.; Sébe, G.; Grelier, S.; Militz, H., 2009: Modification of *Fagus sylvatica* L. with 1,3-dimethylol-4,5-dihydroxy ethylene urea (DMDHEU). Part 2: Pore size distribution determined by differential scanning calorimetry. Holzforschung, 63: 89-93. https://doi.org/10.1515/HF.2009.023
11. Doh, G. H.; Lee, S. Y.; Kang, I. A.; Kong, Y. T., 2005: Thermal behavior of liquefied wood polymer composites (LWPC). Composite structures, 68 (1): 103-108. https://doi.org/10.1016/j.compstruct.2004.03.004
12. Emmerich, L.; Bollmus, S.; Militz, H., 2019: Wood modification with DMDHEU (1.3-dimethylol-4,5-dihydroxyethyleneurea) – State of the art, recent research activities and future perspectives. Wood Material Science & Engineering, 14 (1): 3-18. https://doi.org/10.1080/17480272.2017.1417907
13. Emmerich, L.; Brischke, C.; Militz, H., 2021: Wood modification with N-methylol and N-methyl compounds: a case study on how non-fixated chemicals in modified wood may affect the classification of their durability. Holzforschung, 75 (11): 1061-1065. https://doi.org/10.1515/hf-2021-0037
14. González-Peña, M. M.; Hale, M. D., 2011: Rapid assessment of physical properties and chemical composition of thermally modified wood by mid-infrared spectroscopy. Wood Science and Technology, 45 (1): 83-102. https://doi.org/10.1007/s00226-010-0307-9
15. Hill, C. A. S., 2006: Wood modification – chemical, thermal and other processes. Wiley Series in Renewable Resources, Wiley and Sons, Chichester, UK, pp. 260.
16. Jiang, T.; Gao, H.; Sun, J.; Xie, Y.; Li, X., 2014: Impact of DMDHEU resin treatment on the mechanical properties of poplar. Polymers and Polymer Composites, 22 (8): 669-674. https://doi.org/10.1177/096739111402200803
17. Larsson-Brelid, P., 2013: Benchmarking and state of the-art report for modified wood. SP Report no. 54, SP Technical Research Institute of Sweden, Stockholm, Sweden, pp. 1-31.
18. Li, W.; Chen, L.; Li, X., 2019: Comparison of physical-mechanical and mould-proof properties of furfurylated and DMDHEU-modified wood. BioResources, 14 (4): 9628-9644.
19. Li, W.; Chen, L.; Li, Y.; Li, X., 2020: Bamboo modification with 1,3-dimethylol-4,5-dihydroxyethyleneurea (DMDHEU) catalyzed by maleic anhydride. Journal of Wood Chemistry and Technology, 40 (2): 126-135. https://doi.org/10.1080/02773813.2019.1697293
20. Lopes, D. B.; Mai, C.; Militz, H., 2013: Bending creep of maritime pine wood (*Pinus pinaster* Ait.) chemically modified. Folia Forestalia Polonica, 55 (3): 120-131.
21. Militz, H.; 1993. Treatment of timber with water soluble dimethylol resins to improve their dimensional stability and durability. Wood Science and Technology, 27 (5): 347-355. https://doi.org/10.1007/BF00192221
22. Militz, H.; Lande, S., 2009: Challenges in wood modification technology on the way to practical applications. Wood Material Science and Engineering, 4 (1-2): 23-29. https://doi.org/10.1080/17480270903275578
23. Nicholas, D. D.; William, A. D., 1987: Dimensional stabilisation of wood with dimethylol compounds, Doc. No. IRG/WP 3412. International Research Group on Wood Preservation, Stockholm, Sweden.
24. Okon, K. E.; Lin, F.; Lin, X.; Chen, C.; Chen, Y.; Huang, B., 2018: Modification of Chinese fir (*Cunninghamia lanceolata* L.) wood by silicone oil heat treatment with micro-wave pretreatment. European Journal of Wood and Wood Products, 76 (1): 221-228. https://doi.org/10.1007/s00107-017-1165-z
25. Pandey, K. K., 1999: A study of chemical structure of soft and hardwood and wood polymers by FTIR spectroscopy. Journal of Applied Polymer Science, 71 (12): 1969-1975. https://doi.org/10.1002/(SICI)1097-4628(19990321)71:12<1969:AID-APP6>3.0.CO;2-D
26. Pfeffer, A.; Mai, C.; Militz, H., 2012: Weathering characteristics of wood treated with water glass, siloxane or DMDHEU. European Journal of Wood and Wood Products, 70 (1-3): 165-176. https://doi.org/10.1007/s00107-011-0520-8
27. Popescu, M. C.; Froidevaux, J.; Navi, P.; Popescu, C. M., 2013: Structural modifications of Tilia cordata wood during heat treatment investigated by FT-IR and 2D IR correlation spectroscopy. Journal of Molecular Structure, 1033: 176-186. https://doi.org/10.1016/j.molstruc.2012.08.035
28. Rowell, R. M., 1983: Chemical modification of wood: a review. Commonwealth Forestry Bureau, 6: 363-382. https://doi.org/10.1080/17480270600670923
29. Sandberg, D.; Kutnar, A.; Mantanis, G., 2017: Wood modification technologies a review. iForest-Biogeosciences and Forestry, 10 (6): 895. https://doi.org/10.3832/ifor2380-010
30. Schaffert, S.; Nunes, L.; Krause, A.; Militz, H., 2006: Resistance of DMDHEU-treated pinewood against termite

and fungi attack in field testing according to EN 252. Results after 30 months. The International Research Group on Wood Protection, IRG/WP/06-40354.
31. Schindler, W. D.; Hauser, P. J., 2004: Chemical finishing of textiles. (Cambridge: Woodhead).
32. Shebani, A. N.; Van Reenen, A. J.; Meincken, M., 2008: The effect of wood extractives on the thermal stability of different wood species. Thermochimica Acta, 471 (1-2): 43-50. https://doi.org/10.1016/j.tca.2008.02.020
33. Shen, D. K.; Gu, S.; Bridgwater, A. V., 2010: The thermal performance of the polysaccharides extracted from hardwood: cellulose and hemicellulose. Carbohydrate Polymers, 82 (1). 39-45. https://doi.org/10.1016/j.carbpol.2010.04.018
34. Xie, Y.; Krause, A.; Mai, C.; Militz, H.; Richter, K.; Urban, K.; Evans, P. D., 2005: Weathering of wood modified with the N-methylol compound 1,3-dimethylol-4,5-dihydroxyethyleneurea. Polymer Degradation and Stability, 89 (2). 189-199. https://doi.org/10.1016/j.polymdegradstab.2004.08.017
35. Xie, Y.; Xiao, Z.; Grüneberg, T.; Militz, H.; Hill, C. A.; Steuernagel, L.; Mai, C., 2010: Effects of chemical modification of wood particles with glutaraldehyde and 1,3-dimethylol-4,5-dihydroxyethyleneurea on properties of the resulting polypropylene composites. Composites Science and Technology, 70 (13): 2003-2011. https://doi.org/10.1016/j.compscitech.2010.07.024
36. Van Acker, J.; Nurmi, A.; Gray, S.; Militz, H.; Hill, C.; Kokko, H.; Rapp, A., 1999: Decay resistance of resin treated wood. International Research Group on Wood Preservation, Doc. No. IRG/WP 99-30206.
37. Van der Zee, M. E.; Beckers, E. P.; Militz, H., 1998: Influence of concentration, catalyst and temperature on dimensional stability of DMDHEU modified Scots pine. The International Research Group on Wood Preservation, IRG/WP/98-40119.
38. Verma, P.; Junga, U.; Militz, H.; Mai, C., 2009: Protection mechanisms of DMDHEU treated wood against white and brown rot fungi. Holzforschung, 63: 371-378. https://doi.org/10.1515/HF.2009.051
39. Videlov, C. L., 1989: Biological degradation resistance of pine wood treated with dimethylol compounds. International Research Group on Wood Preservation, Doc. No. IRG/WP 3528.
40. Yuan, J.; Hu, Y.; Li, L.; Cheng, F., 2013: The mechanical strength change of wood modified with DMDHEU. BioResources, 8 (1): 1076-1088.
41. ***EN 113, 2006: Wood preservatives. Test method for determining the protective effectiveness against wood destroying basidiomycetes – determination of the toxic values. European Committee for Standardization, Brussels, Belgium.
42. ***EN 350-2, 1994: Durability of Wood and Wood-based Products e Natural Durability of Solid Wood. Part 2: Guide to Natural Durability and Treatability of Selected Wood Species of Importance in Europe. European Committee for Standardization, Brussels, Belgium.
43. ***ENV 807, 1997: Wood preservatives – Determination of the effectiveness against soft rotting micro-fungi and other soil inhabiting micro-organisms. European Committee for Standardization, Brussels, Belgium.
44. ***TS 2474, 1976: Wood-determination of ultimate strength in static bending, Ankara.
45. ***TS 2595, 1976: Wood-determination of ultimate stress in compression parallel to grain, Ankara.

Corresponding address:

HÜSEYIN SİVRİKAYA
Bartin University, Faculty of Forestry, Department of Forest Industrial Engineering, 74100 Bartin, TURKEY,
e-mail: hsivrikaya@bartin.edu.tr

Abdurrahman Karaman[1]

Effects of Wooden Dowel Species, Edge Banding Thickness, and Adhesive Types on Embedded Strength in Particleboard

Utjecaj vrste drva moždanika, debljine rubnih traka i vrste ljepila na izvlačnu čvrstoću moždanika u iverici

ORIGINAL SCIENTIFIC PAPER
Izvorni znanstveni rad
Received – prispjelo: 17. 4. 2021.
Accepted – prihvaćeno: 13. 12. 2021.
UDK: 544.722.54; 674.812
https://doi.org/10.5552/drvind.2022.2116

ABSTRACT • *Composite materials, edge banding, and wooden dowels are used in inner decoration and construction of furniture frames. However, there is little information available concerning the embedded strength of various fasteners and, in particular, dowels in these materials. The aim of this study was to determine the embedded strengths of PVC edge bandings with the thickness of 0.8, 1, and 2 mm, and dowels produced from five different wood species bonded parallel to the surfaces of a melamine coated particleboard (YL-Lam) with polyvinyl acetate (PVAc-D4) or polyurethane (PUR-D4). In accordance with TS 4539 standard, the effect of wooden dowel species, thickness of edge banding, and type of adhesives on embedded strength were determined. Embedded strength values of polyurethane (PUR-D4) were found 10 % higher than the embedded strength values of polyvinyl acetate (PVAc-D4). The highest embedded strength was obtained for beech dowel bonded with polyurethane (PUR-D4) adhesive in the samples with 0.8 mm PVC edge banding (2.004 N/mm²), while the lowest embedded strength was obtained for Scots pine dowel with polyvinyl acetate (PVAc-D4) adhesive in the samples without PVC edge banding (0.826 N/mm²). This value is higher than the predicted value that allows designers to estimate the embedded strength of dowels.*

KEYWORDS: *PUR-D4; PVC edge banding; embedded strength of dowel; particleboard; dowel*

SAŽETAK • *Pri unutarnjem uređenju i za izradu okvira namještaja upotrebljavaju se kompozitni materijali, rubne trake i drveni moždanici. Međutim, malo je dostupnih podataka o izvlačnoj čvrstoći spojnih elemenata, posebice moždanika. Cilj ovog istraživanja bio je utvrditi izvlačnu čvrstoću moždanika proizvedenih od pet različitih vrsta drva zalijepljenih polivinil acetatnim (PVAc-D4) ili poliuretanskim ljepilom (PUR-D4) u rubove iverice (YL-Lam) paralelno s površinama obloženim melaminom. Rubovi iverice obloženi su PVC trakama debljine 0,8; 1 i 2 mm. Prema standardu TS 4539, određen je utjecaj vrste drva moždanika, debljine rubne trake i vrste ljepila na izvlačnu čvrstoću moždanika. Pokazalo se da su vrijednosti izvlačne čvrstoće moždanika zalijepljenih poliuretanskim ljepilom (PUR-D4) 10 % veće od vrijednosti izvlačne čvrstoće moždanika zalijepljenih polivinil acetatnim ljepilom (PVAc-D4). Najveća izvlačna čvrstoća dobivena je za moždanik od bukovine zalijepljen poliuretanskim (PUR-D4) ljepilom na uzorke s rubnom trakom od PVC-a debljine 0,8 mm (2,004 N/mm²), dok je najniža vrijednost izvlačne čvrstoće zabilježena za moždanik od borovine zalijepljen polivinil acetatnim (PVAc-D4) ljepilom na uzorcima bez PVC rubnih traka (0,826 N/mm²). Ta je vrijednost viša od predviđene vrijednosti koja omogućuje dizajnerima da procijene izvlačnu čvrstoću moždanika.*

KLJUČNE RIJEČI: *PUR-D4; PVC rubna traka; izvlačna čvrstoća moždanika; iverica; moždanik*

[1] Author is associated professor at Uşak University, Vocational School Banaz, Forestry and Forest Program, Department of Forestry, Uşak, Turkey.

1 INTRODUCTION
1. UVOD

Generally, particleboard has been made with forest products in the world. However, due to government restriction, wildlife protection, and other environmental concerns, the availability of these raw materials has been decreasing. The demand for particleboard products continues to increase, leaving an increasing gap between raw materials and products demand (Cheng *et al*., 2004). Dowel joints are widely used in furniture frame construction, both as (load-bearing structure) connections and as simple locators for parts. Joints constructed with dowels may be subjected to withdrawal, bending, shear, and tensional forces. Individual dowel pins used in the joints, however, are subjected to withdrawal and shear forces only (Eckelman and Erdil, 1999).

In order to apply dowel-type joints efficiently, the key thing is to understand their mechanical behavior when undergoing the load (e.g. load-slip relation, stress distributions, ultimate strength and failure modes). The mechanical behavior of wooden joints is a complex problem governed by a number of geometric, solid wood and loading parameters (e.g. wood species, fastener diameter, end distances, edge distances, spacing, number of fasteners, fastener/hole clearances, friction and loading configuration) (Santos *et al.,* 2010). Englesson and Osterman (1972) reported that plain dowels and spiral-grooved dowels with fine grooving gave greater withdrawal strength from the face of particleboard than multi-groove dowels did, at least when an excess adhesive was applied in the holes and subsequently forced into the substrate as the dowels were inserted into the holes. Englesson and Osterman (1972) found that applying glue on both walls of the holes and surface of the dowels (double gluing) resulted in a 35 % increase in holding strength compared to coating the walls of holes or surface of the dowels alone.

Edge banding is perceived as the most important accessory and protection in furniture making. Laminates, wood, polyvinyl chloride (PVC), acrylonitrile butadiene styrene (ABS), acrylic, melamine, wood or wood veneer comprise the types of edge banding materials. The purpose of the edge banding is to suppress the absorption of water and humidity, providing a contrasting finish for all decorative surfaces. The edge bands are in the form of 0.4, 0.8, 1 and 2 mm PVC edge bands (Sözen, 2008).

Örs *et al.* (1999a) investigated the effects of the thickness of solid wood edge banding strips on the withdrawal strength of beech dowels in medium-density fiberboard (MDF). Test samples with 5, 8, and 12 mm beech wood edge banding strips were bonded with PVAc adhesive. The study revealed that the highest tensile strength was obtained with MDF covered with 8 mm thick beech wood material (2.294 N/mm^2), while the lowest value was obtained with 10 mm diamater dowel and with unprocessed MDF (1.314 N/mm^2). Dowels of 6, 8, and 10 mm in diameter bonded with PVAc adhesive were tested according to the procedure in ASTM-D 1037 standard on waferboard (WFB), whose edges were drilled 25 mm in depth and that were covered with beech wood 5, 8 and 12 mm thick. The result of the face withdrawal strength test showed that the highest value (2.338 N/mm^2) was obtained in 6 mm diameter dowel with WFB with 8 mm-thick beech wood, while the lowest value (1.160 N/mm^2) was obtained in 10 mm diameter dowel with unprocessed WFB (Örs *et al.,* 2000). Uysal and Özçifçi (2003) studied the tensile strength of 10-mm-diameter dowels produced from medium-density fiberboard (MDF), plywood, scotch pine (*Pinus sylvestris* L.), and beech (*Fagus orientalis* lipsky), bonded parallel and vertical to the surface of MDF and particleboard (PB) with polyvinyl acetate (PVAc) and Desmodur-VTKA (D-VTKA). The results showed that the highest tensile strength was obtained in beech dowels bonded vertically with PVAc adhesive to the surface of MDF at 7.91 N/mm^2. Tankut (2005) presented the results of evaluating the effect of dowel spacing on bending moment capacity of L-type corner joints in 32 mm case construction. Uysal and Kurt (2007) investigated the effects of the thickness of solid wood edge banding strips and dowel diameter on the withdrawal strength of beech dowels in particleboard test samples with 5, 8, and 12 mm beech wood edge banding strips bonded with PVAc adhesive and the holes with 25 mm depth drilled into the edges of the test samples. The results showed that the highest withdrawal strength was obtained in MDF with 6 mm dowel diameter and 5 mm thick solid wood edge banding strip bonded with hot-melt adhesive, while the lowest withdrawal strength was obtained in case of particleboard with no edge banding strip, with 10 mm dowel diameter. Kurt *et al.* (2009) investigated the withdrawal strengths of 6, 8, 10 mm diameter dowels produced from beech with respect to edge of a medium-density fiberboard (MDF) or particleboard (PB) edged with 5, 10 and 15 mm thickness of solid wood edge banding of uludag fir, bonded with different adhesives. They found that the highest withdrawal strength was obtained in beech dowels with 8 mm diameter for MDF with 5 mm thickness of solid wood edge banding of Uludag fir bonded with D-VTKA adhesive, while the lowest withdrawal strength was obtained in particleboard with 10 mm diameter of dowel and without solid wood edge banding. Tankut and Tankut (2010) investigated the effects of the edge banding material, namely polyvinyl chloride (PVC), melamine and wood veneer, thickness of edge banding

material (0.4, 1, and 2 mm), and wood composite panel type on the diagonal compression and tension strength properties of particleboard surfaced with synthetic resin sheet (LamPb) and MDF surfaced with synthetic resin sheet (LamMDF). They found that the melamin type edge banding material gave more diagonal tension and compression strength than others. The lowest tension and compression strength was obtained in PVC edge banding material. Yapıcı *et al.* (2011) investigated the connection resistance of dowels produced from beech wood and the effects of thickness, dimension of dowels, type of composite materials (MDF and particleboard) and type of adhesives used for edge banding on the withdrawal strength. They found that the highest withdrawal strength was obtained in beech dowels with 8 mm diameter for MDF with 5 mm thickness of solid wood edge banding (6.689 N/mm^2), while the lowest withdrawal strength was obtained in particleboard with 10 mm diameter of dowel and without solid wood edge banding (2.696 N/mm^2).

Vick (1999) reported that the quality of adhesion in adhesives, as well as dispersion on the surface on which the adhesives are applied and penetration to both surfaces, depend on the fluidity of adhesives, which are effective in forming layers and wetting surfaces. Penetration of the hardening adhesives into the porous wood skeleton on several scales are rather complicated. It is strongly influenced by wood factors like wood species, anatomical orientation or surface roughness, adhesive factors, such as adhesive type or viscosity, and process factors, such as applied pressure or temperature, with a big influence on the bonding performance (Kamke and Lee, 2007). D-VTKA adhesive gave higher withdrawal strength values than PVAc. As D-VTKA cures, it swells and fills the gaps in the dowel holes, resulting in better mechanical adhesion. These results confirm earlier reports by Erdil and Eckelman, who stated that the use of excess adhesives in the construction of joints largely outweighed the importance of the other factors and ensured construction of joints with maximum strength (Erdil and Eckelman, 2001). Kurt *et al.* (2009) studied the dowel withdrawal strength of the edge banding thickness, dimension of dowels, type of composite materials and adhesives. They reported that D-VTKA adhesive gave higher withdrawal strength values than PVAc and hot-melt adhesives. Uysal and Kurt (2007) found that the withdrawal strength of dowels with D-VTKA adhesive gave higher withdrawal strength values than PVAc and hot melt adhesives. In the literature, some authors reported that the bond strength for PUR adhesives was higher than the joint strength of PVAc adhesives (Sterley *et al*., 2004; Bomba *et al*., 2014).

This study was performed (1) to evaluate the effects of thickness of edge banding (control, 0.8, 1, and 2 mm) on the embedded strength, (2) to determine the effects of wooden dowel species, namely, beech, chestnut, olive, Scots pine and Turkish fir on the embedded strength, (3) to evaluate adhesive types, namely, polyvinyl acetate (PVAc-D4) and polyurethane (PUR-D4) on the embedded strength.

2 MATERIALS AND METHODS
2. MATERIJALI I METODE

2.1 Materials
2.1. Materijali

The following composite test panel was used. Melamine coated particleboard (YL-Lam) was provided by Güçlüer Forest Products Industry and Trade Ltd. Company (Uşak, Turkey). **Average moisture content, density, bending strength (***MOR***)** and modulus of elasticity (*MOE*) of the YL-Lam were determined to be 7.5 %; 0.620 g/m^3; 19.20 N/mm^2 and 2620 N/mm^2.

The wood of beech (*Fagus orientalis* Lipsky), Scots pine (*Pinus sylvestris* Lipsky), Turkish fir (*Abies bornmülleriana* Mattf.), and Chestnut (*Castanea sativa* Mill) is used extensively in the wood construction sector. This wood was also used as dowel material for these experiments. The wood was chosen randomly from timber merchants of Ankara, Turkey, while the Olive wood (*Ole europaea* L.) as massive material was obtained from the timber enterprises in Akhisar district of Manisa, Turkey. A special emphasis was put on the selection of wood material. Accordingly, non-deficient, proper, knotless, normally grown (without zone line, reaction wood, decay, insect and mushroom damages) wood material was selected. In accordance with TS 2472 (1976), the air-dry density properties of wood materials used in this study are shown in Table 1. The wood dowels were prepared with a cylindrical shape in nominal dimensions of 8 mm × 70 mm (Figure 1).

PVC edge banding is manufactured from first-quality resins and high-impact modifiers resulting in a product of excellent machinability, impact resistance, durability, and overall appearance. The edge bands, which are commonly used in the furniture industry, are in the form of PVC (polyvinyl chloride) edge bands of 0.4, 0.8, 1, and 2 mm. The PVC edge bands with the thickness of 0.8, 1, and 2 mm were used in this study.

The polyvinyl acetate (PVAc) and polyurethane, which are commonly used in the wood industry and box- type furniture manufacture, were used in this study. The single-component polyvinyl acetate (PVAc) adhesive, Kronen Holzleim D4, manufactured by the German Kronen Company (Fenstertechnik Institut Rosenheim, Germany) was used in this study. Polyvinylacetate adhesive, which falls into durability class D4 according to DIN EN 204 (2016), was used as an adhesive. This polyvinylacetate glue, odorless and fireproof, is easy to apply, has quick setting and it is applied

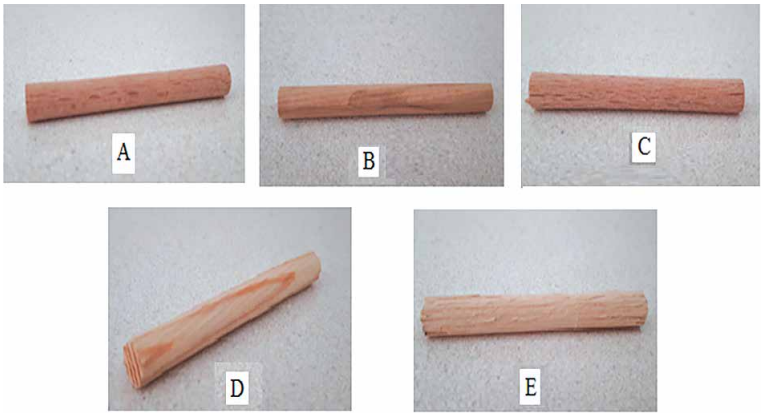

Figure 1 Types of dowel woods used in experiments: A) Beech, B) Olive, C) Chestnut, D) Scots pine, E) Turkish fir
Slika 1. Moždanici od različitih vrsta drva upotrijebljenih u istraživanju: A) bukovina, B) maslinovina, C) kestenovina, D) borovina, E) drvo turske jele

Table 1 Density of wood species used in my research
Tablica 1. Gustoća drva obuhvaćenog istraživanjem

Wood material and wood composite material *Drvni materijal i drvno-kompozitni materijal*	D_{12}, g/cm^3
Beech (*Fagus orientalis* Lipsky)	0.65
Chestnut (*Castanea sativa* Mill)	0.57
Scots pine (*Pinus sylvestris* Lipsky)	0.50
Turkish fir (*Abies bornmülleriana* Mattf.)	0.42
Olive (*Olea europaea*)	0.84

D_{12} – Air dry density at 20 °C and 65 % relative humidity / *gustoća drva sušenoga pri 20 °C i 65 %-tnoj relativnoj vlažnosti zraka*

cold. According to the producer's recommendations, the adhesive was applied in the amount of (180±10) g/m^2 to the surfaces. The properties of this glue were determined as follows: press compression 0.1-0.8 N/mm^2, pH 3.5, viscosity (20 °C) 16000-15000 mPas, density 1.08 g/cm^3 and wood bonding time at 20 °C for 35-40 minutes, by the company (Kronen, 2019). The polyurethane (PUR-D4; Egger Decor, Gebze, Kocaeli, Turkey) is a single component polyurethane-based adhesive, fast curing and polyurethane-based wood adhesive. The gluing process was carried out at 20 °C and 65 % relative humidity. According to the producer's recommendations, the adhesive was applied in the amount of (180±10) g/m^2 to the surfaces. It is easy to apply, water-resistant and has low viscosity and high bonding strength. (Romabant, 2019). In this study, the hot-melt was used as a thermoplastic synthetic resin, commonly used as PVC edge banding adhesive in the furniture industry. Its application is recommended in locations subjected to 8 - 10 % relative humidity. The temperature for the adhesive gluing was 200 - 230 °C.

2.2 Preparation of test samples
2.2. Priprema ispitnih uzoraka

Wood materials were held for approximately 3 months in the conditioning room at (20±2) °C and (65±3) % relative humidity until their weight became stable. Then, 1000 mm ×11 mm ×11 mm pieces were cut from beech sapwood, Scots pine sapwood, Turkish fir sapwood, Chestnut sapwood and olive sapwood. Dowels with 8 mm diameter were produced from these pieces using a dowel machine. These dowels were produced striated. Then, in total 200 samples were prepared for this study (YL-Lam, two different adhesives PVAc-D4, PUR-D4, five different wooden dowel species, three different PVC edge banding with the thickness of 0.8 mm, 1 mm, 2 mm and control). YL-Lam material was prepared as follows: Randomly chosen YL-Lam board was cut into 200 pieces for each member in the dimensions of (18 mm × 75 mm × 75 mm) ± 1 mm with a wood milling machine. An amount of 150 pieces for each composite material was banded on one edge with three different types of edge banding (PVC edge bands with the thickness of 0.8 mm, 1 mm, and 2 mm). The PVC bands were banded by using a hot-melt adhesive on the edge banding machine (Figure 2). In addition, 50 pieces were not included into any process. Dowels of 25 mm depth for embedded tests were glued into matching holes and were drilled into each specimen according to the TS 4539 (1985) standard. All holes were drilled with standard twist drills. The diameter of the holes was 8 mm. Before the dowels were inserted, adhesives (180 g/m^2) were applied both on the sides of the dowels and on the surfaces of the holes. The configuration of test samples is shown in Figure 2. Before the embedded test, the samples were stabilized at (20±2) °C and (65±3) % relative humidity until the samples had 12 % moisture content.

2.3 Test method
2.3. Ispitna metoda

All tests were carried out on a universal testing machine, ZwickRoell Z050, placed in the laboratory of Gümüşhane University and Gümüşhane Vocational High School, having a capacity of 50 kN and equipped with jigs to hold the specimens as shown in Figure 3. A loading rate of 5 mm/min was used in all tests according to ASTM 1037 (1988) standards. The embedded strength was determined as Eq. 1:

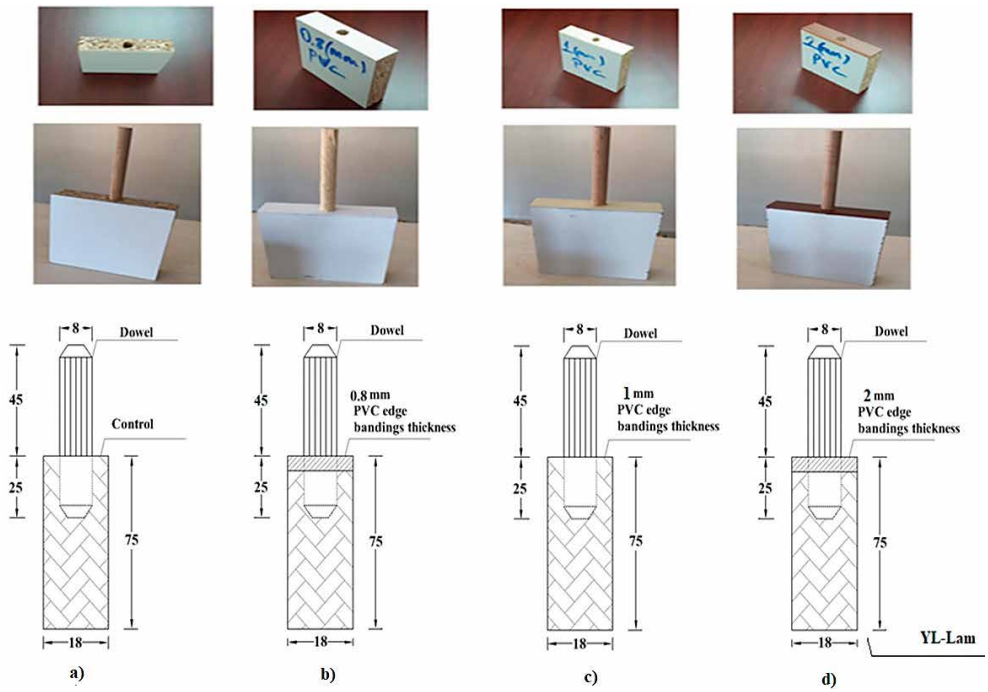

Figure 2 Configuration of test samples; a) Control (non-edge banding), b) 0.8 mm edge banding, c) 1 mm edge banding, d) 2 mm edge banding
Slika 2. Konfiguracija ispitnih uzoraka: a) kontrolni uzorak (bez rubnih traka), b) uzorak s rubnom trakom od 0,8 mm, c) uzorak s rubnom trakom od 1 mm, d) uzorak s rubnom trakom od 2 mm

$$\sigma_k = \frac{F_{max}}{A} = \frac{F_{max}}{h \cdot (2 \cdot \pi \cdot r)} \quad (1)$$

Where is embedded strength (N/mm^2), F_{max} is the maximum load (N), r is radius of dowel (mm), h is depth of dowel (mm).

2.4 Data analyses
2.4. Analiza podataka

The multiple variance analysis was performed to determine the differences among the factors (wooden dowel species, thickness of PVC edge banding, adhesive types) by using the SPSS program (Statistical Software, a computer-based statistical package, version 22). The Tukey's test was used to determine if there was a meaningful difference among the groups.

3 RESULTS AND DISCUSSION
3. REZULTATI I RASPRAVA

The average embedded strength values obtained from the test samples are given in Table 2, and the average values of interactions between the factors are presented in Table 3. The results of the multiple variance analyses connected with these values are given in Table 4.

For the samples without PVC edge banding (control), the highest embedded strength was obtained from the Beech dowel bonded with PUR-D4 adhesive (1.616 N/mm^2), while the lowest embedded strength was obtained from the Scots pine dowel with PVAc-D4 adhesive (0.826 N/mm^2). In terms of the embedded strength values of used PVC edge banding with the thickness of 0.8 mm, the highest embedded strength was obtained

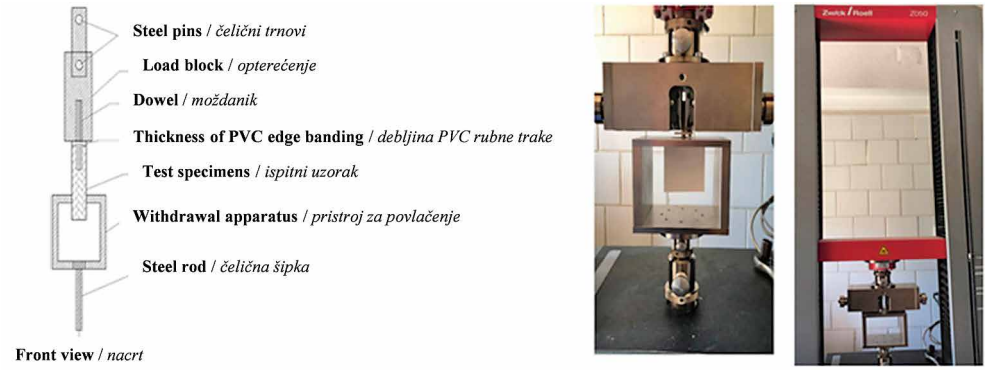

Figure 3 Apparatus used to hold specimens for embedded strength tests
Slika 3. Pristroj za prihvat uzoraka za ispitivanja izvlačne čvrstoće

Table 2 Average values of embedded strength (N/mm²)
Tablica 2. Srednje vrijednosti izvlačne čvrstoće (N/mm²)

Factor source / *Čimbenik*		$\bar{x}$	***SD***	**HG**
Adhesive type *Vrsta ljepila*	PUR-D4	1.298 (22.34)*	0.29	A
	PVAc-D4	1.176 (29.71)	0.35	B
Thickness of PVC edge banding *Debljina PVC rubne trake*	Control	1.176 (24.66)	0.29	B
	0.8 mm	1.485 (25.60)	0.38	A
	1 mm	1.192 (23.50)	0.28	B
	2 mm	1.096 (20.07)	0.22	B
Wooden dowel species *Vrsta drva moždanika*	Beech / *bukovina*	1.342 (29.06)	0.39	A
	Chestnut / *kestenovina*	1.217 (20.54)	0.25	A
	Olive / *maslinovina*	1.278 (24.26)	0.31	A
	Scots pine / *smrekovina*	1.047 (25.79)	0.27	B
	Turkish fir / *drvo turske jele*	1.301 (25.36)	0.33	A

*Values in the parentheses are coefficients of variation, *SD* – Standard deviation, HG – Homogeneity group.
**Vrijednosti u zagradama koeficijenti su varijacije, SD – standardna devijacija, HG – grupa homogenosti.*

Table 3 Average values of interaction for embedded strength (N/mm²)
Tablica 3. Srednje vrijednosti interakcije za izvlačnu čvrstoću (N/mm²)

Thickness of PVC edge bandings *Debljina PVC rubne trake*	**Wooden dowel species** *Vrsta drva moždanika*	**Adhesives** *Ljepilo*	$\bar{x}$	***SD***
Control / *kontrolni uzorci*	Beech / *bukovina*	PVAc-D4	1.322	0.12
		PUR-D4	1.616	0.29
	Chestnut / *kestenovina*	PVAc-D4	1.124	0.21
		PUR-D4	1.358	0.14
	Olive / *maslinovina*	PVAc-D4	1.264	0.22
		PUR-D4	0.964	0.19
	Scots pine / *borovina*	PVAc-D4	0.826	0.16
		PUR-D4	0.965	0.19
	Turkish fir / *drvo turske jele*	PVAc-D4	1.124	0.26
		PUR-D4	1.196	0.24
0.8 mm	Beech / *bukovina*	PVAc-D4	1.280	0.20
		PUR-D4	2.004	0.39
	Chestnut / *kestenovina*	PVAc-D4	1.024	0.37
		PUR-D4	1.498	0.13
	Olive / *maslinovina*	PVAc-D4	1.612	0.33
		PUR-D4	1.554	0.37
	Scots pine / *borovina*	PVAc-D4	1.248	0.22
		PUR-D4	1.394	0.13
	Turkish fir / *drvo turske jele*	PVAc-D4	1.426	0.28
		PUR-D4	1.806	0.31
1 mm	Beech / *bukovina*	PVAc-D4	1.236	0.38
		PUR-D4	1.176	0.23
	Chestnut / *kestenovina*	PVAc-D4	0.952	0.22
		PUR-D4	1.328	0.15
	Olive / *maslinovina*	PVAc-D4	1.485	0.13
		PUR-D4	1.186	0.09
	Scots pine / *borovina*	PVAc-D4	1.032	0.27
		PUR-D4	0.868	0.07
	Turkish fir / *drvo turske jele*	PVAc-D4	1.348	0.11
		PUR-D4	1.306	0.38
2 mm	Beech / *bukovina*	PVAc-D4	0.914	0.18
		PUR-D4	1.190	0.11
	Chestnut / *kestenovina*	PVAc-D4	1.170	0.16
		PUR-D4	1.280	0.14
	Olive / *maslinovina*	PVAc-D4	1.010	0.17
		PUR-D4	1.146	0.08
	Scots pine / *borovina*	PVAc-D4	1.066	0.37
		PUR-D4	0.980	0.20
	Turkish fir / *drvo turske jele*	PVAc-D4	1.054	0.19
		PUR-D4	1.146	0.32

from samples with Beech dowel bonded with PUR-D4 adhesive, while the lowest embedded strength was obtained from Chestnut dowel with PVAc-D4 adhesive. When the samples with 1 mm PVC edge banding was examined, the highest embedded strength was obtained from Olive dowel bonded with PVAc-D4 adhesive (1.485 N/mm^2), while the lowest embedded strength was obtained from Scots pine dowel with PVAc-D4 adhesive (0.868 N/mm^2). When embedded strength values of used PVC edge banding with the thickness of 2 mm was considered, the highest embedded strength was obtained with PUR-D4 adhesive, while the lowest embedded strength was obtained from Beech dowel with PVAc-D4 adhesive (Table 3).

The reasons for this are the density differences of wood materials, structural properties, mechanical properties and provided better bonding strength. The density of beech wood was higher than the density of the other woods used in the experiments. This may be due to the thick cell walls of beech wood, large number of tracheae, narrow lumen space and high material density, and thin lumen of the cell walls in Scots pine and low material density. An excess density may have caused the surface area in contact with each other to grow and increase the amount of molecules involved in adhesion, hence the molecules to adhere to each other by creating more adhesion force. In addition, in trees with an excess density, hydrogen bridges formed between the cellulose molecules of the wood material and the hydroxyl groups (OH) of the glue are deemed more excessive.

As polyurethane (PUR-D4) cures, it swells and fills the gaps in the dowel holes, resulting in better mechanical adhesion. According to the results, if the hole wall of the dowel and surface of the dowel are smoother than the PVAc-D4, it gives better mechanical adhesion with dowels.

Results of multiple variance analysis of the impact of adhesive types, the thickness of PVC edge banding, and wooden dowel species for dowel embedded strength are given in Table 4.

The effects of the main factors including the adhesive types (A), thickness of PVC edge banding (B), and wooden dowel species (C) were found to be statistically significant at the level of 0.05. All two-way interactions were also statistically significant ($p \leq 0.05$). Three factor interactions of adhesive types × thickness of PVC edge banding × wooden dowel species (A × B × C) were statistically insignificant ($p \leq 0.05$). Tukey's test was carried out in order to determine these differences and results are given in Table 2.

With respect to the mean values in Table 2, regarding the adhesive types, the dowel embedded strength was found to be the highest in the polyurethane adhesive (PUR-D4). The dowel embedded strength values of polyurethane PUR-D4) were found 10 % higher than the embedded strength values of polyvinyl acetate (PVAc-D4). The PUR-D4 adhesive expands its volume after being applied to the wood material.

For the thicknesses of PVC edge banding, the dowel embedded strength of 0.8 mm PVC edge banding was approximately 25 %, 26 % and 35 % higher than for 1 mm PVC edge banding, the samples with control (without PVC edge banding), and 2 mm PVC edge banding, respectively (Table 2). It has been determined that the dowel tensile strength increases when the edges of the YL-Lam board are covered with a PVC edge band. These values correspond to the values given in the literature (Örs *et al*., 1999; Tankut and Tankut 2010; Yapici *et al.,* 2011).

Örs *et al.* (1999b) reported that the tensile strength of dowels increases if the edges of the YL board are massified. YL boards without solid edges show lower

Table 4 Results of multiple variance analysis of dowel embedded strength
Tablica 4. Analiza varijance višestruke linearne regresije rezultata izvlačne čvrstoće moždanika

Source of variance / *Izvor varijacije*	***df.***	**Sum of square** *Zbroj kvadrata*	**Mean square** *Sredina kvadrata*	***F* value**	***P* value**
Adhesive types (A)[a] / *vrsta ljepila* (A)[a]	1	0.746	0.746	13.434	0.000
Thickness of PVC edge banding (B)[b] *debljina PVC rubne trake* (B)[b]	3	4.355	1.452	26.147	0.000
Wooden dowel species (C)[c] / *vrsta drva moždanika* (C)[c]	4	2.128	0.532	9.585	0.000
A × B	3	0.895	0.298	5.375	0.001
A × C	4	1.425	0.356	6.418	0.000
B × C	12	2.134	0.178	3.203	0.000
A × B × C	12	0.832	0.069	1.249	0.254*
Error / *pogreška*	160	8.883	0.056		
Total / *ukupno*	200	327.399			
Corrected Total / *ispravljeno ukupno*	199	21.397			
Squared = .585 (Adjusted R Squared = .484)					

*Not significant, *df* – Degrees of freedom, [a]Adhesive types (PVAc-D4, PUR-D4), [b]Thickness of PVC edge banding (0.8, 1 and 2 mm), [c]Wooden dowel species (Beech, Chestnut, Olive, Scots pine, Turkish fir)
**Nije značajno, df – stupnjevi slobode, [a]vrsta ljepila* (PVAc-D4, PUR-D4), [b]*debljina PVC rubne trake (0,8; 1 i 2 mm), [c]vrsta drva moždanika (bukovina, kestenovina, maslinovina, borovina i drvo turske jele).*

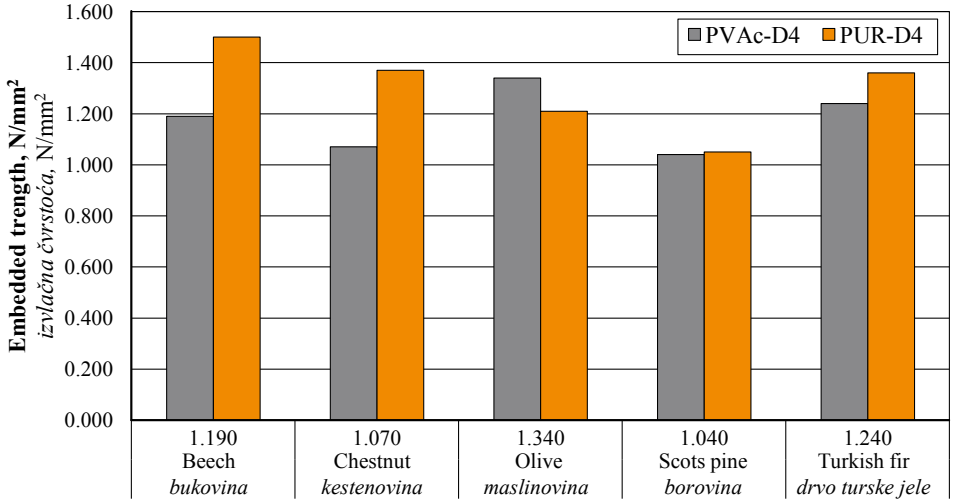

Figure 4 Effect of interactions of types of adhesives and wooden dowel species on embedded strength
Slika 4. Utjecaj interakcije vrste ljepila i vrste drva moždanika na izvlačnu čvrstoću

tensile strength than solid YL boards. Tankut and Tankut (2010) reported that the highest compression strength was obtained in 0.4 mm melamine edge banding, the lowest in PVC edge banding with 1 mm thickness. Yapici *et al.* (2011) determined that the highest withdrawal strength was obtained in beech dowels with 5 mm thickness of solid wood edge banding of beech bonded with D-VTKA adhesive.

For wooden dowel species, the highest embedded strength values of wooden dowel species were obtained from beech. The lowest embedded strength values of dowels were obtained from samples taken from chestnut and Scots pine (Table 2). It is inferred from the results that the highest embedded strength was obtained due to the density of the solid wood. Likewise, in their study, Özcan *et al.* (2013) observed that the highest withdrawal strength values were obtained from dowels made from oak and beech.

Interactions between adhesive type and wooden dowel species, adhesive type and thickness of PVC edge banding wooden dowel species and thickness of PVC edge banding are given Figure 4, 5 and 6.

As shown in Figure 4, the highest average embedded strength was observed in the beech dowel with PUR-D4, while the lowest average embedded strength was observed in Scots pine dowel with PVAc-D4.

As indicated in Figure 5, the samples of PUR-D4 adhesive with 0.8 mm thickness of PVC edge banding showed the highest average embedded strength, the PVAc-D4 with 2 mm thickness of PVC edge banding showed the lowest average embedded strength.

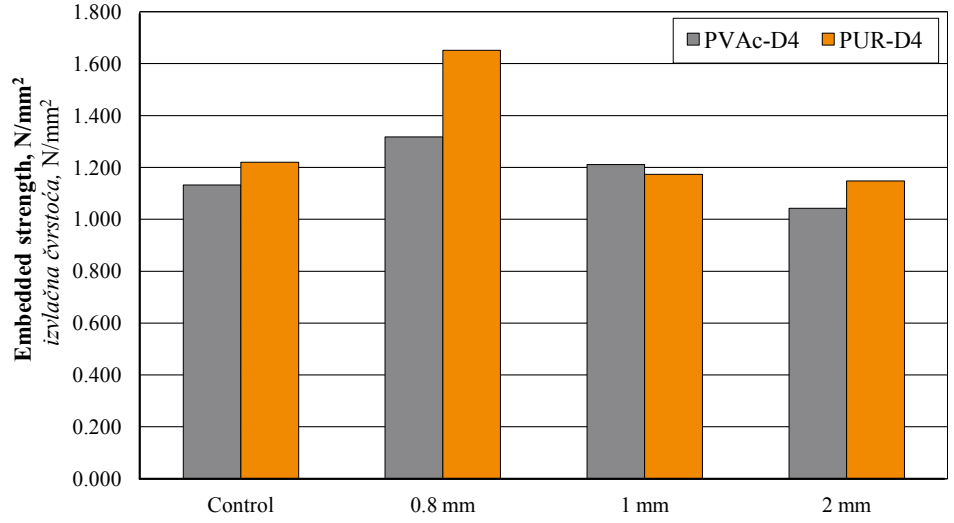

Figure 5 Effect of interactions of types of adhesives and thickness of PVC edge banding on embedded strength
Slika 5. Utjecaj interakcije vrste ljepila i debljine PVC rubne trake na izvlačnu čvrstoću

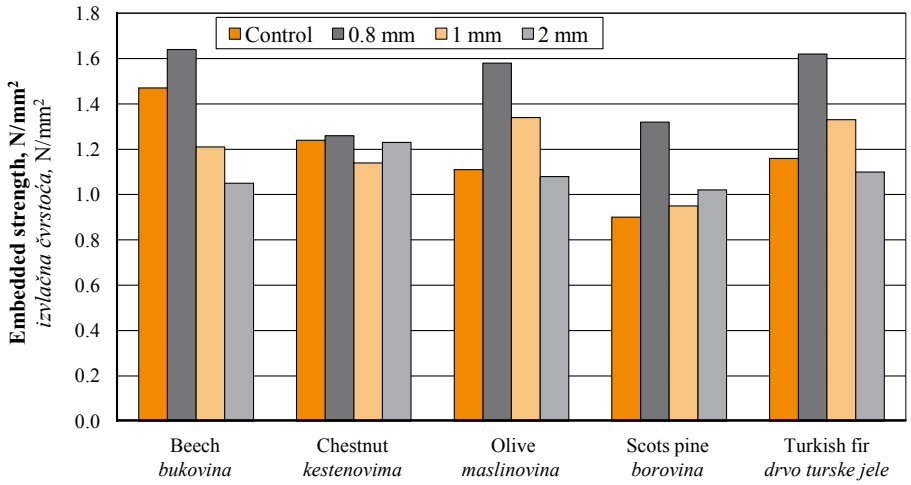

Figure 6 Effect of interactions of thickness of PVC edge banding and wooden dowel species on embedded strength
Slika 6. Utjecaj interakcije debljine PVC rubne trake i vrste drva moždanika na izvlačnu čvrstoću

4 CONCLUSIONS
4. ZAKLJUČAK

The joints assembled with polyurethane (PUR-D4) adhesive had 10 % higher embedded strength than the joints glued with polyvinyl acetate (PVAc-D4) adhesive. As polyurethane (PUR-D4) cures, it swells and fills the gaps in the dowel holes, resulting in better mechanical adhesion. According to the results, if the hole wall of the dowel is smoother than the adhesives, it provides better mechanical adhesion with dowels.

The beech dowel had the highest embedded strength values, and there were significant differences between these five wooden dowel species in this study. The reasons for this may be due to the density of wooden materials.

In terms of embedded strength of dowels from the edges of YL-Lam, PVC edge banding with 0.8 mm thickness was 25 % higher than PVC edge banding with 1 mm, 26 % higher than the control (without edge banding), and 36 % higher than PVC edge banding with 2 mm.

The highest embedded strength values were obtained with the beech dowel as the wooden dowel species, polyurethane (PUR-D4) as the adhesive, PVC edge banding with 0.8 mm thickness as the edge band. According to the results, if the hole wall and surface of the dowel are smoother, then the adhesives provide better mechanical adhesion with dowels and YL-Lam. Moreover, if the dowels are subjected to embedded strength, it is advised that beech dowel should be used on YL-Lam with polyurethane (PUR-D4) as the adhesive in the case-type furniture.

As a result, in building elements where adhesion performance is important, it may be recommended to use beech dowels, which are especially high in density, if wood material is to be used. In addition, since the highest tensile strength occurs in the combination of 0.8 mm thick PVC edge band, polyurethane adhesive, and beech dowel, applying these criteria in dowel joints will provide an advantage.

5 REFERENCES
5. LITERATURA

1. Bomba, J.; Sedivka, P.; Böhm, M.; Devera, M., 2014: Influence of moisture content on the bond strength and water resistance of bonded wood joints. BioResources, 9 (3): 5208-5218. https://doi.org/10.15376/biores.9.3.5208-5218
2. Cheng, E.; Sun, X.; Karr, G. S., 2004: Adhesive properties of modified soybean flour in wheat straw particleboard. Composites Part A: Applied Science and Manufacturing, 35 (3): 297-302. https://doi.org/10.1016/j.compositesa.2003.09.008
3. Eckelman, C. A.; Erdil, Y. Z., 1999: Joint design manual for furniture frames constructed of plywood and oriented strand board. In: Proceeding of 1st International Furniture Congress Proceedings. Istanbul, Turkey, pp. 266-268.
4. Erdil, Y. Z.; Eckelman, C. A., 2001: Withdrawal strength of dowels in plywood and oriented strand board. Turkish Journal of Agricultural Forestry, 25 (5): 319-327.
5. Englesson, T. A.; Osterman, A., 1972: Assembly of chipboard with round dowels. Swedish Forest Products Reseach Laboratory, Stockholm, Report No. 28.
6. Kamke, F. A.; Lee, J. N., 2007: Adhesive penetration in wood: a review. Wood and Fiber Science, 39 (2): 205-220.
7. Kronen, 2019: PVAc-D4 White Adhesive, İzmir._(online). https://www.kronen.com.tr/pva-d4-beyaz-tutkal (Accessed Oct 14., 2019).
8. Kurt, S.; Uysal, B.; Özcan, C.; Yildirim, M. N., 2009: The effects of edge banding thickness of uludağ bonded with some adhesives on withdrawal strengths of beech dowel pins in composite materials. BioResources, 4 (4): 1682-1693. https://doi.org/10.15376/biores.4.4.1682-1693
9. Romabant, 2019: Industrial Glues Professional Adhesive Solution. Kocaeli.
10. Örs, Y.; Atar, M.; Özçifçi, A., 1999a: Tensile resistance of dowel with the pvac and polymerin from different types

wood or particle or fiberboards. Turkish Journal of Agriculture and Forestry, 23 (1): 151-156.
11. Örs, Y.; Atar, M.; Özçifçi, A., 1999b: Effects of edge covering on tensile strength of MDF. Pamukkale University Engineering College Journal of Engineering Sciences, 5 (2-3): 1173-1177.
12. Özcan, C., Uysal, B., Kurt, Ş.; Esen, R., 2013: Effect of dowels and adhesive types on withdrawal strength in particleboard and MDF. Journal of Adhesion Science and Technology, 27 (8): 843-854. https://doi.org/10.1080/01694243.2012.727157
13. Santos, C. L.; De Jesus, A. M. P.; Morais, J. J. L.; Lousada, J. L. P. C., 2010: A comparison between the EN 383 and ASTM D 5764 test methods for dowel-bearing strength assessment of wood: experimental and numerical ınvestigations. Strain, 46 (2): 159-174. https://doi.org/10.1111/j.1475-1305.2008.00570.x
14. Sözen, E., 2008: Effect of type and thickness of edge banding materials on the strength of corner joints used case furniture. Master Thesis, Zonguldak Karaelmas University. Graduate School of Natural and Applied Sciences, Zonguldak.
15. Sterley, M.; Blümer, H.; Wålinder, M. E. P., 2004: Edge and face gluing of green timber using a one-component polyurethane adhesive. Holz Roh- Werkstoff, 62: 479-482. https://doi.org/10.1007/s00107-004-0517-7
16. Tankut, A. N., 2005: Optimum dowel spacing for corner joints in 32-mm cabinet construction. Forest Product Journal, 55 (12): 100-104.
17. Tankut, A. N.; Tankut, N., 2010: Evaluation the effects of edge banding type and thickness on the strength of corner joints in case-type furniture. Materials and Design, 31: 2956-2963. https://doi.org/10.1016/j.matdes.2009.12.022
18. Uysal, B.; Özçifçi, A., 2003: Effects of dowels produced from various materials on withdrawal strength in MDF and PB. Journal of Applied Polymer Science, 88(2): 531-535.
19. Uysal, B.; Kurt, S., 2007: The effect of edge banding thickness of white oak bonded with different adhesives on withdrawal strengths of beech dowels in composite material. Journal of Adhesion Science and Technology, 21 (8): 735-744. https://doi.org/10.1163/156856107781362626
20. Vick, C. B., 1999: Adhesive bonding of wood materials. In: Wood Handbook: Wood as an Engineering Material. Forest Products Laboratory, pp. 9-1 – 9-24.
21. Yapici, F.; Likos, E.; Esen, R., 2011: The effect of edge banding thickness of some trees on withdrawal strength of beech dowel pins in composite material. Wood Research, 56 (4): 601-612.
22. ***ASTM D1037, 1998: Standard test method for evaluating properties of wood-base fiber and particle panel materials. ASTM International. West Conshohocken, PA.
23. ***DIN EN 204, 2016: Classification of thermoplastic wood adhesives for non-structural applications.
24. ***TS 2472, 1976: Wood – determination of density for physical and mechanical tests. TSE, Ankara, Turkey.
25. ***TS 4539, 1985: Wood joints-rules of dowel joint. TSE, Ankara, Turkey.

Corresponding address:

Assoc. Prof. ABDURRAHMAN KARAMAN, PhD
Uşak University, Vocational School Banaz, Forestry and Forest Program, Department of Forestry, Uşak, TURKEY, e-mail: abdurrahman.karaman@usak.edu.tr

Sezgin Koray Gülsoy[1], Ülkü Burcu Gitti[1], Ayhan Gençer[1]

Comparison of Soda, Kraft, and DES Pulp Properties of European Black Poplar

Usporedba svojstava natronske, kraft i DES celuloze od drva europske crne topole

ORIGINAL SCIENTIFIC PAPER
Izvorni znanstveni rad
Received – prispjelo: 28. 3. 2021.
Accepted – prihvaćeno: 13. 12. 2021.
UDK: 630*86; 676.01; 676.1
https://doi.org/10.5552/drvind.2022.2112

ABSTRACT • *Kraft pulping as the dominant pulping method contributes to several environmental problems. To overcome these problems, environmentally friendly pulping methods have been investigated. In the last years, deep eutectic solvents (DESs) have been identified as up-and-coming reagents in the lignocellulosic material processing and they are characterized as environmentally friendly. This study investigated the use of DES in pulp production from European black poplar chips. The DES mixture was prepared from choline chloride (ChCl) and ethylene glycol (EG). In addition, traditional soda and kraft pulping methods were carried out with poplar chips for comparison with the DES pulps. It was found that pulp production from poplar chips using DES was comparable to the soda and kraft pulps in terms of pulp yield, pulp viscosity, and opacity. The DES pulps easily reached target pulp freeness levels. However, the strength properties and brightness of the DES pulps were lower than those of the soda and kraft pulps. The strength properties of DES pulps can be improved with paper strength enhancers such as starch and micro or nanofibrillated cellulose. Also, the utilization of DES in pulp production may have an important role in cleaner production and it represents a greener alternative to traditional pulp production methods.*

KEYWORDS: *DES; European black poplar; green chemistry; cleaner production; pulp properties*

SAŽETAK • *Celuloza se najčešće proizvodi kraft postupkom koji je povezan s nekoliko ekoloških problema. Kako bi se ti problemi prevladali, istražene su ekološki prihvatljive metode proizvodnje celuloze. Posljednjih su godina duboka eutektička otapala (DES) prepoznata kao ekološki prihvatljivi reagensi za preradu lignoceluloznih materijala u budućnosti. U ovom je radu istraživana uporaba DES-a u proizvodnji celuloze od sječke drva europske crne topole. DES smjesa pripremljena je od kolin-klorida (ChCl) i etilen-glikola (EG). Osim toga, tradicionalnim je natronskim i kraft postupkom proizvedena celuloza od sječke drva topole radi usporedbe s celulozom proizvedenom s dodatkom DES smjese. Utvrđeno je da je celuloza proizvedena od sječke drva topole uz upotrebu DES-a u smislu prinosa, viskoznosti i neprozirnosti usporediva s celulozom dobivenom natronskim i kraft postupkom. Celuloza proizvedena uz dodatak DES-a lako je dosegnula ciljani stupanj slobode celuloze. Međutim, svojstva čvrstoće i svjetlina celuloze proizvedene uz dodatak DES-a bili su lošiji od tih svojstava natronske i kraft celuloze. Svojstva čvrstoće DES celuloze mogu se poboljšati pojačivačima čvrstoće papira kao što su škrob i mikrofibrilirana ili nanofibrilirana celuloza. Osim toga, upotreba DES-a u proizvodnji celuloze može imati važan doprinos čišćoj proizvodnji i čini zeleniju alternativu tradicionalnim metodama proizvodnje celuloze.*

KLJUČNE RIJEČI: *DES; europska crna topola; zelena kemija; čišća proizvodnja; svojstva celuloze*

[1] Authors are researchers at Bartın University, Forestry Faculty, Forest Industry Engineering, Bartın, Turkey.

1 INTRODUCTION
1. UVOD

Although kraft pulping is the dominant method used in pulp industry, it has some serious disadvantages such as air pollution, water pollution, and high investment costs (Muurinen, 2000). For this reason, a number of new pulp processing methods have been studied. Organosolv (solvent-based) pulping is a chemical pulping method having minimum environmental impact, high pulp yield, and low investment costs (Saberikhah *et al*., 2011). EG pulping has been carried out with various biomasses such as palm oil tree residues (Alriols *et al*., 2009), olive tree trimmings (Jiménez *et al*., 2004), birch (Gast and Puls, 1984; Rutkowski *et al*., 1993), aspen and beech (Rutkowski *et al*., 1993), tagasaste (Jiménez *et al*., 2008; Rodríguez *et al*., 2008), vine shoots (Rodríguez *et al*., 2008; Jiménez *et al*., 2009), cotton stalks and leucaena (Rodríguez *et al*., 2008), pine (Nakamura and Takauti, 1941), and larch (Uraki and Sano, 1999).

Deep eutectic solvents (DESs) consist of a mixture of at least two components: a hydrogen-bond acceptor (HBA) and a hydrogen-bond donor (HBD) (Pena-Pereira and Namieśnik, 2014). They are non-toxic, eco-friendly, easily prepared, inexpensive, readily available, biodegradable, and recyclable green solvents. Because of these extraordinary advantages, interest in DESs continues to grow (Zhang *et al*., 2012). The usage potential for DESs in organic synthesis, electrochemistry, catalysis, and biology has been studied (Škulcová *et al*., 2016). In addition, DESs have been extensively used in the field of separation technologies (Hou *et al*., 2018). The solubilizing capacity of DESs on lignocellulosic biomass or its individual components such as lignins was tested by Francisco *et al*. (2012). Since then, studies related to biomass processing using various DESs have received increasing attention (Alvarez-Vasco *et al*., 2016; Hou *et al*., 2018; Chen *et al*. 2019; Jablonsky *et al*. 2019; Oh *et al*. 2020; Soto-Salcido *et al*. 2020).

A number of studies have focused on DES treatment using several types of lignocellulosic biomass. De Dios (2013) studied lignin isolation from wheat straw and pine sawdust using several deep eutectic mixtures and reported that the lignin solubility was increased with the higher content of lactic acid in DES. Abougor (2014) pretreated switchgrass with ChCl/trifluoroacetamide and lignin content was reduced by 6.66 %. In addition, they noted that pretreatment did not cause a reduction in cellulose and hemicellulose content. The wheat straw was pretreated with ChCl based DESs and containing different HBDs such as urea, lactic acid, malic acid, malonic acid, and oxalic acid dehydrate by Jablonský *et al*. (2015). The highest lignin removal was 57.9 % with ChCl/oxalic acid dihydrate at 60 °C and 24 h. Kumar *et al*. (2016) investigated solubility of cellulose, xylan, and lignin from rice straw in DESs containing ChCl, betaine, and lactic acid. Their experiments revealed that xylan and cellulose are not soluble in DESs. The lignin solubility in DES consisting lactic acid/ChCl reached almost 100 %. The lignin removal in the lactic acid/betaine (5:1) was 38 %. Alvarez-Vasco *et al*. (2016) used ChCl based DESs for lignin extraction from Douglas-fir and poplar wood. The lignin amounts removed from biomass with ChCl/lactic acid treatment were 78 % in poplar and 58 % in Douglas-fir. The isolation of willow lignin with the treatment of DESs (ChCl/lactic acid, ChCl/urea, ChCl/glycerol) was evaluated by Li *et al*. (2017). Optimal DES-lignin yield (91.8 %) was obtained at a ChCl/lactic acid molar ratio of 1:10, extraction time of 12 h, and temperature of 120 °C. Pan *et al*. (2017) focused on the effects of DES (ChCl/urea) pretreatment on holocellulose, α-cellulose, and acid-insoluble-lignin contents of rice straw. They observed that ChCl/urea had a selective delignification. Lynam *et al*. (2017) noted that DESs (lactic acid/betaine, lactic acid/ChCl, lactic acid/proline, formic acid/ChCl, and acetic acid/ChCl) were capable of selectively dissolving the lignin at 60 °C. Zulkefli *et al*. (2017) noted that the pretreatment of oil palm trunk with ethylammonium chloride/EG had removed 42 % lignin and 83 % hemicellulose. Hou *et al*. (2018) also reported that DES consisting of ChCl/urea could effectively delignify from the rice straw. Chen and Wan (2018) noted that lignin was recoverable with high purity after microwave-assisted DES pretreatment of Miscanthus, switchgrass, and corn stover. Kiliç-Pekgözlü and Ceylan (2019) extracted the Scots pine wood with several DESs. They found that DESs could be alternative solvents for organic solvents. Recently, the effects of DESs (ChCl/lactic acid and ChCl/glycerin) treatment on the chemical composition of the sapwood and heartwood of red pine were investigated by Kwon *et al*. (2020). They observed that the solid residue yield after DES treatment decreased with increasing HBD concentration and treatment time. In addition, the solid residue amount in the sapwood was higher compared to the heartwood.

DESs have potential applications in the pulp and paper industry. Choi *et al*. (2016a and 2016b, respectively) investigated the effects of DES treatment of thermomechanical pulp (TMP) and bleached chemithermomechanical pulp (BCTMP) on handsheet properties. Majová *et al*. (2017a) reported the effect of initial kappa number of kraft pulp on the DES pulp delignification efficiency, and determined that kraft pulp having higher kappa number was more easily delignified with DES. A recent study found that DES could be replaced by oxygen in kraft pulp delignifica-

tion (Majová *et al*., 2017b). The hardwood kraft pulp was delignified using two different DESs (ChCl/lactic acid and alanine/lactic acid) and the effects of DES delignification on the chemical and physical properties of the kraft pulp were investigated (Jablonsky *et al*., 2018). The potential of potassium carbonate/glycerol (K_2CO_3/Gly) DES applied as a green solvent in rice straw pulping was evaluated by Lim *et al*. (2019). Smink *et al*. (2019) investigated the effect of ChCl on the pulping of *Eucalyptus globulus* chips. Rapeseed stems, corn stalks, and wheat straw were treated with acidic and alkaline DESs and the effect of DES type on nanocelluloses properties and on the resulting nanopapers was investigated by Suopajärvi *et al*. (2020). Recently, the effect of ChCl based DES treatment on the chemical composition of the low-energy mechanical pulp was reported by Fiskari *et al*. (2020).

Although several DESs have been extensively studied for pretreating biomass, the literature available regarding the use of DESs in pulp production is limited. To the best of our knowledge, to date, no investigation has been carried out comparing DES pulp production with traditional pulping methods. Therefore, the aim of this study was to evaluate the usage possibilities of a DES (ChCl:EG) in pulp production from poplar wood and to compare DES pulping with traditional pulping methods. The effects of different ChCl:EG molar ratios (4:10, 5:10, 6:10) were also investigated in this study.

2 MATERIALS AND METHODS
2. MATERIJALI I METODE

2.1 Material
2.1. Materijal

European black poplar (*Populus nigra* L.) was chosen as the wood material because it has a rapid growth rate and provides easier delignification compared to softwoods. A 10 cm-thick wood disc was taken at breast height from a poplar log originating from Bartın Province (Turkey). This disc was debarked and subdivided into four discs (25 mm-thick). These were manually chipped, using a chisel, as homogeneously as possible to 25 mm × 15 mm × 5 mm in size for pulping.

2.2 Chemical composition and fiber morphology of poplar wood
2.2. Kemijski sastav i morfologija vlakana topolovine

The chemical analysis of poplar wood was carried out according to TAPPI T 257 cm-02. The klason lignin content (TAPPI T 222 om-02), α-cellulose content (TAPPI T 203 cm-09), and holocellulose content (Wise and Karl, 1962) of the poplar wood were determined according to the relevant methods. The cold-hot water, ethanol, and 1 % NaOH solubilities of the poplar were also determined according to TAPPI T 207 cm-99, TAPPI T 204 cm-97, and TAPPI T 212 om-02, respectively. In addition, poplar wood chips were macerated with the chlorite method (Spearin and Isenberg, 1947). After maceration, the fiber length (L) and width (D), lumen width (d), and cell wall thickness (w) of fibers were measured. The slenderness ratio (L/D), flexibility ratio [$(d/D) \times 100$], and Runkel ratio [$(2 \times w)/d$] were calculated from the dimensional measurements of fibers.

2.3 DES preparation
2.3. Priprema DES-a

DES was prepared by mixing ChCl with EG. All chemicals were acquired commercially (Merck) and used as received. The ChCl and EG were mixed in different mole ratios (4:10, 5:10, and 6:10) and used as DES. The solution was heated at 100 °C for 60 min. until a transparent liquid retaining no solid particles was formed. The mixture was stored in a desiccator until use after being cooled to room temperature.

2.4 DES and traditional pulping
2.4. DES i tradicionalna proizvodnja celuloze

DES and traditional pulping conditions are shown in Table 1. In DES cookings, the oven-dried (o.d.) poplar chip weight was calculated for each cooking experiment using the ChCl/EG molar ratio and cooking liquor/chip ratio. In DES-1 (4ChCl/10EG), 558.48 g ChCl (ChCl molecular weight × 4) and 620.7 g EG (EG molecular weight × 10) were used. The total weight of ChCl and EG was 1179.18 g. The o.d. poplar chip weight in the 2.5/1 cooking liquor/chip was 471.73 g (1179.18/2.5). According to the same calculation, 527.52 g and 583.37 g o.d. poplar chips were used in DES-2 (5ChCl/10EG) and DES-3 (6ChCl/10EG) cooking experiments, respectively (Table 1).

The air-dried poplar wood chips were cooked in a rotary digester. After cooking, the DES pulps and traditional pulps were washed to remove the black liquor with tap water. The DES pulps were also washed in ethanol. All pulps were disintegrated in a laboratory-type pulp mixer with 2-L capacity. The pulps were screened with a Somerville-type pulp screen according to TAPPI T 275 sp-02. After screening, all the pulp samples were beaten to 25 °SR and 35 °SR in a Valley Beater according to TAPPI T 200 sp-15.

2.5 Pulp and paper properties
2.5. Svojstva celuloze i papira

The screened yield (TAPPI T 210 cm-02), kappa number (TAPPI T 236 om-99), viscosity (SCAN-CM 15-62), and freeness of the pulps (ISO 5267-1) were determined. The handsheets (75 g/m^2) were made by a Rapid-Kothen Sheet Former (ISO 5269- 2) at three different freeness levels (unbeaten, 25 °SR, and 35 °SR).

Table 1 DES and traditional pulping conditions
Tablica 1. DES i tradicionalni uvjeti proizvodnje celuloze

Pulps *Celuloza*	**ChCl/EG mole ratios in cooking** *ChCl/EG molarni omjer pri kuhanju*	**Active alkali** *Aktivna lužina*	**Sulfidity** *Sulfidnost*	**Wood weight in cooking, o.d.** *Masa drva pri kuhanju,* o.d.	**Liquor/wood ratio** *Omjer tekućina/drvo*	**Cooking time to max. temp., min** *Vrijeme kuhanja do najviše temperature,* min	**Cooking time at max. temp., min** *Vrijeme kuhanja pri najvišoj temperaturi,* min	**Cooking temp., °C** *Temperatura kuhanja,* °C
DES-1	4ChCl/10EG	-	-	471.67	2.5/1	60	150	190
DES-2	5ChCl/10EG	-	-	527.52	2.5/1	60	150	190
DES-3	6ChCl/10EG	-	-	583.37	2.5/1	60	150	190
Soda	-	18	-	700	4/1	60	60	170
Kraft	-	16	20	700	4/1	60	60	170

Table 2 Chemical composition and fiber morphology of poplar wood
Tablica 2. Kemijski sastav i morfologija vlakana topolovine

Experiments / *Eksperimenti*	***Populus nigra***	***Populus tremula*** **(Gulsoy and Tufek, 2013)**
Holocellulose, % / *Holoceluloza,* %	81.25	82.68
α-cellulose, %	46.30	49.03
Klason lignin, %	18.51	16.69
Ethanol solubility, % / *Topljivost u etanolu*, %	2.22	3.22
1 % NaOH solubility, % / *Topljivost u 1-postotnom NaOH,* %	14.65	15.34
Hot water solubility, % / *Topljivost u vrućoj vodi,* %	3.59	3.04
Cold water solubility, % / *Topljivost u hladnoj vodi,* %	2.18	1.73
Fiber length, mm / *Duljina vlakana,* mm	1.05	1.10
Fiber width, µm / *Širina vlakana,* µm	27.47	23.90
Lumen width, µm / *Širina lumena,* µm	15.53	11.40
Cell wall thickness, µm / *Debljina stanične stijenke,* µm	5.97	6.30
Slenderness ratio / *Omjer vitkosti*	38.22	46.00
Flexibility ratio / *Omjer fleksibilnosti*	56.53	47.70
Runkel ratio / *Runkelov omjer*	0.77	1.10

After conditioning in accordance with TAPPI T 402 sp-03, the tensile index, stretch, and tensile energy absorption (TEA) (ISO 1924-3), tear index (TAPPI T 414 om-98), burst index (TAPPI T 403 om-02), opacity (TAPPI T 519 om-02), and brightness (TAPPI T 525 om-02) of the handsheets were determined.

2.6 Statistical analysis
2.6. Statistička analiza

The data related to properties of the DES, kraft, and soda pulps from poplar chips were analyzed using analysis of variance (ANOVA) and the Duncan test at a 95 % confidence level (p <0.05). The effects of the methods and conditions of pulping on the paper properties were evaluated statistically using SPSS software. In Figures 2-8, the same letters on the columns denote no statistically significant differences between the groups. In addition, there were no significant differences among the values with the same letters in the same column of Table 3 and Table 4.

3 RESULTS AND DISCUSSION
3. REZULTATI I RASPRAVA

The results of the chemical composition analysis and fiber morphology of the *Populus nigra* wood are presented in Table 2. These results are similar to those of *Populus tremula*.

The pulp properties of DES, soda, and kraft pulps are presented in Table 3. The screened yield of the DES pulps was higher than that of the soda and kraft pulps. The highest screened yield was obtained from DES-3 pulp. The screened yields of the DES pulps after washing with ethanol were similar to those of the traditional pulps (Table 3).

The effect of ChCl molar ratio on kappa number of DES pulp was insignificant (p >0.05). The kappa numbers of DES pulps were higher than for the traditional pulps (p <0.05). This result can be ascribed to the insufficient delignification of DES pulping compared to the traditional pulping methods. Alvarez-Vas-

Table 3 Pulp properties of DES, soda, and kraft pulps
Tablica 3. Svojstva DES celuloze, natronske i kraft celuloze

Pulps *Celuloza*	**Screened yield, %** *Prinos prosijavanja, %*	**Reject, %** *Škart, %*	**Total yield, %** *Ukupan prinos, %*	**Weight loss at washing, %** *Gubitak mase pri ispiranju, %*	**Screened yield after washing, %** *Prinos prosijavanja nakon ispiranja, %*	**Total yield after washing, %** *Ukupan prinos nakon ispiranja, %*	**Kappa number** *Kappa broj*	**Viscosity, cm^3/g** *Viskoznost,* cm^3/g
DES-1	52.02	9.27	61.29	14.29	44.59	53.86	72.55a*	1154a
DES-2	49.07	2.47	51.54	14.65	41.88	44.35	69.52a	1170a
DES-3	52.78	5.46	58.24	17.22	43.69	49.15	70.47a	1199a
Soda	40.65	7.81	48.46	-	-	-	37.40b	1126a
Kraft	46.42	17.31	63.73	-	-	-	41.08b	1185a

*There were no significant differences among the values with the same letters in the same column. / *Nema značajnih razlika između vrijednosti s istim slovom unutar istog stupca.*

co *et al*. (2016) reported that DESs can selectively cleave ether bonds without affecting the C-C linkages in lignin and can facilitate lignin extraction from wood fibers. Choi *et al*. (2016a) treated thermomechanical pulp (TMP) with DES (lactic acid and betaine) and identified a linear correlation between the delignification of the TMP and the molar ratio of lactic acid in DES. Yiin *et al*. (2016) noted that the lignin solubility capacity of DES was improved with the increased molar ratio of HBA. Majová *et al*. (2017a) noted that the kappa number of kraft pulp decreased from 21.7 to 12.3 with alanine/lactic acid treatment. Jablonsky *et al*. (2018) reported that the kappa number of untreated hardwood kraft pulp was reduced from 21.7 to 13.5 with ChCl/lactic acid treatment and to 12.3 with alanine/ lactic acid treatment. Lim *et al*. (2019) found that the lignin content in rice straw significantly decreased after DES (K_2CO_3/Gly) pulping. Fiskari *et al*. (2020) stated that DESs consisting of ChCl/lactic acid, ChCl/urea, and ChCl/ oxalic acid reduced the lignin content of Asplund fibers by approximately 50 %. On the other hand, the viscosity of the DES, soda, and kraft pulps had similar values (p >0.05). Majová *et al*. (2017a) reported that the viscosity of kraft pulp decreased slightly, from 789 to 784 ml/g, with alanine/ lactic acid treatment.

Pulp refinability (beatability) is a significant parameter in terms of energy consumption of a pulp mill and usually depends on the chemical composition of the pulps (Gulsoy and Eroglu, 2011). Pulp beating consumes up to 15-18 % of the total electric energy used for paper production (Bajpai *et al*., 2006; Cui *et al*., 2015). Therefore, the pulp should reach the desired freeness level as soon as possible. DES pulps easily reached 25 ºSR and 35 ºSR freeness levels despite their higher kappa numbers (Table 3, Figure 1). DES-2 pulp reached 25 ºSR in 240 s., whereas soda pulp reached the same freeness level in 660 s. DES-1 pulp and soda pulp reached 35 ºSR in 420 s and 900 s, respectively.

The tensile index of the unbeaten and beaten DES pulps was significantly lower (p <0.05) than that of the traditional pulps (Figure 2). In the unbeaten, 25

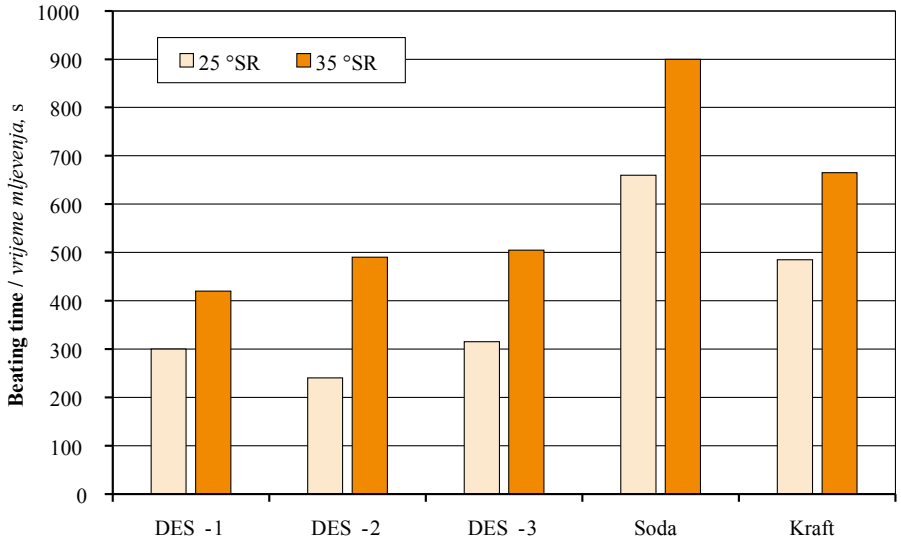

Figure 1 Beating time required for a given freeness level of DES, soda, and kraft pulps
Slika 1. Vrijeme mljevenja potrebno za dani stupanj slobode DES celuloze, natronske i kraft celuloze

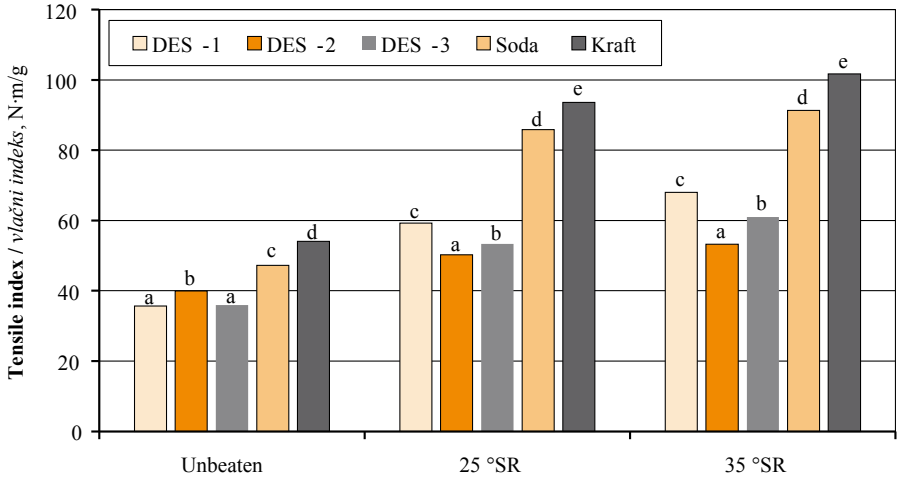

Figure 2 Tensile index of DES, soda, and kraft pulps (The same letters on the columns denote no statistically significant differences between the groups)
Slika 2. Vlačni indeks DES celuloze, natronske i kraft celuloze (ista slova iznad stupaca znače da nema statistički značajne razlike među skupinama)

°SR and 35 °SR DES pulps, the highest tensile index was determined in DES-2, DES-1, and DES-1 pulps as 39.94, 59.24, and 68.02 N·m/g, respectively. The highest tensile index values in the unbeaten, 25 °SR and 35 °SR DES pulps compared to the soda and kraft pulps, respectively, were lower by 15.42 % and 26.17% (unbeaten pulp), 30.98 % and 36.72 % (25 °SR pulp), and 25.47 % and 33.12 % (35 °SR pulp). At all pulp freeness levels, the highest tensile index values were obtained with kraft pulp. Moreover, the tensile index of the DES pulps was irregularly affected by the ChCl amount in the DES cooking liquor. The tensile index of the DES pulps was significantly increased with beating (p <0.05) (Table 4). However, the tensile index increases due to beating were a little more obvious in the traditional pulps. For example, the tensile index of DES-1 pulp was increased by 66.26 % and 90.91 % with beating to 25 °SR and 35 °SR, respectively. In the soda and kraft pulps, these values were 81.77 % & 93.29 % and 73.03 % & 87.99 %, respectively.

The stretch values of the unbeaten DES pulps were higher than those of the traditional pulps, whereas the stretch values of the beaten DES pulps were lower than those of the traditional pulps (Figure 3, p <0.05). In the unbeaten pulps, the highest and the lowest stretch values were obtained from DES-2 pulp and soda pulp as 1.37 % and 0.85 %, respectively. On the other hand, the stretch values of the unbeaten and 25 °SR DES pulps were irregularly affected by the ChCl amount in the DES cooking liquor. In the 35 °SR pulps, the effect on stretch of the ChCl amount in the DES cooking liquor was statistically insignificant (p >0.05). Stretch values of the DES pulps, as for the traditional pulps, were significantly increased with beating (p <0.05) (Table 4).

In the unbeaten pulps, the highest TEA value was 28.86 J/m^2 (DES-2 pulp). In the 25 °SR and 35 °SR

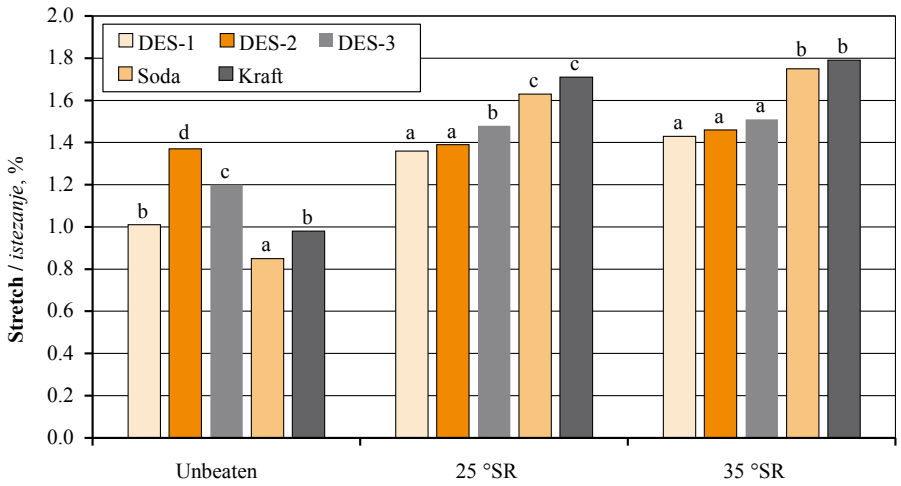

Figure 3 Stretch of DES, soda, and kraft pulps
Slika 3. Istezanje DES celuloze, natronske i kraft celuloze

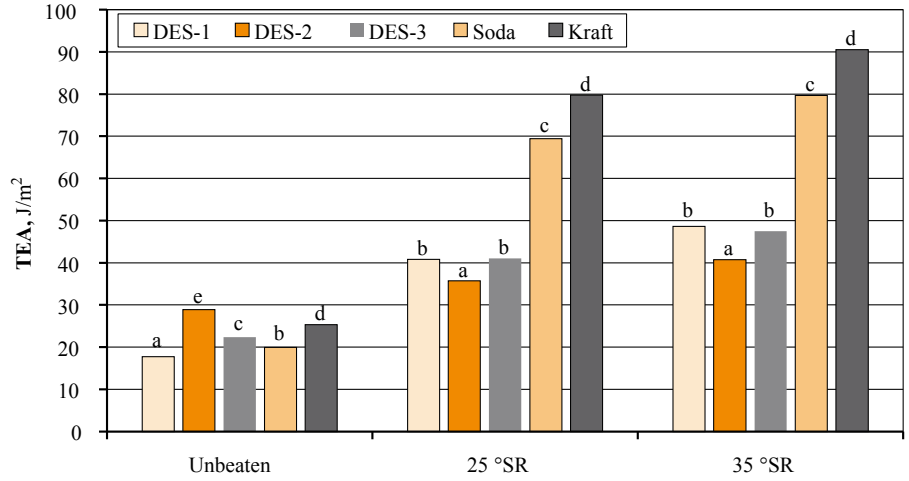

Figure 4 TEA of DES, soda, and kraft pulps
Slika 4. TEA za DES celulozu, natronsku i kraft celulozu

pulps, the stretch values of DES pulps were lower than those of soda and kraft pulps (Figure 4, p <0.05). Moreover, the TEA of DES pulps changed irregularly with the rising ChCl amount in the DES cooking liquor. The pulp beating had a positive effect on the TEA values of DES and traditional pulps (Table 4). However, the effect of beating on TEA was more pronounced in the traditional pulps.

In the unbeaten and beaten pulps, the tear index values of the DES pulps were lower than those of the soda and kraft pulps (p <0.05). The highest tear index values of the DES pulps were determined in DES-3 pulp samples. At all pulp freeness levels, the effect on the tear index of the ChCl amount in the DES cooking liquor was statistically insignificant (Figure 5, p >0.05). In terms of the tear index, the response of DES pulps to beating was different from that of traditional pulps. The tear index increased when the traditional pulps were beaten up to 25 °SR. With increasing beating levels, their tear index values decreased. In contrast, the tear index values of the DES pulps regularly decreased with increasing beating levels (Table 4).

The burst index values of the unbeaten samples of DES-2, soda, and kraft pulps were 1.54, 1.38, and 1.62 kPa·m^2/g. The burst index values of the DES pulps were lower than those of the soda and kraft pulps except for the unbeaten DES-2 pulp (Figure 6). The burst index values of the unbeaten and 35 °SR pulps varied irregularly with increasing ChCl amounts in the cooking liquor. However, the decrease in the burst index with increasing ChCl amount was insignificant (p >0.05). The relationship between the burst index of DES pulps and increasing pulp beating levels was linear (p <0.05) (Table 4). However, the tensile index increases after pulp beating were more pronounced in the traditional pulps. For example, the burst index of DES-1 pulp was increased by 71.09 % and 97.66 % with beating to 25 °SR and 35 °SR, respectively. The burst index increases with beating in the soda and kraft pulps were 152.17 and 181.16 % and 138.27 and 161.11 %, respectively.

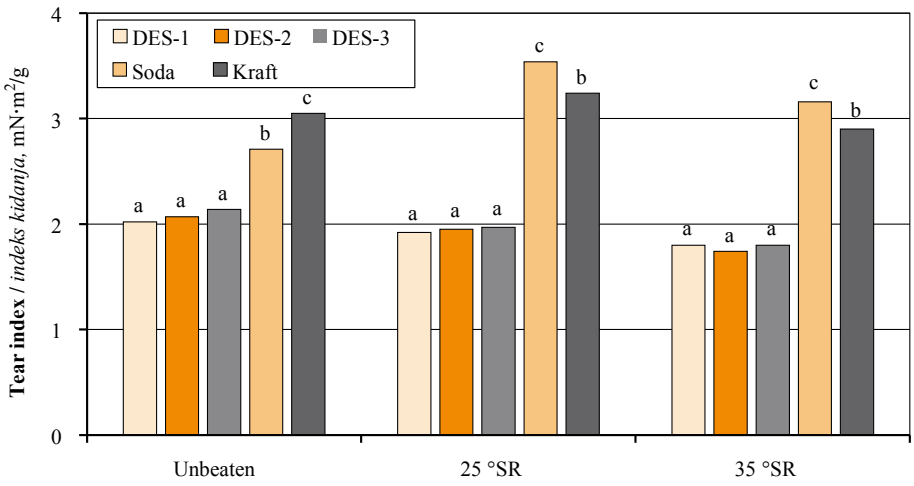

Figure 5 Tear index of DES, soda, and kraft pulps
Slika 5. Indeks kidanja DES celuloze, natronske i kraft celuloze

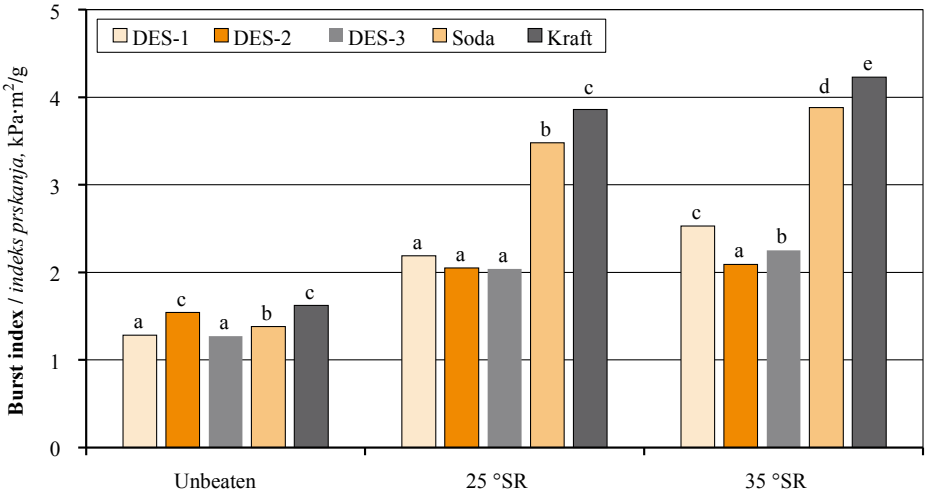

Figure 6 Burst index of DES, soda, and kraft pulps
Slika 6. Indeks prskanja DES celuloze, natronske i kraft celuloze

Choi *et al*. (2016a) reported that the burst and tensile indices of TMP pulps increased when a higher molar ratio of lactic acid was used in the DES preparation. The authors also reported that the tear index of TMP pulps was reduced with the increasing molar ratio of lactic acid in the DES. Jablonsky *et al*. (2018) noted that the burst, tensile, and tear indices of untreated hardwood kraft pulp decreased with ChCl/lactic acid and alanine/lactic acid treatment. Untreated Asplund fiber pulp had a higher or equal tensile index compared to DES-treated pulp at all pulp freeness levels (Fiskari *et al*., 2020). Suopajärvi *et al*. (2020) stated that nanopapers from alkaline DES-treated wheat straw, rapeseed stems, and corn stalks had better tensile strength and strain compared with nanopapers from acidic DESs.

At all pulp freeness levels, the DES pulp had lower brightness values compared to soda and kraft pulps (Figure 7) because of the higher kappa numbers and insufficient delignification of the DES pulps (Table 3). Pulp brightness was significantly reduced with the increase of ChCl in the DES (p <0.05). In addition, the brightness of DES-1 pulp was reduced with beating, whereas for DES-2 and DES-3 pulps, the changes were irregular (Table 4). As expected, the brightness of kraft and soda pulps was reduced with beating. This result can be explained by the homogeneous lignin distribution of the DES fibers in the cell walls.

In the unbeaten and beaten samples, the DES pulp exhibited higher opacity values compared to the soda and kraft pulps (Figure 8). The effect of the amount of ChCl in DES on pulp opacity was statistically insignificant (p >0.05). Although the opacity of the traditional pulps changed with beating (p <0.05), the opacity of the DES pulps did not change (p >0.05) (Table 4). This experiment demonstrated that, compared to traditional pulping methods, DES pulping had a negative effect on pulp brightness, although it had a positive effect on pulp opacity. Choi *et al*. (2016a) noted that lactic acid and betaine DES treatment had no effect on the optical properties of TMP pulp. An in-

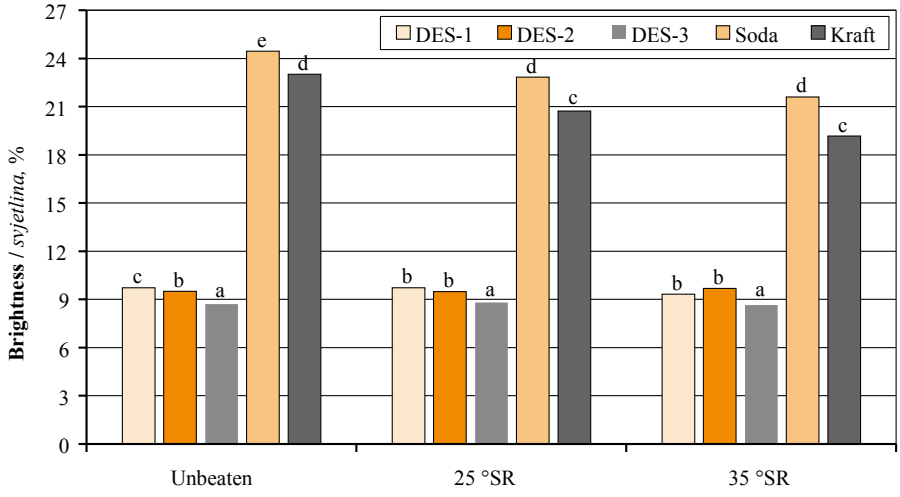

Figure 7 Brightness of DES, soda, and kraft pulps
Slika 7. Svjetlina DES celuloze, natronske i kraft celuloze

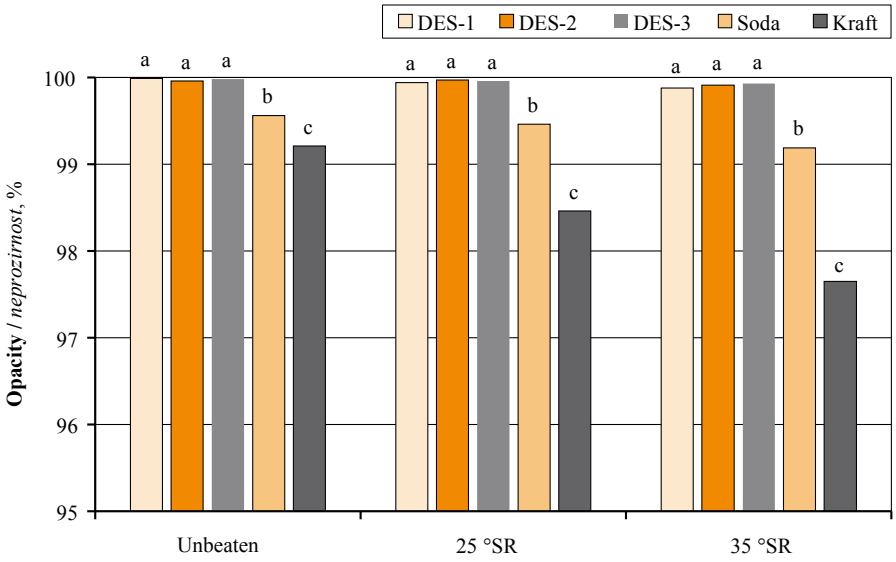

Figure 8 Opacity of DES, soda, and kraft pulps
Slika 8. Neprozirnost DES celuloze, natronske i kraft celuloze

crease in the brightness of kraft pulp was observed with DES treatment (Škulcová *et al*., 2017). Jablonsky *et al*. (2018) reported that the brightness of untreated hardwood kraft pulp increased from 27.02 to 34.05 with ChCl/lactic acid treatment and to 33.38 with alanine/lactic acid treatment.

4 CONCLUSIONS
4. ZAKLJUČAK

In this new century, sustainable development challenges pulp and paper industry to develop new and cleaner technological processes. DESs have potential applications in the pulp and paper industry. The novelty of this study is the utilization of DES in pulp production and comparison of traditional pulps and DES pulps. The results of this study showed that the use of DES was an effective method for the pulping of poplar lignocellulosic biomass (*Populus nigra* L.). The DES formed by ChCl and EG (molar ratios = 4:10, 5:10, 6:10) applied at 190 °C for 3.5 h enabled pulp production from poplar chips. The DES pulps were comparable to those produced by traditional pulping methods in terms of pulp yield, pulp viscosity, and opacity. The DES-1 pulp exhibited the best cooking conditions in terms of total pulp yield. On the other hand, the beata-

Table 4 Effect of beating level on handsheet properties of DES, soda, and kraft pulps
Tablica 4. Utjecaj stupnja mljevenja na svojstva ručno izrađenog papira od DES celuloze, natronske i kraft celuloze

Pulps *Celuloza*	**Freeness, °SR** *Stupanj slobode,* °SR	**Tensile index, N·m/g** *Vlačni indeks,* N·m/g	**Stretch, %** *Istezanje,* %	**TEA,** J/m²	**Tear index, mN·m²/g** *Indeks kidanja,* mN·m²/g	**Burst index, kPa·m²/g** *Indeks prskanja*	**Brightness, %** *Svjetlina,* %	**Opacity, %** *Neprozirnost,* %
DES-1	15	35.63a*	1.01a	17.76a	2.02a	1.28a	9.73a	99.99a
	26	59.24b	1.36b	40.79b	1.92a	2.19b	9.72a	99.94a
	37	68.02c	1.43b	48.60c	1.80b	2.53c	9.33b	99.88a
DES-2	17	39.94a	1.37a	28.86a	2.07a	1.54a	9.51a	99.96a
	25	50.26b	1.39a	35.69b	1.95a	2.05b	9.48a	99.97a
	35	53.28c	1.46a	40.69c	1.74b	2.09b	9.68b	99.91a
DES-3	16	35.91a	1.20a	22.36a	2.14a	1.27a	8.71a	99.98a
	25	53.33b	1.48b	41.00b	1.97b	2.04b	8.80a	99.96a
	35	61.02c	1.51b	47.47c	1.80c	2.25c	8.64a	99.93a
Soda	12	47.22a	0.85a	19.92a	2.71a	1.38a	24.46a	99.56a
	25	85.83b	1.63b	69.43b	3.54c	3.48b	22.84b	99.46a
	36	91.27c	1.75b	79.66c	3.16b	3.88c	21.61c	99.19b
Kraft	12	54.10a	0.98a	25.34a	3.05a	1.62a	23.03a	99.21a
	24	93.61b	1.71b	79.70b	3.24c	3.86b	20.73b	98.46b
	35	101.70c	1.79b	90.50c	2.90b	4.23c	19.16c	97.65c

*There were no significant differences among the values with the same letters in the same column. / *Nema značajnih razlika među vrijednostima s istim slovom unutar istog stupca.*

bility of the pulp was positively affected by the DES pulping. However, the strength properties and brightness of the DES pulps were lower than those of the traditional pulps. In the unbeaten and beaten DES pulps, the highest strength values were obtained from the DES-2 and DES-1 pulps.

This study demonstrated that DES composed of ChCl and EG can be used as green solvent for pulp production from biomass. It can be readily applicable to pulp production. The DES pulping process is an alternative to traditional pulping due to its low-environmental-impact. Inexpensive and biodegradable DESs, used in pulping, are characterized as economically and environmentally viable solvents. These solvents could offer unique opportunities for cleaner pulp production. Therefore, in order to reveal true potential of DESs and to improve pulp properties, further research is needed on the use of DESs as green solvents in pulping.

Acknowledgements – Zahvala

The authors thank the Scientific Research Fund of Bartın University for its financial support (Project Number: 2017-FEN-CY-011).

5 REFERENCES
5. LITERATURA

1. Abougor, H., 2014: Utilization of deep eutectic solvent as a pretreatment option for lignocellulosic biomass. PhD Thesis, Tennessee Technological University.
2. Alriols, M. G.; Tejado, A.; Blanco, M.; Mondragon, I.; Labidi, J., 2009: Agricultural palm oil tree residues as raw material for cellulose, lignin and hemicelluloses production by ethylene glycol pulping process. Chemical Engineering Journal, 148: 106-114. https://doi.org/10.1016/j.cej.2008.08.008
3. Alvarez-Vasco, C.; Ma, R.; Quintero, M.; Guo, M.; Geleynse, S.; Ramasamy, K. K.; Wolcott, M.; Zhang, X., 2016: Unique low-molecular-weight lignin with high purity extracted from wood by deep eutectic solvents (DES): A source of lignin for valorization. Green Chemistry, 18 (19): 5133-5141. https://doi.org/10.1039/C6GC01007E
4. Bajpai, P.; Mishra, S. P.; Mishra, O. P.; Kumar, S.; Bajpai, P. K., 2006: Use of enzymes for reduction in refining energy-laboratory studies. TAPPI Journal, 5: 25-31.
5. Chen, Z.; Wan, C., 2018: Ultrafast fractionation of lignocellulosic biomass by microwave-assisted deep eutectic solvent pretreatment. Bioresource Technology, 250: 532-537. https://doi.org/10.1016/j.biortech.2017.11.066
6. Chen, Y.; Zhang, L.; Yu, J.; Lu, Y.; Jiang, B.; Fan, Y.; Wang, Z., 2019: High-purity lignin isolated from poplar wood meal through dissolving treatment with deep eutectic solvents. Royal Society Open Science, 6: 181757. https://doi.org/10.1098/rsos.181757
7. Choi, K. H.; Lee, M. K.; Ryu, J. Y., 2016a: Effect of molar ratios of DES on lignin contents and handsheets properties of thermomechanical pulp. Journal of Korea TAPPI, 48: 28-33. https://doi.org/10.7584/ktappi.2016.48.2.028
8. Choi, K. H.; Nam, Y. S.; Lee, M. K.; Ryu, J. Y., 2016b: Changes of BCTMP fibers and handsheets properties by the treatment of LB DES at different molar ratios. Journal of Korea TAPPI, 48: 75-81. https://doi.org/10.7584/ktappi.2016.48.1.075
9. Cui, L.; Meddeb-Mouelhi, F.; Laframboise, F.; Beauregard, M., 2015: Effect of commercial cellulases and refining on kraft pulp properties: Correlations between treatment impacts and enzymatic activity components. Carbohydrate Polymers, 115: 193-199. https://doi.org/10.1016/j.carbpol.2014.08.076
10. De Dios, S. L. G., 2013: Phase equilibria for extraction processes with designer solvents. PhD Thesis, University of Santiago De Compostela.
11. Francisco, M.; van den Bruinhorst, A.; Kroon, M. C., 2012: New natural and renewable low transition temperature mixtures (LTTMs): screening as solvents for lignocellulosic biomass processing. Green Chemistry, 14: 2153-2157. https://doi.org/10.1039/C2GC35660K
12. Fiskari, J.; Ferritsius, R.; Osong, S. H.; Persson, A.; Höglund, T.; Immerzeel, P.; Norgren, M., 2020: Deep eutectic solvent delignification to low-energy mechanical pulp to produce papermaking fibers. BioResources, 15: 6023-6032.
13. Gast, D.; Puls, J., 1984: Ethylene glycol-water pulping. Kinetics of delignification, in: Ferrero, G. L. (ed.), Anaerobic Digestion and Carbohydrate Hydrolysis of Waste. Elsevier, Essex, pp. 450-453.
14. Gulsoy, S. K.; Eroglu, H., 2011: Influence of sodium borohydride on kraft pulping of European black pine as a digester additive. Industrial & Engineering Chemistry Research, 50: 2441-2444. https://doi.org/10.1021/ie101999p
15. Gulsoy, S. K.; Tufek, S., 2013: Effect of chip mixing ratio of *Pinus pinaster* and *Populus tremula* on kraft pulp and paper properties. Industrial & Engineering Chemistry Research, 52(6): 2304-2308. https://doi.org/10.1021/ie302709e
16. Hou, X. D.; Li, A. L.; Lin, K. P.; Wang, Y. Y.; Kuang, Z. Y.; Cao, S. L., 2018: Insight into the structure-function relationships of deep eutectic solvents during rice straw pretreatment. Bioresource Technology, 249: 261-267. https://doi.org/10.1016/j.biortech.2017.10.019
17. Jablonský, M.; Škulcová, A.; Kamenská, L.; Vrška, M.; Šima, J., 2015: Deep eutectic solvents: fractionation of wheat straw. BioResources, 10: 8039-8047.
18. Jablonsky, M.; Majova, V.; Skulcova, A.; Haz, A., 2018: Delignification of pulp using deep eutectic solvents. Journal of Hygienic Engineering and Design, 22: 76-81.
19. Jablonsky, M.; Haz, A.; Majova, V., 2019: Assessing the opportunities for applying deep eutectic solvents for fractionation of beech wood and wheat straw. Cellulose, 26: 7675-7684. https://doi.org/10.1007/s10570-019-02629-0
20. Jiménez, L.; Rodríguez, A.; Díaz, M. J.; Lopez, F.; Ariza, J., 2004: Organosolv pulping of olive tree trimmings by use of ethylene glycol/soda/water mixtures. Holzforschung, 58: 122-128. https://doi.org/10.1515/HF.2004.017
21. Jiménez, L.; Perez, A.; De la Torre, M. J.; Rodríguez, A.; Angulo, V., 2008: Ethyleneglycol pulp from tagasaste. Bioresource Technology, 99: 2170-2176. https://doi.org/10.1016/j.biortech.2007.05.044
22. Jiménez, L.; Angulo, V.; Rodríguez, A.; Sánchez, R.; Ferrer, A., 2009: Pulp and paper from vine shoots: Neural fuzzy modeling of ethylene glycol pulping. Bioresource Technology, 100: 756-762. https://doi.org/10.1016/j.biortech.2008.07.019
23. Kiliç-Pekgözlü, A.; Ceylan, E., 2019: Application of DES (deep eutectic solvents) to wood extractives. Wood Industry and Engineering, 1: 52-56.

24. Kumar, A. K.; Parikh, B. S.; Pravakar, M., 2016: Natural deep eutectic solvent mediated pretreatment of rice straw: bioanalytical characterization of lignin extract and enzymatic hydrolysis of pretreated biomass residue. Environmental Science and Pollution Research, 23: 9265-9275. https://doi.org/10.1007/s11356-015-4780-4
25. Kwon, G. J.; Yang, B. S.; Park, C. W.; Bandi, R.; Lee, E. A.; Park, J. S.; Han, S. Y.; Kim, N. H.; Lee, S. H., 2020: Treatment effects of choline chloride-based deep eutectic solvent on the chemical composition of red pine (*Pinus densiflora*). BioResources, 15: 6457-6470.
26. Li, T.; Lyu, G.; Liu, Y.; Lou, R.; Lucia, L. A.; Yang, G.; Chen, J.; Saeed, H. A. M., 2017: Deep eutectic solvents (DESs) for the isolation of willow lignin (*Salix matsudana* cv. Zhuliu). International Journal of Molecular Sciences, 18: 2266. https://doi.org/10.3390/ijms18112266
27. Lim, W. L.; Gunny, A. A. N.; Kasim, F. H.; AlNashef, I. M.; Arbain, D., 2019: Alkaline deep eutectic solvent: a novel green solvent for lignocellulose pulping. Cellulose, 26: 4085-4098. https://doi.org/10.1007/s10570-019-02346-8
28. Lynam, J. G.; Kumar, N.; Wong, M. J., 2017: Deep eutectic solvents' ability to solubilize lignin, cellulose, and hemicellulose; thermal stability; and density. Bioresource Technology, 238: 684-689. https://doi.org/10.1016/j.biortech.2017.04.079
29. Majová, V.; Horanová, S.; Škulcová, A.; Šíma, J.; Jablonský, M., 2017a: Deep eutectic solvent delignification: Impact of initial lignin. BioResources, 12: 7301-7310.
30. Majová, V.; Jablonský, M.; Strizincová, P.; Škulcová, A.; Vrška, M., 2017b: Replacement of oxygen delignification by use of deep eutectic solvents. FP1306 COST Action, Third Workshop & Fourth MC Meeting, Torremolinos, 27-28 March 2017, P28.
31. Muurinen, E., 2000: Organosolv pulping: A review and distillation study related to peroxyacid pulping. PhD Thesis, University of Oulu.
32. Nakamura, H.; Takauti, E., 1941: Zellstoffherstellung mittels aethylenglykol. Cellulose Industry, 17: 19-26. https://doi.org/10.2115/fiber1925.17.en19
33. Oh, Y.; Park, S.; Jung, D.; Oh, K. K.; Lee, S. H., 2020: Effect of hydrogen bond donor on the choline chloride-based deep eutectic solvent-mediated extraction of lignin from pine wood. International Journal of Biological Macromolecules, 165: 187-197. https://doi.org/10.1016/j.ijbiomac.2020.09.145
34. Pan, M.; Zhao, G.; Ding, C.; Wu, B.; Lian, Z.; Lian, H., 2017: Physicochemical transformation of rice straw after pretreatment with a deep eutectic solvent of choline chloride/urea. Carbohydrate Polymers, 176: 307-314. https://doi.org/10.1016/j.carbpol.2017.08.088
35. Pena□Pereira, F.; Namieśnik, J., 2014: Ionic liquids and deep eutectic mixtures: sustainable solvents for extraction processes. ChemSusChem, 7: 1784-1800. https://doi.org/10.1002/cssc.201301192
36. Rodríguez, A.; Pérez, A.; de la Torre, M. J.; Ramos, E.; Jiménez, L., 2008: Neural fuzzy model applied to ethylene-glycol pulping of non-wood raw materials. Bioresource Technology, 99: 965-974. https://doi.org/10.1016/j.biortech.2007.03.007
37. Rutkowski, J.; Mroz, W.; Surna-Slusarsaka, B.; Perlinskasipa, K., 1993: Glycolic delignification of hardwood. In: Progress 93 Conference Proceeding, 1: 190-205.
38. Saberikhah, E.; Mohammadi Rovshandeh, J.; Rezayati-Charan, P., 2011: Organosolv pulping of wheat straw by glycerol. Cellulose Chemistry and Technology, 45: 67-75.
39. Smink, D.; Juan, A.; Schuur, B.; Kersten, S. R., 2019: Understanding the role of choline chloride in deep eutectic solvents used for biomass delignification. Industrial & Engineering Chemistry Research, 58: 16348-16357. https://doi.org/10.1021/acs.iecr.9b03588
40. Soto-Salcido, L. A.; Anugwom, I.; Ballinas-Casarrubias, L.; Mänttäri, M.; Kallioinen, M., 2020: NADES-based fractionation of biomass to produce raw material for the preparation of cellulose acetates. Cellulose, 27: 6831-6848. https://doi.org/10.1007/s10570-020-03251-1
41. Spearin, W. E.; Isenberg, I. H. 1947: Maceration of woody tissue with acetic acid and sodium chlorite. Science, 105: 214-214. https://doi.org/10.1126/science.105.2721.214
42. Suopajärvi, T.; Ricci, P.; Karvonen, V.; Ottolina, G.; Liimatainen, H., 2020: Acidic and alkaline deep eutectic solvents in delignification and nanofibrillation of corn stalk, wheat straw, and rapeseed stem residues. Industrial Crops and Products, 145: 111956. https://doi.org/10.1016/j.indcrop.2019.111956
43. Škulcová, A.; Kamenská, L.; Kalman, F.; Ház, A.; Jablonský, M.; Čížová, K.; Šurina, I., 2016: Deep eutectic solvents as medium for pretreatment of biomass. Key Engineering Materials, 688: 17-24. https://doi.org/10.4028/www.scientific.net/KEM.688.17
44. Škulcová, A.; Majová, V.; Šima, J.; Jablonský, M., 2017: Mechanical properties of pulp delignified by deep eutectic solvents. BioResources, 12: 7479-7486.
45. Uraki, Y.; Sano, Y., 1999: Polyhydric alcohol pulping at atmospheric pressure: An effective method for organosolv pulping of softwoods. Holzforschung, 53: 411-415. https://doi.org/10.1515/HF.1999.068
46. Wise, L. E.; Karl, H. L., 1962: Cellulose and Hemicellulose in Pulp and Paper Science and Technology. McGraw Hill Book Co., New York.
47. Yiin, C. L.; Quitain, A. T.; Yusup, S.; Sasaki, M.; Uemura, Y.; Kida, T., 2016: Characterization of natural low transition temperature mixtures (LTTMs): Green solvents for biomass delignification. Bioresource Technology, 119: 258-264. https://doi.org/10.1016/j.biortech.2015.07.103
48. Zhang, Q.; Vigier, K. D. O.; Royer, S.; Jerome, F., 2012: Deep eutectic solvents: Syntheses, properties and applications. Chemical Society Reviews, 41: 7108-7146. https://doi.org/10.1039/C2CS35178A
49. Zulkefli, S.; Abdulmalek, E.; Rahman, M. B. A., 2017: Pretreatment of oil palm trunk in deep eutectic solvent and optimization of enzymatic hydrolysis of pretreated oil palm trunk. Renew. Energy, 107: 36-41. https://doi.org/10.1016/j.renene.2017.01.037
50. ***ISO 1924-3, 2005: Paper and board – Determination of tensile properties. Part 3: Constant rate of elongation method (100 mm/min). ISO, Geneva, Switzerland.
51. ***ISO 5267-1, 1999: Pulps – Determination of drainability. Part 1: Schopper-Riegler method. ISO, Geneva, Switzerland.
52. ***ISO 5269-2, 2004: Pulps – Preparation of laboratory sheets for physical testing. Part 2: Rapid-Köthen method. ISO, Geneva, Switzerland.
53. ***SCAN-CM 15-62, 1962: Viscosity of cellulose in cupriethylenediamine solution (CED). SCAN, Stockholm, Sweden.
54. ***TAPPI T 200 sp-15, 2015: Laboratory Beating of Pulp (Valley Beater Method). TAPPI, Atlanta, GA, USA.
55. ***TAPPI T 203 cm-09, 2009: Alpha-, beta- and gamma-cellulose in pulp. TAPPI, Atlanta, GA, USA.

56. ***TAPPI T 204 cm-97, 1997: Solvent extractives of wood and pulp. TAPPI, Atlanta, GA, USA.
57. ***TAPPI T 207 cm-99, 1999: Water solubility of wood and pulp. TAPPI, Atlanta, GA, USA.
58. ***TAPPI T 210 cm-03, 2003: Sampling and testing wood pulp shipments for moisture. TAPPI, Atlanta, GA, USA.
59. ***TAPPI T 212 om-02, 2002: One percent sodium hydroxide solubility of wood and pulp. TAPPI, Atlanta, GA, USA.
60. ***TAPPI T 222 om-02, 2002: Acid-insoluble lignin in wood and pulp. TAPPI, Atlanta, GA, USA.
61. ***TAPPI T 236 om-99, 1999: Kappa number of pulp. TAPPI, Atlanta, GA, USA.
62. ***TAPPI T 257 cm-02, 2002: Sampling and preparing wood for analysis. TAPPI, Atlanta, GA, USA.
63. ***TAPPI T 275 sp-02, 2002: Screening of pulp (Somerville-type equipment). TAPPI, Atlanta, GA, USA.
64. ***TAPPI T 402 sp-03, 2003: Standard conditioning and testing atmospheres for paper, board, pulp handsheets, and related products. TAPPI, Atlanta, GA, USA.
65. ***TAPPI T 403 om-15, 2015: Bursting strength of paper. TAPPI, Atlanta, GA, USA.
66. ***TAPPI T 414 om-98, 1998: Internal tearing resistance of paper (Elmendorf-type method). TAPPI. Atlanta, GA, USA.
67. ***TAPPI T 519 om-02, 2002: Diffuse opacity of pulp. TAPPI, Atlanta, GA, USA.
68. ***TAPPI T 525 om-02, 2002: Diffuse brightness of pulp. TAPPI, Atlanta, GA, USA.

Corresponding address:

Assoc. Prof. SEZGIN KORAY GÜLSOY
Bartin University, Forestry Faculty, 74100, Bartin, TURKEY, e-mail: sgulsoy@bartin.edu.tr

Zoran Vlaović, Marko Jaković, Danijela Domljan[1]

Smart Office Chairs with Sensors for Detecting Sitting Positions and Sitting Habits: A Review

Pametne uredske stolice sa senzorima za otkrivanje položaja i navika sjedenja – pregled literature

REVIEW PAPER
Pregledni rad
Received – prispjelo: 13. 12. 2021.
Accepted – prihvaćeno: 23. 3. 2022.
UDK: 630*83; 686.87
https://doi.org/10.5552/drvind.2022.0002

ABSTRACT • *The health consequences of prolonged sitting in the office and other work chairs have recently been tried to be alleviated or prevented by the application of modern technologies. Smart technologies and sensors are installed in different parts of office chairs, which enables monitoring of seating patterns and prevents positions that potentially endanger the health of users. The aim of this paper is to provide an overview of previous research in the field of the application of smart technologies and sensors built into office and other types of chairs in order to prevent diseases. The articles published in the period 2010-2020 and indexed in WoS CC, Scopus, and IEEE Xplore databases, with the keywords "smart chair" and "sensor chair" were analysed. 15 articles were processed, with their research being based on the use of different types of sensors that determine the contact pressures between the user's body and stool parts and recognise different body positions when sitting, which can prevent negative health consequences. Analysed papers prove that the use of smart technology and a better understanding of sitting, using various sensors and applications that read body pressure and determine the current body position, can act as preventive health care by detecting proper heart rate and beats per minute, the activity of individual muscle groups, proper breathing and estimates of blood oxygen levels. In the future research, it is necessary to compare different types of sensors, methods used and the results obtained in order to determine which of them are most suitable for the future development of seating furniture for work.*

KEYWORDS: *office chair; smart chair; sensors; smart seating; internet of things; health*

SAŽETAK • *Posljedice dugotrajnog sjedenja na uredskim i drugim radnim stolicama u posljednje se vrijeme pokušavaju ublažiti ili spriječiti primjenom suvremenih tehnologija. U različite dijelove uredskih stolica ugrađuju se pametne tehnologije i senzori, što omogućuje praćenje rasporeda sjedenja i izbjegavanje položaja koji potencijalno ugrožavaju zdravlje korisnika. Cilj ovog rada jest davanje pregleda dosadašnjih istraživanja u području primjene suvremenih pametnih tehnologija i senzora ugrađenih u uredske i ostale vrste stolica radi prevencije obolijevanja korisnika. Analizirani su članci objavljeni u razdoblju od 2010. do 2020. i indeksirani su u bazama podataka WoS CC, Scopus i IEEE Xplore, a izdvojeni su prema ključnim riječima pametna stolica i senzorska stoli-*

[1]Authors are associate professor, student and associate professor at University of Zagreb, Faculty of Forestry and Wood Technology, Zagreb, Croatia.

ca. Obrađeno je 15 članaka u kojima su se istraživanja temeljila na primjeni različitih vrsta senzora koji određuju kontaktne tlakove između korisnikova tijela i dijelova stolice te raspoznaju različite položaje tijela pri sjedenju, čime se mogu prevenirati negativne posljedice za zdravlje. U analiziranim istraživanjima autori su dokazali da primjena pametne tehnologije i bolje razumijevanje sjedenja uporabom različitih senzora i aplikacija kojima se očitava pritisak tijela i određuje njegov trenutačni položaj može preventivno djelovati zahvaljujući praćenju rada srca i broja otkucaja u minuti, aktivnosti pojedinih mišićnih skupina, pravilnog disanja, procjene razine kisika u krvi i sl. U budućim istraživanjima potrebno je usporediti različite tipove senzora, primijenjene metode i dobivene rezultate kako bi se uočilo koji su od njih najprikladniji za budući razvoj radnog namještaja za sjedenje.

KLJUČNE RIJEČI: *uredska stolica; pametna stolica; senzori; pametno sjedenje; internetske stvari; zdravlje*

1 INTRODUCTION
1. UVOD

Sitting in office and other work chairs has become an almost unavoidable body position in today's work environment. However, as much as sitting offers comfort unlike many physically strenuous body positions, prolonged sitting at work has consequences for the human body and leads to back pain, musculoskeletal deformities, headaches, swelling of the lower extremities and similar phenomena. The reason for these phenomena is in sitting positions, which are an unconscious act folr the majority of the working population, which includes pupils, students, office workers, in short, all age groups who sit and work at the desk.

Because of numerous health problems, mostly in office workers, recent research deals with the application and installation of smart technology and modern sensors in work chairs and other types of seats in order to analyse and monitor data using supporting applications, aiming to promote user health.

One of the well-known networks that provides the use of smart sensors is the more ubiquitous Internet of Things (IoT) – which has already entered our daily lives and is used in various areas of our life habits. Griffiths and Ooi (2018) quoted Gartner's definition of IoT as "the network of physical objects that contains embedded technology to communicate and sense or interact with their internal states or the external environment", whose possibilities are endless. In their work, they stated that "mass digitalisation and IoT will transform many industries". The furniture industry is no exception. Every day more and more types of furniture accept and implement modern technology, increasing its functionality and usability. Moreover, the furniture gets some new features and provides the user with new possibilities.

It is well known that prolonged passive sitting is not healthy, and body position should be changed frequently during sitting. In modern times, intensive digitalisation and computerisation of work requires longer sitting during working hours and life in general. It is interesting that we as humans have existed for approximately 200,000 years, but we have been sitting much more often only for the last 200 years (Harari, 2015). Sitting has become an unavoidable daily habit, and the chair becomes an "icon" in our environment wherever we are. This means that our body has had plenty of time to biomechanically adapt to walking and active living, and only 200 years to living in a predominantly sitting position. Such a relatively sudden change certainly contributes to the occurrence of pain in the human body caused by irregular and excessive sitting.

Excessive and irregular sitting is the subject of many studies as a potential cause of various (especially spine) diseases (Liebenson, 2002; Vergara and Page, 2002; Gallagher, 2005; Scena and Steindler, 2008; Hartvigsen *et al.,* 2018). The way people sit is not likely to cause pain at the end of the day, but daily prolonged sitting will create a physical problem and body aches. The way of life of modern man in industrialised and economically developed countries has brought the human body into an unenviable physical state, and deformations and musculoskeletal disorders (MSD) are increasing. MSD such as neck and low back pain, but also muscular pain in arms and legs are by far the most common, and have been widely reported as being of significant health and economic concern in industrialised countries (Grimes and Legg, 2004; Lima and Coelho, 2011; Besharati *et al.,* 2020). Because of the above problems, people want to sit healthier. According to Ahn *et al.* (2015), the health care paradigm has changed from the former medical diagnostic service and treatment to today's health service dealing with continuous health management and prevention. Sitting at office is especially emphasised because on an average 8-hour workday employees are expected to work diligently and spent more time sitting in a chair. Since their frequent and intensive use during office work is assumed, office chairs are a suitable medium for this type of research and the most common objects in/on which various sensors are installed (Vlaović *et al.,* 2007; Goossens *et al.,* 2012; Zemp *et al.,* 2016).

The literature describing the use of different sensors and technologies that detect the way we sit, how long we sit and what impact it has on our health has been studied. There are a number of different methods and sensors for reading pressures and obtaining data during and about sitting (Jürgens, 1997; De Looze *et*

al., 2001; Kuijt-Evers and Van Dien, 2003; Aissaoui *et al.,* 2001; Ragan *et al.,* 2002; Gyi and Porter, 1999; Davies *et al.,* 2000; Vlaović *et al.,* 2012). However, the question is how to interpret such data and how to process them so as to use them for the purpose of preventing diseases caused by prolonged, irregular and uncomfortable sitting on the chairs, which can often be unsuitable for work, improperly adjusted for sitting and with other defects. Another, no less important problem is the position and location of the installation of sensors that can significantly affect user behaviour and comfort (Bibbo *et al.,* 2018).

1.1 Sitting as a cause of disease in office jobs

1.1. Sjedenje kao uzrok obolijevanja tijekom obavljanja uredskih poslova

Office work plays a significant role in the health of modern employee, especially since today's jobs are based on the use of information technology, robotics and long-term sitting. Unfortunately, in addition to the positive consequences of the introduction of digitalisation, there are more and more negative consequences for the health of the office workers.

Wahlström (2005) quoted many authors who believed that musculoskeletal symptoms of visual display units (VDU) users have a multifactorial aetiology: non-neutral wrist, arm and neck postures, the work station design and the duration of VDU work; psychological and social factors, such as time pressure and high-perceived workload, are believed to interact in the development of these symptoms. Several other studies (quoted in Parvez *et al.*, 2019) pointed out seat-related MSDs between prolonged sitting and back pain, and many analyses even suggested that sitting and satisfaction with furniture were linked to some MSDs symptoms. For employees who work with computers and on physically inactive jobs, prolonged sitting at work becomes a major body posture. Data from the Netherlands and Australia indicate that employed adults can spend up to half of their working day sitting, while in the U.S., time-use surveys have shown that people in full-time employment spend an average of 9.2 hours working on weekdays, much of which will involve sitting. A study of sitting habits of Australian workers found that persons who work full-time sit for an average of 4.2 hours per day at work, and the remaining 2.9 hours are spent in their free time sitting (Van Uffelen *et al.,* 2010). Another study (Ertel *et al.,* 1997) shows that the average office worker spends about 50,000 hours seated during his working life, in typical office workplace such as a computer workstation. About 40 % of office workers develop problems with back pain and deformities that result from a lack of physical activity when working with a computer.

Eurobarometer's survey (quoted in Schwartz, 2016) showed that 11 % of all Europeans over the age of 14 sit for more than 8.5 hours a day. Unfortunately, the nowadays situation caused by the COVID-19 pandemic and restrictions increased this problem on a global scale (Amelot *et al*., 2021).

To avoid, or at least to reduce pains and deformations, sport engagements or physical activities for at least 30 minutes a day are recommended. Owen (2009) finds that a large number of sedentary activities on a daily basis, regardless of the amount of physical activity, is associated with the development of chronic spinal diseases or so-called MSD/LBPs. Referring to several authors, Bontrup *et al.* (2019) state that lower back pain (LBP) is the third leading cause of absenteeism due to self-diagnosed inability to work without pain at work, and that sitting for periods longer than seven hours a day significantly contributes to the risk of lower back disease. On the other hand, the same authors refer to several articles that have failed to confirm the association of excessive sitting while working in the office with the risks of lower back disease, mainly due to the deceptive nature of lower back pain, possible data processing error or unreliable measuring devices, short measurement time and potentially insufficient number of respondents.

Schoberth (1962) (quoted in Harrison *et al.,* 1999) defined three different sitting postures on the basis of the proportion of body weight transmitted to the floor by the feet and the location of the centre of grav-

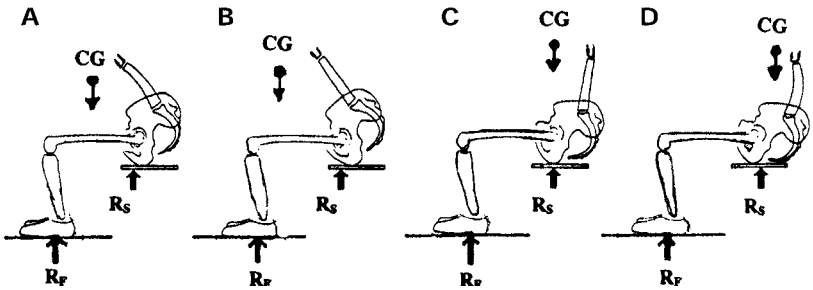

Figure 1 Sitting categories based on centre of gravity (Schoberth (1962) cited in Harrison *et al.,* 1999) RS – reaction force through seat bottom, RF – reaction force from ground to feet, CG – centre of gravity of body mass above pelvis
Slika 1. Kategorije sjedenja s obzirom na težište tijela (Schoberth, 1962.; citirano u: Harrison *et al.,* 1999.)
RS – sila reakcije kroz sjedalo, RF – sila reakcije poda na stopala, CG – težište mase tijela iznad zdjelice

ity of the body. These sitting postures (Figure 1) were termed as: anterior (A and B), middle (C), and posterior (D). Schoberth noted that these three postures also differed with respect to the shape of the lumbar spine. Later works based on this principle (Ribeiro *et al.,* 2015; Ishaku *et al.,* 2019; Mizumoto *et al.,* 2020) aimed at monitoring and recognising sitting position.

A major cause of the disease due to improper sitting could be the fact that different types of office chairs, produced by different producers, have different adjustable parameters and solutions that mostly confuse the users. Users often do not use all of the adjustments, and thus do not use the office chair in the optimal ergonomic way (Goossens *et al.,* 2012). The next problem connected to disease due to improper sitting could be incompatibility of seating furniture dimensions and user's anthropometry, and this starts quite early in school time (Dowell, 1995; Gouvali and Boudolos, 2006; Asif *et al.,* 2012; Adu *et al.,* 2014; Iliev *et al.,* 2019).

Prolonged sitting is also recognised as a serious metabolic health problem due to several pathogenic mechanisms that link muscle inactivity with increased health risks due to low energy consumption, leading to fat accumulation, and may lead to mild inflammation, decreased endocrine function of the glands which can cause poor work of several organs and tissues accompanied by decreased secretion of antioxidants (Grooten *et al.,* 2013).

1.2 Aim of paper
1.2. Cilj rada

The aim of this paper is to present the state-of-the-art techniques and sensors technology applied when sitting in office chairs and other types of chairs, in order to prevent certain diseases and increase the health of users.

In order to monitor our own sitting behaviour and determine how our sitting positions affect our health, research on sitting in chairs with various types of sensors has been conducted in recent times. In addition to understanding our body postures while sitting and permitting to monitor the body postures for a certain period of time, these sensors have the purpose of preventing body deformities and body positions that affect pain, and encourage us to sit more comfortably and appropriately to our body and to improve the quality of sitting and consequently the quality of our lives.

2 MATERIALS AND METHODS
2. MATERIJALI I METODE

2.1 Method of selecting relevant literature
2.1. Metoda odabira relevantne literature

The paper presents the review obtained by searching open source articles published from 2010 to 2020 and indexed in the Web of Science Core Collection (WoS CC), Scopus and IEEE Xplore databases,

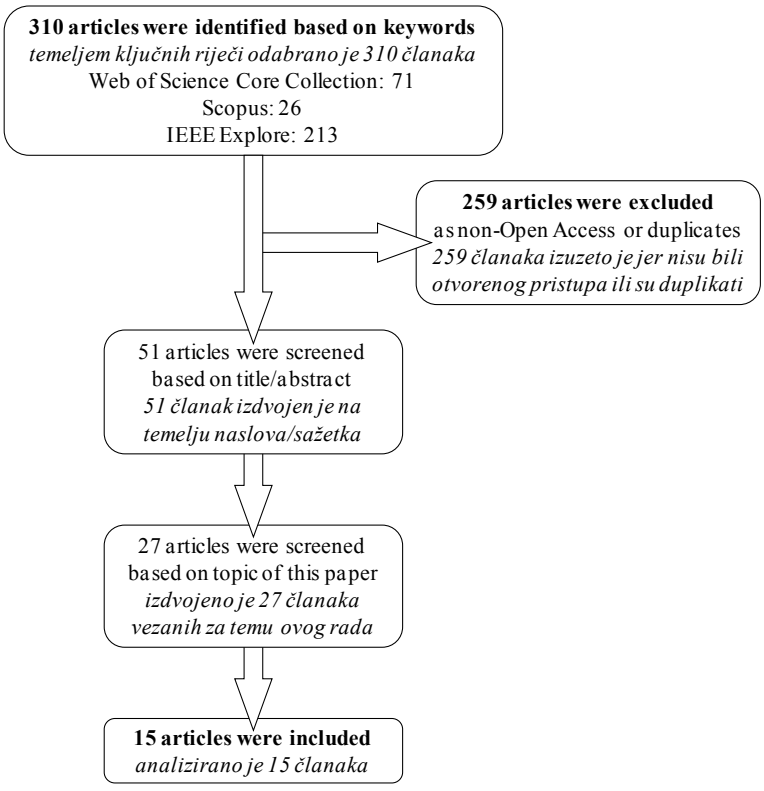

Figure 2 A schematic structure of article selection
Slika 2. Shematski prikaz probira članaka

which were found by March 18, 2020. Keywords were "smart chair" and "sensor chair".

After selecting a large number of "raw" articles, the narrower favourable criteria related to the topic of this paper were applied, such as: sensors integrated in the seat or other parts of the chair; use of sensors that detect sitting position and sitting habits; and systems that give the chair the adjective "smart chair".

Searching of open-source articles by keywords in all three databases resulted in 51 papers. After reviewing the papers and assessing the similarities with the research topic, 15 papers remained (Figure 2).

3 RESULTS AND DISCUSSION
3. REZULTATI I RASPRAVA

Further selection and presentation of articles was based on the type of sensor (pressure, tension, capacitive, heart rate), the mode of operation of the sensor (contact, contactless, wireless), the method of processing the collected data and the existence of the application software for the user.

Lee *et al.* (2019) developed a smart chair that can detect and classify some common daily activities of elderly people. The proposed smart chair is built from simple and sophisticated devices yet robust enough to detect five activities of individuals in sedentary positions. These activities include eating, working at the desk, watching TV, napping, and coughing. The smart chair is composed of six pressure sensors, an analogue-to-digital converter, mini-computer, and a conventional office chair. Four pressure sensors are placed on the seat to collect data while the subject is sitting upright and two on the backrest to collect information when the subject leans back. These sensors generate analogue signals, and the A/D converter is used to convert the collected signals to digital signals for the mini-computer, which transmits the digital signals to a server for pre-processing and analysis (Figure 3).

For the purpose of their research, three different machine learning algorithms were employed. These algorithms were the random forest (RF), extremely randomised trees (ERTs), and support vector machine (SVM). Two phases of experiments were conducted on the collected data upon submission to the server, namely, user-dependent and user-independent experiments. The RF and ERT classifiers demonstrated a very high classification performance during the experiments, the highest being attained by ERT. ERT obtained up to 98 % in the user-dependent phase and 97 % in user-independent phase. According to authors, the results obtained by the classifiers on the five activities showed that the proposed algorithm outperformed all the others mentioned in the literature. The chair has the potential to be a huge source of information on the behaviour of people since most indoor activities are performed in sedentary positions.

A cushion-based system to assess activity levels and recognise the activity from the information hidden in sitting postures of sedentary lifestyle population was developed by Ma *et al.* (2017). It is suitable for monitoring the sitting behaviour in contexts such as workplace, car, or on wheelchairs and can be easily implemented with low-cost embedded devices. Authors use the smart cushion on the chair, equipped with the effective combination of pressure and inertial sensors for non-invasive monitoring of users' postures and body swings (Figure 4). Also, they constructed a body posture analysis model to recognise sitting behaviours and a method to assess the activity levels based on the evaluation of the activity assessment index. An activity can be recognised and activity levels can be quantified so as to provide users with reminders to exercise or take a break and therefore to minimise the health risk as well as to give the users timely necessary interventions.

The results showed that, using the newly designed smart cushion and the standard deviation features, the present system is able to achieve the accuracy higher than 89 % for activity recognition and higher than 98 % for activity level recognition.

Zazula *et al.* (2015) presented a smart chair with unobtrusive sensors that measure functional health pa-

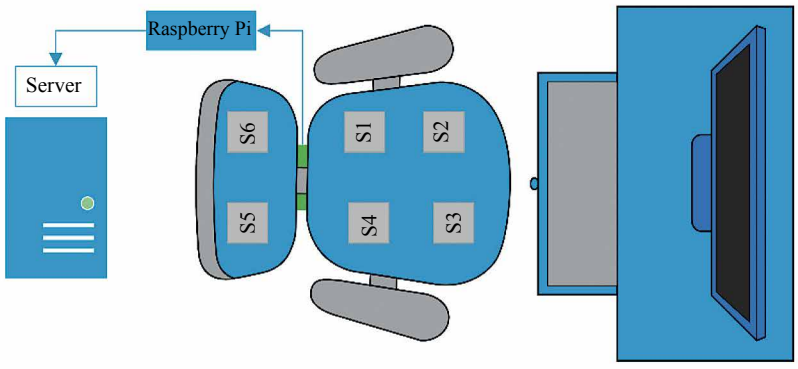

Figure 3 System architecture of smart chair for activity recognition (Lee *et al*., 2019)
Slika 3. Arhitektura sustava pametne stolice za prepoznavanje aktivnosti (Lee *et al*., 2019.)

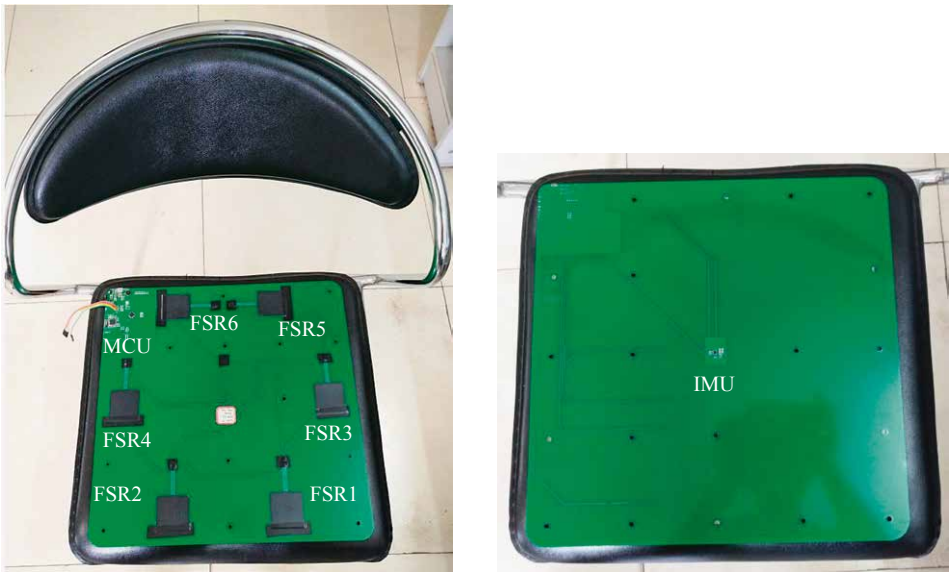

a) Circuit board – front side/ *Prednja strana* b) Circuit board – back side / *Stražnja strana*

Figure 4 Smart cushion circuit board on a chair (Ma *et al*., 2017)
Slika 4. Tiskana pločica pametnog jastuka na stolici (Ma *et al*., 2017.)

rameters of a person sitting on the chair. Although capacitive sensors are placed in the chair's backrest and seat, authors were focused on measurements made by a combined sensory device in the chair armrests. It captures photoplethysmographic (PPG) and electrocardiographic (ECG) signals in parallel, which enables the assessment of various cardiovascular parameters (Figure 5).

Experiments described in respective paper analyse parallel recordings of the PPG and ECG signals only. All acquired measurements were synchronised by a microcontroller build in the chair and wirelessly transmitted to a host computer. Analysis algorithms extracted relevant features and estimated parameters of functional health, and rendered those data by user interface adapted to run on mobile devices. Authors modelled the relationship between pulse transit times and subject's blood pressure by linear model in four situations, i.e. for systolic and diastolic referential pressures at rest and after the exercise. Results show that agreement between the references and modelled estimates is not accurate enough for systolic pressures, but is acceptable for diastolic pressures. Relationship between referential blood pressures and estimated pulse transit times unveiled inferior fitting of systolic blood pressures, both at rest and after exercise and, according to authors, a possible reason might be individ-

a) Unobtrusive sensors in backrest, seat, and armrests / *Nenametljivi senzori u naslonu, sjedalu i naslonima za ruke* b) U-shaped ECG electrode under armrest / *EKG elektroda U-oblika ispod naslona za ruke*

Figure 5 Gaming chair modified for experiment (Zazula *et al*., 2015)
Slika 5. Stolica za igrače računalnih igara prilagođena pokusu (Zazula *et al*., 2015.)

ual differences in vascular parameters that influence this relationship.

An ergonomic chair with embedded IoT technology using support vector machine (SVM, a supervised machine learning algorithm that can be used for both classification and regression challenges) is presented in the work of Prueksanusak *et al.* (2019). The research proposes smart IoT chair that can classify sitting posture by means of artificial intelligent techniques. In the present paper, traditional machine learning techniques were applied to find the best sitting posture classification model. Five algorithms were selected: SVM, Bernoulli, Gaussian, MLP (multi-layer perceptron) Classifier and Logistic Regression, and conducted in terms of comparison of system performance. On hardware side, there were six force sensors set under the chair surface and four force sensors at the chair backrest. Collected data were sent to the server for predicting five sitting postures, such as: straight, sitting with left leg crossed, sitting with right leg crossed, only sitting on half chair and leaning against a chair. Results showed that all machine learning techniques achieved the accuracy over 90 %, while SVM achieved the highest accuracy in the setting environment with 96.2 %. Therefore, the authors chose this algorithm to develop a model for predicting sitting position in a mobile application, with the aim to reduce the incidence of office syndrome promoting the user to have a proper understanding of seating and recognising the problem of office syndrome in sitting posture. The user can monitor the results of predictions via mobile application in real-time, and in case the user has wrong sitting posture, he or she will be warned about it.

Research of Kumar *et al.* (2016) brings results of sedentary activities and behaviour assessment with smart sensing on chair backrest. Authors designed a smart chair system named *Care-Chair*, which can non-intrusively detect and analyse chair occupant's daily sedentary activities and behaviour. The system uses only four force sensitive resistor type sensors on the chair backrest to recognise and classify very fine-grained and complex activities while sitting. Additionally, the *Care-Chair* system is designed to estimate user's breathing rate during relatively static activities (Figure 6).

Interesting findings are that the sensors placed on chair backrest are more sensitive to various functional and emotional activities in sedentary position, as compared to the sensors on the seat. Namely, according to authors, the key difference between the present paper and other relevant studies is that their interest is focused on functional and emotional activity contexts rather than only on static/movement postures. Thirteen machine learning classifiers were used for comparing their accuracy performance and training delay: Linear

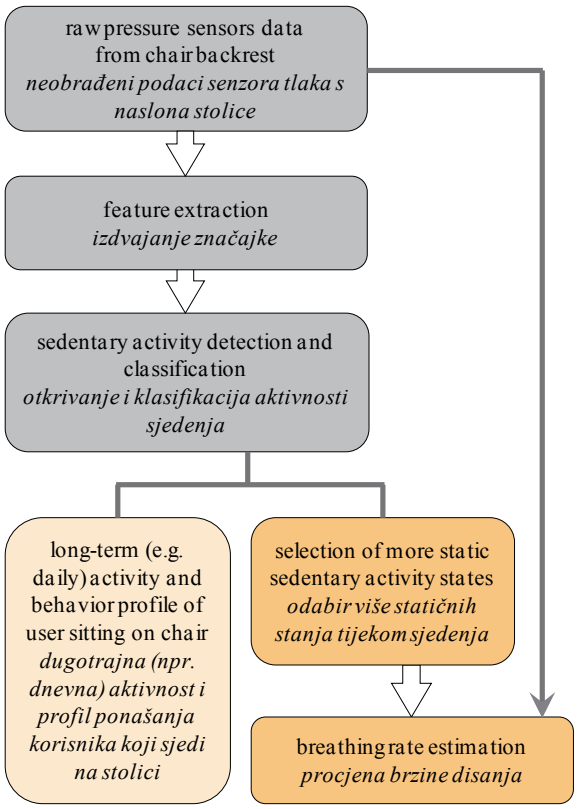

Figure 6 Flowchart of overall functionality of Care-Chair product (Kumar *et al.*, 2016)
Slika 6. Dijagram toka ukupne funkcionalnosti proizvoda Care-Chair (Kumar *et al.*, 2016.)

Discriminant Analysis (LDA), Quadratic Discriminant Analysis (QDA), Stochastic Gradient Descent (SGD), Support Vector Machine (SVM), K-Nearest Neighbors (kNN), Gaussian Naive Bayes (GNB), Multinomial Naive Bayes (MNB), Bernoulli Naive Bayes (BNB), Decision Tree (DT), Random Forest (RF), Extremely Randomised Trees (ERT), AdaBoost (AB), and Gradient Boosting Trees (GBT); finally ERT classifier was chosen for further analysis due to high accuracy and low delay in training phase. The *Care-Chair* system is validated to be able to classify a large number of 19 fine grained and complex user sedentary activities including user functional and emotion-based activities, not only the static and movement based sedentary activities and postures. The system is also validated to estimate user's breathing rate with high accuracy performance.

Anwary *et al.* (2019) dealt with the real time visualisation of asymmetrical sitting posture (ASP), which undoubtedly affects the body mechanics and puts various body segments under strain. That strain may lead to health problems such as musculoskeletal and low back pain, spinal deformity, etc. Therefore, authors developed an automatic real time asymmetric sitting posture monitoring system based on a multi-layered architecture of flexible pressure sensors compatible with human biomechanics, which could be embedded in complex interfac-

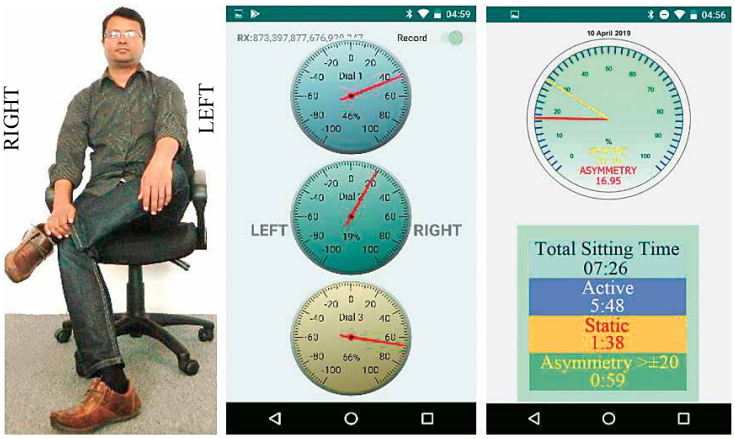

a) b) c)

Figure 7 Example of asymmetrical sitting posture in experiment (a) and mobile application monitoring interfaces (b, c) (Anwary *et al*., 2019)
Slika 7. Primjer asimetričnog položaja sjedenja u pokusu (a); sučelja za praćenje mobilnih aplikacija (b, c) (Anwary *et al*., 2019.)

es, such as seat cover or chair and mobile application for real time data visualisation. Figure 7 shows the asymmetrical sitting posture with cross-leg position (a), dial based asymmetrical sitting posture visualisation (b) and a sitting score with a day summary (c).

According to authors, during a sitting posture, the pressure distribution of both right and left side should theoretically give identical results and therefore perfect asymmetry should give dial indicator readings of zero. The dials (Figure 7b) display asymmetry for thigh, buttock and shoulder regions, where it can be seen that there is a difference in the level of asymmetry. Positive value readings indicate that the pressure distribution of the right region is higher than the left, while a negative value indicates the pressure of the left region is higher than the right region. A high reading indicates higher asymmetry and a reading around zero value indicates good sitting posture. The app records daily reading and estimates the duration of total sitting, active, static and asymmetry sittings (Figure 7c). The present system differs from the existing ones in the meaning of integrating posture visualisation in real time with post analysis of collected data, which provides an easy, user friendly, private and secure way to visualise and monitor the sitting posture. According to the authors, the system can be used for monitoring and rehabilitation of diseases associated with sitting posture in different clinical setting, work place, school and patient's home.

The smart chair cover for posture correction (Kim and Lim, 2019) recognises the postures through the pressure sensor, informs the user of the real-time posture, and precisely distinguishes the correct posture from the incorrect by deep learning. The smart cushion system uses two pairs of 30 pressure sensors embedded in flexible pad (one on the seat, the other on the backrest) and connected to Arduino module. The data was transmitted to the smart device via wireless communication, and from this data, the posture was identified by the system. The identified posture was then compared to the value previously stored in the database. The image and text apt for the posture defined were transmitted to the smartphone and informed the user about his correct or incorrect sitting posture. Despite the fact that only 10 participants were involved in the experiment, authors demonstrated this idea using deep learning system to augment data from a small number of participants and confirmed the effectiveness of the developed system. Moreover, they are convinced that the suggested system can tell the exact posture of the users and that the users can correct the posture by themselves, which will be further bolstered by future research with various and expanded experimental groups.

Sifuentes *et al.* (2019) developed a measurement system to detect and confirm the presence of a subject (or object) on a chair. They propose a novel measurement method for detecting and classifying seat occupancy using a single force sensitive resistor (FSR). The proposed system first detects the subject by monitoring his/her weight and then confirms his/her presence by monitoring the respiration.

For the subject/object classification, additional information is usually required, and in this case, it was extracted from the FSR itself, which is also used to monitor the respiratory signal (Figure 8). The occupancy was expected to cause a large-signal variation of the FSR, whereas the respiration generates a small-signal variation enabling the confirmation of the presence of a human rather than an object. It should be noted that the same FSR sensor was used to wake the microcontroller unit in the presence of the subject/object and then to monitor the respiratory signal to confirm the presence of the subject. It should be mentioned that the system functions without using any intermediate analogue electronics, thus resulting in low-energy consumption and good energy efficiency.

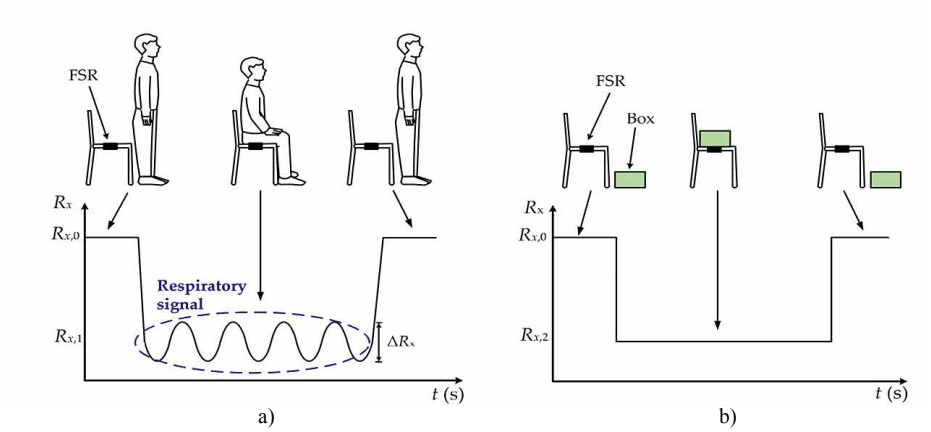

Figure 8 Display of signal variations when a person (a) or an object (b) is on the chair (Sifuentes *et al*., 2019)
Slika 8. Prikaz varijacije signala kada je na stolici osoba (a) ili predmet (b) (Sifuentes *et al*., 2019.)

Therefore, the present method can be attractive for autonomous sensor applications that require the detection and confirmation of people sitting in chairs, such as intelligent airbag deployment systems and aircraft boarding systems.

Offices are not the only places that can be enhanced with smart seating. Smart home environment is more and more present in our daily life, and smart chairs become an unavoidable item of that system (Hesse *et al.,* 2017). The presented chair development is a part of the wider project where parties involved from industry, research (…) and health providers address the question of how "intelligent" and "trustworthy" technical systems can be realised to help people in their everyday lives. In terms of the above, smart armchair is an example of ubiquitous interaction system with the goal to improve the user's well-being (Figure 9).

Figure 9 Smart chair with integrated sensors locations (F – FSR, R – radar) (Hesse *et al*., 2017)
Slika 9. Pametna stolica s rasporedom integriranih senzora (Hesse *et al*., 2017.)

The integrated sensors and actuators enable a multiplicity of applications. The sensors in the seating can be used for presence detection, they can serve as simple push buttons and form an input device, and user's posture can be determined by analysing patterns in the sensor data that can be used to emphasise a healthy sitting posture, etc. The integrated radar sensor can measure the movements of the body caused by the heart beating and respiration, and therefore it can be used to calculate the respiration rate and heart rate. With these, contactless acquired data, it is possible to track the user's health status, detect potentially harmful conditions and provide biofeedback for the relaxation modes. The actuators are used to assist the user while sitting down or standing up, which is especially important for elderly people, or can be used to adjust the chair to the actual user's need. Information about the individual needs is based on the identification of the user and can be gathered from the connected database. The introduced applications are potentially able to improve the user's well-being by offering qualified fitness training, a relaxation mode and assistive functions. Additional value of this research and system is generated by connecting the chair to a smart home environment, which enables and expands novel features and use.

Hu *et al.* (2020) presented a smart chair sitting posture recognition system using flex sensors and implemented artificial neural network that can categorise seven different health-related sitting postures. This research introduces flex sensors with a machine learning algorithm to build a low-complexity hardware system for sitting posture recognition, in which only six passive flex sensors are attached to the chair (Figure 10).

Comparing their system with the state-of-the-art works, the authors conclude that this work has achieved

Figure 10 Flex sensor based sitting posture recognition system (Hu *et al*., 2020)
Slika 10. Sustav za prepoznavanje sjedećeg položaja uz pomoć senzora savijanja (Hu *et al*., 2020.)

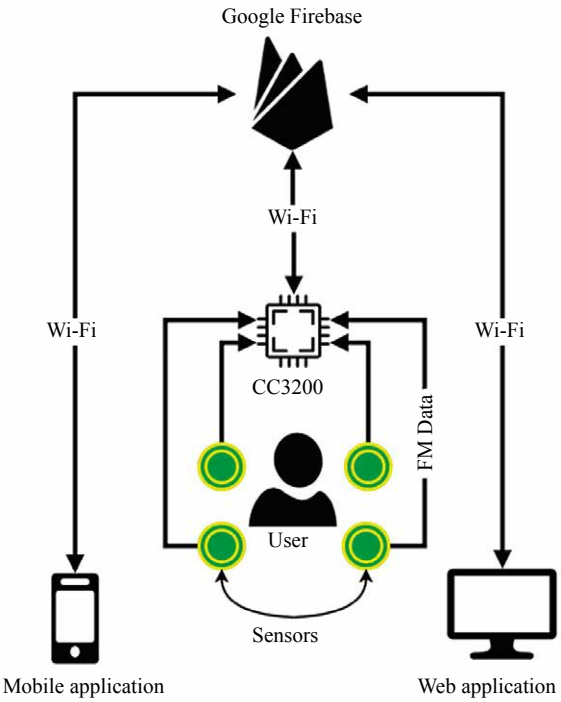

Figure 11 General architecture of Smart Chair system (Flutur *et al*., 2019)
Slika 11. Opća arhitektura sustava Smart Chair (Flutur *et al*., 2019.)

the lowest power consumption, the greatest hardware simplicity and the highest accuracy among the related works. The primary novelty of this research is the new type of sensor combined with fixed-point two-layer artificial neural network model developed to achieve the above goals. The proposed system brings longer battery life, better user experience, and robustness compared to other types of sensing systems. In the future work of these authors, this recognition system will be a part of a smart health monitoring system, which will consider the algorithms with complicated architecture like convolutional neural network.

Flutur *et al.* (2019) developed a smart chair system for posture correction based on a capacitive proximity transducer type of the sensor for remote monitoring. This is a chip-based system. The microcontroller unit measures the frequency signal of each sensor and then sends the data to a Google Firebase cloud via Wi-Fi (Figure 11).

When the subject is in contact with the sensors, the data is correlated with the actual pressure, and when the contact is absent, the measurements data are correlated with distance. In order to collect relevant readings in real-time for the human body position, the capacitive/proximity sensors were placed in six key points: two on the chair seat and four on the user back. To understand in which way and at which time the user is adopting a correct or incorrect posture, he or she can use the data presented in an easy to understand way on mobile application. For the purpose of the present research, it was important to create the user interface so that he/she can easily interact with the information provided by the sensors. The uniqueness of this design for correcting postures comes not from the use of sensors, but the individuality of each feature. The sensors were specifically designed and created for this particular use. The mobile application and the web interface provide ease of access and also a high rate of commodity when using the device.

Design and implementation of a smart chair system for IoT is observed in a research of Park *et al.* (2016), where the system combining a built-in IoT device and a chair with separated seating pads was presented. According to authors, by using "smart IoT chair", the posture can be easily corrected by checking the user's posture on a smart device (phone). Collected posture data can be used for example to further understand user's sitting habits, correct children's posture promoting healthy growth, provide medical information and analyse the time and pattern during studying or working. The system works on the principle of sensing user posture by an embedded IoT device and sev-

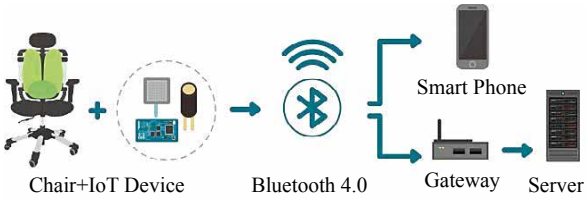

Figure 12 Overview of "Smart IoT Chair" system (Park *et al*., 2016)
Slika 12. Pregled sustava *Smart IoT Chair* (Park *et al*., 2016.)

eral custom designed sensors that are attached to the chair. The embedded IoT device, using Bluetooth technology, sends measured sensor data to a smartphone or a server. At the end, either the server or the smartphone receives, processes, and visualises the posture data sent by the "smart IoT chair" system in real-time (Figure 12). Besides that, a wireless gateway can be used to analyse the pattern of an individual (or groups) and send analysed data to the server by processing data received from a number of smart IoT chairs.

In the smartphone application, the user can visually check his posture, where circles in four colours represent the four levels of pressure sensed by the four pressure sensors, while the four levels of sensed tilt are represented by the tilting of the pad in the figure of the chair itself. Furthermore, actual level values of each sensor are displayed at the bottom of the application. During the research, the limitations were additionally discovered of the existing (off-the-shelf) commercial sensors (pressure, flexible and tilt) and these problems were overcome by developing custom designed sensors.

Different subjects have their distinctive heartbeat patterns due to differences in age, gender, weight, cardiac structure, etc. The heartbeat-based human identification has shown some advantages, basically in resistance against malicious cyber-attacks. A heartbeat is the vibration caused by the passage of blood from the cardiac atria to the ventricles and from the heart cells to the aorta and pulmonary artery (Guyton and Hall, 2012). The heartbeat presents a unique life indicator to represent a subject and it is difficult to manipulate or replicate, and can be represented by ballistocardiography (BCG). BCG is a method of recording the displacement of the body during the ejection of blood from the heart into the aorta at each cardiac contraction. However, the normal record of body displacement changes in some heart patients (aortic stenosis and insufficiency) (***, 2021).

The work of Zhang *et al.* (2019) experimentally presents the unobtrusive continuous identification of a person by BCG using a sensor that works on the principle of micro-bending of the optical fibre (Figure 13).

The authors believe that such a way of identifying a person is appropriate as a person just needs to sit down, lean back, and the chair will recognise who it is. The main goal of this research was to develop a pillow with a sensor to identify a person leaning on a pillow that monitors BCG signals. At the same time, microbending of the optical fibre takes place in the sensor and vibrations are read, including the heartbeat. Experimental results show that the filtered BCG signal reveals an individual pattern of BCG signal. The main advantage of this method of identification in relation to the ECG is that it is much easier and simpler for a person to just sit and lean on a pillow than to be connected to various electrodes.

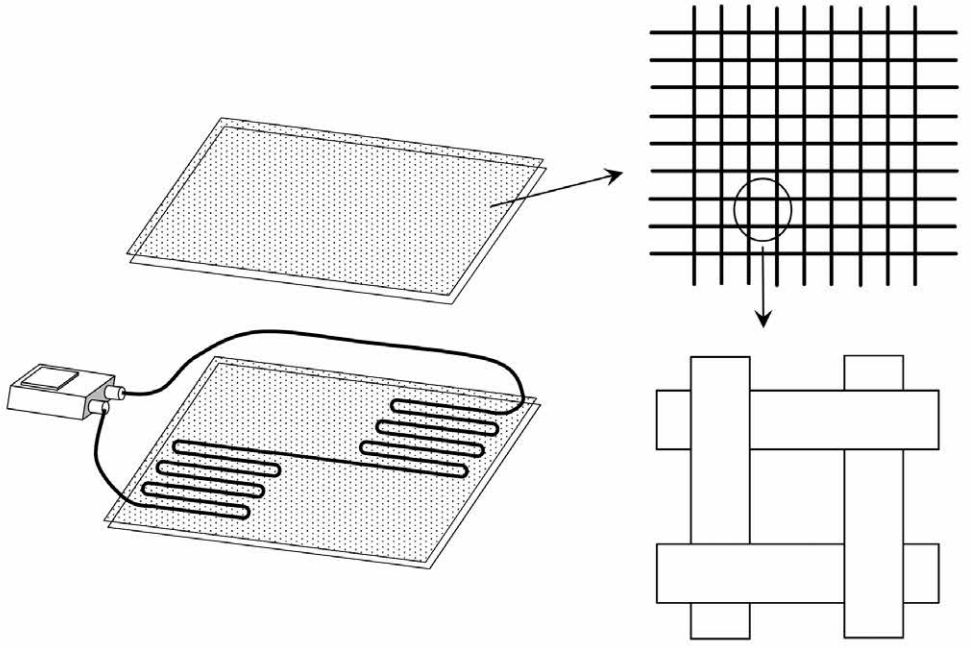

Figure 13 Schematic of microbend fibre sensor (Zhang *et al*., 2019)
Slika 13. Shematski prikaz senzora s mikrosavitljivim vlaknima (Zhang *et al*., 2019.)

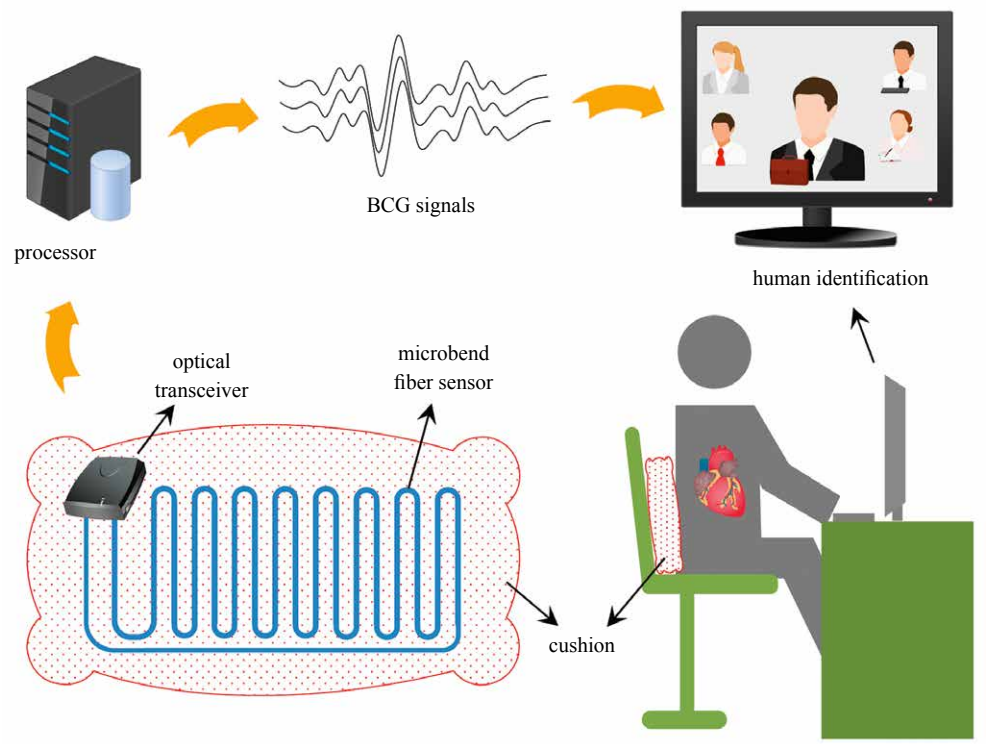

Figure 14 System architecture of continuous human identification system (Zhang *et al*., 2019)
Slika 14. Arhitektura sustava za kontinuiranu identifikaciju ljudi (Zhang *et al*., 2019.)

Figure 14 schematically shows the operation of a pillow for identifying a person, where the convenience and ease of use of such a pillow can be best seen. The authors recommend biometric identification of humans using BCG and prove in their paper that continuous and good recognition results have been obtained. They also emphasise that this is a biometric recognition method that is harder to hack, so it can be used in much more delicate conditions (e.g. military use). It is interesting to mention that the authors conducted an additional experiment where it was found that this method can unlock a smartphone.

However, there are studies that have tried to overcome the problem of contact measurement of electrocardiogram signals, i.e. reducing the occurrence of errors in measurements by combining both BCG and ECG. Ahn *et al.* (2015) developed a smart chair based on multi heart rate detection system. The smart chair implementation is designed to measure a non-contact ECG and an unconstrained BCG at the same time (Figure 15).

The aim was to make up for the shortcomings of the two types of spectrum. The authors succeeded in implementing a non-contact ECG measurement without the need to place electrodes on the body, i.e. while the person is dressed; furthermore BCG provides the possibility of unlimited measurements. In addition, the advantage of such a measurement is that the sitting position does not affect the quality or result of the measurement. However, there are many disadvantages due to the appearance of "noise" in the movements. For non-contact ECG measurements, electrodes are arranged on the contact surfaces of the backrest and seats, i.e. the user's back and buttocks. The BCG measuring system consists of a loadcell located under the

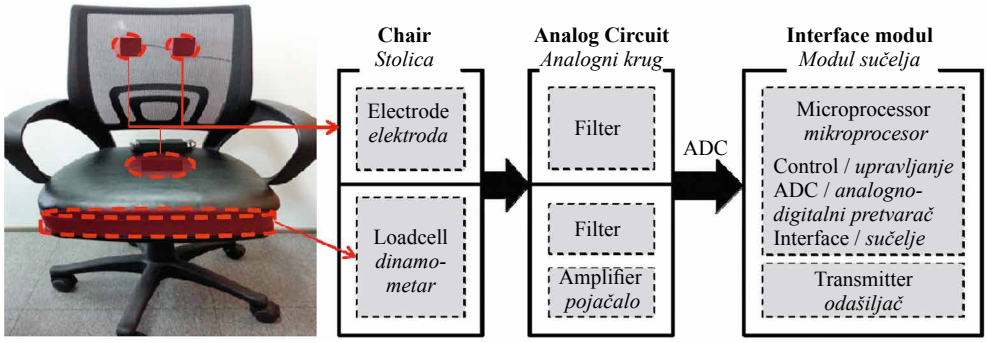

Figure 15 Smart chair system configuration based on heart rate detection system (Ahn *et al*., 2015)
Slika 15. Konfiguracija sustava pametne stolice utemeljena na sustavu za detekciju broja otkucaja srca (Ahn *et al*., 2015.)

seat base to measure the change in weight. The measurement signal is transmitted to the Android smartphone in real time. The authors find that the presented unique and simultaneous measurements of ECG and BCG signals reduce the disadvantages of their separate measurements.

Sodhi and Kunwar (2017) research was motivated by the infinite possibilities provided by the concept of *Inernet of Things* to make surroundings better and smarter. As the research was placed in educational environment, the goal of the *Smart Chair* concept was to verify the presence of a human being and to automate the attendance process in the classroom suggesting the student to maintain a healthy sitting posture. *Smart Chair* helps in the identification of the student and it uses pressure and temperature sensors to maintain the presence record of the student in a local database. It also signals the students to maintain right posture for their healthy lifestyle. The presented prototype of the smart chair system consists of a microcontroller board-based system, which is assembled and implemented to get user ID through radio frequency identification reader and chair occupancy status by pressure sensor and temperature sensor. Moreover, the chair is also equipped with a micro-electromechanical system (MEMS), a 3-axis accelerometer which is used to check the posture of the body and to recommend changing the body posture if the posture is not correct. The functionality of MEMS is not clearly described, but it works on the principle of previously set values for "normal range", i.e. "for the correct body posture", and any other values that are later considered as "not correct postures".

All processed papers on "smart chairs" or "sensors chairs" are shown in Table 1, where an overview of the used sensors, methods of data processing, system accuracy and other summary data are given.

4 CONCLUSIONS
4. ZAKLJUČAK

There is no doubt that mass digitalisation will change the way we live and work.

Industry 4.0 and IoT provide great and new opportunities to improve the world we live in, and can help discover solutions to the great challenges that these new opportunities pose. One of possible and positive improvement could be used for observing our unconscious habits while sitting and working. We will have to tackle the problem of improper sitting and its impact on people's health for many years to come. Nevertheless, it has been shown that the use of modern technology and a better understanding of sitting using a variety of sensors and applications can act preventively in most situations.

This paper singles out 15 current studies whose methods and results are briefly explained in the previous chapter. The selected papers describe various sensors, such as: force-sensitive resistor, heart rate sensor, respiratory monitoring sensor, voice control sensor and acceleration sensor. The system for observing the way of sitting, collecting and processing data and displaying them in real time brings the best results, because in this way it directly influences the user to change the position or keep it. The presented solutions include various applied technologies, ways of functioning and outcomes. Diversity is good and acceptable, but it can cause certain problems, especially if it is not standardised. That has been the case in many of the presented sensor technology solutions that are not always compatible with each other. One of the solutions for wider application and faster implementation of sensor technologies in everyday use in work or home chairs would be the introduction of certain standards that would overcome the obstacles of matching different user needs into a single monitoring system.

Problems that will arise in the future could be related to the acceptance of such built-in monitors by users, mostly due to the risk of invading privacy. There are also possible dangers of malicious intrusions into systems (hacking). Current pandemic problems with poor availability of electronic components (chipsets) due to disrupted supply chains could further slowdown wider implementation of such furniture in everyday life, meaning high prices and low availability on the market. The examples of technologies in this paper show that the previous ideas of "smart furniture" are now functional solutions, but they need to be improved so as to be simpler for installation in furniture, less noticeable and more user friendly.

In future, it should be compared the types of sensors, the methods used and the results obtained in order to determine in which direction the development of certain types of "smart" seating furniture will take place, with emphasis on healthy seating while working.

5 REFERENCES
5. LITERATURA

1. Adu, G.; Adu, S.; Effah, B.; Frimpong-Mensah, K.; Darkwa, N. A., 2014: Office furniture design – correlation of worker and chair dimensions. International Journal of Science and Research, 3 (3): 709-715.
2. Ahn, B. G.; Noh, Y. H.; Jeong, D. U., 2015: Smart chair based on multi heart rate detectionsystem. In: 2015 IEEE Sensors, November, pp. 1-4. https://doi.org/10.1109/ICSENS.2015.7370628
3. Aissaoui, R.; Kauffmann, C.; Dansereau, J.; de Guise, J. A., 2001: Analysis of pressure distribution at the body-seat interface in able-bodied and paraplegic subjects using a deformable active contour algorithm. Medical Engineering & Physics, 23 (6): 359-367. https://doi.org/10.1016/S1350-4533(01)00052-2

Table 1 Related articles on "smart chairs" or "sensors chairs" systems
Tablica 1. Članci koji se odnose na sustave pametnih stolica ili stolica sa senzorima

Chair type *Vrsta stolice*	**Sensor(s) type, quantity, (location)** *Vrsta i broj senzora (lokacija)*	**Data acquisition and processing** *Prikupljanje i obrada podataka*	**Classification method(s)** *Metode klasifikacije*	**User interface/application (connection)** *Korisničko sučelje/aplikacija (veza)*	**Accuracy** *Točnost*	**Authors** *Autori*
office chair / *uredska stolica*	FSR sensor: 4 (on the seat), 2 (on the backrest) *FSR senzori: 4 (na sjedalu), 2 (na naslonu)*	A/D converter MCP 3008, Raspberry Pi	RF; ERT; SVM	n/a	98 %	Lee *et al.*, 2019
wheelchair / *invalidska kolica*	FSR sensor: 6 (on the seat, in the cushion); 3-axis inertial: 1 (in the cushion) *FSR senzori: 6 (na sjedalu, u jastuku);* *3-osni inercijski (u jastuku)*	Arduino Pro Mini	AAI; BPAM; J48	computer, smartphone, tablet (Bluetooth) *računalo, pametni telefon, tablet*	89-98 %	Ma *et al.*, 2017
office (gaming) chair / *uredska stolica*	capacitive sensors: (in the seat and in the backrest); PPG and ECG sensors (under the armrest) *kapacitivni senzori: (u sjedalu i naslonu);* *PPG i ECG senzori (ispod naslona za ruku)*	microcontroller	ECG R-wave peaks; PTTs	mobile devices *mobilni uređaji*	N/A	Zazula *et al.*, 2015
office chair / *uredska stolica*	force sensors: 6 (at the seat), 4 (at the backrest) *senzori sile: 6 (na sjedalu), 4 (na naslonu)*	microcontroller ESPino32, Arduino, cross platform database MongoDB	SVM; Bernoulli; Gaussian; MLP Classifier and Logistic Regression	mobile devices (Bluetooth) *mobilni uređaji*	96.2 %	Prueksanusak *et al.*, 2019
regular chair / *obična stolica*	FSR sensors: 4 (on the backrest) *FSR senzori: 4 (na naslonu)*	RFduino	ERT	mobile devices or another RFduino (Bluetooth) *mobilni uređaji ili neki drugi RFduino*	86 %	Kumar *et al.*, 2016
n/a	RFID EM-18; single point load cell sensor ESP 4-150; LM35 temperature sensor; MEMS *senzor opterećenja u jednoj točki ESP 4-150; LM35 senzor temperature*	microcontroller PIC;	pressure of body; body heat	LCD, Web application (wireless) *mrežna aplikacija (bežična)*	n/a	Sodhi and Kunwar, 2017
n/a	FPS with piezoresistive conductive film: 4 (at the seat), 2 (at the backrest) *FPS senzori s piezootpornim konduktivnim filmom: 4 (na sjedalu), 2 (na naslonu)*	Arduino Nano ATMega328	pressure of body *pritisak tijela*	mobile devices (Bluetooth) *mobilni uređaji*	n/a	Anwary *et al.*, 2019
n/a (only cover cushion) / (*samo dodatni jastuk*)	FSR sensor: 30 on the seat (in the cushion), 30 on the backrest (in the cushion) *FSR senzori: 30 na sjedalu (u jastuku), 30 na naslonu (u jastuku)*	Arduino	pressure of body *pritisak tijela*	mobile devices (Bluetooth) mobilni uređaji	n/a	Kim and Lim, 2019

office chair / *uredska stolica*	FSR sensor: FSR406: 1 (on the seat centre) *FSR senzor: FSR406: 1 (na sredini sjedala)*	Texas instruments MSP430F123 (MCU) applying direct interface circuit (DIC) concept	pressure of subject/object *pritisak subjekta/objekta*	n/a	n/a	Sifuentes *et al.*, 2019
reclining armchair / *naslonjač za opuštanje*	FSR sensor integrated in fabric: FSR406: 7 (in the seat), 2 (in the footrest), 1 (in the backrest); FSR sensor: FSR408: 2 (in armrests); GSR sensor; radar sensor *FSR senzori integrirani u tvornici: FSR406: 7 (na sjedalu), 2 (na podestu za noge), 1 (na naslonu); FSR senzori: FSR408: 2 (na naslonu za ruke); GSR senzor; radarski senzor*	microcontroller: ATSAM-4LC4C, ADC: ADS7953, operational amplifier: MCP6241T; depth camera (Microsoft Kinect); smart watch (heart rate monitor)	pressure of subject; presence of subject *pritisak subjekta; prisutnost subjekta*	TV screen *TV ekran*	n/a	Hesse *et al.*, 2017
office chair / *uredska stolica*	FSR sensor: FS-L-0055-253-ST: 3 (on the seat), 1 (on the backrest), 2 (on the armrests) *FSR senzori: FS-L-0055-253-ST: 3 (na sjedalu), 1 (na naslonu), 2 (na naslonu za ruku)*	Arduino board, ADC board	ANN two-layer; SVM	PC	97.4 % – 97,8 % 88.4 %	Hu *et al.*, 2020
n/a	capacitive proximity transducer: 2 (on the chair seat), 4 (on the user back) *kapacitivni senzor blizine: 2 (na sjedalu stolice), 4 (na leđima korisnika)*	SoC: MCU CC3200; Google Firebase Cloud; OpenEHR	n/a	web and mobile applications *mrežne i mobilne aplikacije*	n/a	Flutur *et al.*, 2019
seating pads (in office chair) / *podlošci (jastuci) za sjedenje*	custom made pressure sensors: 6 (on the seat) 4-level analogue tilt sensor: 2 (under the seat) *senzori tlaka izrađeni po mjeri: 6 (na sjedalu) 4-razinski analogni senzor nagiba: 2 (ispod sjedala)*	Arduino Pro mini; DAC; communication BT module: HM-10	n/a	iOS smart device or a gateway (Bluetooth 4.0, iBeacon) *iOS pametni uređaj ili pristupnik*	n/a	Park *et al.*, 2016
free-cushion (on the backrest) / *slobodni jastuk (na naslonu)*	microbend multi-mode optical fibre sensor *senzori optičkih vlakana*	n/a	LDA; MC-SVM; 1D-CNN	n/a	n/a	Zhang *et al.*, 2019
office chair / *uredska stolica*	non-constrained ECG electrode PS25255; BCG measuring system: SB S-beam loadcell *EKG elektroda bez ograničenja PS25255; BCG mjerni sustav*	MCU ATmega8L; BT module: HC-06	n/a	Android smart device or PC (Bluetooth, Wi-Fi) *Android pametni uređaj ili računalo*	n/a	Ahn *et al.*, 2015

FSR – force-sensitive resistors / *otpornici osjetljivi na silu;* PPG – photoplethysmography / *fotopletizmografija;* ECG – electrocardiography / *elektrokardiografija;* RFID – radio frequency identification / *identifikacija radiofrekvencijom;* MEMS – microelectromechanical systems / *mikroelektromehanički sustavi* ; FPS – flexible pressure sensor / *savitljivi senzor tlaka;* GSR – galvanic skin response sensor / *galvanski senzor reakcije kože;* BCG – ballistocardiography *balistokardiografija*
RF – random forest / *slučajna šuma;* ERT – extremely randomised trees / *ekstremno slučajne šume;* SVM – support vector machine / *stroj s potpornim vektorima;* AAI – activity assessment index / *indeks procjene aktivnosti;* BPAM – body posture analysis model / *model analize držanja tijela;* PTTs – pulse; transit times / *prolazna vremena pulsa;* MLP – multi-layer perceptron / *višeslojni perceptron;* ANN – artificial neural network / *umjetne neuronske mreže;* LDA – linear discriminant analysis / *linearna diskriminantna analiza;* MC-SVM – multi-class support vector machine / *višeklasni stroj s potpornim vektorima;* 1D-CNN – one-dimensional convolutional neural network / *jednodimenzionalna konvolucijska neuronska mreža*

4. Amelot, A.; Jacquot, A.; Terrier, L. M.; Aggad, M.; Planty-Bonjour, A.; Fouquet, B.; Cook, A. R.; Zemmoura, I.; Velut, S.; Destrieux, C.; François, P., 2021: Chronic low back pain during COVID-19 lockdown: is there a paradox effect? European Spine Journal, 1-9. https://doi.org/10.1007/s00586-021-07049-y
5. Anwary, A. R.; Bouchachia, H.; Vassallo, M., 2019: Real time visualization of asymmetrical sitting posture. Procedia Computer Science, 155: 153-160. https://doi.org/10.1016/j.procs.2019.08.024
6. Asif, S.; Qutubuddin, S. M.; Hebbal, S. S., 2012: Anthropometric analysis of classroom furniture used in colleges. International Journal of Engineering Research and Development, 3 (10): 1-7.
7. Besharati, A.; Daneshmandi, H.; Zareh, K.; Fakherpour, A.; Zoaktafi, M., 2020: Work-related musculoskeletal problems and associated factors among office workers. International Journal of Occupational Safety and Ergonomics, 26 (3): 632-638. https://doi.org/10.1080/10803548.2018.1501238
8. Bibbo, D.; Battisti, F.; Conforto, S.; Carli, M., 2018: A non-intrusive system for seated posture identification. In: 2018 IEEE 20th International Conference on e-Health Networking, Applications and Services (Healthcom), September, pp. 1-5. https://doi.org/10.1109/HealthCom.2018.8531165
9. Bontrup, C.; Taylor, W. R.; Fliesser, M.; Visscher, R.; Green, T.; Wippert, P. M.; Zemp, R., 2019: Low back pain and its relationship with sitting behaviour among sedentary office workers. Applied Ergonomics, 81: 102894. https://doi.org/10.1016/j.apergo.2019.102894
10. Davies, O.; Gilchrist, A.; Mills, N. J., 2000: Seating pressure distribution using slow-recovery polyurethane foams. Cellular Polymers, 19 (1): 1-24.
11. De Looze, M. P.; Kuijt-Evers, L. F.; Van Dieen, J. A. A. P., 2003: Sitting comfort and discomfort and the relationships with objective measures. Ergonomics, 46 (10): 985-997. https://doi.org/10.1080/0014013031000121977
12. Dowell, W. R., 1995: An estimation of lumbar height and depth for the design of seating. In: Proceedings of the Human Factors and Ergonomics Society Annual Meeting, 39 (7): 409-411. https://doi.org/10.1177/154193129503900701
13. Ertel, M.; Junghanns, G.; Pech, E.; Ullsperger, P., 1997: Effects of VDU-assisted work on health and well-being. In: Research Report 762. Federal Institute for Occupational Safety and Health (BAuA).
14. Flutur, G.; Movileanu, B.; Károly, L.; Danci, I.; Cosovanu, D.; Stan, O. P., 2019: Smart chair system for posture correction. In: 22nd Euromicro Conference on Digital System Design (DSD), August, pp. 436-441. https://doi.org/10.1109/DSD.2019.00069
15. Gallagher, S., 2005: Physical limitations and musculoskeletal complaints associated with work in unusual or restricted postures: a literature review. Journal of Safety Research, 36 (1): 51-61. https://doi.org/10.1016/j.jsr.2004.12.001
16. Goossens, R. H. M.; Netten, M. P.; Van der Doelen, B., 2012: An office chair to influence the sitting behavior of office workers. Work, 41 (1): 2086-2088. https://doi.org/10.3233/WOR-2012-0435-2086
17. Gouvali, M. K.; Boudolos, K., 2006: Match between school furniture dimensions and children's anthropometry. Applied Ergonomics, 37 (6): 765-773. https://doi.org/10.1080/1463922X.2019.1617909
18. Griffiths, F.; Ooi, M., 2018: The fourth industrial revolution-Industry 4.0 and IoT [Trends in Future I&M]. IEEE Instrumentation & Measurement Magazine, 21 (6): 29-43. https://doi.org/10.1109/MIM.2018.8573590
19. Grimes, P.; Legg, S., 2004: Musculoskeletal disorders (MSD) in school students as a risk factor for adult MSD: A review of the multiple factors affecting posture, comfort and health in classroom environments. Journal of the Human-Environment System, 7 (1): 1-9. https://doi.org/10.1618/jhes.7.1
20. Grooten, W. J.; Conradsson, D.; Äng, B. O.; Franzén, E., 2013: Is active sitting as active as we think? Ergonomics, 56 (8): 1304-1314. https://doi.org/10.1080/00140139.2013.812748
21. Guyton, A. C.; Hall, J. E., 2012: Medicinska fiziologija. Zagreb, Medicinska naklada, 285-301.
22. Gyi, D. E.; Porter, J. M., 1999: Interface pressure and the prediction of car seat discomfort. Applied Ergonomics, 30 (2): 99-107. https://doi.org/10.1016/S0003-6870(98)00018-0
23. Harrison, D. D.; Harrison, S. O.; Croft, A. C.; Harrison, D. E.; Troyanovich, S. J., 1999: Sitting biomechanics part I: review of the literature. Journal of Manipulative and Physiological Therapeutics, 22 (9): 594-609. https://doi.org/10.1016/S0161-4754(99)70020-5
24. Hartvigsen, J.; Hancock, M. J.; Kongsted, A.; Louw, Q.; Ferreira, M. L.; Genevay, S.; Hoy, D.; Karppinen, J.; Pransky, G.; Sieper, J.; Smeets, R. J., 2018: What low back pain is and why we need to pay attention. The Lancet, 391 (10137): 2356-2367. https://doi.org/10.1016/S0140-6736(18)30480-X
25. Hesse, M.; Krause, A. F.; Vogel, L.; Chamadiya, B.; Schilling, M.; Schack, T.; Jungeblut, T., 2017: A connected chair as part of a smart home environment. In: IEEE 14th International Conference on Wearable and Implantable Body Sensor Networks (BSN), May, pp. 47-50. https://doi.org/10.1109/BSN.2017.7936004
26. Hu, Q.; Tang, X.; Tang, W., 2020: A smart chair sitting posture recognition system using flex sensors and FPGA implemented artificial neural network. IEEE Sensors Journal, 20 (14): 8007-8016. https://doi.org/10.1109/jsen.2020.2980207
27. Iliev, B.; Domljan, D.; Vlaović, Z., 2019: Compliance of Preschool Chair Dimensions, Drvna industrija, 70 (2): 175-182. https://doi.org/10.5552/drvind.2019.1850
28. Ishaku, A. A.; Tranganidas, A.; Matúška, S.; Hudec, R.; McCutcheon, G.; Stankovic, L.; Gleskova, H., 2019: Flexible force sensors embedded in office chair for monitoring of sitting postures. In: IEEE International Conference on Flexible and Printable Sensors and Systems (FLEPS), July, pp. 1-3. https://doi.org/10.1109/FLEPS.2019.8792250
29. Jürgens, H. W., 1997: Seat pressure distribution. Collegium Antropologicum, 21 (2): 359-366.
30. Kim, W. L.; Lim, S. B., 2019: Smart chair cover for posture correction. International Journal of Emerging Trends in Engineering Research, 7 (8): 191-196. https://doi.org/10.30534/ijeter/2019/14782019
31. Kumar, R.; Bayliff, A.; De, D.; Evans, A.; Das, S. K.; Makos, M., 2016: Care-chair: Sedentary activities and behavior assessment with smart sensing on chair backrest. In: 2016 IEEE International Conference on Smart Computing (SMARTCOMP), May, pp. 1-8. https://doi.org/10.1109/SMARTCOMP.2016.7501682
32. Lee, C. C.; Saidy, L.; Fitri, 2019: Human Activity Recognition Based on Smart Chair. Sensors and Materials, 31 (5): 1589-1598. https://doi.org/10.18494/SAM.2019.2280
33. Liebenson, C., 2002: Are prolonged sitting postures bad for the back? Journal of Bodywork & Movement Thera-

pies, 3 (6): 151-153. https://doi.org/10.1054/jbmt.2002.0293
34. Lima, T. M.; Coelho, D. A., 2011: Prevention of musculoskeletal disorders (MSDs) in office work: A case study. Work, 39 (4): 397-408. https://doi.org/10.3233/WOR-2011-1190
35. Ma, C.; Li, W.; Gravina, R.; Cao, J.; Li, Q.; Fortino, G., 2017: Activity level assessment using a smart cushion for people with a sedentary lifestyle. Sensors, 17 (10): 2269. https://doi.org/10.3390/s17102269
36. Mizumoto, T.; Otoda, Y.; Nakajima, C.; Kohana, M.; Uenishi, M.; Yasumoto, K.; Arakawa, Y., 2020: Design and Implementation of Sensor-Embedded Chair for Continuous Sitting Posture Recognition. IEICE Transactions on Information and Systems, 103 (5): 1067-1077. https://doi.org/10.1587/transinf.2019EDP7226
37. Owen, N.; Bauman, A.; Brown, W., 2009: Too much sitting: A novel and important predictor of chronic disease risk? British Journal of Sports Medicine, 43 (2): 81-83. http://dx.doi.org/10.1136/bjsm.2008.055269
38. Park, M.; Song, Y.; Lee, J.; Paek, J., 2016: Design and implementation of a smart chair system for iot. In: International Conference on Information and Communication Technology Convergence (ICTC), October, pp. 1200-1203. https://doi.org/10.1109/ICTC.2016.7763406
39. Parvez, M. S.; Rahman, A.; Tasnim, N., 2019: Ergonomic mismatch between students anthropometry and university classroom furniture. Theoretical Issues in Ergonomics Science, 20 (5): 603-631. https://doi.org/10.1080/1463922X.2019.1617909
40. Prueksanusak, B.; Rujivipatand, P.; Wongpatikaseree, K., 2019: An ergonomic chair with Internet of thing technology using SVM. In: 4th Technology Innovation Management and Engineering Science International Conference (TIMES-iCON), December, pp. 1-5. https://doi.org/10.1109/TIMES-iCON47539.2019.9024488
41. Ragan, R.; Kernozek, T. W.; Bidar, M.; Matheson, J. W., 2002: Seat-interface pressures on various thicknesses of foam wheelchair cushions: a finite modeling approach. Archives of Physical Medicine and Rehabilitation, 83 (6): 872-875. https://doi.org/10.1053/apmr.2002.32677
42. Ribeiro, B.; Pereira, H.; Almeida, R.; Ferreira, A.; Martins, L.; Quaresma, C.; Vieira, P., 2015: Optimization of sitting posture classification based on user identification. In: IEEE 4th Portuguese Meeting on Bioengineering (ENBENG), February, pp. 1-6. https://doi.org/10.1109/ENBENG.2015.7088853
43. Scena, S.; Steindler, R., 2008: Methods for sitting posture evaluation: Static posture and applications. Strain, 44 (6): 423-428. https://doi.org/10.1111/j.1475-1305.2007.00334.x
44. Schwartz, B.; Kapellusch, J. M.; Schrempf, A.; Probst, K.; Haller, M.; Baca, A., 2016: Effect of a novel two-desk sit-to-stand workplace (ACTIVE OFFICE) on sitting time, performance and physiological parameters: protocol for a randomized control trial. BMC Public Health, 16 (1): 1-10. https://doi.org/10.1186/s12889-016-3271-y
45. Sifuentes, E.; Gonzalez-Landaeta, R.; Cota-Ruiz, J.; Reverter, F., 2019: Seat occupancy detection based on a low-power microcontroller and a single FSR. Sensors, 19 (3): 699. https://doi.org/10.3390/s19030699
46. Sodhi, S. S.; Kunwar, A. S.; Dhingra, K.; Suganya, G., 2017: Smart chair. In: International Conference on Inventive Computing and Informatics (ICICI), November, pp. 139-148.
47. Van Uffelen, J. G.; Wong, J.; Chau, J. Y.; Van Der Ploeg, H. P.; Riphagen, I.; Gilson, N. D.; Burton, N. W.; Healy, G. N.; Thorp, A. A.; Clark, B. K.; Gardiner, P. A., 2010: Occupational sitting and health risks: A systematic review. American Journal of Preventive Medicine, 39 (4): 379-388. https://doi.org/10.1016/j.amepre.2010.05.024
48. Vergara, M.; Page, Á., 2002: Relationship between comfort and back posture and mobility in sitting-posture. Applied Ergonomics, 33 (1): 1-8. https://doi.org/10.1016/S0003-6870(01)00056-4
49. Vlaović, Z.; Grbac, I.; Bublić, A., 2007: Utjecaj antropometrijskih veličina korisnika na tlakove pri sjedenju na uredskim stolicama. Drvna industrija, 58 (4): 183-191.
50. Vlaović, Z.; Grbac, I.; Gojak, I.; Sekovanić, I.; Salopek, M., 2012: The influence of participants' sex, mass, height and body mass index on pressures and comfort while sitting on office chairs. In: Proceedings of the 23rd international scientific conference, pp. 209-218.
51. Wahlström, J., 2005: Ergonomics, musculoskeletal disorders and computer work. Occupational Medicine, 55 (3): 168-176. https://doi.org/10.1093/occmed/kqi083
52. Zazula, D.; Kranjec, J.; Kranjec, P.; Cigale, B., 2015: Assessing blood pressure unobtrusively by smart chair. In: 38th International Convention on Information and Communication Technology, Electronics and Microelectronics (MIPRO), May, pp. 385-389. https://doi.org/10.1109/MIPRO.2015.7160300
53. Zemp, R.; Taylor, W. R.; Lorenzetti, S., 2016: Seat pan and backrest pressure distribution while sitting in office chairs. Applied Ergonomics, 53 (Part A), 1-9. https://doi.org/10.1016/j.apergo.2015.08.004
54. Zhang, Y.; Chen, Z.; Chen, W.; Li, H., 2019: Unobtrusive and continuous BCG-based human identification using a microbend fiber sensor. IEEE Access, 7: 72518-72527. https://doi.org/10.1109/ACCESS.2019.2919407
55. *** Hrvatska enciklopedija, 2021: http://www.enciklopedija.hr/Natuknica.aspx?ID=5527 (Accessed Nov 3, 2021).

Corresponding address:

DANIJELA DOMLJAN
University of Zagreb, Faculty of Forestry and Wood Technology, Svetošimunska cesta 23,
10000 Zagreb, CROATIA, e-mail: ddomljan@sumfak.unizg.hr

Nikolina Barlović[1], Anka Ozana Čavlović[1], Stjepan Pervan[1],
Miljenko Klarić[1], Silvana Prekrat[1], Nikola Španić[1]

Chemical Changes and Environmental Issues of Heat Treatment of Wood

Kemijske promjene i ekološka problematika toplinske obrade drva

REVIEW PAPER
Pregledni rad
Received – prispjelo: 27. 12. 2021.
Accepted – prihvaćeno: 23. 3. 2022.
UDK: 630*81; 674.04
https://doi.org/10.5552/drvind.2022.0005

ABSTRACT • *The paper gives an overview of chemical changes during heat treatment of wood and their influence on environment. Wood is one of the most used building materials because of its physical and technological properties. Various procedures improve its properties, and due to its environmental acceptability, heat treatment of wood is one of the most commonly used. Heat treatment causes changes in the cell walls and degradation of the main components of the wood structure (cellulose, hemicelluloses, lignin) and extractives. Hemicelluloses, as the most unstable components, are broken down first, followed by cellulose and finally lignin. Degradation results in a change in chemical composition and chemical reactions of colour change causing a technological problem because wood processing tends to make the colour as uniform as possible. The uniformity of colour and the desired colour tone are obtained by the process of steaming and thermal modification. The processing temperature is the most important factor that causes all the changes. Due to its wide use, need has arisen to investigate the ecological consequences of such a heat treatment process, as well as the impact of harmful substances and types of compounds released during the process and their toxicity.*

KEYWORDS: *heat treatment; heat-treated wood; wood components; colour change; ecology*

SAŽETAK • *U radu je naveden pregled kemijskih promjena tijekom procesa toplinske obrade drva te njihova utjecaja na okoliš. Zbog svojih fizikalnih i tehnoloških svojstava drvo je jedan od najčešće upotrebljavanih građevnih materijala. Njegova se svojstva poboljšavaju raznovrsnim postupcima, a toplinska je obrada drva zbog njezine ekološke prihvatljivosti jedna od najzastupljenijih metoda obrade. Pri toplinskoj obradi drva dolazi do promjena u staničnim stijenkama drva i do razgradnje njegovih glavnih gradivnih komponenata (celuloza, hemiceluloze i lignin) i ekstraktivnih tvari. Hemiceluloze se kao najnestabilnije komponenete razgrađuju prve, zatim slijedi razgradnja celuloze te, na kraju, lignina. Razgradnja rezultira promjenom kemijskog sastava drva i kemijskim reakcijama promjene boje, što je tehnološki problem jer se pri preradi drva teži tome da boja bude što ujednačenija. Stoga se ujednačavanje boje i željeni ton nastoje postići procesom parenja i pregrijavanja drva. Najvažniji činitelj koji uzrokuje sve promjene jest temperatura obrade drva. Zbog vrlo česte primjene toplinske obrade drva nametnula se potreba za istraživanjem ekoloških posljedica tog postupka, pri čemu se istražuje i utjecaj nusprodukata i vrsta spojeva koji se oslobađaju za vrijeme tog procesa, kao i toksičnost oslobođenih spojeva.*

KLJUČNE RIJEČI: *obrada drva toplinom; toplinski obrađeno drvo; drvne komponente; promjena boje drva; ekologija*

[1] Authors are researchers at University of Zagreb, Faculty of Forestry and Wood Technology, Zagreb, Croatia.

1 INTRODUCTION
1. UVOD

Wood is one of the most common construction materials with very good aesthetic, acoustic, thermal and mechanical properties; but with some disadvantages, such as dimensional anisotropic instability due to hygroscopicity and low durability. In order to improve these properties, heat treatment of wood is performed, which due to its environmental acceptability has become a better option compared to chemical modification (which is also very commonly used). Heat treatment of wood is a process in which the chemical structure of cell walls changes only in the presence of heat, pressure and moisture, in an oxygen-poor environment, without the addition of chemicals. When the structure is modified, there are changes such as reduced affinity for water, improved dimensional stability, greater resistance to biodegradation, uniform changes in colour to darker tones. At the same time there are negative changes such as reduced mechanical properties, the appearance of cracks and light induced discoloration. The process consists of drying, steaming and thermal modification. Prolonged thermal modification process increases dimensional stability and durability of wood, but at the same time reduces density and mechanical properties (except hardness). That results in brittleness and increased cracking. By prolonging the duration of process and due to chemical changes, the colour of the wood also changes. The observed changes in the structure of cell walls can mainly be attributed to the degradation of hemicelluloses because they are thermally less stable than cellulose, while lignin decomposes over a broad range of temperatures. The occurrence of colour changes and its chemistry is a very complex phenomenon and has been researched for a long time. In heat treatment, drying is used to prevent discoloration, while in the case of steaming and thermal modification, changes are deliberately induced, especially in species with false heartwood. Prolonged exposure to heat darkens the wood (which is often the aim) or equalizes the colour of the false heartwood and the surrounding wood material. With some types of wood, steaming can cause side effects such as reduced strength or appearance of cracks, and in that case cooking treatment is applied (Pervan *et al*., 2008).

In general, heat treatment of wood can be defined as a process that improves its current properties or alters the wood in such a way that it gains new properties. At the end of its life, such wood should not represent a danger to the environment greater than unmodified wood (Hill, 2006). Treated wood should be non-toxic and should not emit any hazardous substances during processing or in later stages of use. Due to the increasing use, there is a need to research the impact of harmful substances from such processes on the environment and ecology in general.

2 CHANGES AND DEGRADATION OF MAIN CHEMICAL COMPONENTS
2. PROMJENE I RAZGRADNJA GLAVNIH KEMIJSKIH KOMPONENATA

Heat treatment causes changes in the cell wall polymers structure, influencing their properties and it also directly affects the chemical degradation of wood, *i.e.* the degradation of its main components (hemicelluloses, cellulose, lignin) and extractives (Figure 1). Chemical changes caused by heat depend on the duration and temperature of the treatment, where temperature is the main factor (Bourgois *et al*., 1989). At temperatures between 20 and 100 ºC, the wood is dried, starting with the loss of free water and ending with the loss of bound water until desired moisture content (MC)

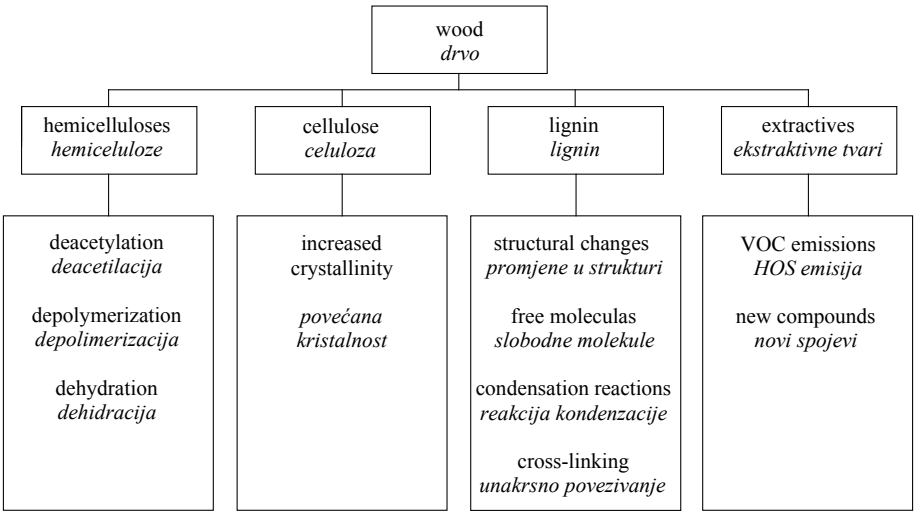

Figure 1 Chemical changes occurring in the main components of wood due to heat treatment (Esteves and Pereira, 2009)
Slika 1. Kemijske promjene glavnih komponenata drva prouzročene toplinskom obradom (Esteves and Pereira, 2009.)

is achieved. At 180 to 250 ºC, which is commonly used for heat treatment, wood undergoes major chemical transformations, and at temperatures above 250 ºC the charring process begins with the formation of CO_2 and other pyrolysis products (Esteves and Pereira, 2009).

Kubovský *et al*. (2020) performed thermal modification of wood at temperatures from 160 to 210 °C and concluded that the higher the processing temperature, the better the durability, stability and biological properties of wood became (except for the mechanical properties that are lowered in such conditions). FT-IR analysis and HPLC revealed that heat treatment leads to an increase in the number of carboxyl groups in lignin with splitting of aliphatic side chains and demethoxylation. Degradation of hemicelluloses results in deacetylation, and the acetic acid released catalyses the hydrolysis of polysaccharide chains. This process is more visible at a temperature of 180 °C, which leads to a decrease in molecular weight and an increase in polydispersity. In addition to the splitting of polysaccharide chains, crosslinking reactions take place at 210 °C, with an increase in molecular weight and polydispersity. Fengel and Wegener (1984) state that the hemicelluloses are the most sensitive of the structural components to thermal degradation, as they are the first to degrade at temperatures of 160 to 260 °C. The reason for this is their low molecular weight and branched structure, which helps faster degradation compared to other components present in wood. However, Funaoka *et al*. (1990) observed that the degradation of hemicelluloses begins as early as 100 °C, with the cellulose and lignin contents remaining constant up to 150 °C. Degradation of cellulose results in reduction of hydroxyl groups and the formation of O-acetyl groups. By subsequently creating cross-links between the wood fibres, the wood becomes more hydrophobic. At the same time, cellulose is degraded to form acetic and formic acid, and the lignin ratio increases as extracted substances from hemicelluloses and cellulose bind to it (Alén *et al*., 1996; Gailliot, 1998). The crystallinity of cellulose is increased by thermal modification up to 200 °C due to the degradation of its amorphous part, which is not only related to temperature but also to the duration of heat treatment, and results in reduced availability of hydroxyl groups to water molecules (Wikberg and Maunu, 2004; Yildiz and Gümüskaya, 2007). Mitsui *et al*. (2008) suggested that hydroxyl groups in cellulose degrade in the following order: amorphous, semi-crystalline, and crystalline regions. Acetic and formic acid, formed during the heat treatment, increase the hydrolysis of hemicelluloses and cellulose, while the degree of polymerization of polysaccharides decreases (Kačíková *et al*., 2013; Nuopponen *et al*., 2004). Degradation of lignin is visible at lower temperatures but takes place at a lower rate than other polysaccharides, while at higher temperatures there is a condensation reaction and an increase in molecular weight. In a study conducted by Bourgois and Guyonnet (1988) on maritime pine (*Pinus pinaster*), the results showed that lignin content at the same temperature increased when longer process duration was applied. The same results were reported for other species by Zaman *et al*. (2000) and Esteves *et al*. (2008b). Kotilainen (2000) and Manninen *et al*. (2002) conducted a research on heat-treated hornbeam (*Carpinus betulus* L.) and Turkish fir (*Abies bornmuelleriana* Mattf.), where the contents of hemicelluloses significantly decreased with increasing temperature and duration of treatment. The reduction in hemicelluloses content was found to be greater than in cellulose content. A significant reduction in hemicelluloses content began at temperatures above 180 °C. Due to the structural heterogeneity of hemicelluloses, it is difficult to detect their behaviour under the influence of heat. Xylan (pentosan) is the most reactive wood hemicellulose, and pentosans are generally very sensitive to degradation and dehydration reactions. For example, the content of pentosan in pine wood treated for 7 hours at 130 °C decreased from 11 % to 9.1 % (Potutkin and Shirayena, 1975). As stated, the cellulose content was reduced compared to the control sample, but to a lesser extent compared to hemicelluloses. The largest and the smallest changes in cellulose content in all heat treatments were found at 170 °C for 4 hours and at 210 °C for 12 hours (Tumen *et al*., 2010). By increasing the temperature above 200 °C, thermal degradation of cellulose and the formation of volatile products take place rapidly (Manninen, 2002; Fengel and Wegener, 1989). Kotilainen (2002) concluded that the most intensive thermal degradation takes place in the temperature range from 200 °C to 260 °C. The lower thermal stability of hemicelluloses compared to cellulose is usually explained by a lack of crystallinity.

Changes in cell walls and individual chemical components of wood also lead to changes such as discoloration. Pervan *et al*. (2006) and Koch (2008) state that it is one of the most common phenomena that occurs during steaming and drying of wood. It is assumed that the main factors involved in the chemical reactions are oxidation and condensation of phenolic compounds (Wengert, 1990), but colour changes can also be caused by hydrolysis, although in many cases the reasons are unknown. Investigating the influence of hemicelluloses, lignin and extractives on the colour, Sundqvist and Moren (2002) found that extractives are involved in the formation of colour during hydrothermal wood processing. This was also proven by Wiberg (1996) in his study of Scots pine (*Pinus sylvestris*) and Norway spruce (*Picea abies*). The results showed that during the drying process the extractives move towards the

surface, making it redder, while the substances that give a yellow colour remain inside. The above authors conclude that this colour change is due to the concentration of low molecular weight carbohydrates and nitrogen on the surface during wood drying. Similar results were obtained by Sandoval-Toress *et al*. (2012) for vacuum-dried samples of oak (*Quercus robur* L.). They concluded that saturation increases with increasing temperature and that the yellow hue is increased by the thermal effect, with red hue associated with extractives. Colour changes were measured on the surface because substances such as sugars, phenols, antioxidants and others move from the centre to the surface layer of wood by evaporating water and are retained there. According to White and Dietenberger (2001), heat darkening of wood is caused by thermal degradation of hemicelluloses and lignin and can start at temperatures below 65 °C (depending on wood pH, moisture content, heating medium and exposure period and wood type). Kosikova´ *et al*. (1999) used ^{13}C CP MAS NMR (carbon cross polarization magic angle spinning nuclear magnetic resonance) spectroscopy to characterise structural changes in cell wall polymers during drying and determined partial depolymerisation of lignin and changes in amorphous and crystalline parts of cellulose. This happened when wood was treated with superheated steam at a temperature of 135 °C, which also affected the colour change. Pervan *et al.* (2008) state that the heating is known to reduce sapwood brightness (in all species), with varying intensity, depending on the humidity, temperature and duration of the process. The influence of the cooking process on the colour change of walnut was studied by Charrier *et al*. (1998). The colour of sapwood changed in parallel with the duration of the process, with the decrease in the value of brightness following the increase of the value of the red component. Brauner and Conway (1964) also studied the colour change in walnut and stated that the black walnut (*Juglans nigra*) sapwood changes colour after 4 to 6 hours of steaming at 100 to 120 ° C. In this particular case the darkening was uniform in width and depth. Gray (1961); Hon (1981); Haluk *et al*. (1991); Klumpers *et al*. (1994); Abe *et al*. (1994); Hon and Shiraishi (2000); White and Dietenberger (2001); Sundqvist (2002); Alén *et al*. (2002); Charrier *et al*. (2002); Koch *et al*. (2003); Stenudd (2004); Thompson *et al*. (2005); Rowell (2006) suggest that the main colour change reactions due to wood steaming are oxidation, hydrolysis, polymerization of phenolic compounds, enzymatic reactions, and thermal degradation of lignin and hemicelluloses.

3 ENVIRONMENTAL ISSUES
3. EKOLOŠKA PROBLEMATIKA

The increasing use of heat-treated materials has made it necessary to investigate the impact of harmful substances of such treatments on the environment, especially on the possible formation of ozone in the lower atmosphere or tropospheric ozone that adversely affects humans, animals and plants. The toxicity of harmful substances was studied, and the types of compounds released during the process were listed. Worldwide standards set strict limits on emissions of volatile organic compounds that occur during wood drying (Zwick *et al*., 1997). In Croatia, these restrictions are currently prescribed by the Regulation on limit values for air pollutants from stationary sources [NN 42/2021] and the Regulation on limit values for exposure to hazardous substances at work and on biological limit values [NN 13/2009]. Exposure limit values are average concentrations of substances (gases, vapours, aerosols, dusts) in the air at the workplace in the breathing zone of workers at a temperature of 20 °C and air pressure of 1013 mbar, which according to current knowledge do not cause damage to health in everyday eight-hour work time. Table 1 shows the exposure limit values for substances that are most often produced by heat treatment of wood, the possible hazards they cause and their harmful effects.

Studies on volatile organic compounds (VOCs) in the atmosphere have shown that atmospheric chemistry

Table 1 Exposure limit values for harmful substances from heat treatment of wood [NN (42/2021)]
Tablica 1. Granične vrijednosti izloženosti štetnim tvarima zbog termičke obrade drva [NN 42/2021]

Substance *Tvar*	**Exposure limit values, mg/m³** *Granična vrijednost izloženosti,* mg/m³	**Hazards and harmful effects** *Opasnost i štetno djelovanje*
Acetaldehyde *acetaldehid*	90	Irritating / *nadražujuće* Extremely flammable / *vrlo zapaljivo* Carcinogenicity / *kancerogeno*
Formaldehyde *formaldehid*	2.5	Very toxic / *vrlo otrovno* Carcinogenicity / *kancerogeno*
Methanol/ *metanol*	260	Very toxic / *vrlo otrovno* Harmful to skin / *štetno djelovanje kroz kožu* Highly flammable / *lako zapaljivo*
Formic acid / *mravlja kiselina*	9	Corrosive / *nagrizajuće*
Acetic acid / *octena kiselina*	25	Corrosive / *nagrizajuće*

is complex and that their degradation and transformation reactions can occur in the gas and water phases (Grosjean *et al*., 1992; Faust, 1994). Organic extracts emitted during the wood drying process include terpenes, methanol, acetic acid, formaldehyde, resin acids and fatty acids (McDonald *et al*., 1999b). In conventional wood drying kiln, such compounds are released into the atmosphere, and the resulting blue haze and unpleasant odours can cause concern for the environment and in some cases health problems (Cronn *et al*., 1983). Harley and Cass (1994) indicate that some toxic compounds found in ambient air are formed in the atmosphere as oxidation products of other volatile organic compounds, and those oxidation products are, for example, ***α***-pinene, formaldehyde, acetone, pinonaldehyde, and glyoxal (Grosjean *et al*., 1992). Terpenes have also been found to react rapidly with ozone, hydroxyl or nitrate radicals to give various organic compounds. McDonald *et al*. (2002) conducted a research on pine and found that volatile components condense with water vapour during the vacuum drying process. Those VOCs were mainly monoterpenes, methanol, formaldehyde, furfural and diterpenes. Additionally, it was observed that the amount of oxygen and carbon suggest that it is necessary to reduce the concentration of organic compounds. Bicho *et al*. (1966) also found harmful substances such as formic, acetic and levulinic acid, furfural, hydroxymethyl-furfural, formaldehyde and acetaldehyde in the analysis of condensates at vacuum drying of ash, beech and oak. The analysis of condensate, obtained during the drying of California pine (*Pinus radiata*) in an experimental vacuum dryer, showed that the condensate contained 10 % monoterpenes, and alcoholic monoterpenes (endoborneol, ***α***-terpineol and 1,4-terpineol), methanol, acetic acid, formaldehyde, furfural and diterpenes were found as organic compounds. The values of BOD (a measure of the amount of oxygen required by bacteria to decompose organic components present in water/wastewater) and COD (chemical oxygen demand; i.e. the total measurement of all chemicals (organic and inorganic) in water/wastewater), for experimental condensate from vacuum kiln dryer indicate the fact that before the condensate is discharged, its treatment will be required in order to reduce the concentration of organic compounds (McDonald *et al*., 1999). According to Mayes and Oksanen (2002), VOC emissions from heat-treated wood are lower than from air-dried wood, as terpene emissions such as pinene, camphene and limonene during drying of untreated wood are higher than for treated wood. Similar results were obtained by Manninen *et al*. (2002), whose results show that VOC emissions from air-dried white pine (*Pinus sylvestris*) were about eight times higher than those of heat-treated wood and consisted of ***α***-pinene, 3-carnene, hexanal, 2-furancarboxaldehyde, acetic acid and 2-propanone. Peters *et al*. (2008) state that furfural and 5-methylfurfural are the main emission products from treated wood and Marutzky and Roffael (1977) conducted a study in which, by applying heat treatment independently of temperature, formaldehyde was formed due to the degradation of lignin and other hydrocarbons.

4 CONCLUSIONS
4. ZAKLJUČAK

Heat treatment is one of the most common wood treatments that results in changes in the structure of the cell walls, degradation of major components (hemicelluloses, cellulose and lignin) and extractives, and changes in chemical composition. The changes that occur due to heat treatment depend on the temperature and duration of treatment, and to a large extent on a number of external conditions due to which the results differ for the same wood species. Treated wood results in lower hygroscopicity with a positive effect on dimensional stability and durability, but very often with a negative effect on mechanical properties, which are reduced (except for hardness which causes an increase in brittleness). In the research on the degradation of the main chemical components of wood, most results showed that hemicelluloses are the most unstable components and they are the first to decompose due to their low molecular weight and branched structure. This is followed by cellulose, which is thermally more stable due to its crystallite structure. Lignin is more unstable at lower temperatures, while at higher temperatures there is an increase in molecular weight. The main components also affect the colour change, which is a common occurrence during thermal modification. The most common causes of discoloration are reactions of phenolic compounds and reactions and thermal decomposition of hemicelluloses and lignin. Although heat treatment is the most environmentally acceptable process, because it is performed under controlled conditions in the presence of heat and moisture without chemical additives, many volatile organic compounds (VOCs) are formed and released, such as alcohols, resins, terpenes, formic and acetic acid, resins and fatty acids, aldehydes, furfurals. Due to the increased use of heat-treated wood and compounds that are formed in the atmosphere during the process, it is necessary to investigate its impact on ecology. It should be emphasized that after heat treatment wood is environmentally acceptable, which means that it is not toxic and that at the end of its life cycle it does not pose a danger to the environment.

Acknowledgements – Zahvala

The article was published as part of the project "Development of innovative products from modified Slavonian oak" by Spin Valis d.d. and partner Univer-

sity of Zagreb, Faculty of Forestry and Wood Technology. The total value of the project is HRK 55,064,343.84, while the amount co-financed by the EU is HRK 23,941,527.32. The project was co-financed by the European Union from the Operational Program Competitiveness and Cohesion 2014-2020, European Fund for Regional Development.

5 REFERENCES
5. LITERATURA

1. Abe, Z.; Oda, K.; Matsumura, J., 1994: The color change of sugi (*Criptomeria japonica*) heartwood from reddish brown to black, 1: The color-change and its causes. Mokuzai Gakkaishi, 40 (10): 1119-1125.
2. Alén, R.; Kuoppala, E.; Oesch, P., 1996: Formation of the main degradation compounds groups from wood and its components during pyrolysis. The Journal of Analytical and Applied Pyrolysis, 36: 137-148. https://doi.org/10.1016/0165-2370(96)00932-1
3. Alén, R.; Kotilainen, R.; Zaman, A., 2002: Thermochemical behavior of Norway spruce (*Picea abies*) at 180-225 ºC. Wood Science and Technology, 36: 163-171. https://doi.org/10.1007/s00226-001-0133-1
4. Bicho, P. A.; Chen, T.; Avramidis, S.; Zwick, R. L.; Breuil, C.; Saddler, J. N., 1996: Characterisation and treatment of condensates generated from softwoods that have been radio-frequency/vacuum kiln dried. Forest Products Journal, 46 (10): 51-56.
5. Bourgois, J.; Guyonnet, R., 1988: Characterisation and analysis of torrefied wood. Wood Science and Technology, 22: 143-155.
6. Bourgois, J.; Bartholin, M.; Guyonnet, R., 1989: Thermal treatment of wood: Analysis of the obtained product. Wood Science and Technology, 23: 303-310.
7. Brauner, A.; Conway, E. M., 1964: Steaming walnut for color. Forest Products Journal, 14: 525-527.
8. Charrier, B.; Charrier, F.; Janin, G., 1998: European walnut wood classification. In individual progress report. Walnut basic research for agroforestry and industry: network and standards, pp. 8.
9. Charrier, B.; Charrier, F.; Janin, G.; Kamdem, P.; Irmouli, M.; Goncalez, J., 2002: Study of industrial boiling process on walnut colour: experimental study under industrial conditions. Holz als Roh- und Werkstoff, 60: 259-264.
10. Cronn, D. R.; Truitt, S. G.; Campbell, M. J., 1983: Chemical characterisation of plywood veneer dryer emissions. Atmospheric Environment, 7: 201-211. https://doi.org/10.1016/0004-6981(83)90034-3
11. Esteves, B.; Graça, J.; Pereira, H., 2008b: Extractive composition and summative chemical analysis of thermally treated eucalypt wood. Holzforschung, 62: 344-351. https://doi.org/10.1515/HF.2008.057
12. Esteves, B. M.; Pereira, H. M., 2009: Wood modification by heat treatment: a review. *BioResources*, 4 (1): 370-404.
13. Faust, B. C., 1994: Photochemistry of clouds, fogs and aerosols. Environmental Science and Technology, 28 (5): 217A-222A. https://doi.org/10.1021/es00054a001
14. Fengel, D.; Wegener, G., 1984: Wood: Chemistry, ultrastructure, reactions. Walter de Gruyter, Berlin and New York, pp. 613. https://doi.org/10.1002/pol.1985.130231112
15. Fengel, D.; Wegener, G., 1989: Wood: Chemistry, ultrastructure, reactions, 2nd ed. Walter de Gruyter, Berlin and New York, pp. 613.
16. Funaoka, M.; Kako, T.; Abe, I., 1990: Condensation of lignin during heating of wood. Wood Science and Technology, 24: 277-288.
17. Gailliot, F. P., 1998: Extraction and Product Capture in Natural Product Isolation, Cannell. Humana Press, Totowa, pp. 59-68.
18. Gray, V. R., 1961: The color of wood and its changes. Journal of the Institute of Wood Science, 8: 35-57.
19. Grosjean, D.; Williams, E. L.; Seinfeld, J. H., 1992: Atmospheric oxidation of selected terpenes and related carbonyls: gas phase carbonyl products. Environmental Science and Technology, 26 (8): 1526-1533. https://doi.org/10.1021/es00032a005
20. Haluk, J. P.; Schoegel, F.; Metche, M., 1991: Chimie de la couleur du bois. Etude comparative des constituants polyphe´noliques dans le cheˆne sain et le cheˆne colore. Holzforschung, 45 (6): 437-444.
21. Harley, R. A.; Cass, G. R., 1994: Modelling the concentration of gas-phase organic air pollutants: Direct emissions and atmospheric formation. Environmental Science and Technology, 28 (1): 88-98. http://dx.doi.org/10.1021/es00050a013
22. Hill, C., 2006: Wood Modification-Chemical, Thermal and Other Processes, Wiley Series in Renewable Resources, John Wiley & Sons, Ldt.
23. Hon, D. N. S., 1981: Photochemical degradation of lignocellulosic materials. In: Development in Polymer Degradation-3, N. Grassie (ed.). Applied Science Publishers Ltd., London, UK.
24. Hon, D. N. S.; Shiraishi, N., 2000: Wood and cellulosic chemistry. Marcel Dekker, New York, pp. 1020.
25. Kačíková, D.; Kačík, F.; Cabalova, I.; Durković, J., 2013: Effects of thermal treatment on chemical, mechanical and colour traits in Norway spruce wood. Bioresource Technology, 144: 669-674. https://doi.org/10.1016/j.biortech.2013.06.110
26. Klumpers, J.; Scalbert, A.; Janin, G., 1994: Ellagitannins in European oak wood: polymerization during wood ageing. Phytochemistry, 36: 1249-1252. https://doi.org/10.1016/S0031-9422(00)89646-6
27. Koch, G.; Puls, J.; Bauch, J., 2003: Topochemical characterisation of phenolic extractives in discolored beechwood (*Fagus sylvatica* L.). Holzforschung, 57: 339-345. https://doi.org/10.1515/HF.2003.051
28. Koch, G., 2008: Discoloration of wood in the living tree and during processing. Conference COST E53, 29-30 October 2008, Delft, The Netherlands.
29. Kosikova´, B.; Hricovı´ni, M.; Consentino, C., 1999: Interaction of lignin and polysaccharides in beech wood (*Fagus sylvatica*) during drying process. Wood Science and Technology, 33: 373-380. https://doi.org/10.1007/s002260050123
30. Kotilainen, R., 2000: Chemical changes in wood during heating at 150-260 °C. PhD Thesis, Jyvaskyla University, Research report 80, Finland. https://doi.org/10.3390/polym12020485
31. Kubovský, I.; Kačiková, D.; Kačik, F., 2020: Structural Changes of Oak Wood Main Components Caused by Thermal Modification. Polymers, 12 (2): 485. https://doi.org/10.3390/polym12020485
32. Manninen, A.; Pasanen, P.; Holopainen, J., 2002: Comparing the VOC emissions between air-dried and heat-treated Scots pine wood. Atmosphere Environment, 36: 1763-1768. https://doi.org/10.1016/S1352-2310(02)00152-8

33. Marutzky, V. R.; Roffael, E., 1977: On the formaldehyde liberation by drying of wood chips. Holzforschung, 31: 8-12.
34. Mayes, D.; Oksanen, O., 2002: Thermowood Handbook. Thermowood, FinnForest, Stora.
35. McDonald, A. G.; Gifford, J. S.; Dare, P. H.; Steward, D., 1999: Characterisation of the condensate generated from vacuum-drying of radiata pine wood. Holz als Roh- und Werkstoff, 57: 251-258. https://doi.org/10.1007/s001070050052
36. McDonald, A. G.; Steward, D.; Franich, R. A., 1999b: Monoterpene composition of radiata pine (*Pinus radiata* D. Don) sapwood from a 13 year old progeny trial. Holz als Roh- und Werkstoff, 57: 301-302. https://doi.org/10.1007/s001070050063
37. McDonald, A. G.; Dare, P. H.; Gifford, J. S.; Steward, D.; Riley, S., 2002: Assessment of air emissions from industrial kiln drying of *Pinus radiata* wood. Holz als Roh- und Werkstoff, 60: 181-190. https://doi.org/10.1007/s00107-002-0293-1
38. Mitsui, K.; Inagaki, T.; Tsuchikawa, S., 2008: Monitoring of hydroxyl groups in wood during heat treatment using NIR spectroscopy. Biomacromolecules, 9: 286-288. https://doi.org/10.1021/bm7008069
39. Nuopponen, M.; Vuorinen, T.; Jamsä, S.; Viitaniemi, P., 2004: Thermal modifications in softwood studied by FT-IR and UV resonance Raman spectroscopies. Journal of Wood Chemistry and Technology, 24: 13-26. https://doi.org/10.1081/WCT-120035941
40. Pervan, S.; Antonović, A.; Humar, M.; Straže, A.; Gorišek, Ž., 2006: Kemizam promjene boje parene i kuhane orahovine (*Juglans regia* L.). Drvna industrija, 57 (3): 127-133.
41. Pervan, S.; Draščić, G.; Antonović, A., 2008: Ekološka problematika nusprodukata hidrotermičkih procesa obrade drva. Drvna industrija, 59 (1): 29-34.
42. Peters, J.; Fischer, K.; Fisher, S., 2008: Characterization of emissions from thermally modified wood and their reduction by chemical treatment. BioResources, 3 (2), 491-502.
43. Potutkin, G.; Shirayena, L., 1975: Changes in chemical components of wood during high temperature drying. Izv. Vyssh. Uchebn. Zaved. Lesn. Zh., 18: 127-129.
44. Rowell, M. R., 2006: Chemical modification of wood: a short review. Wood Material Science & Engineering, 1: 29-33. https://doi.org/10.1080/17480270600670923
45. Sandoval-Torres, S.; Jomaa, J.; Marc, F.; Puiggali, J. R., 2012: Colour alteration and chemistry changes in oak wood (*Quercus pedunculata* Ehrh) during plain vacuum drying. Wood Science and Technology, 46: 177-191. https://doi.org/10.1007/s00226-010-0381-z
46. Stenudd, S., 2004: Color response in Silver birch during kiln-drying. Forest Product Journal, 54 (6): 31-36.
47. Sundqvis, B., 2002: Color response of scots pine (*Pinus sylvestris*), Norway spruce (*Picea abies*) and birch (*Betula pubescens*) subjected to heat treatment in capillary phase. Holz als Roh- und Werkst, 60: 106-114. https://doi.org/10.1007/s00107-001-0273-x
48. Sundqvist, B.; Morén, T., 2002: The influence of wood polymers and extractives on wood colour induced by hydrothermal treatment. Holz als Roh- und Werkst, 60: 375-376. https://doi.org/10.1007/s00107-002-0320-2
49. Thompson, D. W.; Kozak, R. A.; Evans, P. D., 2005: Thermal modification of color in red alder veneer. I. effects of temperature, heating time and wood type. Wood Fiber Science, 37 (4): 653-661.
50. Tumen, I.; Aydemir, D.; Gunduz, G.; Birol, U.; Hakan, C., 2010: Changes in the chemical structure of thermally treated wood. *BioResources,* 5 (3): 1936-1944. https://doi.org/10.15376/biores.5.3.1936-1944
51. Wengert, E. M., 1990: Chemical stain and stain control in hardwood lumber drying. In: Drying softwood and hardwood lumber for quality and profit, M. P. Hamel (ed.). For. Prod. Soc., USA, pp. 81-84.
52. White, R. H.; Dietenberger, M. A., 2001: Wood products: thermal degradation and fire. Encyclopedia of Materials: Science and Technology, pp. 9712-9716. https://doi.org/10.1016/B0-08-043152-6/01763-0
53. Wiberg, P., 1996: Color changes of Scots pine and Norway spruce. Holz als Roh- und Werkst, 54: 349-354.
54. Wikberg, H.; Maunu, S. L., 2004: Characterization of thermally modified hard and softwoods by 13C COMAS NMR. Carbohydrate Polymers, 58: 461-466. https://doi.org/10.1016/j.carbpol.2004.08.008
55. Yildiz, S.; Gümüskaya, E., 2007: The effects of thermal modification on crystalline structure of cellulose in soft and hardwood. Building and Environment, 42: 62-67. https://doi.org/10.1016/j.buildenv.2005.07.009
56. Zaman, A.; Alén, R.; Kotilainen, R., 2000: Heat behavior of *Pinus sylvestris* and *Betula pendula* at 200-230 ºC. Wood Fiber Science, 32 (2): 138-143.
57. Zwick, R. L.; Bicho, P. A.; Avramidis, S.; Chen, T.; Breuil, C.; Saddler, J. N., 1997: Effluent from radio frequency/vacuum drying of softwoods: Characterization and treatment. WDKA 53-63.
58. *** Official Gazette, 2009: Ordinance on limits for exposure to hazardous substances at work and on biological limit values. Zagreb, Narodne novine JSC, NN 13/2009 (in Croatian).
59. ***Official Gazette, 2021: Decree on limit values of pollutant emissions into air from stationary sources. Zagreb, Narodne novine JSC, NN 42/2021 (in Croatian).

Corresponding address:

NIKOLA ŠPANIĆ
University of Zagreb, Faculty of Forestry and Wood Technology, Svetošimunska cesta 23, 10000 Zagreb, CROATIA, e-mail: nspanic@sumfak.unizg.hr

Upute autorima

Opće odredbe

Časopis *Drvna industrija* objavljuje znanstvene radove (izvorne znanstvene radove, pregledne radove, prethodna priopćenja), stručne radove, izlaganja sa savjetovanja, stručne obavijesti, bibliografske radove, preglede te ostale priloge s područja biologije, kemije, fizike i tehnologije drva, pulpe i papira te drvnih proizvoda, uključujući i proizvodnu, upravljačku i tržišnu problematiku u drvnoj industriji.

Predaja rukopisa podrazumijeva uvjet da rad nije već predan negdje drugdje radi objavljivanja ili da nije već objavljen (osim sažetka, dijelova objavljenih predavanja ili magistarskih radova odnosno disertacija, što mora biti navedeno u napomeni) te da su objavljivanje odobrili svi suautori (ako rad ima više autora) i ovlaštene osobe ustanove u kojoj je istraživanje provedeno. Cjelokupni sadržaj Drvne industrije dostupan je za skidanje s interneta, tiskanje, daljnju distribuciju, čitanje i ponovno korištenje bez ograničenja sve dok se naznače autor(i) i originalni izvor prema Creative Commons Attribution 4.0 International License (CC BY). Autor(i) zadržavaju izdavačka prava bez ograničenja.

Znanstveni i stručni radovi objavljuju se na engleskom jeziku, uz sažetak na hrvatskome. Također, naslov, podnaslovi i svi važni rezultati trebaju biti napisani dvojezično. Uredništvo osigurava inozemnim autorima prijevod na hrvatski. Ostali se članci uglavnom objavljuju na hrvatskome. Znanstveni i stručni radovi podliježu temeljitoj recenziji najmanje dvaju recenzenata. Izbor recenzenata i odluku o klasifikaciji i prihvaćanju članka (prema preporukama recenzenata) donosi Urednički odbor.

Svi prilozi podvrgavaju se jezičnoj obradi. Urednici će od autora zahtijevati da tekst prilagode preporukama recenzenata i lektora, te zadržavaju i pravo da predlože skraćivanje ili poboljšanje teksta. Autori su potpuno odgovorni za svoje priloge. Podrazumijeva se da je autor pribavio dozvolu za objavljivanje dijelova teksta što su već negdje objavljeni te da objavljivanje članka ne ugrožava prava pojedinca ili pravne osobe. Radovi moraju izvještavati o istinitim znanstvenim ili tehničkim postignućima. Autori su odgovorni za terminološku i metrološku usklađenost svojih priloga. Radovi se šalju elektronički putem poveznice http://journal.sdewes.org/drvind

Upute

Predani radovi smiju sadržavati najviše 15 jednostrano pisanih A4 listova s dvostrukim proredom (30 redaka na stranici), uključujući i tablice, slike te popis literature, dodatke i ostale priloge. Dulje je članke preporučljivo podijeliti na dva ili više nastavaka. Tekst treba biti u *doc formatu*, u potpunosti napisan fontom *Times New Roman* (tekst, grafikoni i slike), normalnim stilom, bez dodatnog uređenja teksta.

Prva stranica poslanog rada treba sadržavati puni naslov, ime(na) i prezime(na) autora, podatke o zaposlenju autora (ustanova, grad i država) te sažetak s ključnim riječima (duljina sažetka približno 1/2 stranice A4).

Posljednja stranica treba sadržavati titule, zanimanje, zvanje i adresu (svakog) autora, s naznakom osobe s kojom će Uredništvo biti u vezi.

Znanstveni i stručni radovi moraju biti sažeti i precizni. Osnovna poglavlja trebaju biti označena odgovarajućim podnaslovima. Napomene se ispisuju na dnu pripadajuće stranice, a obrojčavaju se susljedno. One koje se odnose na naslov označuju se zvjezdicom, a ostale uzdignutim arapskim brojkama. Napomene koje se odnose na tablice pišu se ispod tablica, a označavaju se uzdignutim malim pisanim slovima, abecednim redom.

Latinska imena trebaju biti pisana kosim slovima (italicom), a ako je cijeli tekst pisan kosim slovima, latinska imena trebaju biti podcrtana.

U uvodu treba definirati problem i, koliko je moguće, predočiti granice postojećih spoznaja, tako da se čitateljima koji se ne bave područjem o kojemu je riječ omogući razumijevanje ciljeva rada.

Materijal i metode trebaju biti što preciznije opisane da omoguće drugim znanstvenicima ponavljanje pokusa. Glavni eksperimentalni podaci trebaju biti dvojezično navedeni.

Rezultati trebaju obuhvatiti samo materijal koji se izravno odnosi na predmet. Obvezatna je primjena metričkog sustava. Preporučuje se upotreba SI jedinica. Rjeđe rabljene fizikalne vrijednosti, simboli i jedinice trebaju biti objašnjeni pri njihovu prvom spominjanju u tekstu. Za pisanje formula valja se koristiti Equation Editorom (programom za pisanje formula u MS Wordu). Jedinice se pišu normalnim (uspravnim) slovima, a fizikalni simboli i faktori kosima (italicom).

Formule se susljedno obrojčavaju arapskim brojkama u zagradama, npr. (1) na kraju retka.

Broj slika mora biti ograničen samo na one koje su prijeko potrebne za objašnjenje teksta. Isti podaci ne smiju biti navedeni i u tablici i na slici. Slike i tablice trebaju biti zasebno obrojčane, arapskim brojkama, a u tekstu se na njih upućuje jasnim naznakama ("tablica 1" ili "slika 1"). Naslovi, zaglavlja, legende i sav ostali tekst u slikama i tablicama treba biti napisan hrvatskim i engleskim jezikom.

Slike je potrebno rasporediti na odgovarajuća mjesta u tekstu, trebaju biti izrađene u rezoluciji 600 dpi, crno-bijele (objavljivanje slika u koloru moguće je na zahtjev autora), formata jpg ili tiff, potpune i jasno razumljive bez pozivanja na tekst priloga.

Svi grafikoni i tablice izrađuju se kao crno-bijeli prilozi (osim na zahtjev). Tablice i grafikoni trebaju biti na svojim mjestima u tekstu te originalnog formata u kojemu su izrađeni radi naknadnog ubacivanja hrvatskog prijevoda. Ako ne postoji mogućnost za to, potrebno je poslati originalne dokumente u formatu u kojemu su napravljeni (*excel* ili *statistica* format).

Naslovi slika i crteža ne pišu se velikim tiskanim slovima. Crteži i grafikoni trebaju odgovarati stilu časopisa (fontovima i izgledu). Slova i brojke moraju biti dovoljno veliki da budu lako čitljivi nakon smanjenja širine slike ili tablice. Fotomikrografije moraju imati naznaku uvećanja, poželjno u mikrometrima. Uvećanje može biti dodatno naznačeno na kraju naslova slike, npr. "uvećanje 7500 : l".

Diskusija i zaključak mogu, ako autori žele, biti spojeni u jedan odjeljak. U tom tekstu treba objasniti rezultate s obzirom na problem postavljen u uvodu i u odnosu prema odgovarajućim zapažanjima autora ili drugih istraživača. Valja izbjegavati ponavljanje podataka već iznesenih u odjeljku *Rezultati*. Mogu se razmotriti naznake za daljnja istraživanja ili primjenu. Ako su rezultati i diskusija spojeni u isti odjeljak, zaključke je nužno napisati izdvojeno. Zahvale se navode na kraju rukopisa. Odgovarajuću literaturu treba citirati u tekstu, i to prema harvardskom sustavu (*ime – godina*), npr. (Bađun, 1965).

Nadalje, bibliografija mora biti navedena na kraju teksta, i to abecednim redom prezimena autora, s naslovima i potpunim navodima bibliografskih referenci. Popis literature mora biti selektivan, a svaka referenca na kraju mora imati naveden DOI broj, ako ga posjeduje (http://www.doi.org) (provjeriti na http://www.crossref.org).

Primjeri navođenja literature

Članci u časopisima: Prezime autora, inicijal(i) osobnog imena, godina: Naslov. Naziv časopisa, godište (ev. broj): stranice (od – do). Doi broj.

Primjer

Kärki, T., 2001: Variation of wood density and shrinkage in European aspen (*Populus tremula*). Holz als Roh- und Werkstoff, 59: 79-84. http://dx.doi.org/10.1007/s001070050479.

Knjige: Prezime autora, inicijal(i) osobnog imena, godina: Naslov. (ev. izdavač/editor): izdanje (ev. svezak). Mjesto izdanja, izdavač (ev. stranice od – do).

Primjeri

Krpan, J., 1970: Tehnologija furnira i ploča. Drugo izdanje. Zagreb, Tehnička knjiga.

Wilson, J. W.; Wellwood, R. W., 1965: Intra-increment chemical properties of certain western Canadian coniferous species. U: W. A. Cote, Jr. (Ed.): Cellular Ultrastructure of Woody Plants. Syracuse, N.Y., Syracuse Univ. Press, pp. 551- 559.

Ostale publikacije (brošure, studije itd.)

Müller, D., 1977: Beitrag zür Klassifizierung asiatischer Baumarten. Mitteilung der Bundesforschungsanstalt für Forstund Holzvvirt schaft Hamburg, Nr. 98. Hamburg: M. Wiederbusch.

Web stranice

***1997: "Guide to Punctuation" (online), University of Sussex, www.informatics.sussex.ac.uk/department/docs/punctuation/node 00.html. First published 1997 (pristupljeno 27. siječnja 2010).

Autoru se prije konačnog tiska šalje pdf rada. Rad je potrebno pažljivo pročitati, ispraviti te vratiti Uredništvu s listom ispravaka. Autori znanstvenih i stručnih radova besplatno dobivaju po jedan primjerak časopisa. Autoru svakog priloga također se dostavlja besplatan primjerak časopisa.

Dodatne informacije o načinu pisanja znanstvenih radova mogu se naći na web adresi:
www.ease.org.uk/publications/author-guidelines

Instructions for authors

General terms

The "Drvna industrija" ("Wood Industry") journal publishes scientific papers (original scientific papers, review papers, previous notes), professional papers, conference papers, professional information, bibliographical and survey articles and other contributions related to biology, chemistry, physics and technology of wood, pulp and paper and wood products, including production, management and marketing issues in the wood industry.

Submission of a paper implies that the work has not been submitted for publication elsewhere or published before (except in the form of an abstract or as part of a published lecture, review or thesis, in which case it must be stated in a footnote); that the publication is approved by all co-authors (if any) and by the authorities of the institution where the research has been carried out. The complete content of the journal *Drvna industrija* (Wood Industry) is available on the Internet permitting any users to download, print, further distribute, read and reuse it with no limits provided that the author(s) and the original source are identified in accordance with the Creative Commons Attribution 4.0 International License (CC BY). The authors retain their copyrights.

The scientific and professional papers shall be published in English with summary in Croatian. The titles, headings and all the relevant results shall be also presented bilingually. The Editor's Office shall provide the translation into Croatian for foreign authors. Other articles are generally published in Croatian. The scientific and professional papers will be subject to a thorough review by at least two selected referees. The Editorial Board shall make the choice of reviewers, as well as the decision about the classification of the paper and its acceptance (based on reviewers' recommendations).

All contributions are subject to proofreading. The editors will require authors to modify the text in the light of the recommendations made by reviewers and language advisers, and they reserve the right to suggest abbreviations and text improvements. Authors are fully responsible for the contents of their contributions. It shall be assumed that the author has obtained the permission for the reproduction of portions of text published elsewhere, and that the publication of the paper in question does not infringe upon any individual or corporate rights. Papers shall report on true scientific or technical achievement. Authors are responsible for the terminological and metrological consistency of their contributions. The contributions are to be submitted by the link http://journal.sdewes.org/drvind

Details

Papers submitted shall consist of no more than 15 single-sided DIN A-4 sheets of 30 double-spaced lines, including tables, figures and references, appendices and other supplements. Longer papers should be divided into two or more continuing series. The text should be written in doc format, fully written using Times New Roman font (text, graphs and figures), in normal style without additional text editing.

The first page of the paper submitted should contain full title, name(s) of author(s) with professional affiliation (institution, city and state), abstract with keywords (approx. 1/2 sheet DIN A4).

The last page should provide the full titles, posts and address(es) of each author with indication of the contact person for the Editor's Office.

Scientific and professional papers shall be precise and concise. The main chapters should be characterized by appropriate headings. Footnotes shall be placed at the bottom of the same page and consecutively numbered. Those relating to the title should be marked by an asterix, others by superscript Arabic numerals. Footnotes relating to the tables shall be printed under the table and marked by small letters in alphabetical order.

Latin names shall be printed in italics and underlined.

Introduction should define the problem and if possible the framework of existing knowledge, to ensure that readers not working in that particular field are able to understand author's intentions.

Materials and methods should be as precise as possible to enable other scientists to repeat the experiment. The main experimental data should be presented bilingually.

The results should involve only material pertinent to the subject. The metric system shall be used. SI units are recommended. Rarely used physical values, symbols and units should be explained at their first appearance in the text. Formulas should be written by using Equation Editor (program for writing formulas in MS Word). Units shall be written in normal (upright) letters, physical symbols and factors in italics. Formulas shall be consecutively numbered with Arabic numerals in parenthesis (e.g. (1)) at the end of the line.

The number of figures shall be limited to those absolutely necessary for clarification of the text. The same information must not be presented in both a table and a figure. Figures and tables should be numbered separately with Arabic numerals, and should be referred to in the text with clear remarks ("Table 1" or "Figure 1"). Titles, headings, legends and all the other text in figures and tables should be written in both Croatian and English.

Figures should be inserted into the text. They should be of 600 dpi resolution, black and white (color photographs only on request), in jpg or tiff format, completely clear and understandable without reference to the text of the contribution.

All graphs and tables shall be black and white (unless requested otherwise). Tables and graphs should be inserted into the text in their original format in order to insert them subsequently into the Croatian version. If this is not possible, original document should be sent in the format in which it was made (excel or statistica format).

The captions to figures and drawings shall not be written in block letters. Line drawings and graphs should conform to the style of the journal (font size and appearance). Letters and numbers shall be sufficiently large to be readily legible after reduction of the width of a figure or table. Photomicrographs should have a mark indicating magnification, preferably in micrometers. Magnification can be additionally indicated at the end of the figure title, e.g. "Mag. 7500:1".

Discussion and conclusion may, if desired by authors, be combined into one chapter. This text should interpret the results relating to the problem outlined in the introduction and to related observations by the author(s) or other researchers. Repeating the data already presented in the "Results" chapter should be avoided. Implications for further studies or application may be discussed. A conclusion shall be expressed separately if results and discussion are combined in the same chapter. Acknowledgements are presented at the end of the paper. Relevant literature shall be cited in the text according to the Harvard system ("name – year"), e.g. (Bađun, 1965). In addition, the bibliography shall be listed at the end of the text in alphabetical order of the author's names, together with the title and full quotation of the bibliographical reference. The list of references shall be selective, and each reference shall have its DOI number (http://www.doi.org) (check at http://www.crossref.org).:

Example of references

Journal articles: Author's second name, initial(s) of the first name, year: Title. Journal name, volume (ev. issue): pages (from - to). DOI number.

Example:
Kärki, T., 2001: Variation of wood density and shrinkage in European aspen (*Populus tremula*). Holz als Roh- und Werkstoff, 59: 79-84. http://dx.doi.org/10.1007/s001070050479.

Books:
Author's second name, initial(s) of the first name, year: Title. (ev. Publisher/editor): edition, (ev. volume). Place of publishing, publisher (ev. pages from - to).

Examples:
Krpan, J. 1970: Tehnologija furnira i ploča. Drugo izdanje. Zagreb: Tehnička knjiga.
Wilson, J.W.; Wellwood, R.W. 1965: Intra-increment chemical properties of certain western Canadian coniferous species. U: W. A. Cote, Jr. (Ed.): Cellular Ultrastructure of Woody Plants. Syracuse, N.Y., Syracuse Univ. Press, pp. 551-559.

Other publications (brochures, studies, etc.):
Müller, D. 1977: Beitrag zur Klassifizierung asiatischer Baumarten. Mitteilung der Bundesforschungsanslalt für Forst- und Holzwirtschaft Hamburg, Nr. 98. Hamburg: M. Wiederbusch.

Websites:
***1997: "Guide to Punctuation" (online), University of Sussex, www.informatics.sussex.ac.uk/department/docs/punctuation/node00.html. First published 1997 (Accessed Jan. 27, 2010).

The paper will be sent to the author in pdf format before printing. The paper should be carefully corrected and sent back to the Editor's Office with the list of corrections made. Each contributor will receive 1 copy of the journal.

Further information on the way of writing scientific papers can be found on the following website:

www.ease.org.uk/publications/author-guidelines

SVEUČILIŠTE U ZAGREBU • FAKULTET ŠUMARSTVA I DRVNE TEHNOLOGIJE
UNIVERSITY OF ZAGREB • FACULTY OF FORESTRY AND WOOD TECHNOLOGY
Svetošimunska 23, 10000 Zagreb, Hrvatska / *Croatia* IBAN: HR0923600001101340148
tel: 00385 1 2352 454 e-mail: dcvetan@sumfak.hr OIB / *VAT ID*: HR07699719217

PRETPLATNI LIST / *SUBSCRIPTION SHEET*

Izašao je **broj 1** časopisa Drvna industrija, **volumen 73 (2022. godina)**. Pozivamo Vas da obnovite svoju pretplatu ili se pretplatite na časopis, te na taj način pomognete njegovo izlaženje. Cijena sva četiri broja jednog godišta (volumena) je 300,00 HRK bez PDV-a u Hrvatskoj, odnosno 55 EUR u inozemstvu. Ukoliko ste suglasni s uvjetima pretplate za jedno godište časopisa, molimo Vas da popunite obrazac za pretplatu i pošaljete ga na našu poštansku ili elektroničku adresu.

Issue 1, Volume 73 (2022) *of the journal* Drvna industrija *is published. We invite you to renew your subscription or subscribe to a journal to support it. The price of all four issues of one year (volume) is 300 HRK in Croatia, or 55 EUR, without VAT, in EU or elsewhere. If you agree to the subscription terms for one volume, please complete the subscription form and send it to our postal or e-mail address.*

Predsjednik Izdavačkog savjeta
časopisa Drvna industrija
President of Publishing Council

izv. prof. dr. sc. Vjekoslav Živković

Glavna i odgovorna urednica
časopisa Drvna industrija
Editor-In-Chief

prof. dr. sc. Ružica Beljo Lučić

PRETPLATA NA ČASOPIS
SUBSCRIPTION TO JOURNAL

DRVNA INDUSTRIJA

Pretplaćujemo se na časopis Drvna industrija u količini od ___ godišnje pretplate (četiri broja).
Cijena jednog godišta (volumena) iznosi 300 HRK, bez PDV-a. Pretplata obuhvaća sve brojeve jednog godišta.
We subscribe to the journal Drvna industrija *in amount of ___ annual subscription(s) (four issues).*
Price of one volume (year) is 55 EUR, without VAT. The subscription covers all issues of one volume.

Hrvatska:
HR0923600001101340148
s naznakom "Za časopis Drvna industrija"
poziv na broj: 3-02-03

EU / World:
Bank: Zagrebačka banka
IBAN: HR0923600001101340148
Swift: ZABA HR 2X

Osoba / *Name*: _____ e-mail: _____

Tvrtka, ustanova / *Company, institution*: _____

OIB / *VAT ID*: _____ Telefon / *Phone*: _____

Adresa / *Address*: _____ Pošta. broj: _____
(ulica / street) *Postal code:*

Grad / *City*: _____ Regija / *Region*: _____

Država / *Country*: _____

spinvalis

Kvaliteta s potpisom Slavonije.

Industrijska 24, 34000 Požega | Avenija Dubrovnik 14, 10 000 Zagreb
+385 34 311 150 | spinvalis@spinvalis.hr

www.spinvalis.hr